EVOLUTION OF EARLY PROTEROZOIC PASSIVE-MARGIN CARBONATE PLATFORM, ROCKNEST FORMATION, WOPMAY OROGEN, N.W.T., CANADA

by

John P. Grotzinger

Dissertation submitted to the Faculty of the

Virginia Polytechnic Institute and State University

in partial fulfillment of the requirements for the degree of

DOCTOR OF PHILOSOPHY

in

Geology

APPROVED:

J.F. Read

K.A. Eriksson

A.K. Sinha

R.K. Bambach

C. Simpson

February, 1985
Blacksburg, Virginia

EVOLUTION OF EARLY PROTEROZOIC PASSIVE-MARGIN CARBONATE PLATFORM, ROCKNEST FORMATION, WOPMAY OROGEN, N.W.T., CANADA

by

John P. Grotzinger

(ABSTRACT)

The superbly exposed Rocknest Formation, Wopmay Orogen, N.W.T., Canada, is an early Proterozoic (1.89 Ga) passive-margin carbonate platform. It is an eastward-thinning prism, 0 to 1,100 m thick, extending for over 220 km parallel to strike, and over 200 km perpendicular to strike. It contains from west to east, slope, outer-shelf, shoal-complex, and inner-shelf facies. Slope facies are rhythmites, megabreccias and rhythmite breccias. Outer-shelf facies include stromatolitic reefal boundstone and backreef ooid/intraclast grainstore. Shoal-complex facies are shallowing-upward cycles of tufa, cryptalgalaminite, laminated dolosiltite/lutite, overlain by tepees, breccias and pisolite; these formed a paleotopographic high, restricting an eastern "lagoon" from western ocean. Inner-

shelf facies are dominantly asymmetric, shallowing-upward cycles of "lagoonal" mixed carbonates and siliciclastics, that grade up into intertidal stromatolitic dolomites; cyclic facies pass eastward into non-cyclic siliclastics of central and eastern "lagoon". The shelf was terminally drowned during attempted subduction of the margin.

Individual cycles are correlatable for over 200 km parallel to strike and over 120 km perpendicular to strike. Cycles formed in response to small, asymmetric (rapid rise/slow fall) eustatic oscillations in sea-level (= 10 m). An alpine glacio-eustatic model accounts for the origin of cycles best. During sea-level rise, rapid transgression and submergence of tidal flats occurred along eastern margin of the shoal-complex, followed by eastward expansion of the shoal-complex, and slow progradation of tidal flats over lagoonal facies during sea-level fall.
Computer modelling of Rocknest cycle types across the platform provides important information on absolute sedimentation rates and lag times.

ACKNOWLEGEMENTS

It is a pleasure to thank my principle advisors, Drs. Fred Read and Ken Eriksson, for providing much critical advice during the course of this project and helping obtain financial support. Their comments and relentless editing greatly improved this dissertation. Both made the long trip to Wopmay, where they stimulated and encouraged my ongoing field work and made many important observations.

Dr. Paul Hoffman is gratefully acknowledged for suggesting the project, and providing continual advice, enthusiasm, counter-arguments and bop during three field seasons. The Geological Survey of Canada is thanked for generously supporting the project with full-time helicopter assistance and other logistical support. I sincerely thank Rein Tirrul for helpful discussions and advice concerning the structure and stratigraphy of the Wopmay externides.

The support, advice and critical reviews of my examining committee, Drs. Richard Bambach, Carol Simpson, Krishna Sinha, were very helpful. Appreciation is expressed to , , , , , , , , , , , , and for superb field assistance. helped prepare photographic plates.

Financial support was provided by National Science Foundation Grant EAR-8218618, Geological Society of America Grant 2992-82, and a Grant-in-Aid of Research from the Scientific Research Society of Sigma Xi.

Final thanks go to my colleagues in the Carbonate Research Arctic/Appalachian Projects Laboratory;

, , , , and

, for support and advice both on and off the court.

This thesis is dedicated to my uncle,

, a pioneer in both modern carbonate sedimentology and pre-Phanerozoic geology. His enthusiasm, intense curiosity, and uncompromising dedication have shown me how to more accurately define my goals as a scientist.

"Here, interpretations of buildup associations become wildly speculative."

(B.W. Sellwood, page 312, 1983 edition of "Sedimentary Environments and Facies"; stated in reference to descriptions of pre-Phanerozoic carbonate buildups).

TABLE OF CONTENTS

ACKNOWLEGEMENTS iv

Chapter

page

I. EVOLUTION OF ROCKNEST PLATFORM 1

Abstract 1
Introduction 3
Structural and Stratigraphic Setting 5
Rocknest Outer-Shelf 21
Lithofacies 21
Evolution of Outer-Shelf 33
Rocknest Slope 38
Lithofacies 39
Evolution of Slope 56
Rocknest Shoal-Complex 61
Rocknest Inner Shelf 67
Cyclic Lithofacies 73
Evolution of Cyclic Inner-Shelf 76
Incipient Drowning of Shelf 83
Terminal Drowning of Shelf 91
Conclusions and Summary of Shelf Evolution . . . 97

II. ORIGIN OF ROCKNEST INNER-SHELF AND SHALLOWING-UPWARD CYCLES 106

Abstract 106
Introduction 108
Regional Setting 110
Rocknest Outer-Shelf and Slope 113
Rocknest Shoal-Complex 115
Lithofacies 116
Evolution of Shoal-Complex 125
Rocknest Inner-Shelf 127
Cyclic Lithofacies 128
Evolution of Cyclic Inner-Shelf 148
Cycle Development in the Geologic Record: A Discussion of Mechanisms 149
Autocyclic Mechanism 149
Allocyclic Mechanisms 153
Mechanisms of Cycle Development in Rocknest Formation 164
Quantification of Parameters Controlling Cycle Development 164
Development of Cycle Types and Profiles . . 174

"Grand Cycles" and Non-Cyclic Sedimentation on Inner-Shelf 190
Lower Non-Cyclic Interval 190
Middle Non-Cyclic Interval 195
Upper Non-Cyclic Interval 197
Origin of Non-Cyclic Intervals and "Grand Cycles" 199
Conclusions 202

REFERENCES 210

Appendix

page

A. MEASURED SECTIONS 221

VITA 225

LIST OF FIGURES

Figure		page
1.	Regional setting of Wopmay Orogen.	6
2.	Tectono-depositional setting of Rocknest shelf sequence.	8
3.	Rocknest shelf stratigraphy.	13
4.	Rocknest shelf-edge stratigraphy.	15
5.	Correlation diagram of Coronation Supergroup, Wopmay Orogen, with Goulburn Group, Kilohigok Basin.	18
6.	Lowermost rim stratigraphy (a).	22
7.	Reefal rim facies.	25
8.	Trough cross-bedded backreef grainstone (A), and neptunian dike (B) cross-cutting reefal mound.	29
9.	Rocknest shelf paleogeography.	34
10.	Rocknest slope stratigraphy.	40
11.	Slope rhythmite facies.	42
12.	Slope bioherm facies.	48
13.	Slope breccia facies.	53
14.	Paleobathymetric relationships, lowermost rim sequence.	59
15.	Shoal-complex stratigraphy.	63
16.	Shoal-complex facies.	65
17.	Cyclic inner-shelf stratigraphy.	69
18.	Inner-shelf "grand cycles" and cycles.	71
19.	Rocknest cycle types.	74
20.	Lower facies of shale-based cycles.	77

21. Dolosiltite and edgewise conglomerate. 79

22. Stromatolites, thrombolite and tufa. 81

23. Stratigraphy of non-cyclic intervals. 84

24. Paleogeographic cross-sections of non-cyclic intervals. 87

25. Stratigraphy of two "grand cycles". 92

26. Rocknest Formation/Recluse Group contact. 95

27. Summary of shelf evolution. 99

28. Shoal-complex facies. 120

29. Shoal-complex facies (continued). 122

30. Correlation of cycles parallel to depositional strike. 129

31. Correlation diagram of cycles perpendicular to depositional strike. 132

32. Conical stromatolites and thrombolitic microfabric. 141

33. Varieties of Rocknest tidal-flat tufa. 146

34. Plot of cycle period vs. sea-level amplitude. . . 169

35. "Geohistory" diagram of Rocknest cycles. 175

36. Rocknest cycle profiles. 177

36. Rocknest cycle profiles (continued). 179

37. Synthetic models of Rocknest cycles: General model and shoal-complex model. 183

38. Synthetic models of Rocknest cycles: proximal and distal inner-shelf. 187

39. Non-cyclic facies. 192

40. Synthetic model of "Grand Cycle". 203

41. Location of measured sections for Appendix A. . . 224

Chapter I

EVOLUTION OF ROCKNEST PLATFORM

ABSTRACT

The superbly exposed Rocknest Formation, Wopmay Orogen, N.W.T., Canada, is an early Proterozoic (1.89 Ga) carbonate platform that formed along the eastern, passive margin of Slave craton (Archean). The palinspastically restored shelf sequence is an eastward-thinning prism, 0 to 1,100 m thick, extending for over 220 km parallel to strike, and over 200 km perpendicular to strike. It contains from west to east, slope, outer-shelf, shoal-complex, and inner-shelf facies. Slope facies are carbonate rhythmites, megabreccias and platy rhythmite breccias. Outer-shelf facies include stromatolitic reefal boundstone and backreef ooid/intraclast grainstore. Shoal-complex facies are shallowing-upward cycles of tufa, cryptalgalaminite, laminated dolosiltite/lutite, overlain by tepees, breccias and pisolite; these formed a paleotopographic high, restricting an eastern "lagoon" from western ocean. Inner-shelf facies are dominantly asymmetric, shallowing-upward cycles of "lagoonal" mixed carbonates and siliciclastics, that grade up into intertidal stromatolitic dolomites; cyclic facies pass eastward into non-cyclic siliclastics of central and

eastern "lagoon". The Rocknest "lagoon" spanned the width of slave craton (400 to 500 km), and was bounded by a western carbonate shoreline (shoal-complex), and by a tectonically active eastern siliciclastic shoreline.

The Rocknest carbonate shelf developed on an underlying siliclastic shelf. An initial ramp rapidly evolved into a progradational accretionary rim and shoal-complex, followed by vertical aggradation of the rim. Concurrently, the shoal-complex underwent numerous west-to-east progradational events to produce many shallowing-upward cycles in the shelf interior. Subsidence rates ranged from 40 cm/1000 yrs at the rim, to 25 cm/1000 yrs, 135 km to the east. Thus, cycles formed near the rim are thicker, (avg. 12 m) than those formed in the shelf interior (avg. 6 m). Cyclic sedimentation was interrupted during three events of incipient shelf drowning, associated with local backstepping of the rim and non-cyclic sedimentation over most of the shelf, probably caused by fourth order eustatic sea-level oscillations. The shelf was terminally drowned and overlain by deep-water, synorogenic siliciclastics during attempted subduction of the margin. Carbonates capping the shelf are stromatolitic patch reefs which overlie a possible unconformity, suggesting emergence of the shelf prior to drowning.

INTRODUCTION

The stratigraphy and evolution of carbonate shelves formed on Phanerozoic passive continental margins have been well documented (eg. Logan et al., 1969; Ginsburg and James, 1974; Wilson, 1975; Mullins and Neumann, 1979; Cook, 1979). Models of ancient and modern carbonate platforms have been integrated to emphasize platform types, their facies and evolutionary histories (Read, 1982; James and Mountjoy, 1983; James, 1984 a,b). However, several general aspects of passive-margin carbonate shelf evolution are still poorly understood.

First, descriptions of pre-Phanerozoic passive-margin carbonate shelves are lacking, and little is known concerning distribution and genesis of shelf, shelf-edge and slope facies (including stromatolites), general shelf evolution, and the similarities and differences between pre-Phanerozoic and Phanerozoic shelves. Second, because most Mesozoic carbonates are deeply buried beneath modern continental shelf sequences, little is known of shelf evolution during early stages of rapid passive-margin subsidence immediately following continental break-up. Third, although the effect of long-term (low order) eustatic sea-level changes on Phanerozoic shelf stratigraphy has drawn much attention (eg. Vail et al., 1977; Pitman, 1973,

1978), our understanding of the effects of short-term (high order) eustatic sea-level changes is restricted to the Quaternary (Mesolella et al., 1969; Logan et al., 1969; Steinen et al., 1973; Chappel, 1974). There are few exceptions to this (eg. Fischer, 1964; Moore, 1964), despite the probability that these short-term changes occurred throughout most of the geologic record (Morner, 1976), and that they may be the cause of most small-scale shallowing-upward cycles in carbonates (Read et al., in prep).

The extremely well exposed early Proterozoic (1.89 Ga) Rocknest Formation provides a unique opportunity to study the evolution of a pre-Phanerozoic passive-margin carbonate shelf, involving analysis of shelf, shelf-edge and slope facies, major types of platform-to-basin transitions, and distribution and magnitude of subsidence. Because the passive margin was destroyed within 10-15 m.y. of rifting (Hoffman and Bowring, 1984), the Rocknest shelf sequence provides valuable information on the juvenile stage of shelf evolution following break-up. Finally, this study also addresses the problems of genesis of small-scale shallowing-upward cycles in carbonates, and the origin of pre-Phanerozoic carbonate sediment.

STRUCTURAL AND STRATIGRAPHIC SETTING

The early Proterozoic (1.89 Ga) Rocknest Formation, part of the Coronation Supergroup, is exposed in the foreland thrust-fold belt and autochthon of Wopmay Orogen, northwest Canada (Fig. 1). Early Proterozoic sediments unconformably overlie Archean crystalline basement, exposed to the east and south, and are flanked to the west by high-grade equivalents and intrusive rocks of the Hepburn Metamorphic-Plutonic Complex (Hoffman, 1980). These sediments are overlain to the north by gently-dipping middle Proterozoic sedimentary rocks.

The Coronation Supergroup (Fig. 2) is a continental margin sedimentary prism composed of a basal rift sequence (Akaitcho Group), a middle passive-margin sequence (Epworth Group), and overlying foredeep sequence (Recluse Group; Hoffman, 1980). The Akaitcho Group (8 to 10 km thick) contains submarine arkosic sandstone, basinal mudstone, pillow basalts and rhyolite porphyry, and minor reefal carbonate (Easton, 1981).

The lower part of the Epworth Group (Odjick Formation; 0.2 to 1.5 thick) is a shallow-water, siliciclastic shelf sequence composed of siltstone, mudstone and marlstone (lower member), stacked coarsening-upward cycles of quartz arenite and siltstone (middle member), and siltstone with

Figure 1. Regional setting of Wopmay orogen. A; location of foreland thrust-fold belt (zone 2), the autochton (zone 1), and their relationship to Peacock Hills area (P. Hills) of Kilohigok Basin. Simplified geology of zones 1 and 2 are shown in (B), including distribution of Rocknest Formation (included with Odjick Fm. as Epworth Group), and location of sections of Figs. 30-31. Note location of syncline "M"; TL, Takijuq Lake; CG, Coronation Gulf. After Hoffman, 1980; Hoffman et.al., 1984; reproduced and modified with permission of P.F. Hoffman, 1985.

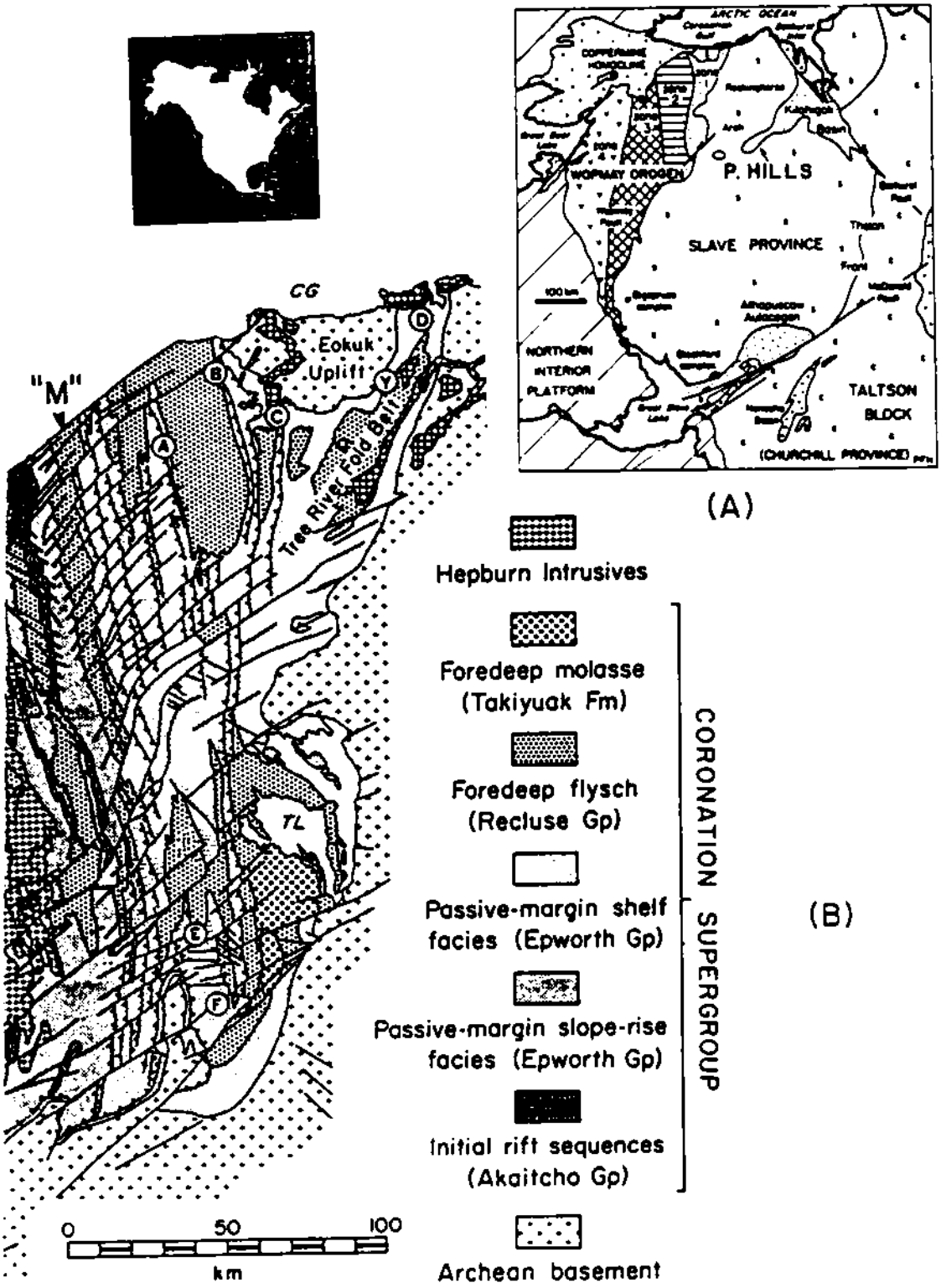
ARCTIC OCEAN
COPPERMINE HOMOCLINE
WOPMAY OROGEN
P. HILLS
SLAVE PROVINCE
NORTHERN INTERIOR PLATFORM
TALTSON BLOCK
(CHURCHILL PROVINCE)
(A)
CG
Eokuk Uplift
"M"
Tree River Fold Belt
TL
Hepburn Intrusives
Foredeep molasse (Takiyuak Fm)
Foredeep flysch (Recluse Gp)
Passive-margin shelf facies (Epworth Gp)
Passive-margin slope-rise facies (Epworth Gp)
Initial rift sequences (Akaitcho Gp)
CORONATION SUPERGROUP
Archean basement
0
50
100
km
(B)

Figure 2. Tectono-depositional setting of Rocknest shelf sequence. Note relationship to other sequences in Coronation Supergroup, and that passive-margin shelf facies overlie predominantly unfaulted Archean basement. After Hoffman et al., 1984; reproduced with permission of P. F. Hoffman, 1985.

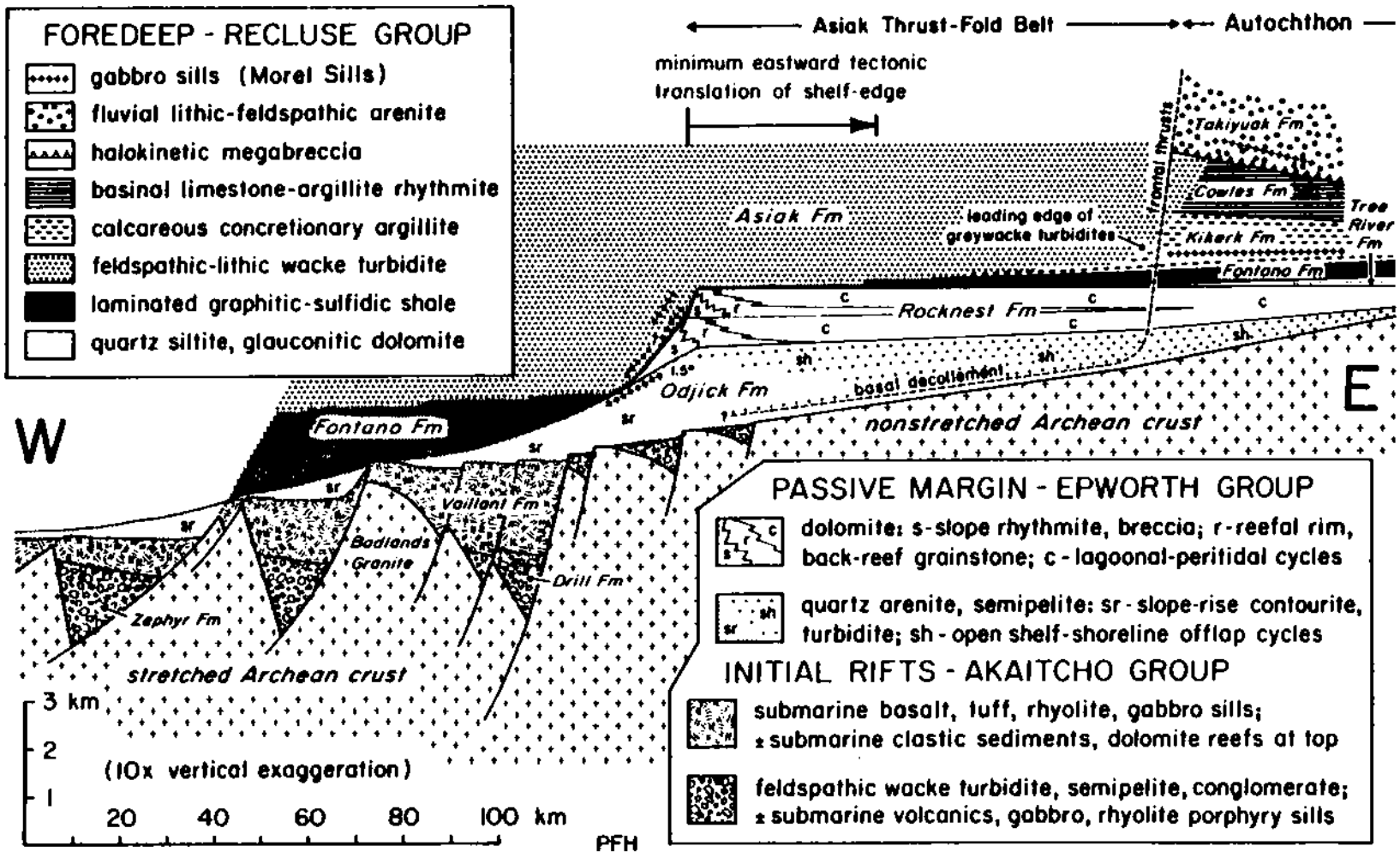
FOREDEEP - RECLUSE GROUP
gabbro sills (Morel Sills)
fluvial lithic-feldspathic arenite
halokinetic megabreccia
basinal limestone-argillite rhythmite
calcareous concretionary argillite
feldspathic-lithic wacke turbidite
laminated graphitic-sulfidic shale
quartz siltite, glauconitic dolomite
Asiak Thrust-Fold Belt
Autochthon
minimum eastward tectonic translation of shelf-edge
frontal thrusts
Takiyuak Fm
Cowles Fm
Tree River Fm
Asiak Fm
leading edge of greywacke turbidites
Kikerk Fm
Fontano Fm
Rocknest Fm
Odjick Fm
basal decollement
nonstretched Archean crust
W
E
Fontano Fm
Vaillant Fm
Badlands Granite
Drill Fm
Zephyr Fm
stretched Archean crust
3 km
2
1
(10x vertical exaggeration)
20 40 60 80 100 km
PFH
PASSIVE MARGIN - EPWORTH GROUP
dolomite: s-slope rhythmite, breccia; r-reefal rim, back-reef grainstone; c-lagoonal-peritidal cycles
quartz arenite, semipelite: sr-slope-rise contourite, turbidite; sh-open shelf-shoreline offlap cycles
INITIAL RIFTS - AKAITCHO GROUP
submarine basalt, tuff, rhyolite, gabbro sills; ± submarine clastic sediments, dolomite reefs at top
feldspathic wacke turbidite, semipelite, conglomerate; ± submarine volcanics, gabbro, rhyolite porphyry sills

minor intercalated pebbly sandstone, and ferruginous and intraclastic dolomite (upper member; Hoffman et al., 1983, 1984). It formed on a prograding, storm-dominated, open-marine shelf (Hoffman et al., 1984). The upper Epworth Group (Rocknest Formation; 450 to 1100 m thick) is a cyclic dolomite shelf-sequence with a stromatolitic reefal rim and flanking debris apron (Hoffman, 1973, 1975). Stratigraphic relationships and facies analysis indicate long-term progradation and aggradation of the shelf, punctuated by relatively short episodes of incipient drowning of the shelf and backstepping of the rim. The shelf was terminally drowned and onlapped by the Recluse Group during continental collision and attempted subduction of the margin (Calderian orogeny; Hoffman and Bowring, 1984).

The Recluse Group (1.5 to 2.5 km thick) is a deep-to-shallow water sequence which sharply overlies the Rocknest Formation. It comprises successively overlying glauconitic siltstone (Tree River Formation), graphitic and pyritic black shale (Fontano Formation), graywacke turbidites (Asiak Formation), limestone/argillite rhythmites, intraclast grainstone, and stromatolitic reefs (Cowles Lake Formation), and solution collapse breccia and fluvial, feldspathic sandstone (Takiyuak Formation; Hoffman, 1973; Hoffman et al., 1983; Jackson, 1984).

During the Calderian orogeny (1.90 to 1.885 Ga), the Coronation Supergroup was detached from its basement and imbricated during west-to-east transport over the craton (Tirrul, 1982; 1983; Hoffman and Bowring, 1984). Subsequently, the thrust-fold belt and autochthon underwent large-scale cross-folding due to NW-SE compression, and later conjugate transcurrent faulting related to E-W compression (Tirrul, 1982, 1983; Hoffman et al., 1983, 1984). Locally, Rocknest sections have been thickened or thinned by either the Calderian deformation (thrusting and folding), or later cross-folding (Tirrul, 1982, 1983; Hoffman et al., 1984). Locally high penetrative strain in Rocknest dolomites developed under Anchi- to epi-metamorphic conditions that locally reached 200 to 350 °C (Lucas, 1984). The conjugate transcurrent event did not produce significant penetrative strain in the Rocknest Formation, although in domains of high shortening, counterclockwise rotations of fault blocks of up to 12 degrees are common (Tirrul, pers. comm., 1984).

Palinspastic cross-sections (Figs. 3,4) constructed from structural cross-sections (Tirrul, 1983), and regional geologic maps (Hoffman, 1984; Campbell and Cecile, 1976) were used to reconstruct the Rocknest shelf. Structural cross-sections were made (Tirrul, 1983) from composite down-

plunge projections of the thrust-fold belt, using bed-length and area balancing and are accurate to less than 10% error (Tirrul, pers. comm., 1985). The correlation datum used in constructing stratigraphic cross-sections is the top of a distinctive set of carbonate-based shallowing-upward cycles. Time control is provided by the upper boundaries of two shelf-wide, shallowing-upward cycles which contain large, fenestral stromatolite domes and small, conical stromatolites (Fig. 3).

The palinspastically restored Rocknest shelf sequence is an eastward-thinning prism, 0 to 1,100 m thick, extending for over 220 km parallel to depositional strike, and over 200 km perpendicular to strike (Fig. 3). Along depositional strike, the Rocknest Formation shows little change in thickness or facies, suggesting that the shelf was continuous beyond the present northern and southern limits of outcrop. The Rocknest Formation may be correlative with the Snare Group (McGlynn and Ross, 1963), 225 km south of the southern end of the thrust-fold belt. The Snare Group contains probable cyclic carbonates with conical stromatolites (J. King, pers. comm., 1983). Correlation of the Rocknest Formation perpendicular to depositional strike with the Goulburn Group in Kilohigok basin to the east (Figs. 1,5; Hoffman et al., 1984) suggests that the original

Figure 3. Rocknest shelf stratigraphy. Note well-developed W-E facies zonation including: slope, outer-shelf (rim boundstone and back-reef grainstone), tufa-based cycles (shoal-complex), dolosiltite-based cycles (proximal inner-shelf), shale-based cycles (distal inner-shelf), and shale (non-cyclic "lagoon"). Cyclic sequences are separated by non-cylcic sequences. Time horizons indicate greatest subsidence midway across shelf sequence. Note that shelf probably extended farther to east in the north than in the south and that the eastern "feather edge" may be time-equivalent to the lower non-cyclic interval (correlation queried).

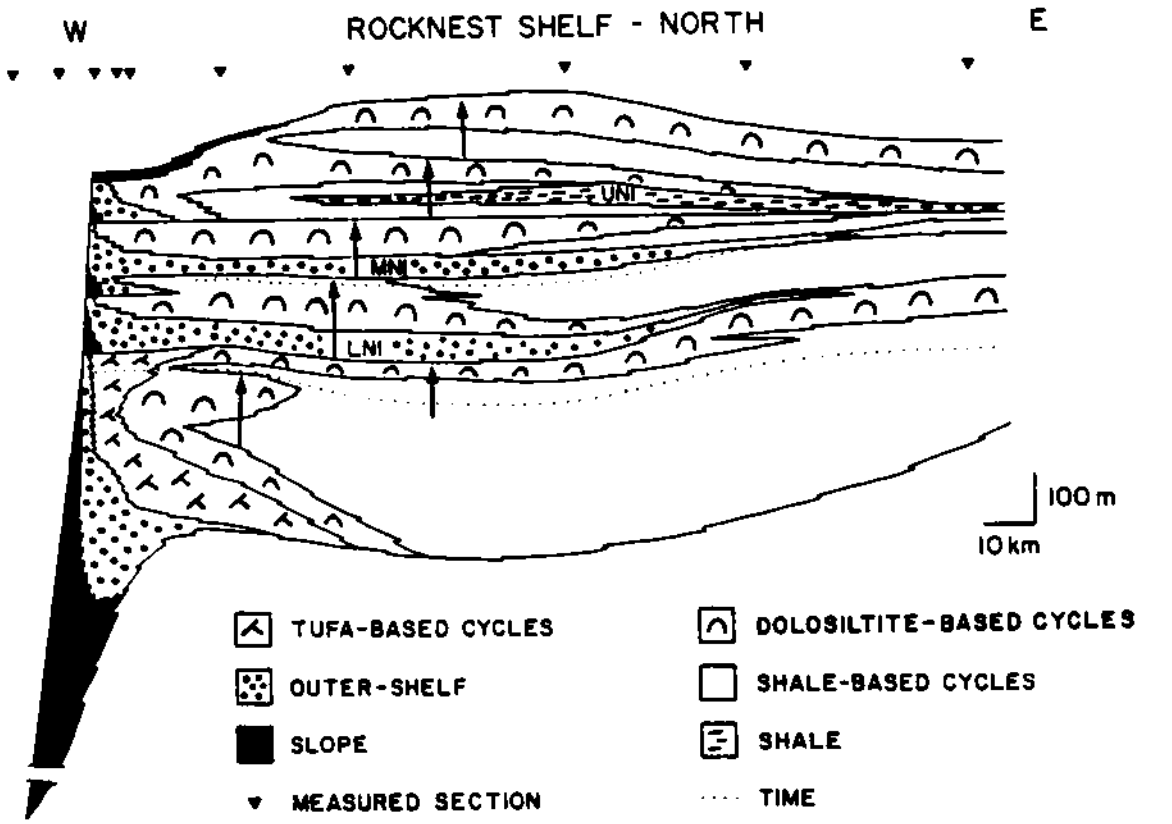
W
ROCKNEST SHELF - NORTH
E
UNI
MNI
LNI
100 m
10 km
TUFA-BASED CYCLES
DOLOSILTITE-BASED CYCLES
OUTER-SHELF
SHALE-BASED CYCLES
SLOPE
SHALE
MEASURED SECTION
TIME

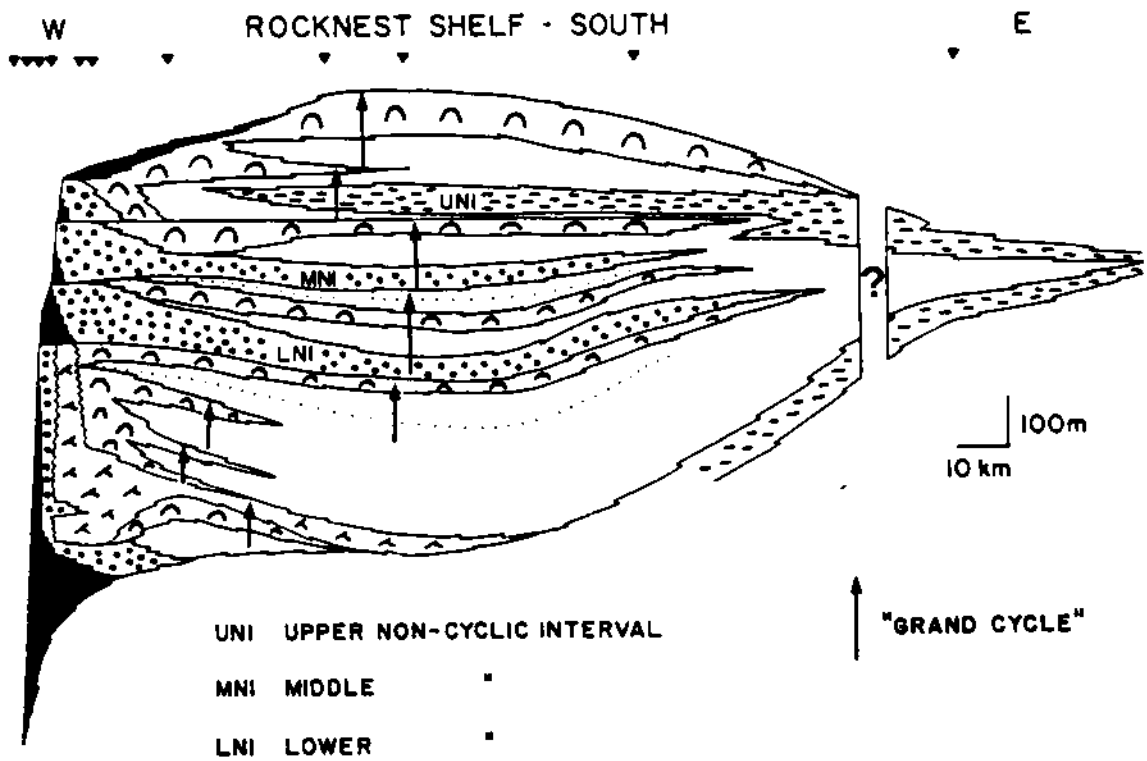
W
ROCKNEST SHELF - SOUTH
E
UNI
MNI
LNI
?
100m
10 km
UNI UPPER NON-CYCLIC INTERVAL
"GRAND CYCLE"
MNI MIDDLE "
LNI LOWER "

Figure 4. Rocknest shelf-edge stratigraphy. Note scale change and subdivision of shallow from deep slope, and boundstone from grainstone. Calculation of average slopes for lowermost rim in south are discussed in text. Rim backstepping events are correlative with non-cyclic intervals (cf. Figure 3).

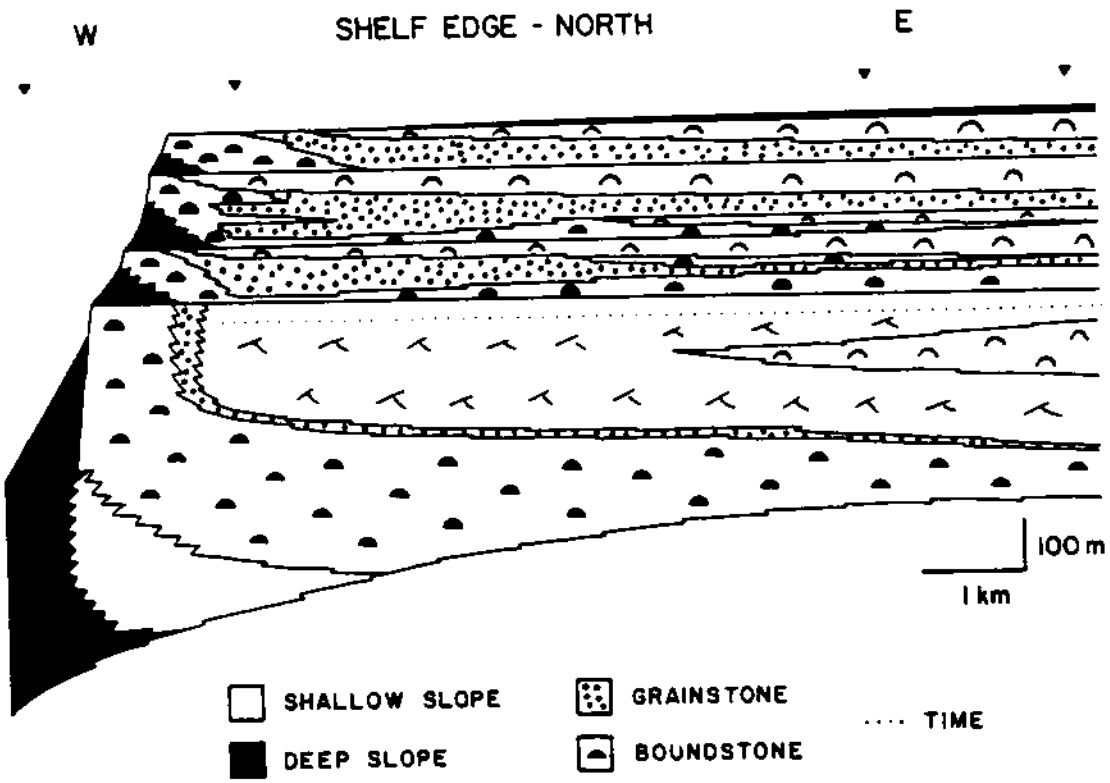
W
SHELF EDGE - NORTH
E
100 m
1 km
SHALLOW SLOPE
DEEP SLOPE
GRAINSTONE
BOUNDSTONE
.... TIME

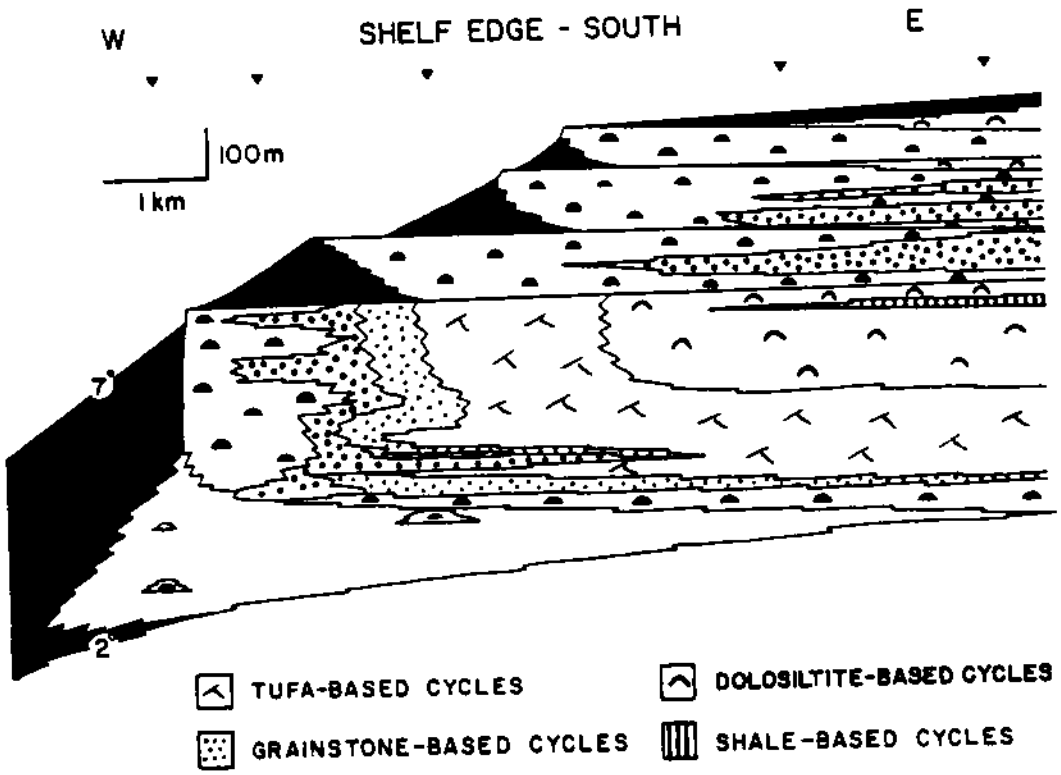
W
SHELF EDGE - SOUTH
E
100m
1 km
1'
2'
TUFA-BASED CYCLES
GRAINSTONE-BASED CYCLES
DOLOSILTITE-BASED CYCLES
SHALE-BASED CYCLES

width of the shelf may have exceeded 260 km at the southern end of the thrust-fold belt; there it is only 40 m thick, 180 km (palinspastic) from the shelf edge (Fig. 3b). However, the shelf probably was much wider at the northern end of the thrust-fold belt where it is 450 m thick, 180 km (palinspastic) from the shelf-edge (Fig. 3a).

The Rocknest shelf sequence (Figs. 3,4) can be divided from west to east into slope, outer-shelf, shoal-complex, and inner-shelf facies. Slope, outer-shelf and shoal-complex facies assemblages are restricted to the western margin of the shelf; inner-shelf facies occur over most of the shelf region, except adjacent to its margin.

The inner-shelf sequence contains three non-cyclic intervals (Fig. 3), which together with sequences of inner-shelf cycles, form "grand cycles", 75 to 200 km thick (Fig. 3). Inner-shelf carbonates pass eastward (Fig. 3) into siliciclastic inner-shelf deposits of the Burnside River Formation, Goulburn Group, Kilohigok Basin (Campbell and Cecile, 1981; Hoffman et al., 1984).

Burnside River siliciclastics thicken from less than 300 m in westernmost exposures (Peacock Hills/Rockinghorse Lake areas) to more than 2,500 m in the east near Bathurst Inlet (Campbell and Cecile, 1981; Hoffman et al., 1984). Western and central parts of the basin contain marine quartz

Figure 5. Correlation diagram of Coronation Supergroup, Wopmay Orogen, with Goulburn Group, Kilohigok Basin. Note pinch-out of Rocknest Formation into time-equivalent siliciclastics of Burnside River Formation, which thickens markedly toward section 10. Burnside River facies are marine except for section 10 (dominantly fluvial), located near Bathurst Inlet.

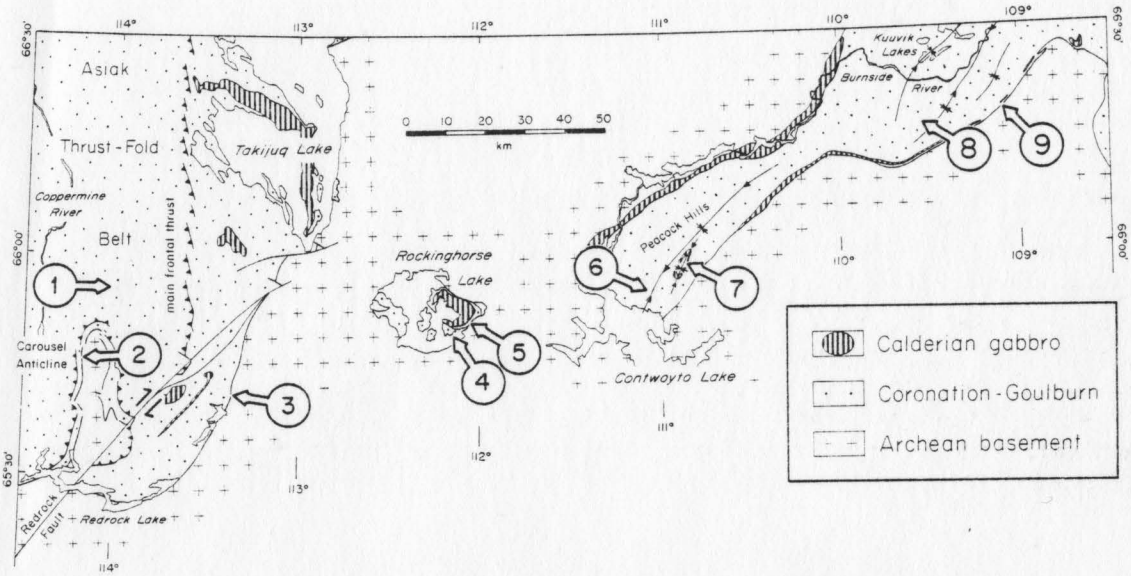
Asiak
Thrust-Fold
Belt
Takijuq Lake
Coppermine River
main frontal thrust
Carousel Anticline
Redrock Fault
Redrock Lake
Rockinghorse Lake
Peacock Hills
Contwoyto Lake
Kuuvik Lakes
Burnside River
0 10 20 30 40 50
km
Calderian gabbro
Coronation-Goulburn
Archean basement

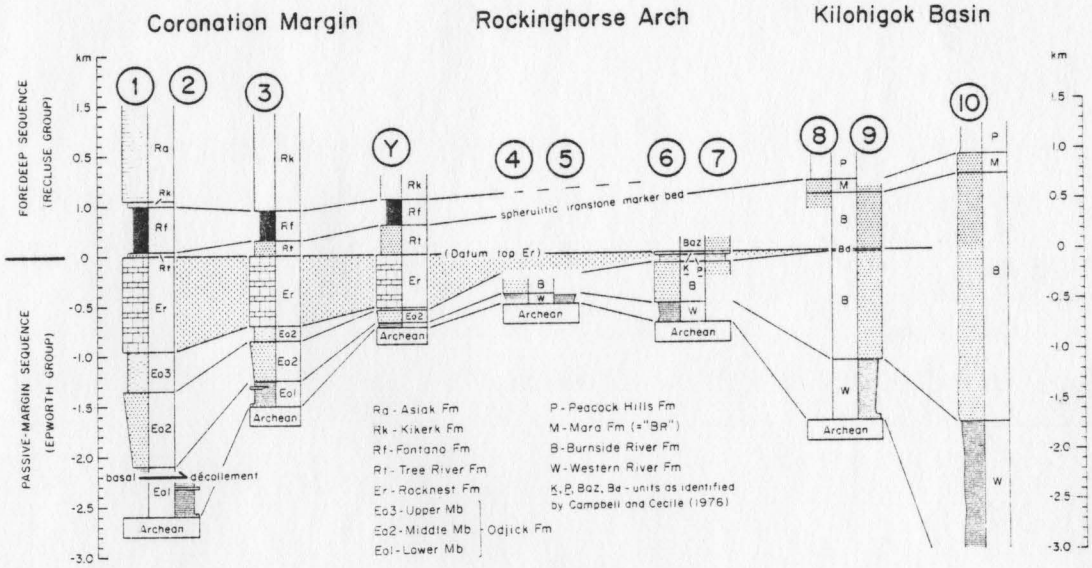
Coronation Margin
Rockinghorse Arch
Kilohigok Basin
FOREDEEP SEQUENCE (RECLUSE GROUP)
PASSIVE-MARGIN SEQUENCE (EPWORTH GROUP)
spherulitic ironstone marker bed
(Datum top Er)
basal décollement
Archean
Ra - Asiak Fm
Rk - Kikerk Fm
Rf - Fontano Fm
Rt - Tree River Fm
Er - Rocknest Fm
Eo3 - Upper Mb
Eo2 - Middle Mb
Eo1 - Lower Mb
Odjick Fm
P - Peacock Hills Fm
M - Mara Fm (="BR")
B - Burnside River Fm
W - Western River Fm
K, P, Baz, Bd - units as identified by Campbell and Cecile (1976)

arenite, siltstone and shale, and were formed as distal "lagoonal" deposits during Rocknest deposition. They pass eastward into fluvial subarkose, arkose and conglomerate. Burnside River siliciclastics probably were derived from unroofing of the Thelon Tectonic Zone, a major structure bounding the eastern side of the Slave Province (Hoffman et al., 1984). The Thelon Tectonic Zone is a late Archean structure that was reactivated during the early Proterozoic, involving major west-directed thrusting of Archean basement and the Goulburn Group (Thompson and Ashton, 1984; Tirrul, 1985). Deposition occurred in a deeply subsiding foredeep, flanking the advancing basement-involved thrust sheets of the Thelon Tectonic Zone. Because the Rocknest Formation is a passive-margin carbonate shelf sequence that interfingers westward with Burnside foredeep clastics, it demonstrates that passive-margin development along the western side of Slave craton was concommitant with convergence and foredeep subsidence along its eastern margin. The Rocknest "lagoon" spanned the width of the Slave craton and was bounded to the west by a carbonate shoreline (shoal-complex), and to the east by a tectonically active, siliciclastic shoreline.

ROCKNEST OUTER-SHELF

Facies of the Rocknest outer-shelf are exposed along the east limb of syncline "M" and in the first two thrust sheets to the east (Fig. 1). Four distinct reefal rim sequences occur, flanked to the east by backreef grainstones (Fig. 4). The lowermost rim sequence is thickest (450 to 500 m), and is overlain by three younger, backstepped rim sequences, 80 to 130 m thick.

The lowermost rim sequence consists dominantly of stromatolite mounds interbedded with intervals of partially-linked columnar stromatolites, and minor ooid-intraclast grainstone and mounded edgewise conglomerate (Fig. 6a). Younger rim sequences contain abundant grainstone (Fig. 4), and different varieties of stromatolite mounds.

Lithofacies

Stromatolite Mounds: These are laterally continuous, dolomitic biostromes, 10 to 150 m thick, of superimposed mound-shaped stromatolites, 1 to 4 m wide and with up to 2 m of synoptic relief (Fig. 7a). Internal lamination is tangential to the mound surface, with a high degree of inheritance within mounds, but poor inheritance between succesively overlying mounds. Rarely, parts of mounds contain partially-linked digitate stromatolites (1 to 3 cm

Figure 6. Lowermost rim stratigraphy (a). Note cross-cutting relationship of neptunian dikes to mounds (b). Dikes cross-cut or run parallel to layering (d), but may be truncated and overlain by more stromatolitic layering (c); morphology of preserved dike-filling marine cements suggests that initial aragonite was followed by hi-Mg(?) calcite (c,d).

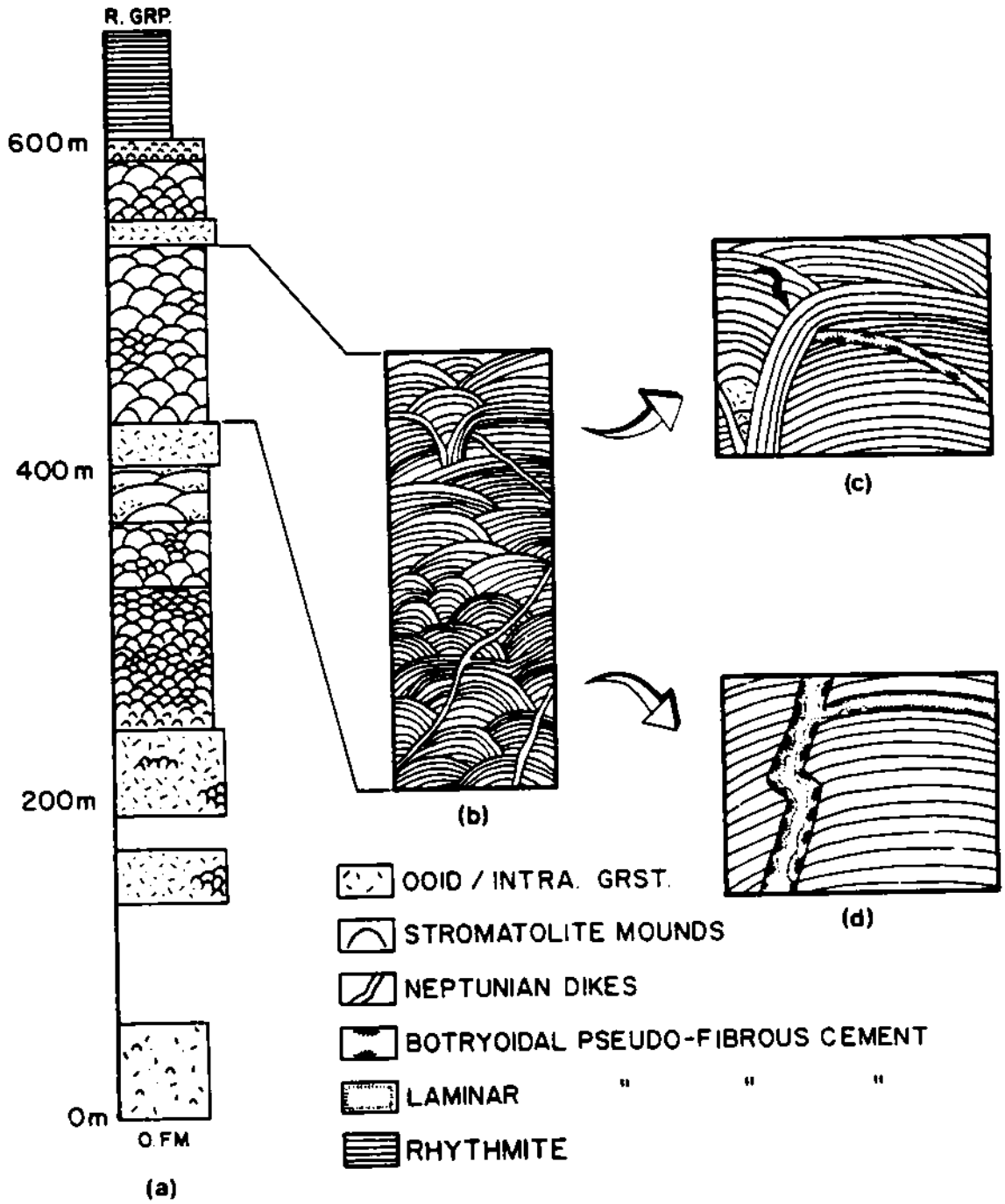
R. GRP.
600m
400m
200m
0m
O. FM
(a)
(b)
(c)
(d)
OOID / INTRA. GRST.
STROMATOLITE MOUNDS
NEPTUNIAN DIKES
BOTRYOIDAL PSEUDO-FIBROUS CEMENT
LAMINAR " " "
RHYTHMITE

wide). Mounds are strongly elongate subnormal to the regional trend of the shelf-edge, deviating 10 to 15 degrees southwest from normal to shelf-edge trend. Channels between stromatolite mounds are narrow (20 to 50 cm wide), steep and filled with intraclast grainstone/packstone or edgewise conglomerate. Mounds are locally brecciated and large fragments are overlain by stromatolitic layering.

The thick sequences of large stromatolite mounds formed a major barrier reef complex in shallow, turbulent water as shown by the strong elongation of mounds, erosion of stromatolite walls and accumulation of fragments as cross-bedded detritus in adjacent narrow channels, and lack of associated mud- and silt-sized carbonate sediment. Prevailing paleowinds impinged on the shelf-edge at such an oblique angle that waves were not refracted parallel to shelf-edge trend, and stromatolites were elongated subnormal to the trend of the shelf-edge. This differs from the normal-to-shelf-edge orientation of stromatolite elongation in the 1.8 Ga Pethei Group (Hoffman, 1974; 1969), which is similar to the normal-to-shelf-edge orientation of most Holocene spur and groove structure. An orthogonal orientation should be most common because waves, upon shoaling at the fore-reef, are commonly refracted parallel to shelf-edge trend. However, if wave approach is

Figure 7. Reefal rim facies. A) Large mounds (M) of lowermost rim. The same neptunian dike cross-cutting mound "M" is enlarged in Figure 8b. B) Partially-linked columns with upward decrease in column width and synoptic relief, possibly due to lowering of sea-level and upward-shallowing; columns are elongate in plan view (C). Such columns form bioherms in upper rims (D). Hammer for scale.

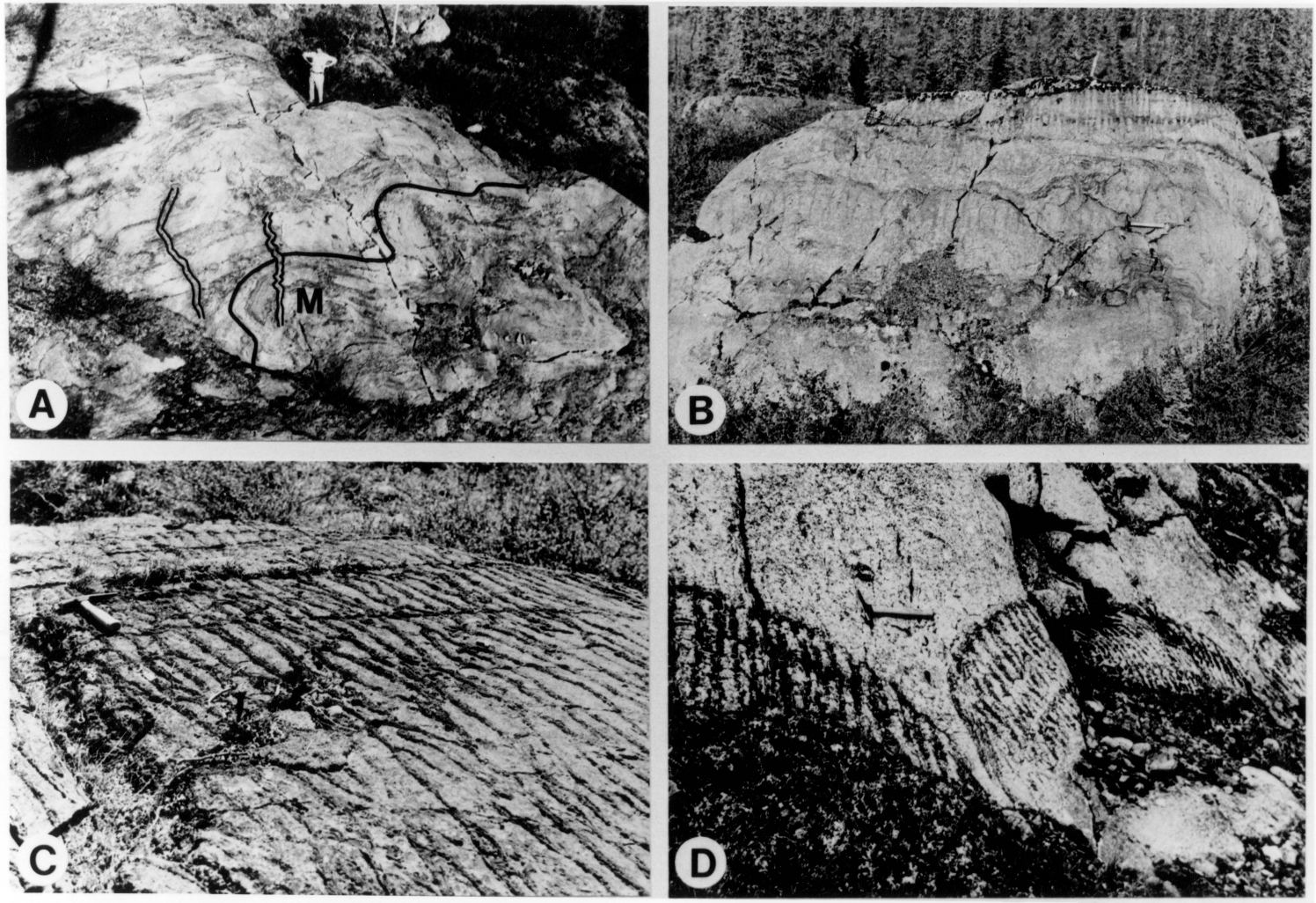
A
M
B
C
D

sufficiently oblique to shelf-edge trend, waves will be incompletely refracted and spurs and grooves will be oriented subnormal to shelf-edge trend (Sneh and Friedman, 1980). This process should also apply to stromatolites, which are elongated by wave attack (Logan et al., 1974). Mounds may have been brecciated during small-scale lowering of sea-level and subaerial dissolution.

Partially-Linked Columnar Stromatolites: This facies is present in the lower rim sequence, and abundant in the younger rim sequences. In the lower rim sequence dolomitic, partially-linked columnar stromatolites, 10 to 50 cm wide and 10 to 200 cm high with up to 30 cm of synoptic relief, occur as laterally continuous beds (Fig. 7b). Individual columns show high inheritance of successive laminae and are strongly elongate (Fig. 7c) subnormal to regional shelf-edge trend. Narrow (5 to 20 cm), steep "gutters" or rills between columns are filled with intraclast grainstone/packstone or edgewise conglomerate.

In the younger rim sequences, partially-linked columnar stromatolites form mounds 5 to 40 m wide and with up to 4 m of synoptic relief (Fig. 7d). Sides are steep and border narrow channels, 40 to 100 cm wide. Internal partially-linked columnar stromatolites (10 to 30 cm wide) are strongly elongate parallel to the elongation of mounds (subnormal to the regional shelf-edge trend).

Partially-linked columnar stromatolites formed part of the barrier reef complex, along with stromatolite mounds. Laterally continuous beds probably formed in water depths shallower than the stromatolite mounds. Bioherms of partially-linked columns probably were formed in water depths comparable to the stromatolite mounds. Subnormal (to shelf-edge trend) orientation of partially-linked columnar stromatolites reflects oblique wind/wave attack. Vertical alternation of large, stromatolite mounds and smaller, partially-linked columnar stromatolites may, if related to water depth, reflect intermittent shoaling of the reef complex.

Ooid/Intraclast Grainstone: This facies is poorly developed in the lower rim, but common in the younger rim sequences as lenses 10 to 50 m wide and 1 to 20 m thick. Laterally continuous sheet-like units of tabular-planar or trough cross-bedded (Fig. 8a) and planar-laminated ooid/intraclast grainstone are characteristic of the transition from reef to shoal-complex. Rare isolated stromatolites and small stromatolitic bioherms (less than 15 m wide and 3 m high) occur locally.

Sheets of ooid and intraclast grainstone are back-reef sands that formed behind the rim. Cross-bedded sands were deposited as bars or in channels, while planar laminated

Figure 8. Trough cross-bedded backreef grainstone (A), and neptunian dike (B). Note cross-cutting dike/mound relationship and well-developed fitted fabric. Same mound is shown in Fig. 7a, cross-cut by dike. Hammer for scale.

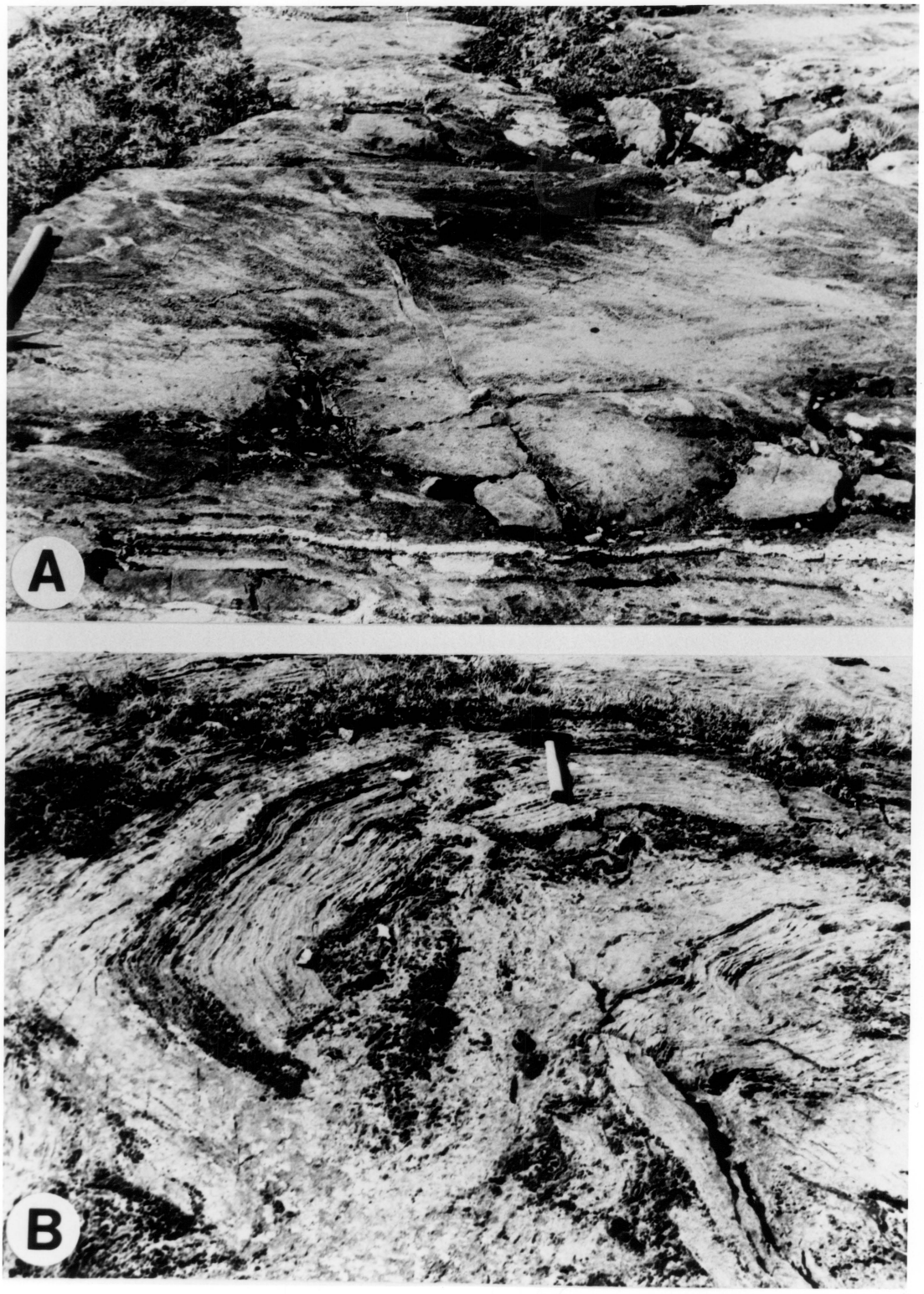
A
B

sands most likely formed in the swash zone along the western margin of the shoal complex. Scarcity of stromatolites in the sand facies probably reflects highly mobile substrates.

Mounded Edgewise Conglomerate: This facies is rare within the rim sequences. The conglomerates occur interbedded with beds of partially-linked columnar stromatolites, forming flat-bottomed, convex-upward lenses, 30 to 300 cm wide and 10 to 50 cm thick. They occur also as a transitional facies between the stromatolite reefs and overlying rhythmites that formed during drowning of the older rim. Intraclasts are platy (up to 10 cm long) fragments of stromatolites and commonly have a subvertical imbrication, which in plan view, form polygonal mosaics.

Mounded edgewise conglomerate beds probably formed on the reefal foreslope by wave action which eroded platy fragments of stromatolites and reworked them into polygonal mosaics with subvertical imbrication. Where developed as a transitional facies into drowned shelf rhythmites, they mantle reefal facies and were probably formed by wave reworking of early lithified rhythmites and uncommon platy stromatolite fragments.

Neptunian Dikes and Cavities, Lower Reefal Rim: Stromatolitic facies of the lower reefal rim are cut by neptunian dikes and sills (a few millimeters to 50 cm wide),

oriented at various angles to shelf-edge trend (Fig. 8b). Most dikes have matching walls suggesting development by fracturing of early cemented sediments (Fig. 6d). Some dikes extended to the seafloor as shown by synsedimentary erosion of host stromatolitic layering and dikes, followed by deposition of younger, discordant stromatolitic layering over irregular surfaces. Other filled voids in rim facies are large, irregular cavities (up to 50 cm wide) whose margins truncate internal layering in stromatolite mounds.

Dikes are filled with dolomitized-silicified marine cements and laminated sediment (Figs. 6c,d). First generation marine cements lining walls of dikes are dolomite and silica pseudomorphs after botryoidal, fibrous cement fans, up to 5 cm in radius. Botryoidal marine cements are overlain by bladed, isopachous marine cements or geopetal sediment fill. The cavities are first filled with dolomite and silica that replaces botryoidal, fibrous marine cements, followed by isopachous linings of bladed dolomite spar. Geopetal sediment fills are interlayered with the cement linings.

Abundant neptunian dikes in the reefal rim indicate early cementation and fracturing of the rim. First-generation cements lining dike walls are pseudomorphs after botryoidal, fibrous aragonite. Later generations of

isopachous, bladed marine cement suggest precursory hi-Mg(?) calcite. Large cavities with irregular and scalloped margins in the Rocknest Formation may have formed by subaerial dissolution. Dissolution was early because cavities are lined by dolomitized marine cements (originally aragonite and hi-Mg(?) calcite).

Evolution of Outer-Shelf

Rocknest outer-shelf facies formed a narrow, barrier reef complex (rim) and flanking back-reef sand belt (Fig. 9). The Rocknest rim is comparable to Phanerozoic rims, because it was a resistant barrier that grew in turbulent water and influenced adjacent environments. It allowed a major subaerial shoal-complex to develop behind the back-reef sand belt, which prevented free exchange between the high energy open ocean, and low energy "lagoon" to the east.

A conspicuous feature of the Rocknest barrier reef complex is the scarcity of clastic carbonate within the rim, which is dominated by stromatolite boundstone. In part, this attests to the very efficient process of trapping and binding by the microbial communities responsible for construction of the reefal rim. However, the Rocknest rim was wave-dominated, and absence of grainstone in the rim also must reflect transport of detritus away from the rim

Figure 9. Rocknest shelf paleogeography. Shown for progradational stage of development. Cyclic deposits form by limited westward and extensive eastward progradation of shoal-complex in response to oscillating sea-level (see Chapt. 2).

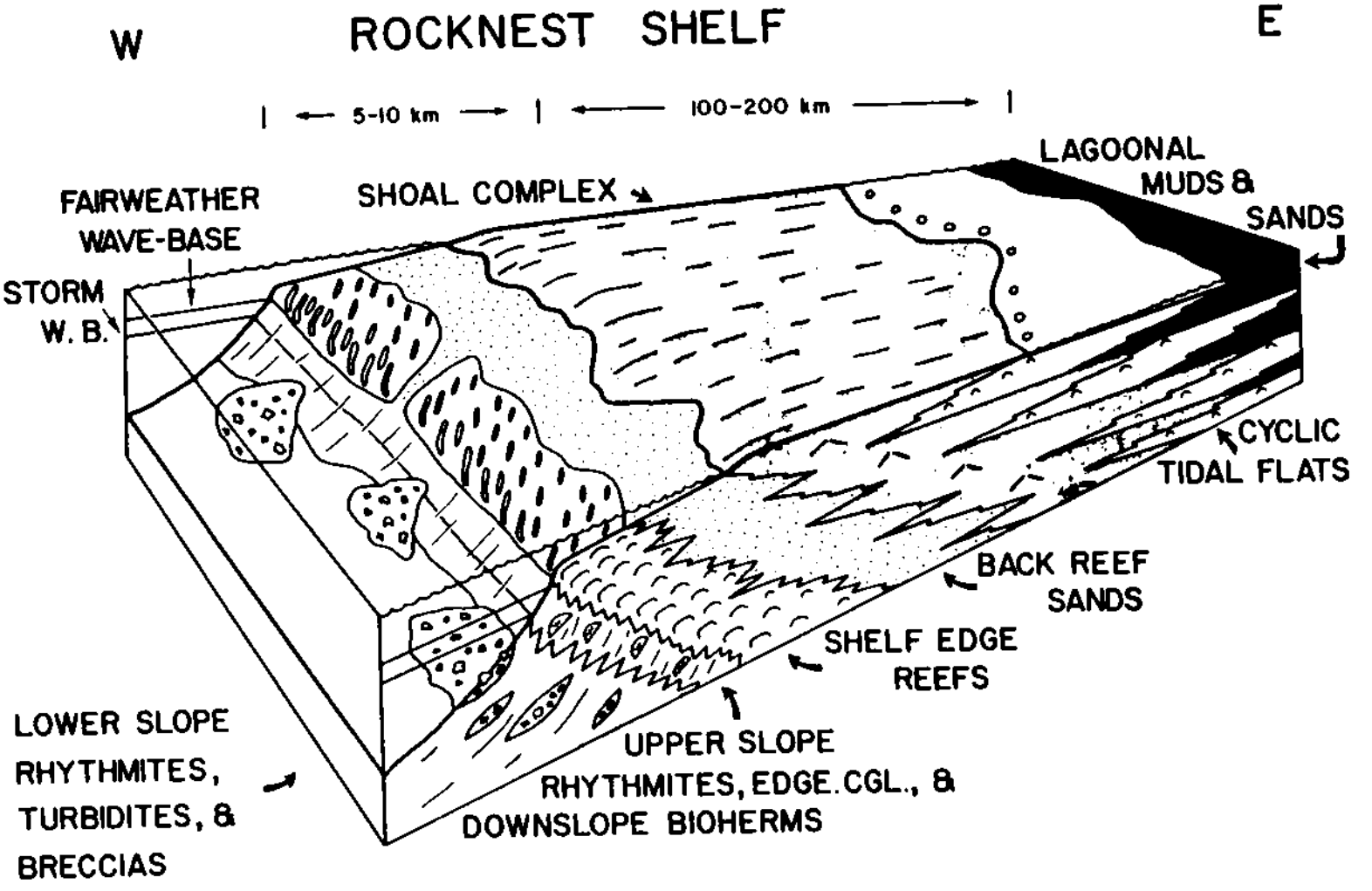
W
ROCKNEST SHELF
E
5-10 km
100-200 km
LAGOONAL MUDS & SANDS
FAIRWEATHER WAVE-BASE
SHOAL COMPLEX
STORM W. B.
CYCLIC TIDAL FLATS
BACK REEF SANDS
SHELF EDGE REEFS
LOWER SLOPE RHYTHMITES, TURBIDITES, & BRECCIAS
UPPER SLOPE RHYTHMITES, EDGE. CGL., & DOWNSLOPE BIOHERMS

and into the backreef sand belt by onshore-directed paleowinds.

As a wave-dominated, windward margin, the Rocknest rim is not entirely comparable to Phanerozoic windward margins which contain more clastic carbonate located in the reefal framework and in tidal channels between reefs (cf. Hine and Neumann, 1977; Mullins and Neumann, 1979). However, numerous grainstone-dominated tidal channels are developed in the reef-tract, in addition to much clastic carbonate within the reef framework. In the Phanerozoic, most clastic carbonate associated with reefs is produced by organisms that erode the frame by rasping, boring and grazing, supplemented by the post-mortem disintegration of segmented and non-segmented benthic organisms that grow in cavities and shelters formed by the larger skeletal metazoa (James, 1984b). Absence of clastic carbonate in the Rocknest reefal framework most likely can be attributed to lack of the organisms in the Precambrian. In the pre-Phanerozoic, ecologic reefs (cf. Dunham, 1970; Heckel, 1974) were formed dominantly by trapping and binding of loose sediment by non-calcareous cyanobacteria. Because of the absence of a porous skeletal frame and fine grain size of trapped sediment, the reefal "frame" was tight, with no place for non-bound clastic carbonate to accumulate, except between individual stromatolites, or breaks in the reef tract.

It is unlikely that clastic carbonate, trapped and bound to form stromatolites, was imported from adjacent environments because this would require uphill transport of slope sediment and/or upwind transport of backreef sediment; on the contrary, it is probable that the reef supplied sediment to both the slope and backreef, and by implication, any model of carbonate production in the rim must also account for the volume of slope and backreef sediment. Over the short term, microbial communities colonizing and building stromatolites probably trapped and bound loose sediment derived from erosion of other early cemented stromatolites within the reef. However, this process only moves carbonate back and forth between adjacent areas and does not provide a mechanism for net growth of the rim. Ultimately, the source of the carbonate must be inorganic precipitation (microbially mediated?) of cement in pores, and possibly as crusts on stromatolites. Inorganic precipitation within the surrounding water column is another possibility. Regardless of the exact mechanism, precipitation must have been prolific in order to provide the volume of sediment represented by the rim, backreef sand belt and slope wedge. Most likely, precipitation was strongly regulated by microbes which would have created favorable conditions for precipitation by extracting CO_2

from the water column during photosynthesis, raising the pH and lowering aragonite/calcite solubility. Early pervasive submarine cementation was important in development of the Rocknest reefal rim, similar to Phanerozoic reefs (cf. Playford, 1980; Hileman and Mazzullo, 1977; James et al., 1976).

ROCKNEST SLOPE

Rocknest slope facies are exposed along the flanks of syncline "M" (Fig. 1). Slope facies are flanked to the east by reefal boundstone, and pinch-out laterally to the west where foredeep deposits of the Recluse Group sit directly on those of the Odjick Formation.

Sections along the east limb of the syncline are 160 to 490 m thick, and consist exclusively of slope facies, or of outer-shelf facies overlain by slope facies, or of slope facies overlain by outer-shelf facies. Slope facies of the east limb are rhythmite, slump-folded rhythmite, megabreccia, and minor mounded edgewise conglomerate and downslope bioherms of conical stromatolites. Along the west limb of the syncline sections are thinner (70 to 230 m; Fig. 10) and consist exclusively of slope facies which include rhythmite and resedimented rhythmite breccia; slump-folded rhythmite and megabreccia are rare, and mounded edgewise

conglomerate and conical stromatolites are absent. In thrust sheets to the east of the syncline the Odjick Formation is directly overlain by Recluse Group foredeep sediments, with no intervening carbonate.

Lithofacies

Rhythmites: Rhythmites form units up to 50 m thick, and are best developed along the east limb of the syncline. They are buff to light gray (tan to brownish-orange on weathered surface), rhythmically interlaminated dololutite and dolosiltite, and gray-green shale (Fig. 11a). Dolosiltites are most common on the east limb; shales are most common on the west limb and near the contacts of the Rocknest Formation, transitional into the shales of the underlying Odjick Formation and overlying Recluse Group. Lamination is sub-millimeter to centimeter scale with dolosiltite composing the thickest laminae. Non-graded laminae are most common, but some laminae are normally graded. Shale forms partings between dolosiltite/lutite laminae.

Slump-folded rhythmite containing truncation surfaces (Fig. 11b) is common along the east limb. Slump folds are a few centimeters to several meters in scale and measurements of verging slump folds indicate east to west transport of allochthonous rhythmite masses.

Figure 10. Rocknest slope stratigraphy. Partial measured section along west limb of syncline "M". Sections along west limb are thin and consist mostly of rhythmite, rhythmite breccia and shale. Megabreccias are rare.

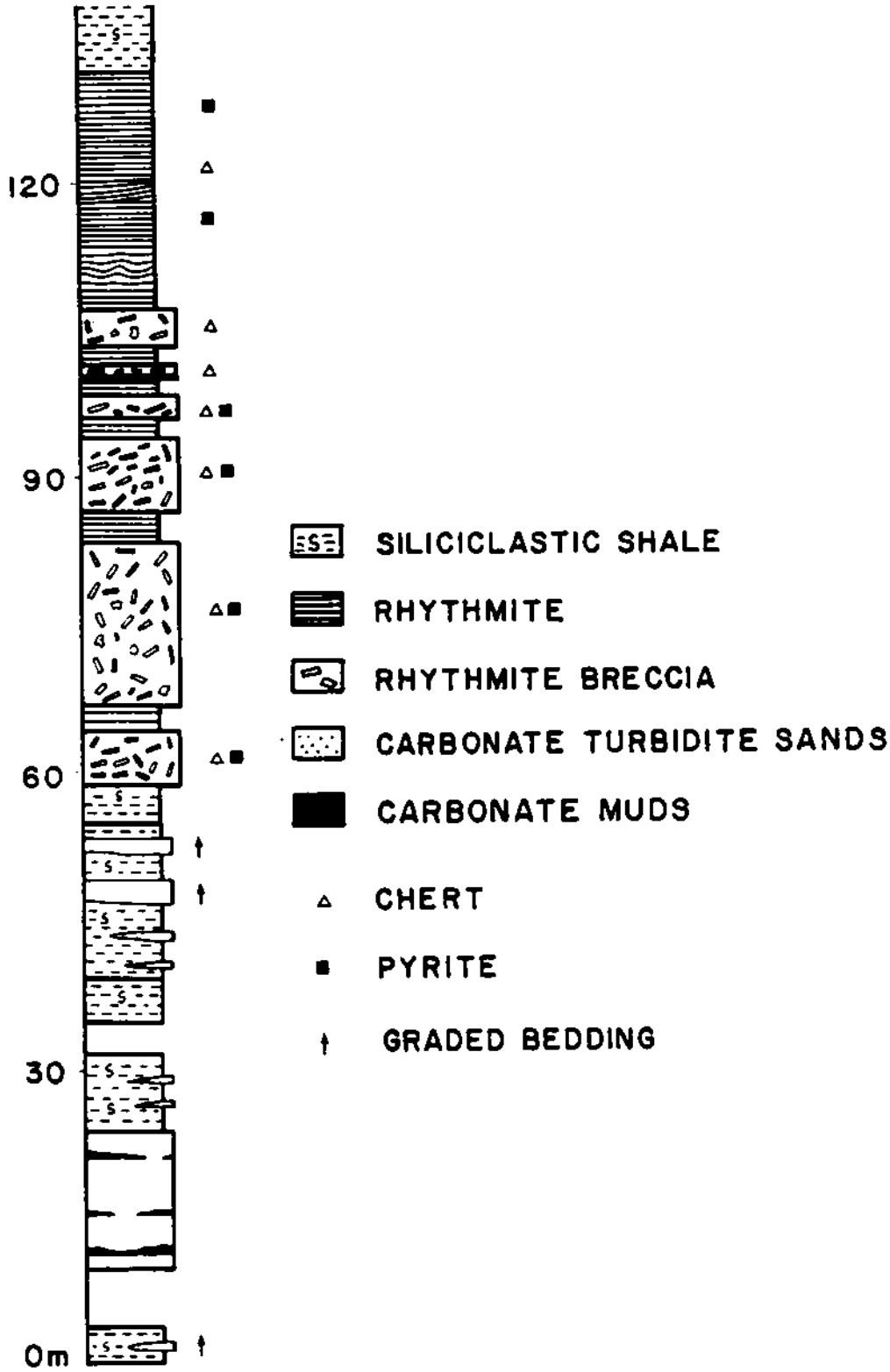
120
90
60
30
0m
SILICICLASTIC SHALE
RHYTHMITE
RHYTHMITE BRECCIA
CARBONATE TURBIDITE SANDS
CARBONATE MUDS
CHERT
PYRITE
GRADED BEDDING

Figure 11. Slope rhythmite facies. A) Rhythmite. Penknife for scale. B) Truncation surface (dashed line); note west-verging drag fold in beds underlying truncation surface. Hammer for scale. C) Edgewise conglomerate hosted in rhythmite. Scale in cm.

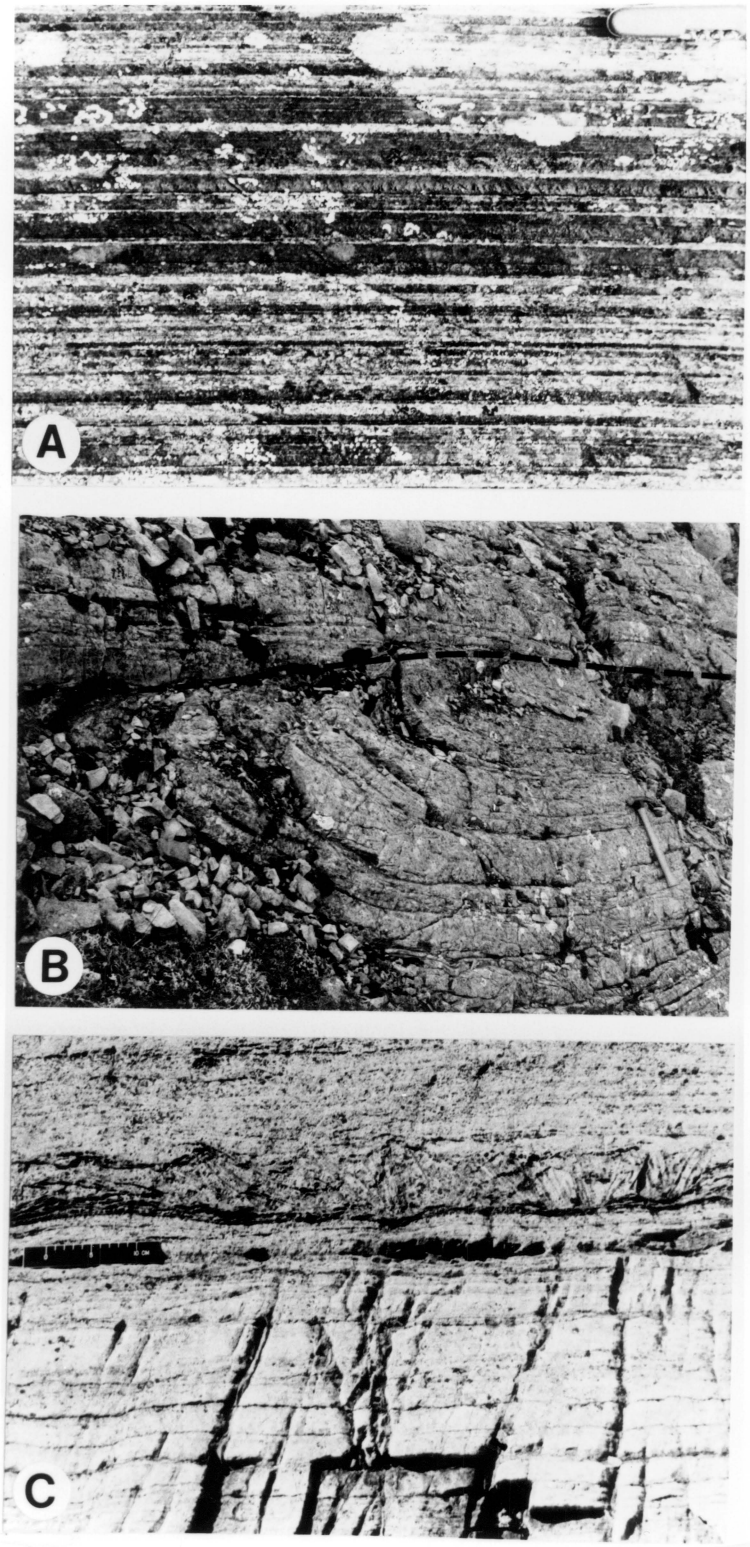
A
B
C

Rhythmites locally are cut by variously oriented sheet-cracks, filled with dolomitized marine cements, laminated sediment, and late, equant dolomite and quartz cements. Initial fillings are linings of bladed, isopachous marine cements, followed by final fillings of blocky dolomite spar and quartz. Geopetal sediment fills are locally present.

Sediments contain pods of massively recrystallized, coarse dolomite, 10 to 20 m thick and 50 to 100 m wide, hosted in fine-grained, well laminated rhythmite. Framboidal pyrite is ubiquitous. Rare gypsum casts are preserved in coarsely recrystallized rhythmite, and are closely related to early fractures which post-date depositional features but pre-date compactional stylolites. Casts are most abundant within and adjacent to the early fractures, decreasing outwards from the fractures. Casts are filled with coarse, dark (ferroan?) dolomite mosaics which contrasts with the lighter, finer-grained host dolomite.

Rhythmites are periplatform fine-grained carbonate (ooze), derived from the shelf margin. Grading suggests episodic influx of sediment, perhaps as distal turbidites produced during off-shelf transport of sediment during storms. The relatively thin sequences of rhythmite (10 to 50 m), compared to the overall thickness of the Rocknest

shelf (1100 m), indicate that off-shelf sediment transport was uncommon, and suggest the rim was a windward margin. Shaly intervals within rhythmites may be diastems, indicating non-deposition of carbonate sediment, during which time siliciclastic mud accumulated as hemipelagic sediment.

Slump-folding and truncation surfaces within rhythmites indicate upper-slope failure and initial down-slope transport of allochthonous rhythmite masses. Abundant early, framboidal and cubic pyrite in rhythmites indicates reducing conditions below the sediment-water interface. The relatively light color of some rhythmites (buff to light grayish green) reflects a low organic content in the sediment, suggesting that organics were destroyed by sulphate-reducing bacteria during pyrite formation; in order for sulphate to be a dominant dissolved species in interstitial fluids, the water column must have been oxidizing at depth for certain periods of time. Darker colored rhythmites may reflect increased organic production, or more reducing bottom waters which would have inhibited sulphate production, discouraged the activity of sulphate-reducing bacteria, and preserved more organic carbon.

First generation cements lining sheet-crack walls are marine, and their isopachous, bladed growth habit suggests

primary (hi-Mg?) calcite. Later, blocky dolomite and quartz cements were probably precipitated from hot, basinal brines during burial.

Pods of massively recrystallized dolomite in host rhythmites and rare gypsum casts associated with fractures and coarse dolomite probably reflect the up-dip migration of dolomitizing, sulphate-rich brines during deep burial diagenesis (cf. Magara, 1976; Moore and Druckman, 1981).

Mounded Edgewise Conglomerate: This facies is restricted to the eastern limb of the syncline. Deposits are flat-bottomed, mounded lenses of dolomitic edgewise intraclastic conglomerate, 30 to 300 cm wide and 10 to 30 cm thick, consisting of rhythmite fragments (Fig. 11c). Rhythmites associated with layers of edgewise conglomerate contain isolated wave-ripples.

Mounded edgewise conglomerates were formed in a reefal foreslope setting, below fairweather wave-base but above storm wave-base. During storms, wave-base was lowered and partially lithified rhythmite was eroded and reworked into imbricated mosaics by oscillatory shear currents. This is suggested by the imbricated, edgewise orientation of platy clasts and presence of wave ripples in enclosing rhythmites. Episodic, storm-related sedimentation is indicated by intercalation of these "high-energy" sediments in fine

grained rhythmites, deposited during fairweather sedimentation.

Conical Stromatolites: This facies is only developed along the eastern limb of the syncline and occurs as isolated or biohermal, dolomitic, cone-shaped columns (Fig. 12). Individual columns are 10 to 250 cm wide, and 10 to 200 cm high with up to 150 cm synoptic relief; they are often coalesced to form bioherms 1 to 40 m wide and up to 20 m thick. Smaller bioherms commonly are cored by one or two, large, central cones constructed of superimposed smaller cones that define large-scale synoptic profiles within bioherms. Axial zones, characteristic of Conophyton, are diffuse. In plan view, lamination within cones is concentric and either circular or eliptical. Eliptical forms are elongate subparallel to shelf-edge trend which is perpendicular to the elongation direction of domes and columns of the reefal rim and inner-shelf. Locally, bioherms are encrusted with layers of bladed, isopachous marine cement which may compose up to 50% of the bioherm. Cement layers are commonly replaced by quartz.

Isolated bioherms of conically-laminated stromatolites probably formed within the photic zone of the reefal foreslope. In the Rocknest Formation, the association of conically-laminated stromatolites with mounded edgewise

Figure 12. Slope bioherm facies. A) Bioherms overlying flat rhythmite and small conical stromatolites. Staff is 1.5 m long. B) Margin of bioherm showing onlapping of rhythmite. Scale in cm.

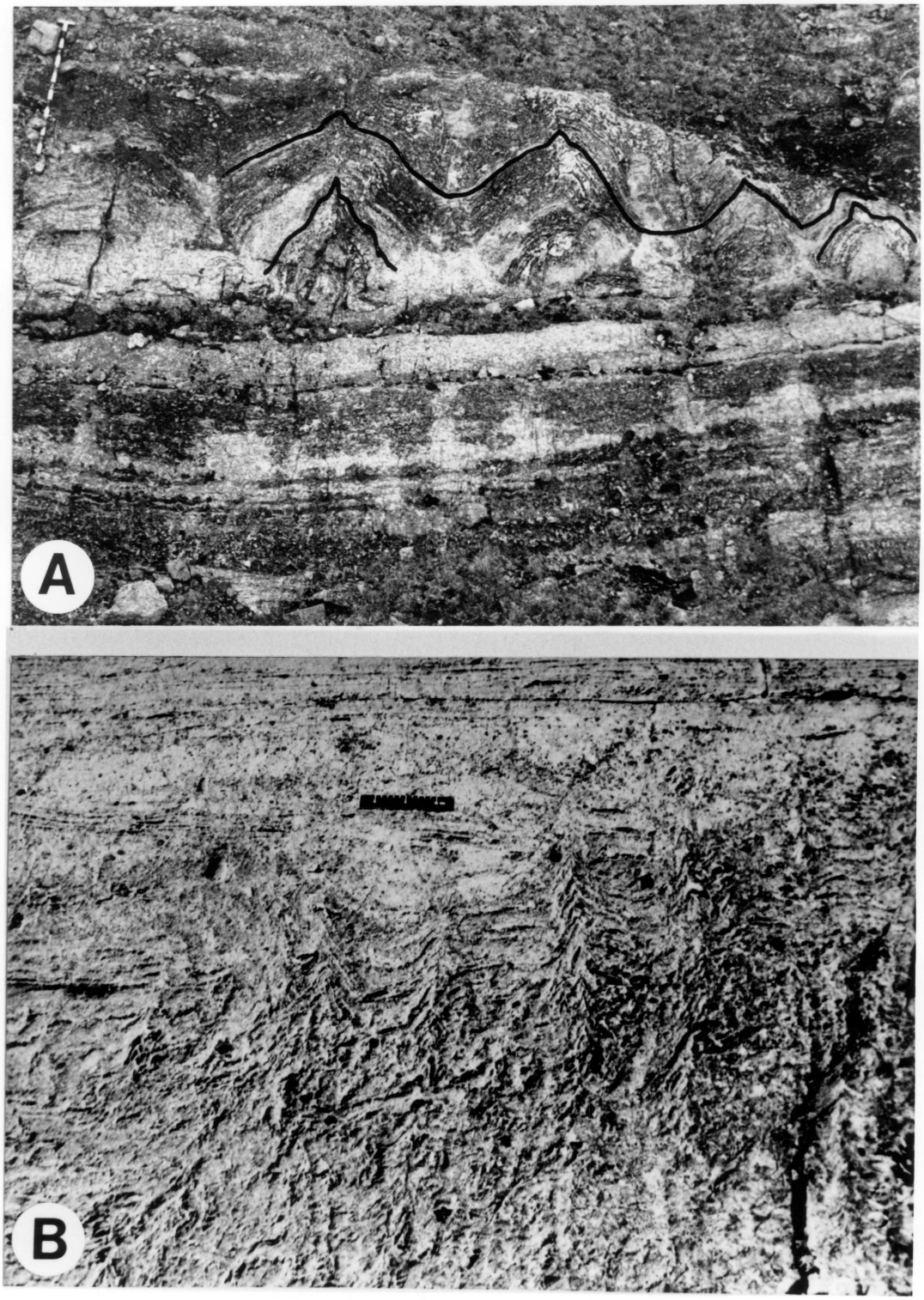
A
B

conglomerate and wave rippled rhythmite indicates deposition above storm wave-base. The weak elongation of cones subparallel to shelf-edge trend may have been produced by contour currents moving parallel to the shelf margin. Cones were unaffected by sustained, wave-produced oscillatory shear currents that caused elongation of other stromatolites on the Rocknest shelf, indicating that they formed below fairweather wave-base.

Similar buildups of conically laminated stromatolites have been documented from Proterozoic deep water carbonates of the Dismal Lakes Group (Donaldson, 1976; Kerans, 1982) and Pethei Group (Hoffman, 1974). Conically laminated stromatolites are also developed in subtidal lagoonal sediments of the Rocknest inner-shelf (Hoffman, 1975) and in subtidal lagoonal sediments of the McArthur Basin (Jackson, 1982). It seems likely that growth of large buildups of conically-laminated stromatolites in the Proterozoic occurred only in subtidal settings, as suggested by Donaldson (1976).

Kerans (1982) noted that some laminae within buildups of conical stromatolites in the Dismal Lakes Group have neomorphic fabrics, suggesting that bladed cement crusts were precipitated on microbial laminae while stromatolites were growing. Hoffman (1974) suggested that deep-water,

poorly laminated conical stromatolites of the Pethei Group must have been precipitated in situ (see Hoffman, 1974, figs. 10, 11; James, 1983, fig. 72). Thus, precipitation of cement crusts to form conical stromatolites was probably microbially mediated. Rocknest stromatolites probably were formed by photosynthetic microbes because buildups are restricted to the eastern limb of the syncline, in shallow-water settings between storm and fairweather wave-base. Conical stromatolites of the Dismal Lakes Group probably also grew within the photic zone, just below wave-base. However, those of the Pethei Group formed in a deep basinal setting, which may have been sub-photic.

Layers of encrusting, bladed marine cement were probably (hi-Mg?) calcite, and record early cementation of bioherms. This cementation may have been related to microbial photosynthesis, which would have taken CO_2 from seawater, raised the pH, and induced calcite precipitation.

Megabreccias: This facies is most abundant along the eastern limb of the syncline. Individual sequences are 2 to 75 m thick and associated with interbedded rhythmite and slump-folded rhythmite. Contacts with enclosing facies are poorly exposed; upper contacts are irregular to slightly hummocky and lower contacts are parallel to the underlying beds.

Internally, most megabreccia beds are massive and lack textural changes from base to top. Inter-clast matrix consists of fine-grained breccia and highly contorted rhythmite. Individual blocks average 1 to 10 m and are up to 150 m (Fig. 13a). Blocks are angular, those smaller than 10 m tending to be oblong to equant, whereas larger blocks are elongate or tabular. Block composition is varied (polymictic), and dominated by shelf-edge boundstone and minor grainstone. In some deposits, small (less than 50 cm) blocks of dolomitized marine cement are common; in others, blocks of rhythmite are important (Fig. 13b).

Megabreccias are restricted to the upper parts of slope sequences, reflecting progradation and upbuilding of the rim when a near vertical escarpment may have developed. Gravitational instability of the early-cemented rim led to fracturing (evidenced by neptunian dikes) and spalling of large blocks which were transported downslope as rock-fall or in debris flows. Megabreccias of reefal origin were deposited as periplatform detritus at the foot of an escarpment, and fine outward in a few kilometers. Downslope, only breccias of resedimented slope rhythmite accumulated.

Rhythmite Breccias: This facies is best developed along the western limb of the syncline. Breccia beds are

Figure 13. Slope breccia facies. A) Megabreccia block (B), east limb of syncline "M". Statigraphic facing (arrow) of host sediments ("H") is from top left to bottom right; in block, from center to center right. Block consists of reefal boundstone and is hosted in rhythmite, rhythmite breccia and finer-grained megabreccia deposits. B) Finer-grained megabreccia consisting dominantly of rhythmite blocks. Brunton for scale. C) Platy, imbricated rhythmite breccia overlying undisturbed rhythmite. Hammer for scale.

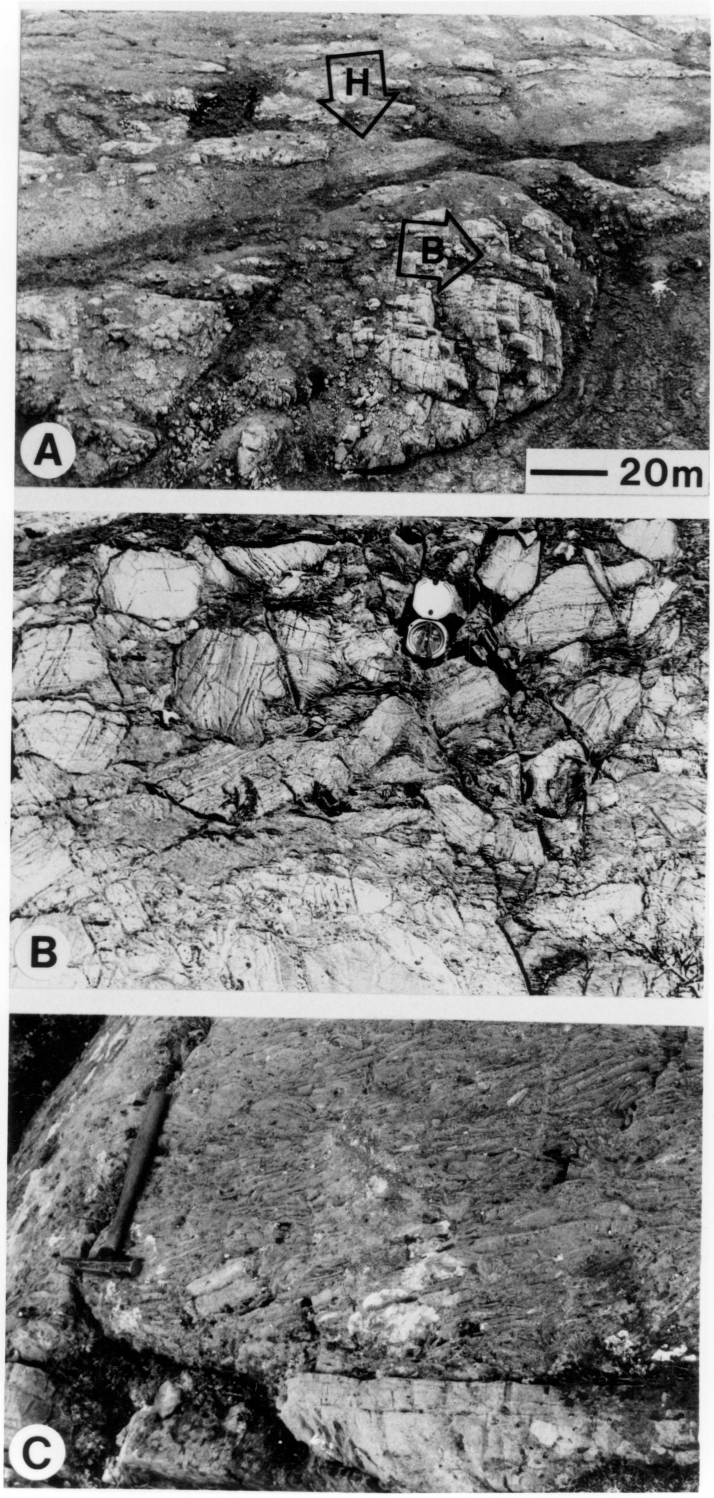
H
B
A
20m
B
C

0.5 to 10 m thick and laterally extensive, with sharp, scoured basal contacts (Fig. 13c). Breccia beds rest on undisturbed rhythmite, or on other breccia beds to form amalgamated sequences. Clasts are subrounded fragments to angular shingles (1 to 50 cm in length) composed of rhythmite lithologies, with rare clasts of shelf-edge boundstone or grainstone.

Clasts form chaotic arrays (commonly matrix supported) or are organized into imbricated and/or graded sequences (commonly clast supported). Grading commonly is normal, and imbricated clasts dip upslope. Most breccia beds are capped by a turbidite which consists of fine-grained, comminuted breccia material. The more complete turbidites contain massive grainstone/packstone bases, followed by planar-laminated and cross-laminated grainstone/packstone, climbing ripple laminated dolosiltite, and are overlain by rhythmite. Breccia beds and associated turbidites contain abundant cubic and framboidal pyrite, pyrite associated with late tectonic fractures. Sediments also are extensively silicified.

Rhythmite breccias reflect slumping of upslope rhythmite masses, transportation as debris flows, and resedimentation farther downslope as breccia deposits. The platy, angular clasts indicate partial early lithification

of rhythmites before slumping. Upslope dip of clast imbrication at the base of debris flow deposits reflects internal shear and clast rotation during movement (cf. Cook and Mullins, 1983). Turbidites that cap rhythmite breccias formed from the overlying, more turbulent part of debris flows (cf. Krause and Oldershaw, 1979).

Evolution of Slope

Mounded edgewise conglomerate, and bioherms of conically-laminated stromatolites are restricted to the east limb of the syncline, in thick sections overlain by offlapping outer-shelf deposits, or rare megabreccia deposits. Along with rhythmites, they are forereef sediments deposited during the initial, progradational stage of the shelf.

Thin sections along the east limb lack mounded edgewise conglomerate and bioherms, but contain abundant megabreccias and slump-folded rhythmite, reflecting deposition further downslope. This lithotope was below storm wave-base, and probably below the photic zone.

Sections along the west side of the syncline (farther down paleoslope) are much thinner, and contain abundant rhythmite breccias, but lack megabreccias. They were deposited in very deep water, close to 1100 m below sea-level at the time of terminal shelf drowning.

Sediment starvation of the slope is indicated by rapid westward thinning of slope facies, probably a result of dominantly on-shelf transport of clastic carbonate due to prevailing onshore-directed winds. Also, backstepping of the rim formed numerous perched ledges which probably trapped allodapic sediments derived from younger rims, preventing their transport down to the main slope leading to the ocean floor.

Average inclinations of the main depositional slope have been calculated by Grotzinger and Hoffman (1983). At the southern end of the syncline, the Rocknest Formation comprises 230 m of slope deposits on the west limb and 660 m of shelf deposits (lowermost rim) on the east limb. The difference in the decompacted thickness of the overlying Recluse Group on both sides of the syncline, as measured from the top of the Rocknest Formation to a marker bed in the Recluse, is 590 m which represents the total bathymetric relief up to the top of the lowermost rim (Fig. 14). However, the difference in thickness of the Rocknest Formation, 430 m, is less than the total paleobathymetric relief which indicates that most, but not all of the total paleobathymetric relief was produced by constructional aggradation of the outer-shelf. The remaining 160 m of relief was inherited from an antecedent slope at the top of

the Odjick Formation and therefore represents the initial relief of the Rocknest slope.

Average inclinations of the Rocknest slope can be calculated given the palinspastic distance between sections (approximately 4500 m). The initial average inclination of the slope is 2 degrees, and the final average inclination of the slope is 7 degrees (Fig. 4b). This data, in addition to facies distributions in the outer-shelf, suggest a depositional model for the Rocknest outer-shelf and slope involving an initial ramp developed on low-gradient topography inherited from the underlying Odjick clastic shelf. A prograding accretionary reefal rim was quickly established and prevailing wind patterns caused sediment starvation of the slope which resulted in slope steepening, leading to development of a near vertical escarpment. By-passing of the steepened slope is indicated by deposition of megabreccias at the top of some sections along the east limb of the syncline. During development of the lowermost rim (Fig. 4), off-shelf sediments were deposited on the main continental slope, covering siliciclastic slope facies of the Odjick Formation. However, following drowning of the lowermost rim, most off-shelf sediments produced during growth of overlying rims (Fig. 4) were probably trapped on perched ledges (drowned rims), and sedimentation on the main continental slope was greatly reduced.

Figure 14. Paleobathymetric relationships, lowermost rim sequence. Values for paleobathymetric relief were converted to average slopes (cf. Fig.4) by unfolding the syncline, utilizing surface dips and down-plunge projections to determine the original horizontal distance between measured sections. Thickness values for Recluse Group are decompacted.

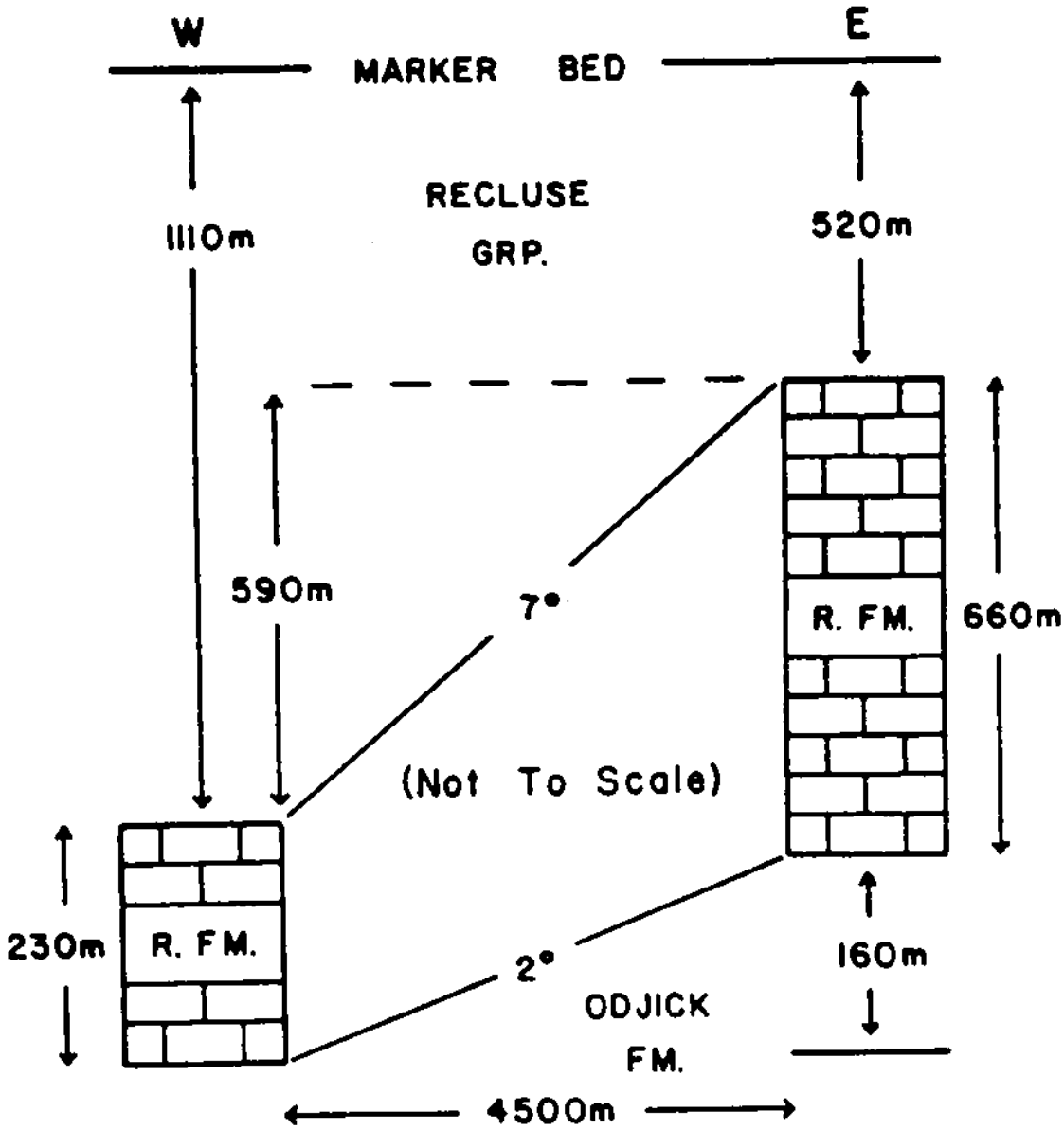
W
MARKER BED
E
1110m
RECLUSE
GRP.
520m
590m
7°
R. FM.
660m
(Not To Scale)
230m
R. FM.
2°
160m
ODJICK
FM.
4500m

At the time of terminal drowning of the entire shelf, the profile of the shelf-margin was nearly vertical, punctuated by several ledges formed during earlier, local drowning of the rim (Figs. 3,4). The outer-shelf had a total thickness of 1100 m, and was flanked by a wedge of slope sediments that thinned from 490 m near its contact with the margin to 230 m, 4500 m to the west. This indicates that the margin had a final relief of 610 m above the most proximal part of the main slope wedge, and 1030 m of relief above the slope wedge, 4500 m to the west.

ROCKNEST SHOAL-COMPLEX

Rocknest shoal-complex facies are exposed along the east limb of syncline "M", and in the first three thrust sheets to the east (Fig. 1). They pass westward into outer-shelf backreef grainstone and reefal boundstone, and eastward into cyclic inner-shelf facies (Figs. 3,4). Shoal-complex facies are described and interpreted in detail in chapter 2. Brief descriptions and interpretations are provided here.

Shoal-complex facies of the lowermost rim sequence occur in a narrow belt, 1 to 5 km wide. Facies are cryptalgalaminite, tufa, and laminated dolosiltite/lutite; these may be deformed into tepees or breccias and contain

pisolite (Fig. 15). Sediments are arranged cyclically, so that undeformed cryptalgalaminite, tufa and laminated dolosiltite/lutite are overlain by syndepositionally deformed equivalents, developed as tepees and breccias with associated pisolite (Fig. 16). Tepee and breccia deposits forming cycle caps are truncated by planar to irregular erosion surfaces and abruptly overlain by undeformed cryptalgalaminite, tufa and dolosiltite/lutite of the succeeding cycle base.

Laminated dolosiltite/lutite, cryptalgalaminite and tufa alternating with sequences containing tepees, breccias and pisolite indicates deposition in the upper intertidal to supratidal zone. Cyclical sequences in the shoal-complex reflect minor oscillations in sea-level. Initially, upper intertidal to supratidal sedimentation occurred during rises in sea-level, transgression of the eastern "lagoon", and very shallow submergence of the shoal-complex. During subsequent falls in sea-level the eastern margin of the shoal-complex prograded away from the rim (up to 200 km), forming the upper intertidal to supratidal caps of inner-shelf cycles. As sea-level fell below the sediment surface, earlier formed sediments of the western shoal-complex were exposed in the vadose zone, and tepees, breccia and pisolite developed as soils.

Figure 15. Shoal-complex stratigraphy. Section is located one thrust east of syncline "M". Shoal-complex facies overlie backreef grainstone and reefal boundstone as part of a long-term progradational sequence. Note thickness of cycles (aug. 10 m), which are defined by alternations of bedded lithologies and brecciated equivalents.

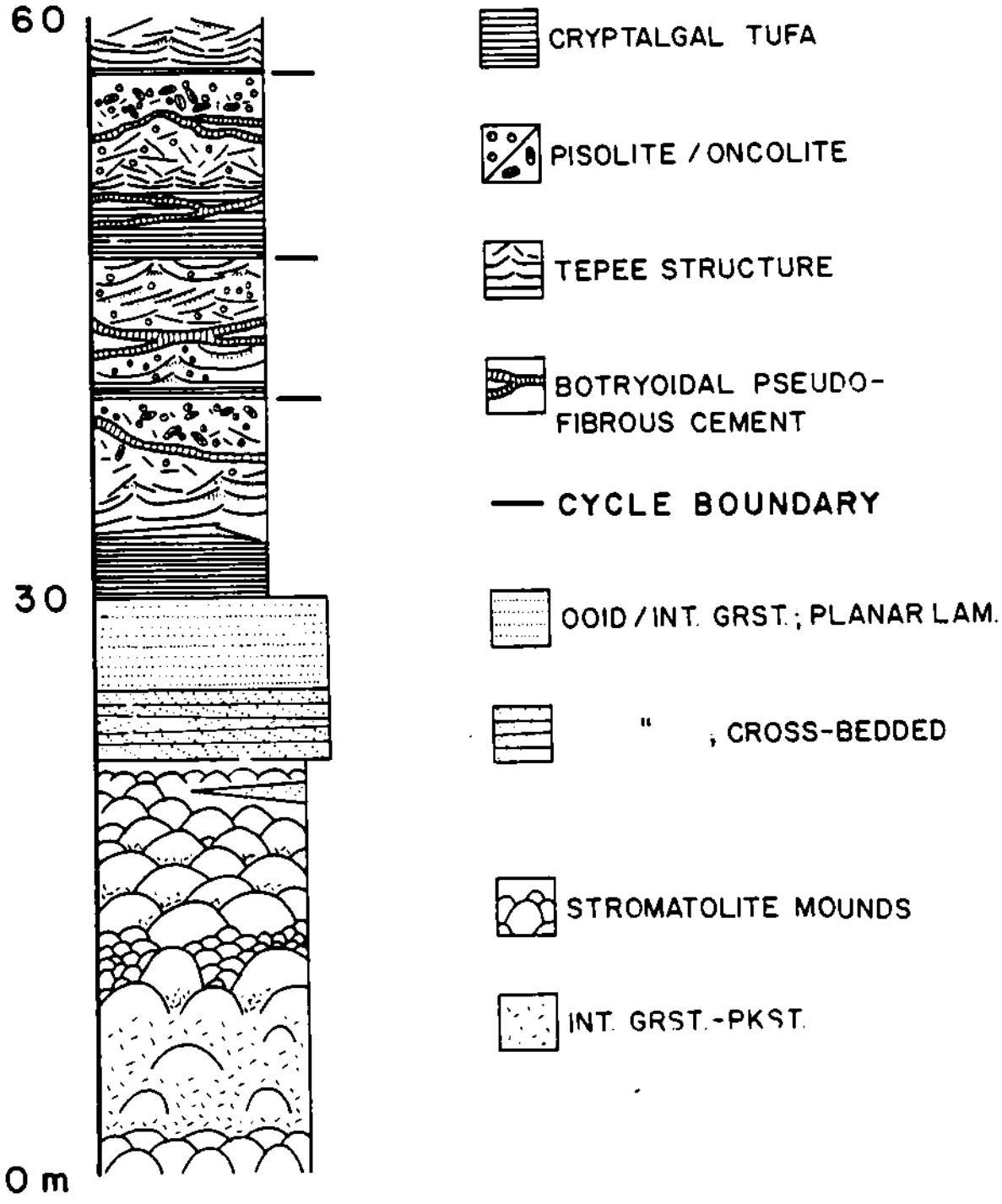
60
30
0 m
CRYPTALGAL TUFA
PISOLITE / ONCOLITE
TEPEE STRUCTURE
BOTRYOIDAL PSEUDO-
FIBROUS CEMENT
CYCLE BOUNDARY
OOID / INT. GRST.; PLANAR LAM.
" ; CROSS-BEDDED
STROMATOLITE MOUNDS
INT. GRST.-PKST.

Figure 16. Shoal-complex facies. A) Cycle composed of partially silicified tufa with minor cryptalgalamite and laminated dolosiltite/lutite, overlain by brecciated equivalents, probably formed during lowering of sea-level and exposure in vadose zone. Hammer for scale in upper left corner. B) Cryptalgalaminite with halite casts (c). C) Colloform tufa, draped by dololutite. Note small tepee near bottom right.

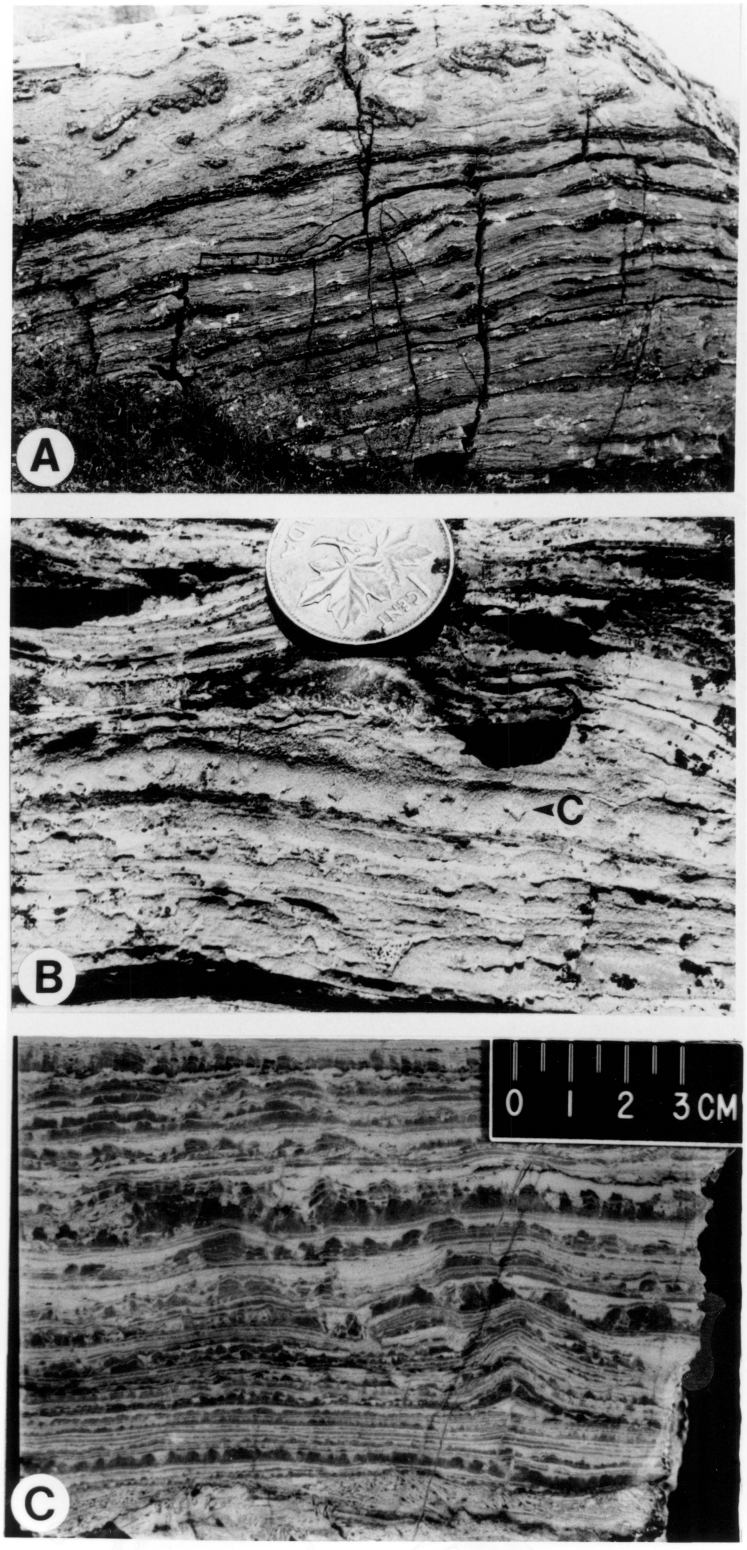
A
B
C
0 1 2 3 CM
C

Submergence of the shoal-complex during subsequent cyclical transgressions was seldom greater than upper intertidal to supratidal depths. Thus the proximal shoal-complex was a permanent, linear barrier of variable width that often was subaerially exposed, isolating the inner shelf lagoon from the open ocean. Such a paleogeographic configuration is very similar to that proposed for Phanerozoic tepee/pisolite complexes (cf. Dunham, 1972; Assereto and Kendall, 1977; Aitken, 1978).

After drowning of the lowermost reefal rim, the shoal-complex subsequently was reestablished as a paleotopographic high behind the younger rims of the upper Rocknest Formation, but was only exposed during the most aggraded phase of each shoaling-upward cycle. During each cyclic transgression it was submerged to intertidal or subtidal depths, followed by aggradation to sea-level and final subaerial exposure during lowering of sea-level.

ROCKNEST INNER SHELF

Rocknest inner-shelf facies are exposed in central and eastern thrust sheets and autochthon of Wopmay orogen, and Peacock Hills area of Kilohigok Basin (Figs. 1,3). Inner-shelf facies pass westward into shoal-complex facies (Fig. 3), and eastward into siliciclastic shale, siltstone and

sandstone of the Goulburn Group (Kilohigok Basin; Campbell and Cecile, 1981; Hoffman et al, 1984). Inner-shelf facies are dominantly asymmetric, shallowing-upward cycles of subtidal to supratidal argillaceous dololutite and cryptalgal dolomite (Figs. 17,18). Individual cycles can be correlated for over 200 km parallel to depositional strike and over 100 km perpendiclar to strike (see chapter 2).

The cyclic sequence contains three non-cyclic intervals which represent incipient drowning of the shelf. The lower and middle non-cyclic intervals consist of stromatolitic boundstone, intraclast/ooid grainstone, and cherty dolosiltite; they form eastward-tapering wedges that pass laterally into cyclic deposits (Fig. 3). The upper non-cyclic interval consists of argillaceous dololutite with intercalated intraclast/ooid packstone-wackestone, and forms a westward-tapering wedge that passes laterally into cyclic deposits (Fig. 3).

Inner-shelf facies are described and interpreted at length in chapter 2. Brief descriptions and interpretations are provided here.

Figure 17. Cyclic inner-shelf stratigraphy. See appendix or figure 30 for key to symbols. Note asymmetry of facies in most cycles, and average cycle thickness (5 m). Interval shown is "thrombolitic" member of Grotzinger and Hoffman (1983). Section is from locality "B", figure 1.

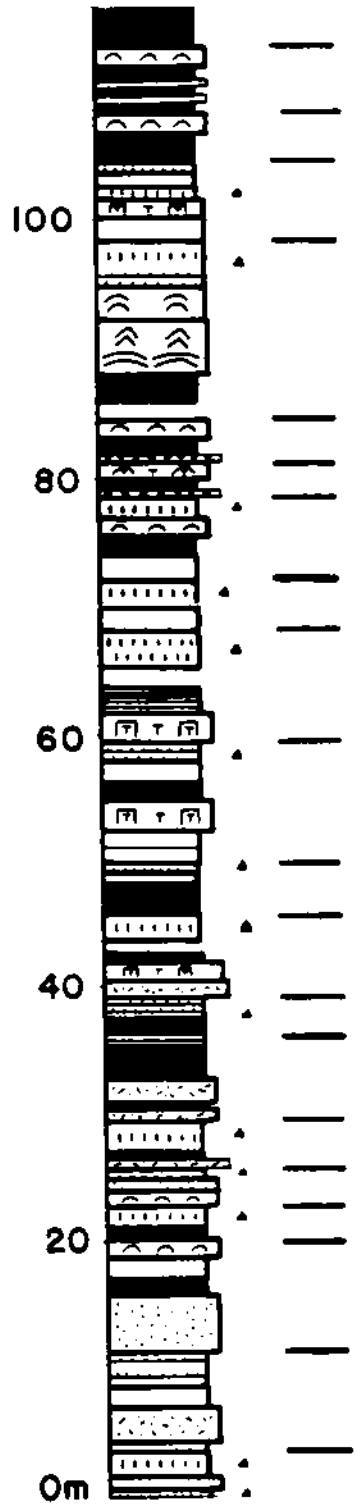
100
80
60
40
20
0m

Figure 18. Inner-shelf "grand cycles" and cycles. A) Aerial view of several Rocknest members, locality "B" of figure 1 (D, Domal Stromatolite member; R, Red Shale member; T, Thin member; S, Striped member; TP, Top member; members discussed further in Grotzinger and Hoffman, 1983). The Red Shale member grades up into Thin member, comprising one "grand cycle", and the Striped member grades up into Top member, comprising another "grand cycle" (cf. figure 25). About 250 meters of section are shown. B) Same members (background), spotlighting "striped member" (foreground), about 20 km (palinspastic) east of "locality B" (Fig. 1). C) Details of small-scale cycles in Striped member. Shales (dark) grade up into dolosiltites (light), then into stromatolitic dolomite, and then into tufa or cryptalgalaminite. Arrows point to cycle boundaries. Staff is 1.5 m long.

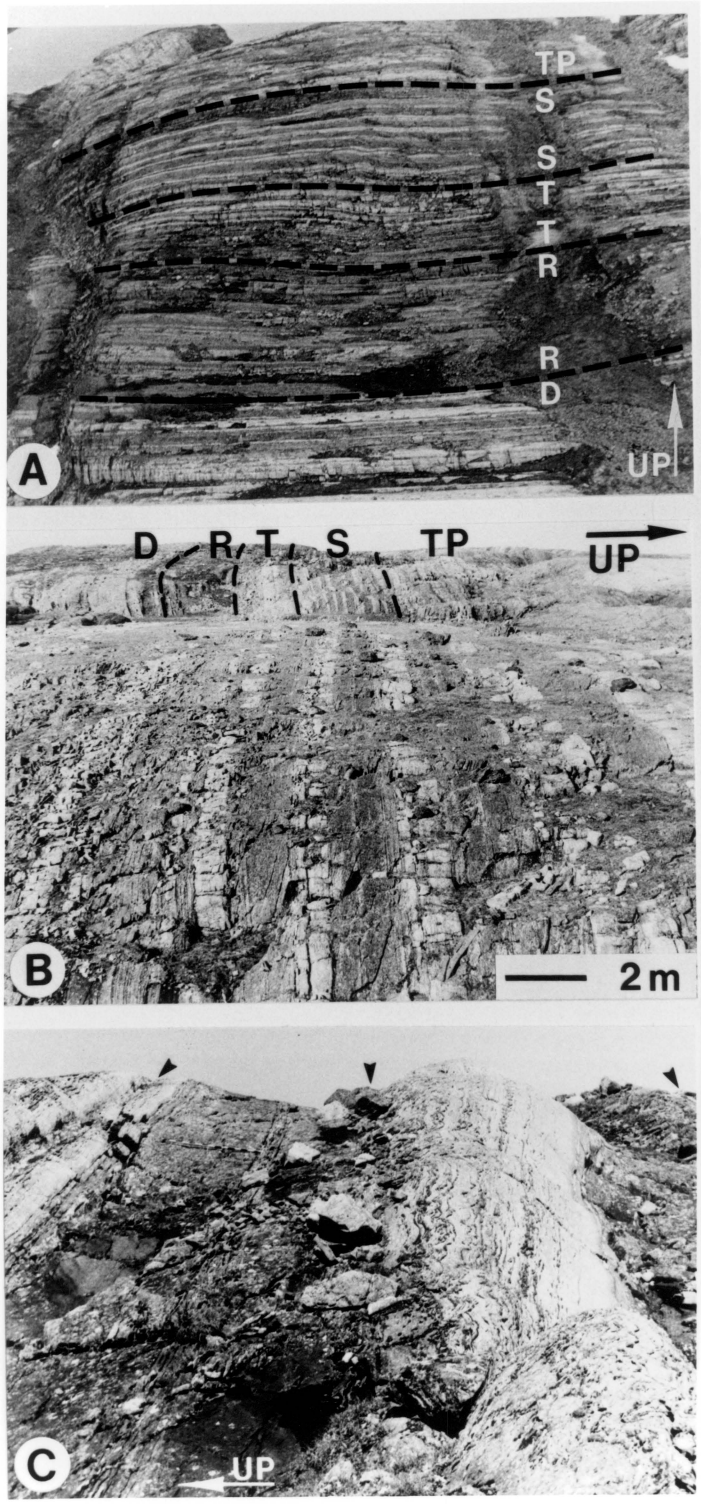
TP
S
S
T
T
R
R
D
UP
A
D
R
T
S
TP
UP
B
2m
C
UP

Cyclic Lithofacies

Cycles have been subdivided (Fig. 19) into four groups based on the dominant cycle base lithology. Shale-based cycles contain argillaceous dololutite or siliciclastic siltstone/sandstone at their bases. Dolosiltite-based cycles lack siliciclastic detritus and contain either thick-laminated dolosiltite or less commonly, stromatolitic/thrombolitic dolomite at their bases. Tufa-based cycles contain only shoal-complex lithologies. Grainstone-based cycles have ooid-intraclast grainstone at their bases.

Cycle type is a function of paleogeographic position. Below the lower non-cyclic interval, shale-based cycles pass westward into dolosiltite-based cycles, then into tufa-based cycles of the shoal-complex, and then into grainstone-based cycles (Figs. 3,4). In contrast, above the lower non-cyclic interval, tufa-based cycles are absent and shale-based cycles pass westward into dolosiltite-based cycles and then directly into grainstone-based cycles backreef and reef facies of the outer-shelf.

Shale-based cycles of the inner-shelf have the greatest diversity of facies and contain from base to top: 1) intraclast packstone (Fig. 20a), 2) siliciclastic siltstone/sandstone and argillaceous dololutite (Fig. 20b),

Figure 19. Rocknest cycle types. See text for description. Average cycle thicknesses range from 10 m where subsidence is highest (grainstone-based, tufa-based) to 5 m where subsidence is lowest (shale-based).

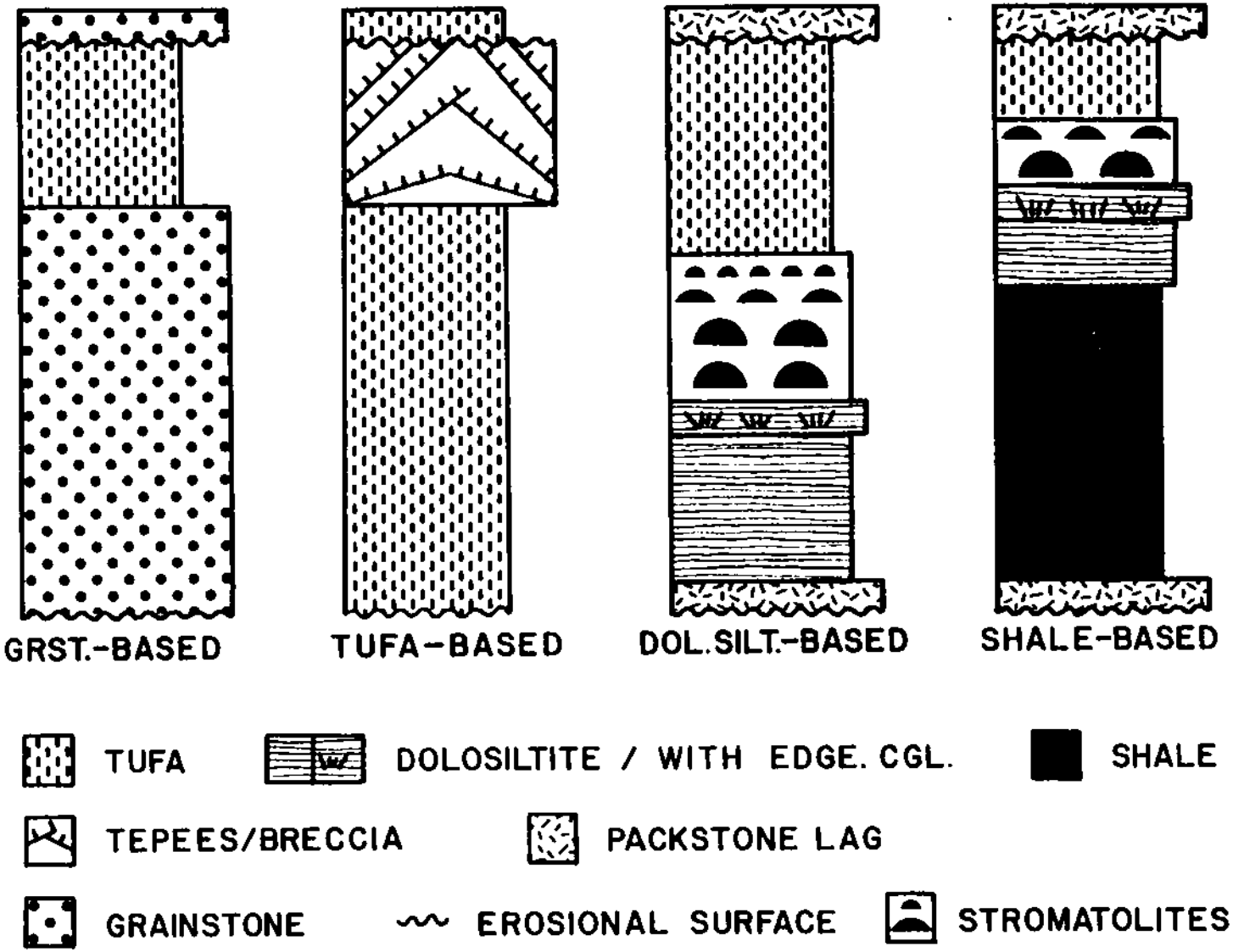
GRST.-BASED
TUFA-BASED
DOL.SILT.-BASED
SHALE-BASED
TUFA
DOLOSILTITE / WITH EDGE. CGL.
SHALE
TEPEES/BRECCIA
PACKSTONE LAG
GRAINSTONE
EROSIONAL SURFACE
STROMATOLITES

3) thick-laminated dolosiltite (Fig. 21), 4) stromatolitic/thrombolitic dolomite (Fig. 22a-c), and 5) laminated to microdigitate tufa (Fig. 22d). Abundance of specific facies depends mostly on proximity to the western margin of the shoal-complex and on amplitude of sea-level oscillation during cycle development (see chapter 2). Component facies are stacked vertically, in predictable sequences, and each cycle usually is bounded by erosional surfaces which become less pronounced away from the shoal-complex.

Evolution of Cyclic Inner-Shelf

Cycles were initiated by rapid transgression and flooding of carbonate tidal flats flanking the eastern margin of the shoal-complex, followed by eastward expansion of the shoal-complex and slow progradation of tidal flats over "lagoonal" facies of the inner-shelf. At the end of each progradation event the shoal-complex had a maximum width of over 200 km, which shrank following each transgression to a minimum width of 1 to 5 km for the shoal-complex behind the older rim. This contrasts with the shoal-complex behind each of the younger rims, which became completely submerged following each cyclical transgression.

Figure 20. Lower facies of shale-based cycles. A) Intraclast packstone lag overlying brecciated cycle cap. Penknife for scale. B) Mixed siliclastic mud (dark) and carbonate mud (light), cut by synaeresis cracks. Pen for scale in upper left. C) Shale-based cycle showing planar laminated (P) and hummocky cross-stratified (H) dolarenite, probably deposited during storms (CB, cycle boundary). Hammer for scale.

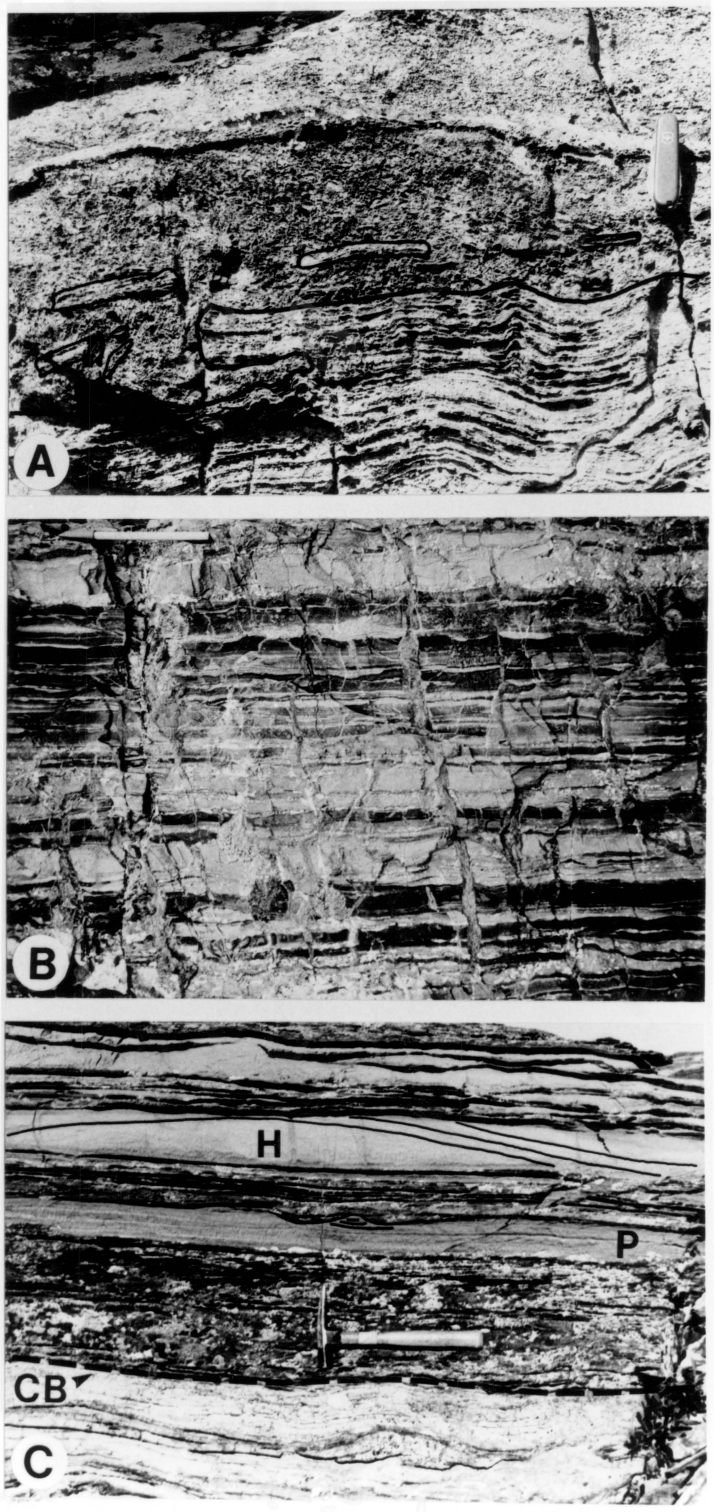
A
B
H
P
CB
C

Figure 21. Dolosiltite and edgewise congolmerate. A) Thick-laminated dolosiltite overlain by thin bed of edgewise conglomerate and stromatolitic layering. B) Edgewise conglomerate interbedded with thick laminae of dolosiltite.

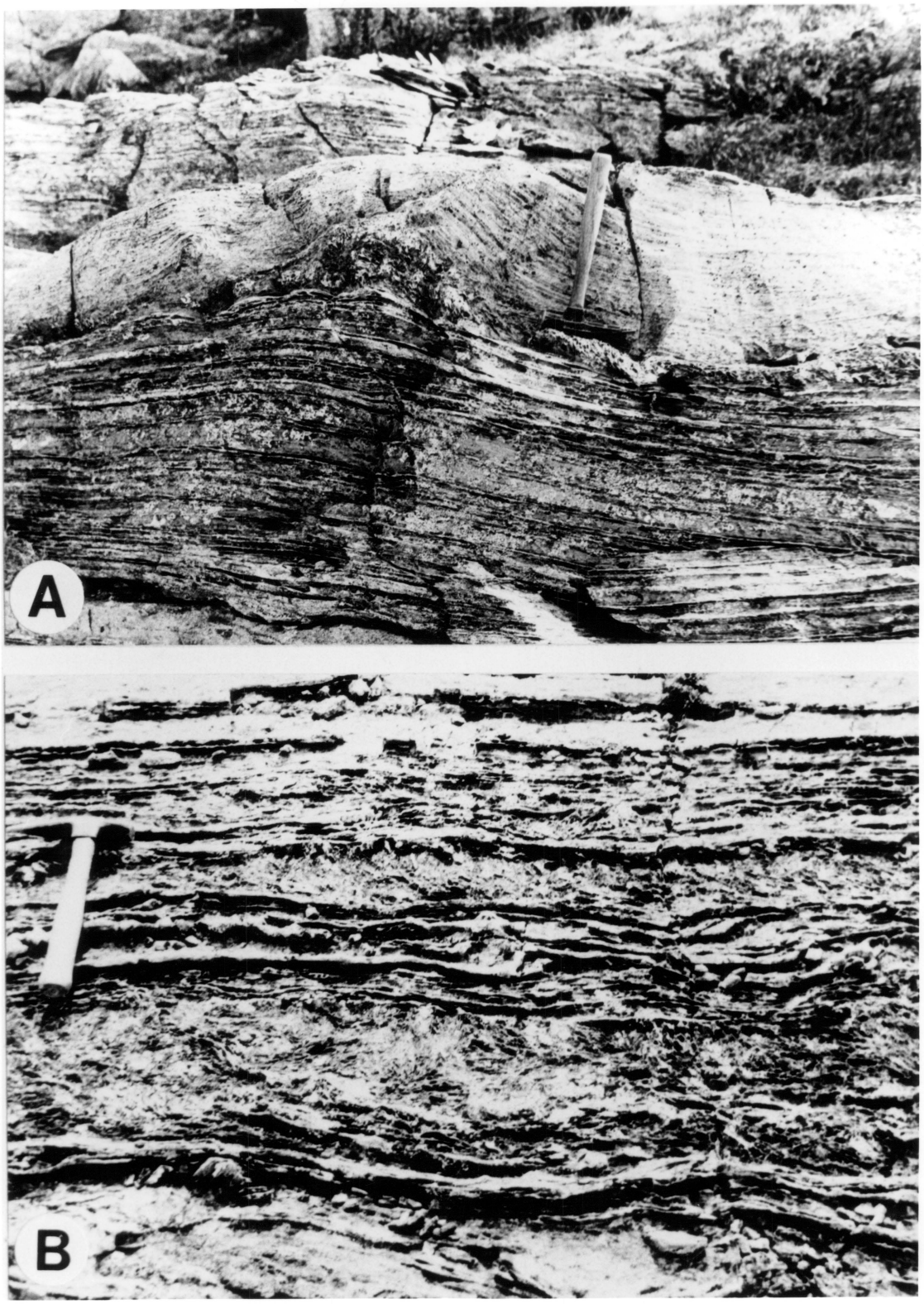
A
B

Figure 22. Stromatolites, thrombolite and tufa. Domal (A) and branching columnar stromatolites (B). Columnar thrombolite (C), with crude internal lamination defined by clots. Microdigitate tufa (D); note that influx of clastic carbonate mud (light) inhibited growth of microcolumns, suggesting growth by precipitation rather than trapping and binding.

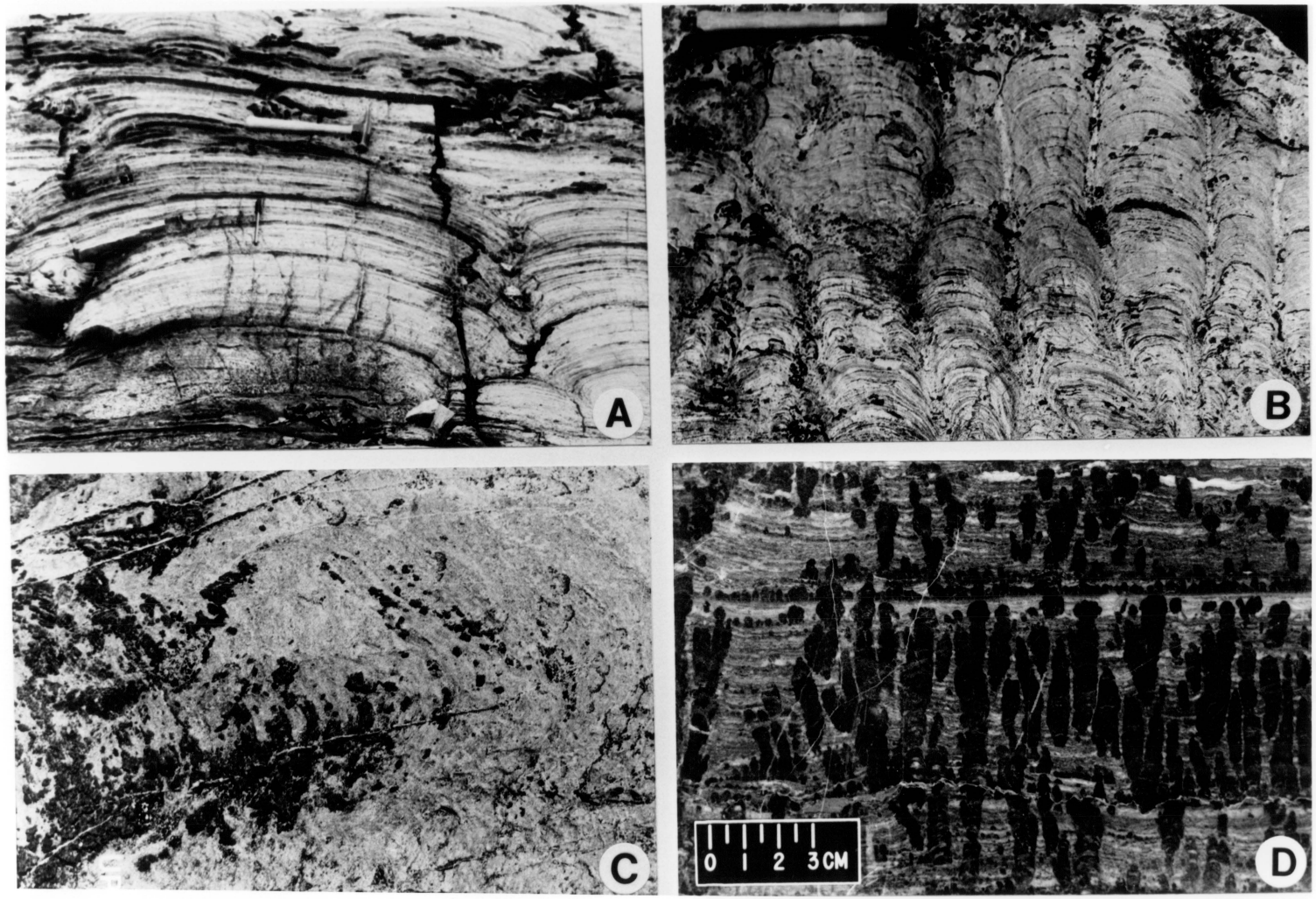
A
B
C
0 1 2 3CM
D

Incipient Drowning of Shelf

Three incipient drowning events are represented by non-cyclic intervals of the inner-shelf sequence (see Chapter 2). The lower and middle non-cyclic intervals formed during long-term onlap of western, high-energy outer-shelf facies. The upper non-cyclic interval formed during long-term onlap of eastern, low-energy "lagoonal" facies.

Lower Non-Cyclic Interval: This interval is a westward-thickening (up to 100 m) wedge of interbedded, partially-linked columnar stromatolites and intraclast/ooid grainstone (Figs. 3,23a). Intraclast grainstone/packstone is common in the western shelf, passing westward into rhythmite facies which mantles the lower rim. To the east, intraclast grainstone/packstone passes into stromatolitic facies of the eastern shelf. In the most eastern part of the shelf, the interval thins and passes laterally into cyclic deposits.

The lower non-cyclic interval formed during drowning of the lowermost rim sequence and incipient drowning of the inner-shelf. The Rocknest inner-shelf was a high-energy platform, open to the west, and lacked a reefal rim (Fig. 24a). Open-marine conditions prevailed over most of the shelf, except in the autochthon where it periodically shoaled to sea-level to form grainstone-based cycles. This

Figure 23. Stratigraphy of non-cyclic intervals. Horizontal lines are cycle boundaries of sequences that bracket non-cyclic intervals. See appendix for key to symbols. A) Lower non-cyclic interval, locality "B" (Fig. 1). B) Middle non-cyclic interval, locality "A" (Fig. 1). C) Upper non-cyclic interval, locality "B".

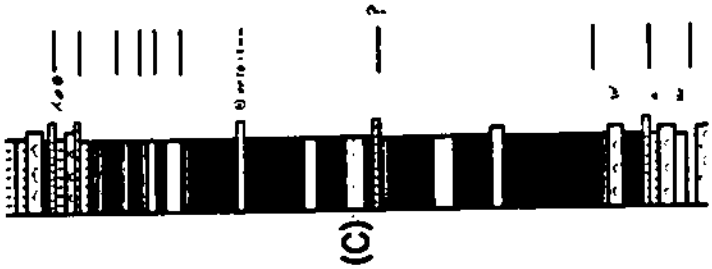

(C)

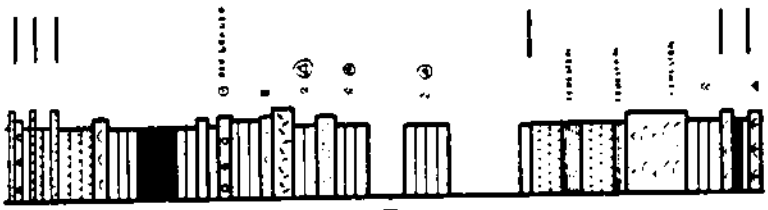

30 20 10 0m

(B)

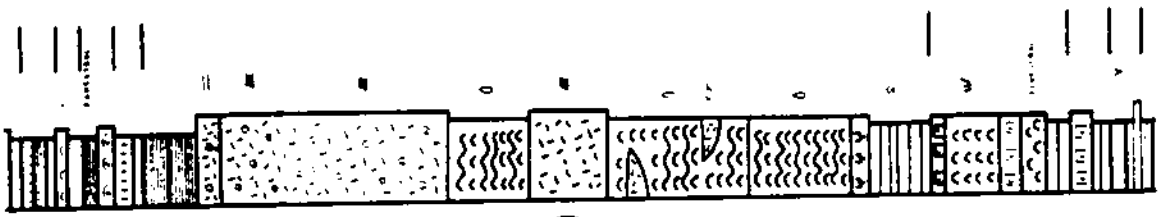

(A)

indicates that the shoal-complex had backstepped to the easternmost part of the shelf, allowing "lagoonal" sedimentation to occur farther east. Reestablishment of cyclic sedimentation over the Rocknest shelf occurred when the shoal-complex prograded westward across the inner-shelf to within several kilometers east of its original location.

Middle Non-Cyclic Interval: This interval is a westward-thickening (0 to 120 m) wedge of cherty, wave-rippled dolosiltite-dolarenite grainstone/packstone with thin interbeds of partially-linked columnar stromatolites (Figs. 3,23b), and minor thin beds of ooid-intraclast packstone and argillaceous dololutite. The interval passes westward into rim facies consisting of abundant stromatolitic boundstone and intraclast-ooid grainstone/packstone. Eastward, the interval thins and passes into shale-based and minor carbonate-based cycles of the eastern shelf.

The middle non-cyclic interval formed during a second event of rim backstepping and incipient drowning of the inner-shelf (Fig. 24b). In contrast to the lower non-cyclic interval, the middle non-cyclic interval is dominated by finer grained sediments and lacks thick stromatolitic units in the central and eastern part of the shelf. This suggests that the inner-shelf was rimmed by a stromatolitic barrier

Figure 24. Paleogeographic cross-sections of non-cyclic intervals. A) Lower non-cyclic interval. Lacks rim, with shoal-complex moved far back on platform. High energy distally steepened (?) ramp. B) Middle non-cyclic interval. Has rim, but shoal complex is located back on platform. Partially restricted "lagoon". C) Upper non-cyclic interval. Has rim and narrow shoal-complex that does not undergo significant lateral expansion (<20 km to east). Restricted, low-energy "lagoon". HS, High stand of sea-level.

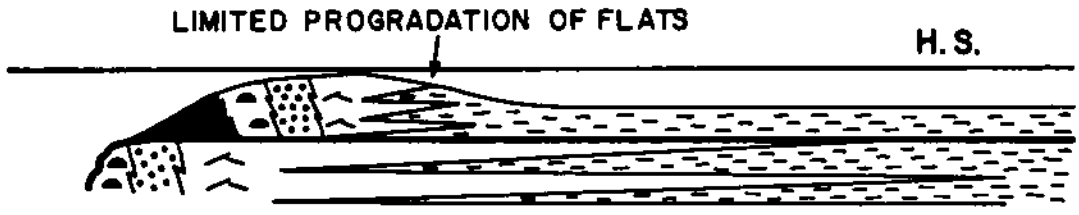

(C)

RHYTHMITE

BOUNDSTONE

GRAINSTONE

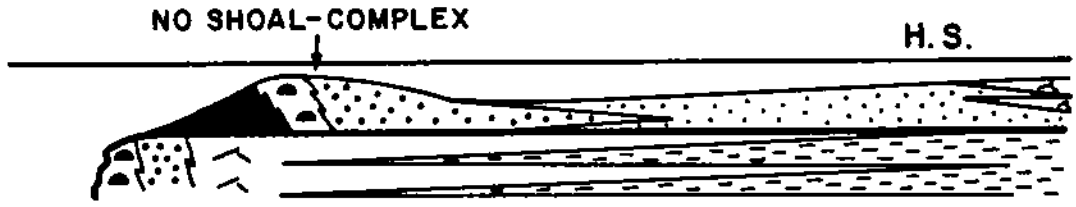

(B)

TIDAL FLAT

MIXED CARBONATE/SILICICLASTIC
SHALE AND SANDS

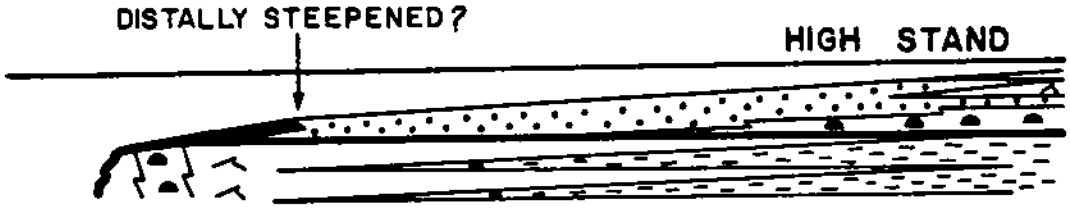

(A)

reef, but lacked an adjacent shoal-complex. The inner-shelf was a high-energy "lagoon", in part shielded by the rim, but lacked the more extensive restriction due to presence of a shoal-complex.

Incipient drowning was less extreme than that which caused the lower non-cyclic interval, suggesting that the amplitude and/or rate of relative sea-level rise may have been less great. Cyclic sedimentation was reestablished over the Rocknest shelf when the shoal-complex prograded westward, back over the inner-shelf to a few kilometers east of its previous location.

Upper Non-Cyclic Interval: This interval is an eastward-thickening (0 to 70 m) wedge of argillaceous dololutite (Figs. 3,23c), lithologically similar to the mixed carbonate/siliciclastic facies of the cyclic inner-shelf. The interval passes westward into shoal-complex facies and eastward into siliciclastic lagoonal facies of the Goulburn Group, Kilohigok Basin. Thin beds of intraclast packstone and reverse-graded ooid packstone are common throughout the interval.

Sediments of the upper non-cyclic interval formed during a third event of incipient drowning of the inner-shelf, concomitant with drowning and backstepping of the rim. However, there was incomplete transgression of the

shoal-complex (Fig. 24c). The combined width of rim and shoal-complex was less than 30 to 40 km, which persisted until the shoal-complex prograded eastward, back over the inner-shelf at the end of the upper non-cyclic interval. Because the shoal-complex was not completely submerged, the inner-shelf was effectively shielded from high-energy, open marine conditions, allowing deposition of mixed siliciclastic and carbonate mud and silt during a prolonged period of low energy "lagoonal" sedimentation.

Water depths were not much greater than after each small-scale cyclic submergence increment responsible for development of inner-shelf cyclic sequences. However, unlike the cyclic sequence in which the tidal flats of the shoal-complex prograded 100 to 200 km back over the inner-shelf after each submergence event, the tidal flats only prograded 10 to 20 km over the inner-shelf during the upper non-cyclic interval.

Relationship Of Non-Cyclic Intervals To "Grand Cycles": Non-cyclic intervals represent net increases in platform water depth due to changes in rates of longer-term (fourth order?) sea-level rise or fall. Incipient drowning can be caused by increasing the rate of longer-term sea-level rise, or decreasing the rate of longer-term sea-level fall (Pitman, 1978). "Grand cycles" consist of large-scale (75

to 200 m) changes in cycle types such that non-cyclic intervals or bundles of shale-based cycles grade up into bundles of carbonate-based or tufa-based cycles (Figs. 3,25). Therefore, "grand cycles" reflect initial net submergence of the platform followed by long-term net aggradation of the platform.

Terminal Drowning of Shelf

Generally, the uppermost deposits of the Rocknest Formation are large, highly aggradational, stromatolitic patch reefs (1 to 10 m thick), which rest sharp on the uppermost tufa bed (Fig. 26a). Individual bioherms and component stromatolites are strongly elongate. Most stromatolites are strongly divergent, branching columns. The uppermost stromatolites commonly contain siliciclastic sand and silt, and are sharply but conformably overlain by siltstone and sandstone of the Tree River Formation (basal Recluse Group). However, in the eastern part of the shelf (northeastern autochthon), the uppermost tufa bed locally is erosionally (unconformably ?) overlain by the Tree River Formation (Fig. 26b). Therefore, the sharp surface which separates the uppermost tufa bed from overlying patch reefs over much of the Rocknest shelf may be the same erosional surface that separates the uppermost tufa bed from overlying

Figure 25. Stratigraphy of two "grand cycles". Section is from locality "B" (Fig. 1). See appendix or figure 30 for key to symbols. Four members are shown (cf. Fig. 18; R, Red Shale member; T, Thin member; S, Striped member; TP, Top member; members discussed in Grotzinger and Hoffman, 1983). Lower "grand cycle" has upper non-cyclic interval (Red Shale member) as "base", and grades up into cycles with very thin shale bases, comprising the Thin member. The lower part of upper "grand cycle" has cycles with thick shale bases, comprising the Striped member, and grades up into dolosiltite-based cycles, comprising the Top member. See text for interpretation.

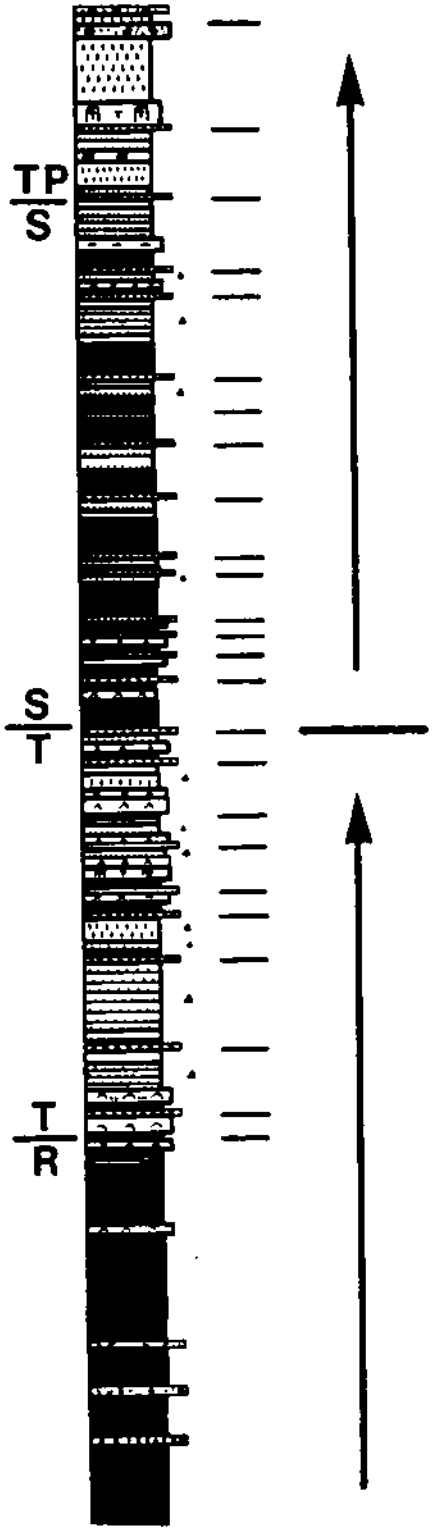
TP
S
S
T
T
R

Tree River Formation in the eastern shelf. If this surface is an unconformity, then it is possible that the shelf was locally emergent prior to terminal drowning.

Growth of large patch reefs at the top of the Rocknest Formation indicates rapid relative sea-level rise. Because the Rocknest Formation is abruptly overlain by deep-water siliciclastics of the Recluse Group, it is likely that rapid relative sea-level rise was initiated by increased subsidence related to tectonic loading and lithospheric flexure during collision (Hoffman, 1980). However, the presence of siliciclastic sediment within the uppermost stromatolite bed suggests that clastic pollution related to progradation of the Tree River Formation also helped drown the shelf. This may explain the absence of an offlap carbonate package formed during progressive drowning of the shelf. Such an assemblage developed during foredeep subsidence of the Cambro-Ordovician carbonate platform in the Appalachians (Read, 1980; Ruppel and Walker, 1984). There, craton-derived siliciclastic influx was negligible, allowing carbonate sedimentation to continue into deeper-water slope settings during progressive drowning.

Following drowning of carbonates and deposition of Tree River clastics, the shelf was mantled by hemipelagic black shale (Fontano Formation), and then onlapped from west to

Figure 26. Rocknest Formation/Recluse Group contact. A) Patch reefs of uppermost Rocknest Formation. Hammer for scale. These are separated from underlying tufa beds by sharp, possibly unconformable surface. B) Farther to east, tufa beds are erosionally overlain by Tree River Formation (siliciclastics). Surface has up to 1 m erosional relief. C) Ultimately, shelf is onlapped by well bedded, synorogenic graywacke turbidites (Asiak Formation).

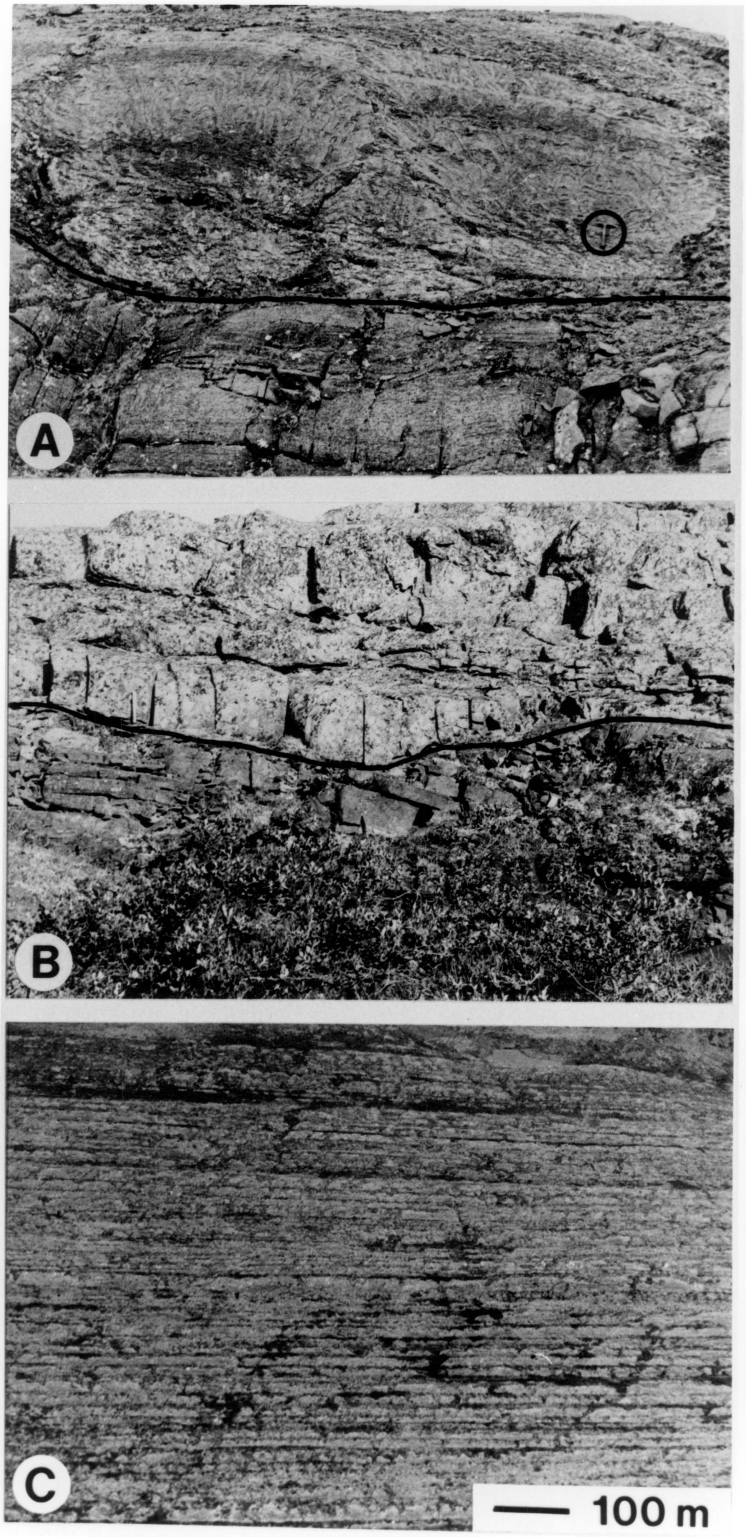
A
B
C
100 m

east by a thick sequence of deep-water, synorogenic graywacke turbidites (Fig. 26c), derived from unroofing the Hepburn metamorphic/plutonic complex (Hoffman, 1973; 1980). Because of this relationship, the rapid rise in relative sea-level required for terminal drowning was originally ascribed to rapid subsidence of the passive margin in response to its attempted subduction (Hoffman, 1973, 1980), an interpretation followed here. Although it was predicted that the subducting margin should be upflexed and exposed prior to drowning as a test of the plate tectonic model (Hoffman, 1980), the apparent absence of such a feature and extreme youth of the margin during collision led Hoffman and Bowring (1984) to consider the margin as hot and ductile, and thus unable to flex elastically in response to thrust loading. However, this interpretation should be reconsidered again given the possibility that an erosional unconformity may occur near the top of the Rocknest Formation over part of the shelf.

CONCLUSIONS AND SUMMARY OF SHELF EVOLUTION

Siliciclastic-to-Carbonate Shelf Transition: Before deposition of Rocknest carbonates, the Epworth continental shelf was siliciclastic dominated (Odjick Formation) and affected primarily by open-marine wave and storm reworking

(Hoffman et al., 1984). Palinspastic reconstruction suggests that the position of shelfbreak was located at the seaward margin of mostly unfaulted continental basement, with slope/rise facies deposited over highly stretched and rifted continental crust. Shallow-shelf sedimentation occurred over a palinspastic width of 400 to 500 km, extending from shelfbreak eastward over the submerged Slave craton and into Kilohigok foredeep. Ultimately, siliciclastic sedimentation was diminished, leading to initial carbonate sedimentation at the outer part of the shelf where a narrow barrier reef was constructed (Fig. 27a). Expansion of the shelf occurred from west to east with time (younging towards craton), by the growth and amalgamation of small bioherms in a broad siliciclastic-dominated lagoon.

Initiation of carbonate production is related to reduced siliciclastic influx, which may have been caused by either long-term sea-level rise (leading to trapping of clastics in estuaries), or decreased rates of uplift and/or erosion in the hinterland source area flanking the eastern side of Kilohigok foredeep. Reduced erosion rates could result from a decrease in hinterland uplift rate, or a climatic change. However, siliciclastics were supplied to the Rocknest "lagoon" throughout most of the carbonate

Figure 27. Summary of shelf evolution. See figure 24 for key to symbols. A) Carbonate ramp. Stromatolitic reef facies develops along outer-shelf where siliclastic influx is low. B) Prograding accretionary rim, stabilized at shelf-break of underlying siliclastic shelf. Well-developed reef-backreef-shoal complex-lagoon facies zonation. Cycles form by eastward expansion of shoal-complex over lagoon. C) Aggrading bypass rim, sheds megabreccia blocks downslope. D) Incipient drowning of inner shelf during development of lower non-cyclic interval, associated with rim drowning. See figure 24 for illustration of other events of incipient shelf drowning. E) Development of new rim in backstepped position. This occurred after each event of incipient shelf drowning. F) Terminal drowning of shelf during attempted subduction of margin. High-aggradational patch reefs form as uppermost deposits, overlying an erosional surface possibly formed during a brief period of shelf emegence preceeding shelf drowning. Shelf is finally mantled by siliclastic sediments which prohibit development of upward-deepening carbonate package.

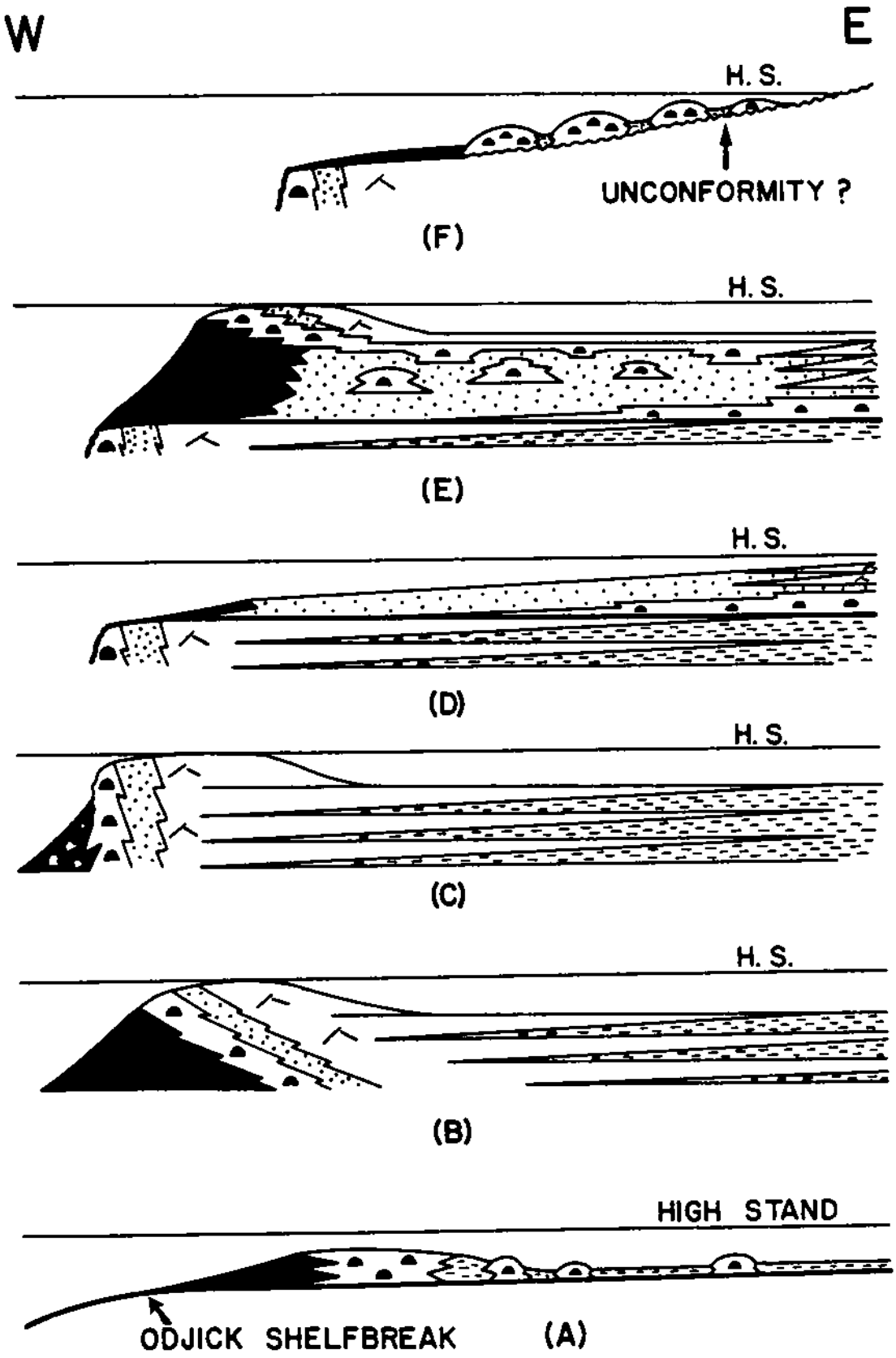
W
E
H. S.
UNCONFORMITY ?
(F)
H. S.
(E)
H. S.
(D)
H. S.
(C)
H. S.
(B)
HIGH STAND
ODJICK SHELFBREAK
(A)

shelf's existence. Siliciclastics may have been transported from the eastern shoreline of the lagoon by wind-forced geostrophic currents, and storm-surge ebb currents either as bed load or in turbidity flows (cf. Walker, 1985).

Progradation and Aggradation of Reefal Rim: Basal deposits of the Rocknest shelf sequence consist of outer-shelf and shoal-complex facies and were formed on a low-gradient ramp, developed on antecedent topography of the Odjick siliciclastic shelf (Fig. 27a). This was followed by long-term progradation of a newly-formed accretionary reefal rim over foreslope rhythmites and bioherms, seaward to a position overlying the earlier Odjick shelfbreak (Fig. 27b). This represents the westernmost limit of rim progradation; advance beyond Odjick shelfbreak was inhibited due to increase in slope and insufficient sedimentation to reduce slope inclination. Consequently, the shelf entered a prolonged period of aggradation (Fig. 27c). During this time, rapid slope steepening occurred, ultimately leading to development of a possible escarpment that shed megabreccias downslope.

The shoal-complex formed early during the progradational stage, and expanded over the inner-shelf lagoon numerous times in response to oscillating sea-level, to form many (70 to 80 in lower Rocknest) small-scale

shallowing-upward cycles. Sea-level rise initiated cycles, causing rapid east-to-west transgression of the shoal-complex by the inner-shelf lagoon, followed by sea-level fall and west-to-east progradation of the shoal-complex over lagoonal facies. This dynamic paleogeography persisted until incipient drowning of the shelf.

Subsidence rates over the platform ranged from approximately 40 cm/1000 yrs at the outer-shelf and shoal-complex, to 25 cm/1000 yrs, 135 km east of the western shoal-complex (see chapter 2). Subsidence did not decrease linearly over the shelf but increased slightly towards the central part of the shelf, then decreased rapidly over the interval 90 to 150 km from western shoal-complex (Fig.3). Minimum subsidence occurred at 180 to 200 km from the western shoal-complex (area of northeast autochthon, and Peacock Hills of Kilohigok basin). East of this arch, subsidence increased rapidly into the axis of Kilohigok foredeep.

Incipient Shelf Drowning and Backstepping of Rim: The Rocknest shelf experienced three events of incipient shelf drowning, associated with local backstepping of the rim and non-cyclic sedimentation over most of the shelf (Figs. 3,27d,e). During the lower non-cyclic interval, the shelf probably was a distally steepened ramp (cf. Read, 1982)

extending from below storm wave-base at the drowned shelf-edge, to sea-level at the shoal-complex, then located approximately 150 km to the east (Fig. 27d). Reefal stromatolite bioherms and cross-bedded grainstone were deposited over most of the shelf, passing into sub-storm wave-base rhythmites overlying the old rim. If water depths were on the order of 40-70 m (a reasonable value for open-shelf storm wave-base; Logan et al., 1969), then the ramp slope was 25 to 45 cm/km (0.015-0.027 degrees). Low ramp slopes are supported by the lack of slump/slide features or breccia deposits in rhythmites.

Diachronous onlap and offlap of outer-shelf facies during the lower non-cyclic interval is indicated by time-slicing parallel to cycle boundaries. Initial onlap was very rapid (almost time parallel, Fig. 3) but slowed as more of the shelf was covered. Similarly, offlap was initially rapid but decreased as the outer-shelf and shoal complex prograded westward were reestablished in backstepped positions (Fig. 27e)

Several mechanisms may cause drowning of carbonate platforms (Schlager, 1981). Of these, rapid increase in relative sea-level by rapid subsidence or eustatic sea-level rise are the most attractive. Mezozoic/Cenozoic passive-margin shelf sequences commonly are cut by growth faults

(Bally, 1983), and compaction within Odjick shales could have led to fracturing and downfaulting of the early cemented rim. Although this might explain drowning and backstepping of the rim, it fails to explain inundation and incipient drowning of the inner shelf, which would have otherwise been at shallow depths (<10 m). However, a eustatic sea-level rise would have favored incipient drowning of the inner-shelf in addition to drowning and backstepping of the rim.

The middle and upper non-cyclic intervals (Fig. 24b,c) similarly may represent periods of rapid sea-level rise, associated with rim backstepping. However, these two events apparently were less severe than that which produced the lower non-cyclic interval, because the rim quickly became reestablished in the middle non-cyclic interval, and the shoal complex did not backstep in the upper non-cyclic interval. Incipient drowning events responsible for the non-cyclic intervals may have been caused by fourth order eustatic sea-level oscillations (Vail et al., 1977), with amplitudes of 50 to 100 m and periods of 500,000 yrs to 1 m.y.

Terminal Drowning of Shelf: During the final phase of evolution (Fig. 27f), the shelf was terminally drowned and overlain by deep-water siliciclastics of the Recluse Group.

Rapid tectonic subsidence combined with clastic pollution to effectively terminate carbonate production, following development of thin stromatolitic patch reefs. Drowning may have followed a period of shelf emergence associated with formation of a regional(?) unconformity. If so, then it suggests that the margin was capable of elastic flexure (Caldwell and Turcotte, 1979; Kominz and Bond, 1984) in response to thrust loading. However, the extreme youth of the margin during loading implies a relatively hotter lithosphere, which should result in greatly reduced flexural rigidity (Kominz and Bond, 1984). Perhaps the poor development of the Rocknest "unconformity" relects a weaker lithospheric plate at that time.

Chapter II

ORIGIN OF ROCKNEST INNER-SHELF AND SHALLOWING-UPWARD CYCLES

ABSTRACT

The Rocknest shelf sequence contains 140 to 160 shallowing-upward cycles (1 to 15 m thick; 18 to 30,000 yr period) which contain distinctive marker beds, and can be correlated for over 200 km parallel to strike and over 120 km perpendicular to strike. Cycles are grouped according to cycle base lithology, which reflects paleogeographic position on the platform. Shale-based cycles of the distal inner-shelf pass westward in dolosiltite-based cycles, then into tufa-based cycles of the shoal-complex, and then into grainstone-based cycles of the outer-shelf. Cycles are bounded by erosional surfaces that become less pronounced away from the shoal-complex.

Cycles formed in response to small, asymmetric (rapid rise/slow fall) eustatic oscillations in sea-level (≈ 10 m). During sea-level rise, rapid transgression and submergence of tidal flats occurred along eastern margin of the shoal-complex, followed by eastward expansion of the shoal-complex, and slow progradation of tidal flats over lagoonal facies during sea-level fall. A glacio-eustatic model for

cyclicity accounts for the data, favoring: asymmetric, eustatic, sea-level oscillations; subaerial exposure and vadose diagenesis of platform during sea-level falls; arrested progradation and incomplete shoaling of many cycles; and cycle periods of 20,000 to 100,000 yrs (18,000 to 30,000 yrs for Rocknest). Given the low amplitude of sea-level oscillation (≈ 10 m), alpine glaciation is favored over continental glaciation.

Inner-shelf slopes ranged from 8 cm/km (avg.) at high sea-level stand, to 2 cm/km (avg.) at low sea-level stand. Tidal flat progradation rates were approximately 7 to 9 km/1000 yrs. Interaction of inner-shelf slope, sea-level fall rate and sedimentation rate generates "complete", "condensed", or "expanded" cycle profiles. One-dimensional computer modelling reveals that: sedimentation rates of shoal-complex facies were ≈ 250 cm/1000 yrs lag times in sedimentation following transgression may have ranged from zero on the shoal-complex to 2000 yrs on the distal inner-shelf; subtidal sedimentation rates may have ranged from 80 cm/1000 yrs for the proximal inner-shelf to 20 cm/1000 yrs for the distal inner-shelf.

INTRODUCTION

Cyclic carbonates comprise many early Proterozoic to Holocene passive-margin sedimentary prisms. Phanerozoic cyclic carbonates have been described in detail (see summaries in Wilson, 1975; Wilkinson, 1982; James, 1984a), in contrast to rare studies of pre-Phanerozoic cyclic carbonates (O'Connor, 1972; Hoffman, 1975; Jackson and Ianelli, 1981). Despite the abundant data which these studies have generated, the mechanisms responsible for cyclicity are poorly understood due to lack of constraints on variables that influence cycle development. Consequently, a controversy exists over whether allocyclic or autocyclic mechanisms are most important.

Proponents of autocyclic models (eg. Ginsburg, 1971) ascribe cyclicity to internal feedback mechanisms within the sedimentary system. On the other hand, advocates of allocyclic mechanisms (eg. Fischer, 1964) believe that extrinsic mechanisms (eg. episodic subsidence, eustatic sea-level changes) drive the sedimentary system and cause cyclicity.

Furthermore, many workers suggest that individual cycles cannot be regionally correlated and models of progradation envisage "islands" shallowing to sea-level, producing a mosaic facies pattern in which tidal flat cycle

caps do not extend from one "island" to the next (eg. James, 1984a). However, inability to correlate cycles may relate more to lack of distinct marker beds, than to real pinchout of facies.

A study of the Rocknest Formation (1.89 Ga), Wopmay orogen, northwest Canada, was undertaken to document a cyclic sequence of early Proterozoic age, and to help resolve some of the problems which prohibit a more thorough understanding general cycle development. The Rocknest Formation is superbly exposed for over 200,000 sq. km and contains 140 to 160 shallowing-upward cycles which contain distinct marker beds. There also are good absolute time constraints on the age of the passive-margin sequence in which it occurs.

As such, the Rocknest Formation is ideal for testing correlatability of cycles and approximating average cycle period, which makes it possible to constrain the possible mechanisms of cycle development. Furthermore, establishment of a detailed regional stratigraphy of cycles adjacent to marker beds, has allowed estimation of inner-shelf paleoslopes, tidal flat progradation rates, amplitude and period of sea-level oscillation, and absolute sedimentation rates. Given these constraints on variables which control cyclic sedimentation, it has been possible to test various

models of cycle development using computer modelling. The modelling results in a greatly enhanced understanding of the relative effect of each variable, and increased knowledge of overall cycle development.

This chapter provides detailed descriptions of cyclic lithofacies and their lateral and vertical distribution. It discusses the general applicability of cyclic mechanisms to generating cyclic carbonates on the Rocknest shelf, as well as on carbonate shelves of other ages. Finally, it quantitatively considers the variables controlling Rocknest cycle development, and establishes a framework which should be useful in interpreting more poorly exposed Proterozoic, and perhaps Phanerozoic cyclic carbonates.

REGIONAL SETTING

The early Proterozoic (1.89 Ga) Rocknest Formation (Coronation Supergroup) is exposed in the foreland thrust-fold belt and autochthon of Wopmay Orogen, northwest Canada (Fig. 1). The Coronation Supergroup (Fig. 2) is a continental margin sedimentary prism composed of a basal rift sequence (Akaitcho Group), a middle passive-margin sequence (Epworth Group), and overlying foredeep sequence (Recluse Group; Hoffman, 1980).

The lower part of the Epworth Group (Odjick Formation; 0.2 to 1.5 km thick) is an open-marine, storm-dominated, siliciclastic shelf sequence composed of quartz arenite, siltstone and mudstone, with rare intraclastic and stromatolitic dolomite (Hoffman et al., 1983, 1984). The upper Epworth Group (Rocknest Formation; 450 to 1100 m thick) is a cyclic-dolomite shelf sequence with a stromatolitic reefal rim and flanking debris apron (Hoffman, 1973; 1975). Stratigraphic relationships and facies analysis indicate long-term progradation and aggradation of the shelf, punctuated by relatively short episodes of incipient drowning of the shelf and backstepping of the rim. The shelf was terminally drowned and onlapped by the Recluse Group during continental collision and attempted subduction of the margin (Calderian orogeny; Hoffman and Bowring, 1984). The passive-margin sequence (Epworth Group) probably was destroyed within 10 to 15 m.y. of rifting (Hoffman and Bowring, 1984).

The palinspastically restored Rocknest shelf sequence (Figs. 3,4) is an eastward-thinning prism, 0 to 1,100 m thick, extending for over 220 km parallel to depositional strike, and over 200 km perpendicular to strike. Originally, it may have extended for over 450 km parallel to depositional strike, and over 260 km perpendicular to

strike. The shelf sequence (Figs. 3,4) can be divided from west to east into slope, outer-shelf, shoal-complex, and inner-shelf facies. Slope, outer-shelf and shoal-complex facies assemblages are restricted to the western margin of the shelf; inner-shelf facies occur over most of the shelf region, except adjacent to its margin.

The Rocknest Formation is laterally equivalent to siliciclastic sediments of the Burnside River Formation, Goulburn Group, Kilohigok Basin (Figs. 1,5; Campbell and Cecile, 1981; Hoffman et al., 1984). Burnside River clastics thicken from less than 300 m in western exposures (Peacock Hills/Rockinghorse Lake areas) to more than 2,500 m in eastern exposures near Bathurst Inlet (Campbell and Cecile, 1981; Hoffman et al., 1984). Western and central parts of the basin contain red and white quartzite, subarkose and siltstone containing hummocky cross-stratification, planar lamination, wave ripples and graded bedding (Campbell and Cecile, 1981; Eriksson, unpub. data). These are shallow-marine facies and pass toward the eastern margin of the basin into fluvial quartzites, subarkose and abundant cobble/boulder conglomerate. Burnside River siliciclastics were derived from an eastern source area (Thelon Front), and deposited in a foredeep flanking an advancing thrust-fold belt. The Rocknest "lagoon" spanned

the width of the Slave craton (400-500 km) and was bounded to the west by a carbonate shoreline (shoal-complex) formed on a passive margin, and bounded to the east by a siliciclastic shoreline adjacent to a rising hinterland.

ROCKNEST OUTER-SHELF AND SLOPE

Outer-shelf and slope facies are described and interpreted in detail in chapter 1. Brief descriptions and interpretations are provided here. Outer-shelf facies (rim boundstone and backreef grainstone) pass westward into slope facies and eastward into shoal-complex facies. Slope facies are flanked to the east by reefal boundstone, and pinch-out laterally to the west where foredeep deposits of the Recluse Group sit directly on those of the Odjick Formation.

Outer-shelf facies comprise four distinct reefal rim sequences and associated backreef sand belts (Figs. 3,4). The lowermost rim sequence is thickest (450 to 500 m), and is overlain by three younger, backstepped rim sequences, 80 to 130 m thick. The lowermost rim sequence consists dominantly of stromatolite mounds (1 to 4 m wide, up to 2 m synoptic relief) interbedded with intervals of partially-linked columnar stromatolites. Mounds and columns are strongly elongate subnormal to regional trend of the shelf edge, and are separated by narrow channels filled with

intraclast grainstone/packstone or edgewise conglomerate. Mounds are locally brecciated, and cut by irregular cavities or neptunian dikes and sills. Younger rim sequences consist dominantly of sheets of partially-linked columnar stromatolites (10 to 50 cm wide, 10 to 200 cm high, up to 30 cm synoptic relief), although bioherms with up to 2 m relief are locally present. Ooid/intraclast grainstone is most common in younger rim sequences, occurring as cross-bedded lenses and sheets.

The Rocknest shelf was a wave-dominated windward margin characterized by a major barrier reef, flanked by backreef sands. Onshore transport of clastic carbonate generated within the reef favored slope starvation and growth of a major supratidal shoal-complex behind the backreef sand belt. This shoal-complex prevented open communication between the high energy open ocean, and lower energy "lagoon" to the east.

Slope facies are rhythmites (with slump folds and truncation surfaces), edgewise conglomerates, downslope bioherms, megabreccias, and rhythmite breccias. Rhythmites consist of interlaminated dololutite, dolosiltite and shale, and represent periplatform sediments derived from the shelf margin. Edgewise conglomerates are composed of imbricated rhythmite fragments, probably formed by reworking of early-

lithified rhythmite as a result of lowering wave-base during storms. Bioherms consist of isolated or coalesced cone-shaped stromatolites, commonly encrusted with layers of marine cement, and probably formed within the photic zone of the reefal foreslope. Megabreccias contain shelf-edge boundstone/grainstone blocks (up to 150 m), spalled off of a near-vertical escarpment during aggradation of the rim. Rhythmite breccias are composed of platy rhythmite fragments in debris flow deposits, commonly capped by carbonate tubidites and reflect slumping of upslope masses.

ROCKNEST SHOAL-COMPLEX

Rocknest shoal-complex facies are exposed along the east limb of syncline "M" and in the first three thrust sheets to the east (Fig. 1). They pass westward into backreef grainstone and reefal boundstone, and eastward into cyclic inner-shelf facies. Shoal-complex facies of the lowermost rim sequence occur in a narrow belt, 1 to 5 km wide. Facies are cryptalgalaminite, tufa, and laminated dolosiltite/lutite; these may be deformed into tepees or breccias and contain pisolite. Sediments are arranged cyclically, so that cryptalgalaminite, tufa and laminated dolosiltite/lutite are overlain by disrupted equivalents, developed as tepees and breccias with associated pisolite

(Fig. 16a). Cycles are up to 15 m thick and the intensity of brecciation generally increases upwards. Tepees and breccia deposits forming cycle caps are truncated by planar to irregular erosion surfaces and abruptly overlain by undeformed cryptalgalaminite, tufa and dolosiltite/lutite of the succeeding cycle.

Lithofacies

Cryptalgalaminite: This facies forms sequences up to 1 m thick of finely laminated, flat to irregularly layered dolosiltite and dololutite (Fig. 16b). Individual laminae are continuous on the scale of a few meters, and are cut by scours filled with thin intraclast layers. Irregular to laminoid fenestrae, desiccation cracks, tepee structures, abundant silica pseudomorphs after displacive halite and casts after skeletal halite, and rare pseudomorphs after gypsum and possibly anhydrite are present.

Cryptalgalaminites were formed in the upper intertidal to supratidal zone by binding of thin storm-deposited silt/mud layers by smooth algal mats (cf. Davies, 1970; Kendall and Skipwith, 1968). Evaporation of pore fluids in sediments produced desiccation cracks, and generated hypersaline fluids which precipitated halite and rarely, gypsum or possibly anhydrite.

Tufas: These form beds up to several meters thick and are associated with cryptalgalaminite and laminated dolosiltite/lutite. Tufas (Fig. 16c) are light-gray to tan or cream, whereas cryptalgalaminites and dolosiltite/lutites are cream or light red. Tufas consist of cement laminae that are continuous, smooth to undulatory or colloform (0.1 to 2.0 mm thick), and interlaminated with cryptalgalaminite or dolosiltite/lutite. They also may form compound, centimeter to decimeter-thick layers that contain tepee structures, desiccation cracks, intraclasts and halite casts. Laminae are confluent from layer to layer and commonly form discrete to partially-linked columnar structures ("microdigitate" stromatolites), 1 to 10 mm wide and with 0.1 to 5 mm relief. Tufas are replaced by mosaics of turbid, golden brown, anhedral dolomite neospar (0.03 to 0.2 mm diameter crystals) in which crystal size increases upward within layers or microcolumns. They are overlain by dololutite that drapes relict square and feathery precursor crystal-bundles.

Tufas formed where the influx of clastic carbonate was low enough to allow the accumulation of cement crusts. Precipitation occurred when sediment-poor waters supersaturated with aragonite were blown over the flats as wind or storm tides, where they were evaporated. Tufa

precipitation probably was aided by microbes which would have consumed CO_2 during photosynthesis, increasing pH and promoting aragonite precipitation. Sediments are pale in the proximal shoal-complex because during low stands in sea-level, subaerial exposure of tufas was prolonged and intense, and organics trapped by cementation were oxidized.

Laminated Dolosiltite/Lutite: This facies commonly is developed as interlaminae in cryptalgalaminites and tufas, or as continuous sequences of thin to thickly laminated, cream to light red dolosiltite and dololutite. Flat to wavy lamination is dominant along with minor normally graded laminae and cross-laminae. Tepee structures, desiccation cracks, irregular solution fenestrae, and halite casts are common. Rare gypsum casts and possible psuedomorphs after anhydrite also are present.

Laminated dolosiltite/lutite formed in the upper intertidal to supratidal zone by suspension settling from storm floodwaters. Sediments may have been bound by thin algal mats, but mechanical sedimentation was dominant.

Tepee/Pisolite Facies: Cryptalgalaminites, tufas and dolosiltite/lutite are deformed into synsedimentary structures ranging from simple flexural buckles (tepees) to extremely complex breccias. Tepees are up to 3 m wide and 2 m high, with spaces between bedding layers up to a few

centimeters (Fig. 28a). Tepees also are transected by numerous sub-vertical to sub-horizontal fractures (Fig. 28b).

In the extreme case, fracturing destroyed tepees to form chaotic masses of angular to sub-rounded blocks. Upper sides of blocks and smaller fragments often are coated by tufa, and fractures are filled with internal sediment (dolosiltite, dololutite, and pisoliths) and cement (silica and dolomite pseudomorphs after downward-diverging botryoidal aragonite; Fig. 28c).

Layers of pisolitic gravel, up to 1.5 m thick, also occur in tepee/ breccia deposits. Pisoliths (Fig. 29a) are 0.1 to 2 cm in diameter and have circumgranular and radial cracks, composite nucleii consisting of encrusted pisolith fragments, solution fenestrae, and rare reverse grading and polygonal fitting. Shelter voids and solution fenestrae are lined with isopachous fringes of dolomitized marine cement and cavities are floored by dolomite crystal silt (Fig. 29b). Oncolitic deposits (Fig. 29c) in tepee/pisolite facies can be distinguished from pisolitic deposits by larger size of oncoliths (up to 20 cm diameter), upward rather than downward elongation (indicating growth at the sediment surface), and microfabric which is more cellular and similar to associated tufa layers.

Figure 28. Shoal-complex facies. A) Large tepee. Note truncation of up-arched layering along cycle boundary (CB), followed by deposition of nearly horizontal beds. Staff is 1.5 m long. B) Sub-horizontal fissures (F) filled with silica pseudomorphs after botryoidal aragonite. C) Close-up of (B) showing silica pseudomorphs after downward divergent (stalactitic) botryoidal aragonite.

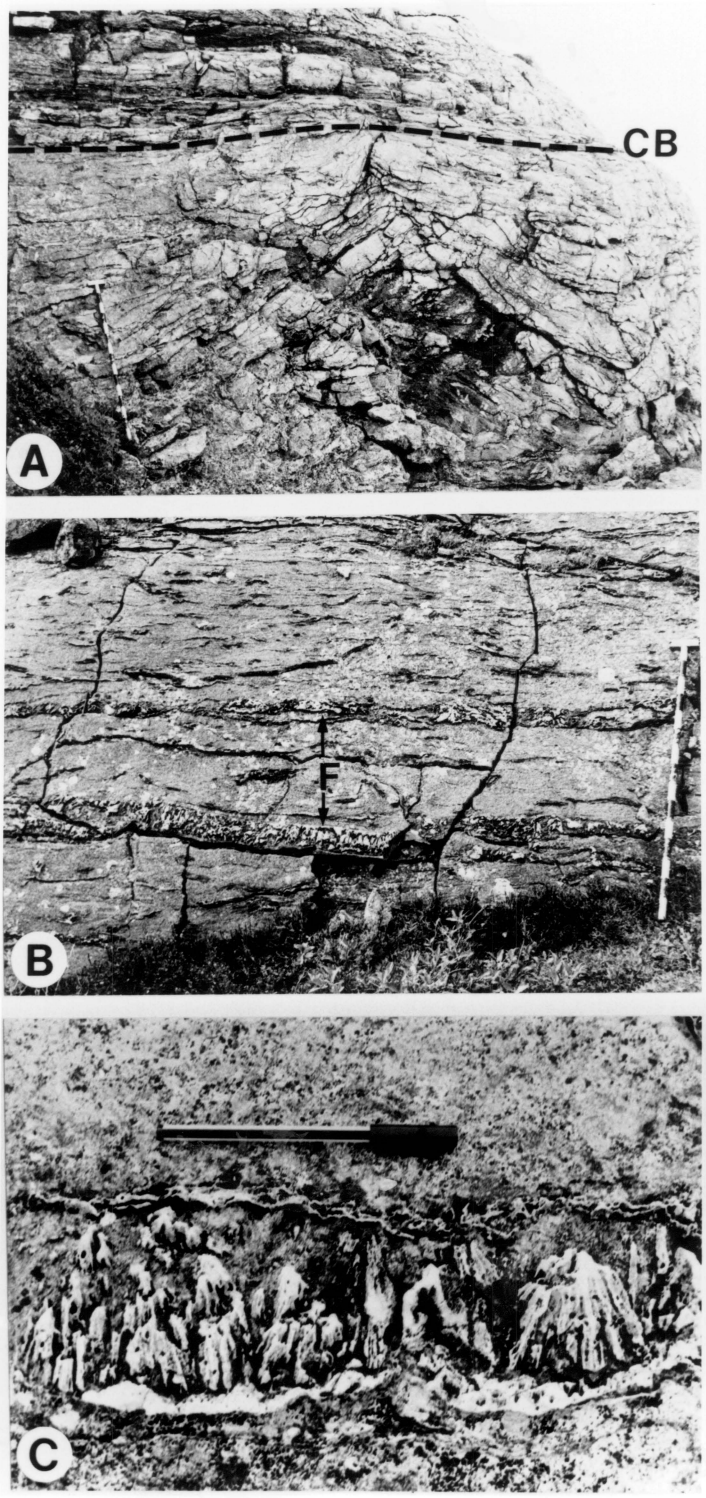
CB
A
F
B
C

Figure 29. Shoal-complex facies continued. A) Pisolite; note concentric, irregular layering, abundant fenestrae, and pisolith-fragment nucleii. B) Photomicrograph of pisolite showing geopetal crystal silt (CS) flooring cement-filled fenestrae. C) Onolitic dolomite; note light color of oncoliths which contrasts with associated dark pisoliths, upward elongation due to encrusting growth, and contrast in microfabric with adjacent pisoliths.

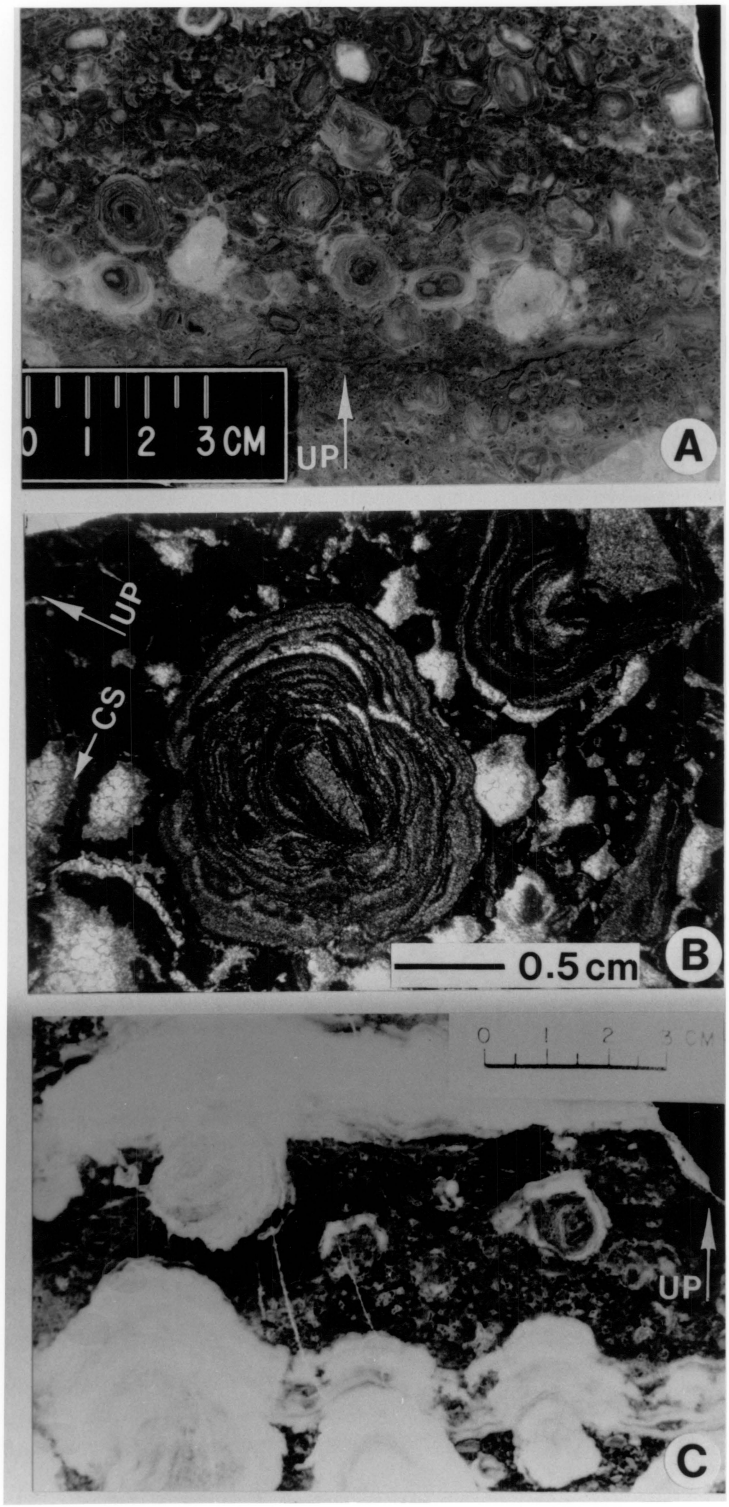
0 1 2 3CM
UP
A
UP
CS
0.5 cm
B
0 1 2 3 CM
UP
C

During the course of cycle development at the shoal-complex, deposition of laminated dolosiltite/lutite, cryptalgalaminite, and tufa was followed by lowering of the water table (caused by falls in sea-level), which favored tepee and pisolite formation through expansion of carbonates by precipitation, moisture and thermal swelling, superimposed on the effects of desiccation and thermal contraction (cf. Assereto and Kendall, 1977). As the water table was lowered and vadose diagenesis became more severe, sediments were increasingly disrupted forming embryonic, mature, and eventually senile (breccias) tepees (cf. Assereto and Kendall, 1977). Pisoliths and tufa-encrusted blocks were formed by precipitation of aragonite and/or hi-Mg calcite during evaporation of infiltrating storm-flood waters.

Vadose diagenesis of the shoal-complex is indicated by development of tepees, pisolite, crystal silt, and fractures filled with silica and dolomite pseudomorphs after downward-diverging botryoidal aragonite. Botryoids commonly are stalactitic, which indicates precipitation of cements from saline fluids percolating down through the vadose zone. Although some of these features (eg. crystal silt and tepees) may have non-vadose origins in other sequences (Malek-Aslani, 1970; Shinn, 1969), a vadose origin in the

Rocknest Formation is supported by the regional correlation of shoaling-upward cycles from the inner shelf into the shoal complex. Westward from the inner-shelf, subtidal and then intertidal facies at bases of cycles progressively pinch-out and are replaced by thicker, upper intertidal and supratidal facies at the tops of cycles, indicating lateral shoaling onto a topographically high area during deposition. Tepee structures, pisoliths and crystal silt are most abundant in the upper, most aggraded parts of cycles; they are absent in basal parts of shoal-complex cycles and lower and middle parts of inner-shelf cycles. Furthermore, they only are marginally developed in shoal complexes adjacent to rims of the upper Rocknest Formation, where each cyclic transgressive event was more complete and subsequent subaerial exposure less prolonged.

Evolution of Shoal-Complex

The occurrence of laminated dolosiltite/lutite, cryptalgalaminite and tufa alternating with sequences containing tepees, breccias and pisolite indicates deposition in the upper intertidal to supratidal zone. During high sea-level stand these facies developed behind (eastward of) back-reef grainstones and formed an emergent barrier, 1 to 5 km wide, that prevented open exchange between the western ocean and eastern lagoon (Fig. 9).

Cyclical sequences in the shoal-complex reflect minor oscillations in sea-level; initially, upper intertidal to supratidal sedimentation occurred, following transgression of the eastern lagoon during rises in sea-level and shallow submergence of the shoal-complex. During subsequent falls in sea-level the eastern margin of the shoal-complex prograded away from the rim (up to 200 km), forming upper intertidal to supratidal caps of inner-shelf cycles; as sea-level fell below the sediment surface, earlier formed sediments of the western shoal-complex were exposed in the vadose zone, and tepees, breccias and pisoliths developed as soils. Depth and intensity of vadose zone development reflects position on the shoal-complex. Because the shoal-complex prograded from west to east, and transgression occurred from east to west, the duration of subaerial exposure of the shoal complex increased westward. Consequently, brecciation and pisolite development are most intense along the western margin of the shoal-complex. Following subaerial exposure and soil development, submergence of the shoal-complex during the next cyclical trangression reinitiated upper intertidal to supratidal sedimentation. Each transgression was minor, and never reached water depths suitable for production of intertidal stromatolites or subtidal carbonates. Thus the proximal

shoal-complex was a permanent, narrow, linear barrier that often was subaerially exposed, isolating the inner shelf lagoon from the open ocean, similar to other ancient carbonate barriers (cf. Dunham, 1972; Assereto and Kendall, 1977; Aitken, 1978).

After drowning of the lowermost reefal rim, the shoal-complex subsequently was reestablished as a paleotopographic high behind each of the younger rims of the upper Rocknest Formation. However, these were commonly submerged to intertidal or subtidal depths during each cyclic transgression, followed by aggradation to sea-level and final subaerial exposure during sea-level fall. Thus, each shoal-complex sequence behind the younger rims lacks a vertically continuous sequence of upper intertidal to supratidal facies, that typifies the older shoal-complex adjacent to the lower rim.

ROCKNEST INNER-SHELF

Rocknest inner-shelf facies are exposed in central and eastern thrust sheets and autochthon of Wopmay orogen, and Peacock Hills area of Kilohigok Basin (Figs. 1,3). Inner-shelf facies pass westward into shoal-complex facies, and eastward into siliciclastic shale, siltstone and sandstone of the Goulburn Group, Kilohigok Basin (Figs. 3,5; Campbell

and Cecile, 1981; Hoffman et al, 1984). Generally, inner-shelf facies occur in asymmetric, shallowing-upward cycles which can be classified according to cycle base lithology, reflecting paleogeographic position on shelf (Fig. 19). Individual cycles can be correlated for over 200 km parallel to depositional strike and over 100 km perpendicular to strike (Figs. 30,31).

Three non-cyclic intervals occur within the cyclic sequence. The lower (0 to 100 m thick) and middle (0 to 120 m thick) non-cyclic intervals consist of stromatolitic boundstone, intraclast/ooid grainstone, and cherty dolosiltite. They form eastward-tapering wedges that pass laterally into cyclic deposits (Fig. 3). The upper non-cyclic interval (0 to 70 m thick) consists of argillaceous dololutite with intercalated intraclast/ooid packstone-wackestone, and forms a westward-tapering wedge that passes laterally into cyclic deposits (Fig. 3). The non-cyclic intervals grade up into sequences of inner-shelf cycles to form "grand cycles", 75 to 200 m thick (Figs. 3,25).

Cyclic Lithofacies

Cycles of the inner-shelf sequence can be grouped according to cycle-base lithology (Fig. 19). Shale-based cycles contain argillaceous dololutite or siliciclastic

Figure 30. Correlation of cycles parallel to depositional strike. Cycles are within thrombolitic member (TM), between underlying Intraclastic member (IM), and overlying Pink Chert member (PCM). Members discussed in Grotzinger and Hoffman, 1983 (note: Intraclastic member = lower non-cyclic interval; Pink Chert member = middle non-cyclic interval). Location of sections shown in Fig. 1.

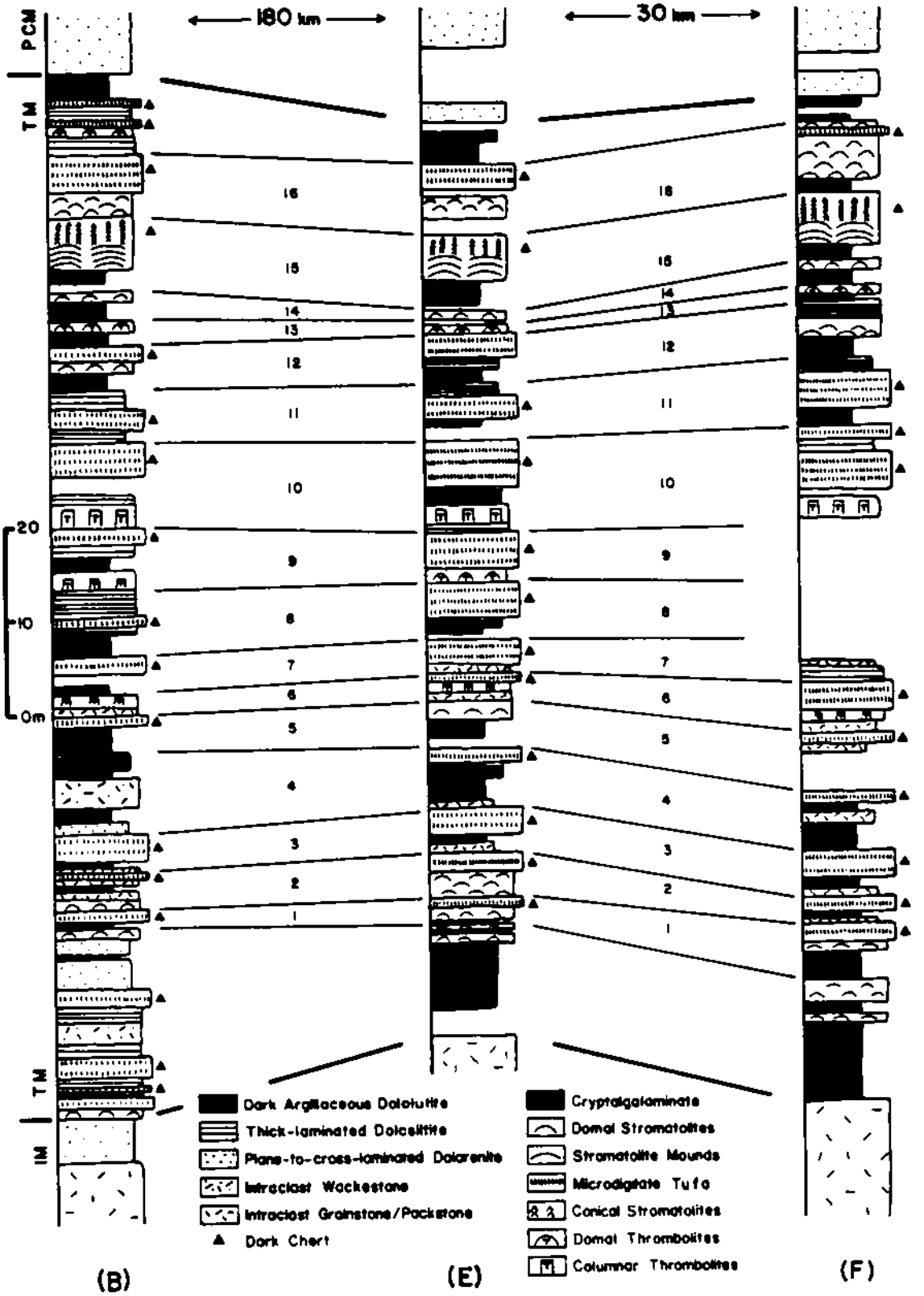
180 km
30 km
PCM
TM
IM
20
10
0m
16
15
14
13
12
11
10
9
8
7
6
5
4
3
2
1
Dark Argillaceous Dololutite
Thick-laminated Dolosiltite
Plane-to-cross-laminated Dolarenite
Intraclast Wackestone
Intraclast Grainstone/Packstone
Dark Chert
Cryptalgalaminate
Domal Stromatolites
Stromatolite Mounds
Microdigitate Tufa
Conical Stromatolites
Domal Thrombolites
Columnar Thrombolites
(B)
(E)
(F)

siltstone/sandstone at their bases. Dolosiltite-based cycles lack siliciclastic detritus and contain thick-laminated dolosiltite or stromatolitic/thrombolitic dolomite at their bases. Tufa-based cycles contain only shoal-complex lithologies. Grainstone-based cycle have ooid-intraclast grainstone at their bases.

Shale-based cycles below the lower non-cyclic interval pass westward into dolosiltite-based cycles, and then into restricted tufa-based (shoal-complex) cycles (Figs. 3,31). Grainstone-based cycles only occur west (oceanward) of the shoal-complex. Above the lower non-cyclic interval, shoal-complex cycles are absent and shale-based cycles pass westward into dolosiltite-based cycles and then directly into reef and backreef facies of the outer-shelf.

Shale-based cycles have the most diverse facies and contain from base to top: 1) intraclast packstone, 2) siliciclastic siltstone/sandstone and argillaceous dololutite, 3) thick-laminated dolosiltite, 4) stromatolitic/thrombolitic dolomite, 5) cryptalgalaminite, and 6) laminated to microdigitate tufa. Facies successions within cycles were defined both by inspection and by using a BMDP computer program (Brown,1983), which is a log-linear model, in conjunction with a stepwise procedure for identification of significant transitions between facies

Figure 31. Correlation of cycles perpendicular to depositional strike. Cycles are from basal part of Lower Shale member of Grotzinger and Hoffman, 1983. Note pinchout of tufas and stromatolites to east. Location of sections shown in Fig. 1.

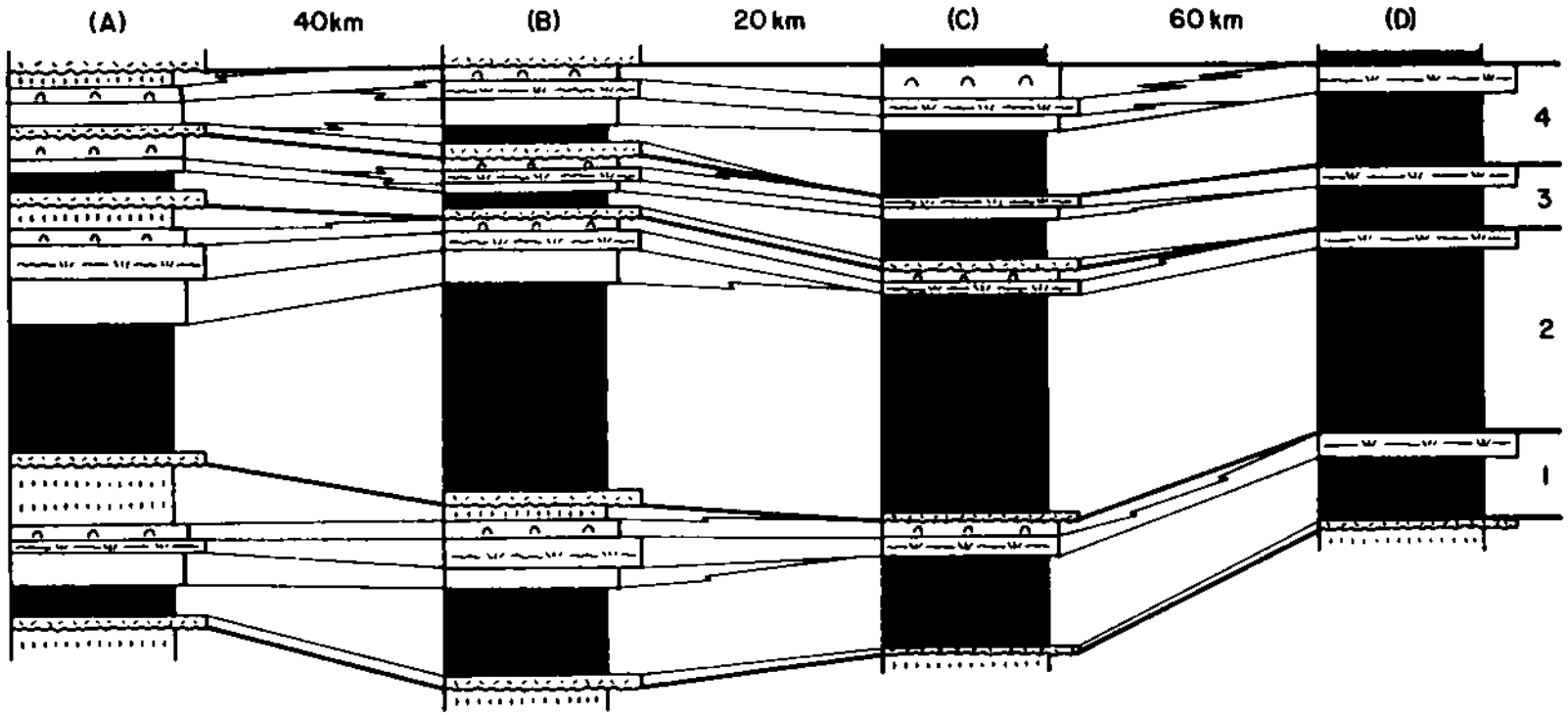

MICRODIGITATE TUFA

DOMAL STROMATOLITES

EDGEWISE CONGLOMERATE

THICK-LAMINATED DOLOSILTITE

ARGILLACEOUS DOLOLUTITE ± QTZ. & DOLO. SILT/SAND

INTRACLAST PACKSTONE

EROSIONAL SURFACE

CYCLE BOUNDARY

FACIES BOUNDARY

10

5

0 m

(cf. Carr, 1982). Abundance of specific facies depends mostly on proximity to the western margin of the shoal-complex, and to a minor extent on cycle thickness. Cycles are bounded by erosional surfaces which become less pronounced away from the shoal-complex.

Intraclast Packstone Lags: Lags form sheets (5 to 30 cm thick) that cover erosional tops of cycles. They consist of reworked fragments (Fig. 20a) derived from the top bed of the underlying cycle, which is tufa and cryptalgalaminite over most of the inner-shelf, except near the eastern limit of cycles where erosional surfaces sit directly on stromatolitic dolomite and lags consist of reworked stromatolite fragments. Clasts generally are well rounded, platy, and less than 1 to 2 cm, although some larger fragments may be up to 10 to 20 cm wide. Grain size commonly decreases upwards. Rarely, small ooids and peloids of glauconite are present. In shale-based cycles, lags are overlain by argillaceous dololutite or siliciclastic siltstone/sandstone; lags separating dolosiltite-based cycles are overlain by thick-laminated dolosiltite or stromatolitic dolomite.

Intraclast packstone lags are initial transgressive sediments, deposited as sheets covering tidal flat lithologies. Brecciated fragments developed during vadose

diagenesis and incipient soil development were reworked in the swash zone during transgression to form smaller, well-rounded clasts with rare oolitic coatings. Glauconite peloids were formed during the hiatus following initial transgression and the onset of subtidal sedimentation.

Intraclast Grainstone/Packstone: These are rare basal deposits of inner-shelf cycles formed behind the younger rims, but abundant in cycles which are laterally equivalent to the lower non-cyclic interval. They commonly overlie erosional surfaces of underlying cycles and pass upwards into thick-laminated dolosiltite or stromatolitic/thrombolitic dolomite. Beds are 50 to 100 cm thick, generally massive, with local cross-bedding.

Beds of intraclast grainstone/packstone formed following submergence of the shoal-complex during cyclic transgression. Wave-generated currents probably caused eastward transport and dispersal of coarse, clastic carbonate over the inner-shelf.

Mixed Carbonate/Siliciclastic Facies: This facies consists of interstratified (1 to 5 cm) argillaceous dololutite, minor dololutite/dolosiltite and siliciclastic mudstone (Fig. 20b). Non-graded and normally-graded laminae are present, and climbing-ripple and wave-ripple lamination is common. These lithologies contain intercalated sheets

and lenses of dolarenite and siliciclastic siltstone/sandstone (up to 30 cm thick) that are massive, planar-laminated or hummocky cross-stratified (Fig. 20c), and capped by climbing-ripple or wave-ripple cross-laminae. Generally, siliciclastic sand and silt increases eastward, and clastic carbonate increases westward and upward within cycles.

Argillaceous laminae are red to olive-gray whereas dolomitic laminae are brownish-yellow to dull-orange. Color of argillaceous laminae is related to the degree of foreland metamorphism (Lucas, 1984), the brighter shades of red corresponding to lowest metamorphic grade and approximating original color. Most sediments are disrupted by synaeresis dikes (Fig. 20b) which are distinguished from desiccation cracks on the basis of numerous mud-filled cracks in coarse layers which open downwards and are filled from below, lack of systematic relationship of cracks to bedding, and absence of mud-chip conglomerate (cf. Hoffman, 1975; Grotzinger, 1981; Soegaard, 1984). Skeletal halite casts are common in siltier laminae; argillaceous layers are compacted around casts indicating growth of skeletal crystals before or during compaction.

Shale-based cycles formed on the inner-shelf when flats were deeply submerged following maximum transgression, and

carbonate silts and muds were deposited along with siliciclastics transported from the eastern shoreline. Parts of the sea floor more proximal to the eastern shoreline received abundant siliciclastic sandstone and siltstone as storm deposits. Thin Bouma sequences in dolarenites and siliciclastics indicate deposition of entrained sediment below storm wave-base by storm-surge ebb or gradient currents (Allen, 1981), whereas hummocky cross-stratified deposits reflect reworking of sediment above storm wave-base by oscillatory shear currents (Hamblin and Walker, 1979). The presence of both sorts of deposits indicates that water depths at maximum transgression were close to storm wave-base.

Siliciclastics may have been transported from the eastern shoreline of the lagoon by wind-forced geostrophic currents, and storm-surge ebb currents either as bed load or in turbidity flows. With regard to transport of sediment from shoreline to final depositional site, bedload transport would occur incrementally over the course of several storms, whereas turbidity transport would occur during one storm (Walker, 1985). Turbidity flows are driven by gravity and therefore would move directly offshore and across the shelf, unlike currents driven by hyraulic pressure and Coriolis forces which would evolve into geostrophic flows parallel to shoreline.

The mechanisms by which shelf sediments are transported over 300 to 400 km (width of Rocknest "lagoon") are poorly understood (Walker, 1985). However, it seems that a combination of wind-forced currents, storm-surge ebb currents and turbidity currents may have been responsible for transporting siliciclastics from the eastern shoreline, across the submerged craton to the western lagoon. Once deposited, storm-generated oscillatory shear currents reworked sediments into hummocks.

Synaeresis structures were formed during plastic deformation of sediments, probably during sediment dewatering and compaction. Skeletal halite was precipitated from hypersaline brines generated in the shoal-complex, percolating down through sediments as tidal flats prograded over subtidal lithologies.

Thick-Laminated Dolosiltite: This facies overlies argillaceous dololutite in shale-based cycles or forms beds above basal lags in some carbonate cycles. It consists of non-graded, laminated dolosiltite (1 to 3 cm thick), that contains abundant wave ripples (Fig. 21a). Intercalated beds (1 to 10 cm thick) of dolarenite and sub-vertically packed sheets of edgewise conglomerate (Fig. 21b) are common and increase in abundance upwards. Conglomerates form polygonal mosaics in plan view and locally are overlain by

wavy, irregular cryptalgalaminite. Dolosiltites contain skeletal halite casts and grade up into cryptalgal dolomite or tufa.

The upward increase in clastic carbonate beds within shale-based cycles, culminating in continuous thick-laminated dolosiltite, indicates progressive migration of the carbonate tidal flats over deeper lagoonal sediments. Thick-laminated dolosiltites accumulated close to fairweather wave-base and have abundant wave ripples and edgewise conglomerates. Carbonate-based cycles that have thick-laminated dolosiltite as basal (deepest water) deposits were only submerged to fairweather wave-base at the maximum extent of transgression.

Stromatolitic/Thrombolitic Dolomite This facies includes both stromatolitic and thrombolitic dolomite. Most cycles contain linked to partially linked stromatolitic domes (10 to 150 cm wide) with smooth-laminated to tufa-laminated or fenestral-laminated microfabrics (22a). Domes are circular or rarely eliptical in plan view. Generally, synoptic relief of domes decreases upwards, whereas linkage between domes increases. Microfabrics change upward from smooth-laminated to tufa-laminated in most cycles capped by tufa, but may also become fenestral-laminated. Well developed fenestral fabrics are restricted to several beds in the upper Rocknest Formation.

Columnar stromatolites are common in the inner-shelf sequences behind the younger rims, but are rare in the inner-shelf sequence behind the lower rim. They are regionally extensive markers, and used for correlating cycles. Forms include isolated to partially-linked, and branching columns (Fig. 22b). Internal lamination varies from curved to box-shaped or cone-shaped (Fig. 32a), and microfabrics are smooth-laminated or fenestral. In plan view columns are circular to rarely eliptical. Columnar stromatolites may grade up into domal stromatolites with similar microfabrics. In branching columnar stromatolites, daughter columns may be parallel, weakly divergent or strongly divergent.

Thrombolites are rare except in one interval of the Rocknest Formation where they are domes, columns, or branching columns (Fig. 22c). The microfabric consists of isolated or connected clots, defining a very crude internal lamination (Fig. 32b). Clots have irregular to wavy concentric internal lamination that contrasts with the massive internal structure of clots in Cambrian and Ordovician thrombolites (Aitken, 1967; Bova, 1982; Pratt and James, 1982).

Stromatolitic/thrombolitic dolomite formed when the sediments shoaled into the upper subtidal and intertidal

Figure 32. Conical stromatolites and thrombolitic microfabric. A) conical columnar stromatolites. B) photomicrograph of thrombolitic fabric. Note crude lamination (dotted line) defined by clots (C) and fenestral voids (V).

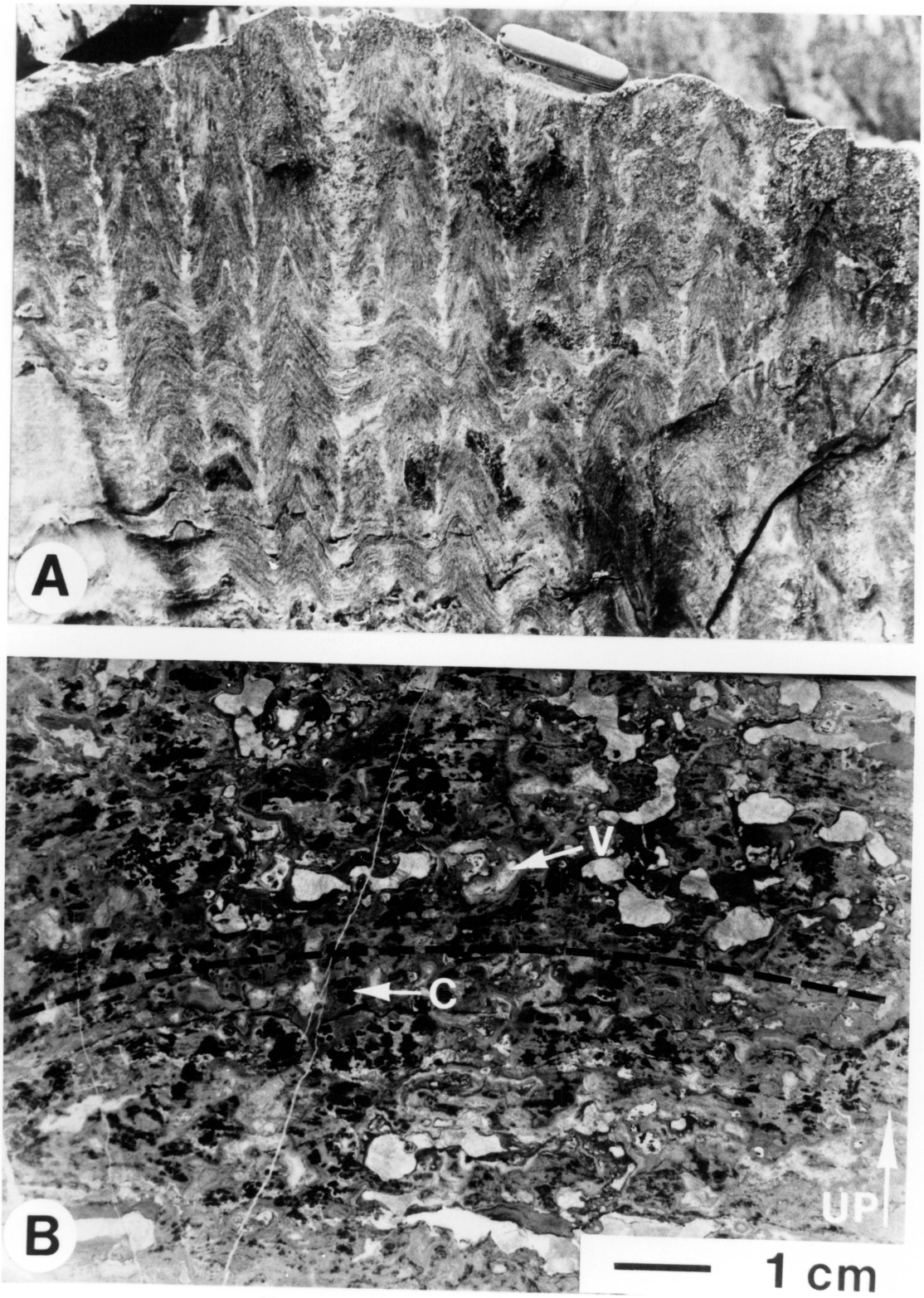
A
B
V
C
UP
1 cm

zone. Columnar stromatolites and thrombolites formed in zones of greater wave agitation than linked domal stromatolites. Columnar forms are restricted to the western and central part of the inner-shelf and pass laterally into domal forms of the eastern inner-shelf. This spatial zonation in stromatolite morphology may relate to regional variations in the ambient wave-energy of the "lagoon". During each cycle, emergence of the shoal-complex behind the rim marked the onset of tidal flat progradation, during which time the "lagoon" was 250 to 300 km wide and wave energy was greatest due to large fetch. Columnar forms grew due to extensive wave reworking between heads, preventing linkage. However, after progradation of tidal flats the "lagoon" was much narrower (50 to 100 km), and the smaller fetch decreased wave energy. Consequently, cryptalgal structures growing in the intertidal zone were not subjected to intense erosion between heads, promoting extensive linkage between heads and the development of linked domes.

During formation of either columns (broad "lagoon") or domes (narrower "lagoon"), wave energy was not sufficiently intense or sufficiently prolonged to cause significant elongation of cryptalgal structures. Modern elongate stromatolites result from sustained wave attack from one direction, induced by the local trade winds (Logan et al,

1974). Lack of significant elongation of Rocknest "lagoonal" stromatolites and thrombolites is consistent with northeasterly-directed (present day coordinates) paleotrade-winds (Hoffman et al., 1983). The western shoreline of the "lagoon" was protected in the lee of the shoal complex, and characterized by low wave energy (except intermittently during storms). The upward decrease in synoptic relief of cryptalgal structures indicates continued shoaling into the upper intertidal zone where cryptalgalaminites or tufas formed.

Cryptalgalaminite: Cryptalgalaminites generally are uncommon, but locally form beds 10 to 120 cm thick capping cycles, or as layers beneath laminated or microdigitate tufa beds. They are tan to buff colored, finely-laminated, flat to irregularly layered dolosiltite and dololutite in which laminae are continuous over a few meters, but locally are scoured and contain thin intraclast layers. Irregular to laminoid fenestrae, desiccation cracks, tepee structures, abundant silica pseudomorphs after displacive halite, and rare pseudomorphs after gypsum and possibly anhydrite occur.

Cryptalgalaminites formed in the upper intertidal to supratidal zone when shoreward transport of clastic carbonate was high. Smooth algal mats trapped and bound loose, storm-deposited silt/mud layers which were desiccated

to form cracks and small tepee structures. Evaporation of pore fluids generated hypersaline brines which precipitated halite, and rarely, gypsum or anhydrite.

Tufas: The tufas described here are similar to those of the western shoal-complex, described previously. However, microdigitate tufas are more abundant and all are dark-gray to black and extensively silicified (Fig. 33). Commonly, tufas contain thin interlaminae of clastic dololutite and dolosiltite which also forms the fill between columns in microdigitate tufas. Clastic interlaminae contain silica pseudomorphs after displacive halite. Tufa beds contain desiccation cracks, very small tepees (less than 15 cm relief), and thin (10 to 20 cm thick) brecciated intervals below tops of cycles.

Tufas formed higher up on the flats, landward of cryptalgalaminites, where influx of clastic carbonate was low enough to allow cement crusts (tufas) to form by precipitation of aragonite. Epilithic microbes were probably essential in creating geochemical conditions favorable for precipitation of tufas, similar to Tertiary and Holocene travertine and tufa (cf. Esteban and Klappa, 1983). Microfossils have been found in silicified clastic carbonate associated with microdigitate tufa (Hofmann and Grotzinger, in prep.)

Figure 33. Varieties of Rocknest tidal-flat tufa. A) microdigitate. B) Laminar to incipient microdigitate (I), associated with oncoliths (O), also composed of laminar tufa. C) Laminar tufa forming small tepee structure. D) Digitate structures forming adjacent to laminar tufa. Over 90% of the rock in this photograph was formed by precipitation of carbonate, probably aragonite.

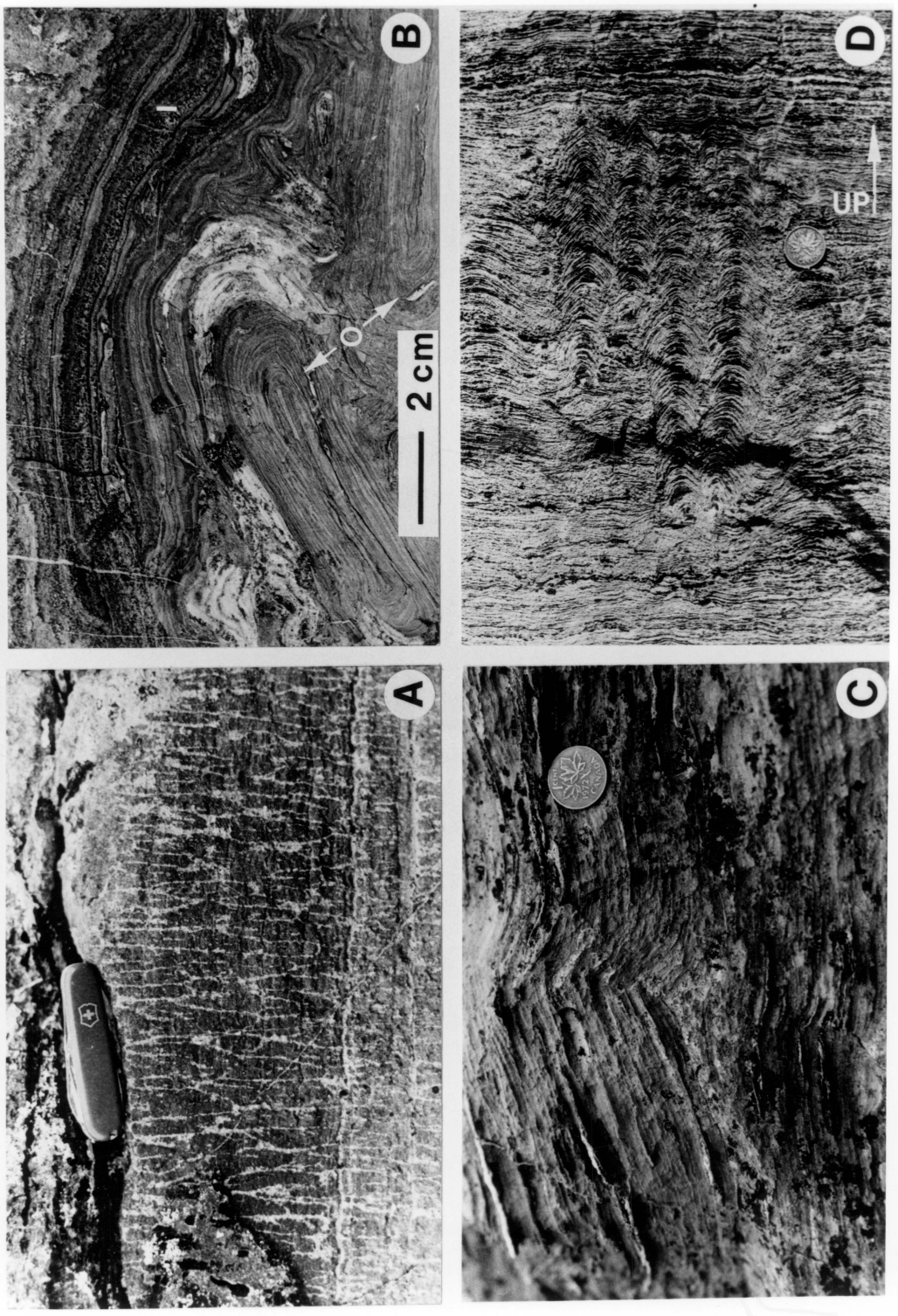
A
B
2 cm
C
D
UP

The dark-gray to black color of tufas over much of the Rocknest shelf indicates that these crusts were organic-rich, with preservation of organics into the burial environment. Such material probably escaped oxidation in the supratidal vadose zone because it was entombed in coatings of carbonate cement. However, near the western margin of the shoal-complex, a thicker vadose zone and more prolonged exposure oxidized organics during low sea-level stands, to form light colored tufas.

Evolution of Cyclic Inner-Shelf

Asymmetric cycles formed by rapid submergence of the inner-shelf followed by gradual shoaling to sea-level. Cycles were initiated by rapid transgression and flooding of carbonate tidal flats flanking the eastern margin of the shoal-complex, followed by eastward expansion of the shoal-complex and slow progradation of tidal flats over "lagoonal" facies of the inner-shelf. At the end of each progradation event the shoal-complex had a maximum width of over 200 km, which shrank following each transgression to a minimum width of 1 to 5 km for the shoal-complex behind the older rim, and became completely submerged behind each of the younger rims. Behind the lower rim, the shoal-complex was still subaerially exposed after most transgressive events.

However, behind the upper rims, the shoal-complex was submerged after transgressive events. In that case, initial shallowing by sedimentation took place immediately behind the rim, and was followed by progradation of tidal flats away from the shoal-complex towards the inner-shelf "lagoon" to the east.

CYCLE DEVELOPMENT IN THE GEOLOGIC RECORD: A DISCUSSION OF MECHANISMS

Autocyclic Mechanism

Shallowing-upward cycles (1 to several 10s of m) in carbonate rocks can be produced by autocyclic or allocyclic mechanisms (Ginsburg, 1971; Wilson, 1975; Wilkinson, 1982; Mathews, 1984; James, 1984a). Cyclicity within the autocyclic model is essentially intrinsic, involving feedback interactions between different parts of the system. Several variations on the autocyclic mechanism have been proposed (Ginsburg, 1971; Wilkinson, 1982), but all are ultimately controlled by the rate of carbonate sedimentation as a function of source area size. Sedimentation takes place on a stable shelf of fixed width, subsiding at differential but constant rates, and under stationary or slowly rising sea-level. Carbonate sediments are produced

in an initially large subtidal area and transported landward (Ginsburg, 1971), resulting in tidal flat progradation. During progradation, the subtidal area (or "carbonate factory") is gradually reduced in size until it fails to provide sufficient sediment to the prograding wedge, and sedimentation is arrested. Finally, background differential subsidence combined with stalled sedimentation results in relative sea-level rise over the platform until water depths are once again deep enough to efficiently generate sediment. This starts the next cycle of progradation. As such, rapid shoaling occurs during progradation and slow deepening occurs during non-depositional, submarine hiatus; most time in a cycle period is represented by the cycle boundary. Autocycles should only be affected by minor vadose diagenesis, related to shallow depression of the water table by evaporative drawdown (cf. Read, 1973).

The autocyclic model is popular because it does not require "sudden" eustatic changes in sea-level or subsidence (James, 1984a), nor does it predict global synchroneity of sea-level oscillation. However, some consequences of the autocyclic model are: 1) progradation can only occur if there is differential subsidence across the platform, 2) progradation must proceed in the direction of increasing subsidence, 3) cycles must always shoal to sea-level, and 4)

cycles should not be significantly affected by vadose diagenesis. Therefore, cycles should be wedge-shaped and show evidence of progradation in the direction of increasing subsidence (cf. Wilkinson, 1982, Fig. 5); contrary evidence would support an allocyclic model. Although some cyclic sequences have been shown to prograde in the direction of increasing subsidence (eg. Lohman, 1976), others clearly prograde in the direction of decreasing subsidence (both grand and small cycles of Aitken, 1978; Koerschner, 1983; Goldsmith, pers. comm; and this study). The latter can only be explained by an allocyclic model.

Furthermore, the autocyclic model has a fundamental weakness in that it fails to adequately explain the transition from prograded platform to submerged platform (ie. the cause of transgression). If progradation rate is only controlled by the rate of sedimentation (implicit in autocyclicity), then certainly it must be highest when the subtidal source area is largest, decreasing with time as the area of the "factory" is reduced. In this system, the direct feedback relationship between sediment supply and progradation requires that the system approach a state of dynamic equilibrium; the prograding wedge will reach a point where the limit of production is such that the tidal flats will remain more or less stationary and track subsidence.

Any advance will be negatively reinforced by slackened production, while an equal retreat will be negatively reinforced by increased production. It is difficult to find any cause or reason for shelf transgression in the autocyclic model. Under such conditions, the carbonate shelf should not be cyclic at all, rather dominated by thick tidal flat deposits.

Also, even if sedimentation was arrested so that transgression could occur, it is unlikely that deepening could occur because subsidence rates on cratons (1 to 5 cm/1000 yrs) and mature passive margins (5 to 10 cm/1000 yrs), where most cyclic carbonates form, are too low to generate sufficient water depths within a reasonable amount of time. For example, at 5 cm/1000 yrs, it would take 20,000 yrs to generate 1 m of water depth. Generating water depths of several meters (typical of subtidal facies of cycles) is difficult with an autocyclic model.

Finally, the autocyclic model cannot explain incomplete shoaling to sea-level. Autocycles must shoal to sea-level in order for carbonate production and progradation to be arrested. Theoretically, progradation should continue to a limit where carbonate production is decreased due to several possible effects (eg. water too shallow; water too deep; siliciclastic influx too high). Since many cycles of

different sequences (eg. this paper; Anderson, et al., 1984) show arrested progradation (incomplete shoaling) before having reached their potential limit, factors other than shoaling to sea-level must be involved in ultimately causing submergence events.

Allocyclic Mechanisms

Cyclicity within the allocyclic model has an extrinsic control, where sedimentary cyclicity is controlled by the forcing effect of an external cyclic or rhythmic system. Fundamentally, the allocyclic model invokes changes in relative sea-level caused by episodic subsidence or eustatic sea-level changes. Consequently, an external control on submergence events can result in premature arrest of prograding tidal flats, and incomplete shoaling of the shelf to sea-level. As in the autocyclic model, progradation occurs in response to deposition of sediment on tidal flats, derived from a subtidal source area. Eustatic sea-level may remain stable if cyclicity is related to periodic subsidence, or falls if eustatically controlled, or any combination of both variables.

Episodic Subsidence: In the episodic subsidence model, progradation is arrested by sudden submergence of the shelf during rapid, incremental subsidence events. Transgression

occurs, initiating a new cycle, followed by progradation and shallowing to sea-level. This model may be tenable for rift basins where intermittant downfaulting results from relief of tensional stress during extension of the crust. Similarly, it may also apply to foredeeps which subside in response to episodic loading of the lithosphere by thrust sheets. Cyclic sequences are known from rift (eg. Jackson and Ianelli, 1981; Aigner, 1984) and foredeep (eg. Read, 1980) settings. However, it is unlikely that such episodic subsidence of 10^4 to 10^5 yrs is important in passive-margin settings, or occurs at all in craton interiors. There, subsidence may occur primarily in response to thermal cooling of uplifted and thinned crust (Sleep, 1971), uniform stretching of the lithosphere (McKenzie, 1978), non-uniform extension of the lithosphere resulting in preferential thinning of lower crust and/or subcrustal lithosphere (Royden and Keen, 1980), and isostatic adjustment due to sediment/water loading (Bond and Kominz, 1984). None of these mechanisms are known to cause episodic subsidence with a period of 10^4 to 10^5 yrs.

Eustatic Causes: A eustatic model for cyclicity probably fits the data best, because other models do not predict significant vadose diagenesis. In the eustatic model, sea-level commonly will drop below the surface of the

platform during each progradation event. Cycles in the Rocknest Formation (particularly in the shoal-complex), and many other cyclic sequences (eg. Permian of west Texas, Triassic of Italy, Cambro-Ordovician of Appalachians) have vadose profiles characterized by large tepees, pisolite, crystal silt, and stalactitic botryoidal aragonite (now dolomite).

Eustatic models generate fluctuations in relative sea-level by oscillations in absolute sea-level and the model is applicable to carbonate platforms in all tectonic settings. Eustatic oscillations in sea-level may arise from changes in climate, which control global ice volume (Hays et al., 1976), changes in the geoid (Morner, 1976), or from changes in the rate of sea-floor spreading (tectono-eustacy; Pitman, 1978).

Tectono-Eustatic Cause: Tectono-eustacy has been important in causing changes (up to 350 m) in Mezozoic and Cenozoic sea-level that occur over periods of 10^7 to 10^8 yrs (Vail et al., 1977; Pitman, 1978). However, it is doubtful that changes in spreading rates over the much shorter period (10^4 to 10^5 yrs) required to produce small-scale cycles in carbonates. Furthermore, the maximum rate of sea-level change due to alteration of the geometry of the mid-ocean ridge system is approximately 1 cm/1000 yrs (Pitman, 1978).

This rate is insufficient to drown or submerge carbonate platforms (Schlager, 1981), and 10 to 1000 times slower than the rates created by waxing and waning of global ice-volume. Therefore, changes in the volume of mid-ocean ridges can be considered as only having a negligible influence on generating small-scale cycles.

Glacio-Eustatic Cause: Glacio-eustatic driven changes in sea-level is the most powerful mechanism for generating cyclic sequences similar to those seen in the Rocknest Formation and elsewhere (eg. Fischer, 1964). In this model, changes in sea-level result from changes in global ice-volume, caused by climatic fluctuations (Hays et al., 1976). These climatic fluctuations are in turn forced by changes in Earth's orbital geometry (Milankovitch hypothesis; Berger, 1980). Essentially, global ice-volume waxes and wanes over the scale of 20,000 to 100,000 yrs in response to variations (of the same period) in the seasonal and latitudinal distribution of incoming solar radiation. These fluctuations in insolation are probably due to changes in precession of Earth's axis (period = 21,000 yrs), obliquity of its equatorial plane (period = 40,000 yrs), and eccentricity of its orbit (period = 100,000 yrs).

Ice volume fluctuations throughout the late Pleistocene have been dominated by a periodic oscillation of 100,000

yrs, and at less strongly defined periods corresponding to the 21,000 yr precession and 40,000 yr obliquity cycles (Hays et al., 1976). However, the dominance of the 100,000 yr period in the Pleistocene record is surprising because the strength of the astronomical forcing at this period is negligibly small (Imbrie and Imbrie, 1980). The answer to this apparent paradox lies in the relationship between input (changes in insolation) and output (changes in sea-level) spectra. Precession and obliquity have linear (direct) effects on the forcing of changes in insolation and changes in ice volume. However, eccentricity must have a nonlinear (indirect) effect on the forcing of changes in insolation and changes in ice volume (Hays et al, 1976; Peltier and Hyde, 1984). Apparently, the eccentricity cycle strongly modulates the precession cycle such that insolation anomalies at times of high eccentricity are 3 to 4 times greater than at times of low eccentricity (Imbrie and Imbrie, 1980).

Hays et al.(1976) suggest that periods of ice melting (transgression) may have occured within as little as 10,000 yrs (10% of cycle period). Galcio-eustatic changes during the late Pleistocene were probably on the order of +70 to -130 m, relative to present levels (Morner, 1976), suggesting that rates of sea-level change may have been very

fast. For a deglaciation period of 10,000 yrs and sea-level amplitude of 100 m, it is possible that some late Pleistocene transgressions could have occured at rates of 10 m/1000 yrs, which is sufficiently fast to drown carbonate platforms, including reefs (Schlager, 1981).

In summary, the glacio-eustatic model is well tailored for generating small-scale carbonate cycles. First, oscillations in sea-level are asymmetric, favoring relatively slow sea-level fall and progradation, followed by rapid transgressions. Second, transgressions are fast enough to effectively terminate carbonate production and cause submergence. Third, sea-level fall below the platform surface explains the development of vadose profiles ranging from incipient soils to thick tepee/pisolite sequences. Fourth, a glacio-eustatic control can explain why many shallowing-upward cycles do not shoal completely to sea-level in that the period of sea-level oscillation dictates how far tidal flats may prograde between submergence events. Fifth, glacio-eustacy is forced by perturbations in Earth's orbit on the scale of 20,000 to 100,000 yrs; this predicts that if small-scale carbonate cycles are glacio-eustatic, they should have a similar period. Periodicities for several cyclic sequences ranging in age from early Proterozoic through Triassic fit that range. They are:

18-30,000 yrs/cycle (Grotzinger, this paper), 50,000 yrs/cycle (Fischer, 1964), 60,000 yrs/cycle (Koerschner, 1983), and 100,000 yrs/cycle (Bova, 1982).

Amplitude of Eustatic Oscillations: Although the range in period of shallowing-upward cycles in several sequences is supportive of astronomic orbital forcing of glacio-eustatic oscillations in sea-level, the apparent range of oscillation amplitude is not. Most small-scale shallowing-upward cycles probably developed in response to sea-level oscillations with less than 10 m amplitude (Read et al., in prep.) Here, the Quaternary is not applicable in that it was dominated by large-scale fluctuations in amplitude (100 m), which produced drowning of platforms (rather than shallow submergence), followed by subaerial exposure so that "cycles" consist of disconformity bounded units with intense vadose diagenesis on the inner shelf, or pelagic facies capped by thin oolite layers or shallow-water muds on the outer shelf (eg. late Pleistocene of Campeche Platform; Logan et al., 1969). Given the very low slopes of most platforms (5 to 25 cm/km), the rates of eustatic sea-level fall could produce shoreline regression rates of 65 km/1000 yrs. Regression would outpace any attempt by the subtidal source area to supply sediment to tidal flats, resulting in stranding of tidal flats near high sea-level stand, if they

were ever produced at all. Consequently, an explanation for the production of lower amplitude glacio-eustatic cycles must be sought.

The present distribution of the continents is very favorable for production of large ice sheets (Berger, 1980). Latitudes greater than 60 degrees north are particularly sensitive to climatic changes produced by perturbations in precession of the Earth's axis (Imbrie and Imbrie, 1980). As there are presently large areas of continental mass at latitudes above 60 degrees north (the case since the earliest Tertiary), this has led to major glaciations in the late Pleistocene and Holocene. Any change in distribution of landmass (or oceanic currents by implication) can effect the extent of glaciation, and consequently the range of sea-level oscillation (Peltier and Hyde, 1984; Berger, 1980). By reducing the amount of land north of this climatically sensitive latitude or altering oceanic currents, the magnitude of sea-level oscillations will be proportionally decreased. For example, during the Tertiary, when it is likely that Antarctica was the only site of major glaciation, deep-sea core data record sea-level oscillations with periodicities between 20,000 and 100,000 yrs, but amplitude is reduced by 30 to 50 m compared to the late Pleistocene (Major and Mathews, 1983; Mathews, 1984).

Accepting continental drift for the Phanerozoic through late Archean (Hoffman, submitted) and that continental glaciation has occurred intermittantly since at least 2.2 Ga (Gowganda tillite; Miall, 1983), which spans the range of known cyclic carbonates, it is reasonable to assume that there may have been times when small-scale glacio-eustatic oscillations in sea-level occurred in response to limited continental glaciation. However, given the area of Earth poleward of 60 degrees, it seems likely that on the average, continents were not in a favorable position for glaciation; eustacy in response to formation of continental ice sheets should have been an exception.

However, alpine glaciation may have been important in that mountain belts are sites of limited glaciation and are very sensitive to climatic changes (Fairbridge, 1961). Thus, they have probably had some effect on sea-level throughout much of Earth history and since they can only store small amounts of ice, sea-level fluctuations have probably been small. Because small-scale carbonate cycles probably formed in response to low amplitude changes in sea-level, it is likely that they may be produced by alpine glaciation as well as limited continental glaciation. Modelling of eustatic-induced, low-amplitude cyclicity can account for most small-scale shallowing-upward cycles in the carbonate rock record (Read et al., in prep).

Period of Glacio-Eustatic Oscillations: Certain latitudes are more sensitive to insolation changes produced by the different astronomic forcing periods (Berger, 1980). Therefore, the period of glacio-eustatic oscillation is dependent on the location of continents and mountain belts with respect to latitude. Consequently, cycle periods will vary in length through time as a function of continental drift. Also, the period of sea-level oscillation depends on response time of lithosphere to ice-loading. In turn, response time is sensitive to mantle viscosity (Peltier, 1984). This suggests that in the pre-Phanerozoic, when a hotter Earth probably had a less viscous mantle, faster isostatic adjustment of ice-loads and shorter cycle periods may have occurred.

There also may be a long-term secular trend in the period of precession, obliquity, and eccentricity orbital parameters. Because these effects result from gravitational interactions between the Earth, Sun, and other planets (Berger, 1980), it may be possible that these relationships have evolved through time, similar to the decay of rate of Earth spin.

Geoidal Cause of Eustacy: The effects of the ocean geoid (or geodetic sea-level) as an independent cause of eustatic oscillations, and as an influence on the amplitude

and period of glacio-eustatic oscillations must be considered. The geoid may change laterally or vertically through time. The geoid is a function of Earth's gravity, in turn a function of its structure, density, and rotation. The present geoid is highly irregular, with maximum deviations of up to 180 m in sea-level between New Guinea and Maldive Islands, although most relief does not exceed 50 to 60 m and is commonly just a few meters (Morner, 1976; 1983). Since geoidal changes can occur over the period of 10,000 to 100,000 yrs or less (Morner, 1976), it is reasonable to assume that for any given shelf in time, over a scale of 20,000 to 100,000 yrs, glacio-eustatic sea-level changes might be influenced by migration of the geoid. In any cyclic sequence, the fundamental range in thickness (ie. 1 to 10 m, rather than 0.1 to 1 or 10 to 100) and periodicity (ie. 20,000 to 100,000 yrs, rather than 2,000 to 10,000 or 200,000 to 1,000,000) of cycles is probably determined by astronomic orbital periods and position of continents and mountain belts with respect to climatically sensitive lattitudes. Variance within the given ranges of cycle thickness and period is probably due to "noise" within the climatic system (one glaciation not being as extensive as the next, etc.), interference due to migration of the geoid and longer-term changes in sea-level, and fluctuations

in subsidence rate. Most importantly, the small-scale glacio-eustatic sea-level changes proposed in this paper (and many other eustatic changes for that matter) may not be globally correlative.

The geoid may also change directly in response to perturbations of the astronomic variables. Because the geoid is strongly influenced by Earth's rotation, which is in turn affected by the astronomic variables (particularly precession), it is possible that geoidal oscillations in sea-level may be possible at the astronomic periods (Morner, 1981).

MECHANISMS OF CYCLE DEVELOPMENT IN ROCKNEST FORMATION

Quantification of Parameters Controlling Cycle Development

Calculation of cycle period, amplitude of sea-level oscillation, slope of the inner-shelf at high and low sea-level stands, and progradation rates of tidal flats is important in identifying the mechanism(s) responsible for cyclic sedimentation. Calculations are only made for "complete" cycles of the lower Rocknest Formation, which are most accurately constrained.

Cycle Period: Average cycle period is calculated given the following:

10 to 15 m.y. = Duration of Epworth passive margin

4.0 to 4.6 km = Minimum & maximum values for decompacted thickness of passive-margin sequence

1.3 to 1.45 km = Minimum & maximum values for decompacted thickness of Rocknest Formation

140 to 160 = Minimum & maximum number of cycles in Rocknest Formation

1) Average Subsidence Rate of Passive Margin:

4.6 km ÷ 10 m.y. = 46 cm/1000 yrs = maximum average rate
4.0 km ÷ 15 m.y. = 27 cm/1000 yrs = minimum average rate

2) Duration of Rocknest Formation:

1.3 km ÷ 46 cm/1000 yrs = 2.8 m.y. = minimum duration
1.45 km ÷ 27 cm/1000 yrs = 5.4 m.y. = maximum duration

3) Cycle Period:

2.8 m.y. ÷ 160 cycles = 18,000 yrs/cycle = minimum period
5.4 m.y. ÷ 140 cycles = 39,000 yrs/cycle = maximum period

This minimum and maximum range of values for the estimated cycle period includes all cummulative error involved in the calculations. Because the Rocknest Formation comprises the upper part of the passive-margin sequence, its subsidence rate was probably less than the average for the passive margin, assuming that passive-margin tectonic subsidence decays with time (eg. Sleep, 1971).

However, because the mechanism(s) for tectonic subsidence of the Epworth passive margin has not been identified (thermal cooling alone is too slow; P.F. Hoffman, pers. comm., 1984), it is difficult to assess the error due to this effect. However, even if Rocknest subsidence was 25% slower than the passive-margin average, this would only shift the period range from 18,000 to 39,000 yrs, to 23,000 to 51,000 yrs, producing a maximum range (for all calculations) of 18,000 to 51,000 yrs.

Although the minimum (18,000 yrs/cycle) and maximum (51,000 yrs/cycle) values for average cycle period span a large range, the fact that these are 10^4 yr cycle periods is important, because this range is typical of values reported for cyclic perturbations of Earth's orbit (20,000 to 100,000 yrs; Berger, 1980), known to have significantly influenced Pleistocene sea-level (Hays et al., 1976). The range of period provides evidence in favor of a glacio-eustatic control on Rocknest cyclicity. It is unlikely that relative sea-level changes over the shelf could produce such regionally extensive cycles with this period if related to autocyclic or other allocyclic (eg. episodic subsidence, tectono-eustacy) mechanisms.

For calculating the slope of the shelf interior and progradation rates of tidal flats, the range of 18,000 to

51,000 yrs/cycle is too broad. In order to narrow the range, it is assumed that the most likely age for the passive-margin sequence is 10 m.y. as suggested by Hoffman and Bowring (1984). This contrains the likely average cycle period at 18,000 to 30,000 yrs, assuming that Rocknest subsidence was 25% slower than average passive-margin subsidence. For the next section, averaged values for period (24,000 yrs) and subsidence (40 cm/1000 yrs) are used.

Amplitude: In cyclic sequences that form by eustatic changes in sea-level, erosional caps bounding cycles are produced only if the rate of sea-level fall exceeds subsidence rate, in which case sea-level drops below the platform surface, exposing it to subaerial weathering and vadose diagenesis. The rate of sea-level fall is controlled by amplitude and period of sea-level oscillation, and therefore allows estimation of minimum amplitude of sea-level oscillation. For a symmetrical oscillation, the rate of sea-level fall is (Amplitude) ÷ (Period). However, it is more likely that during one cycle, sea-level fall is longer than sea-level rise. For Pleistocene 100,000 yr oscillations in sea-level, the length of sea-level fall was commonly 85 to 90% of the total cycle period (Hays et al., 1976). If it is arbitrarily chosen that the duration of

sea-level fall is 70 to 90% of the cycle period, then the most likely range of minimum amplitude is approximately 7 to 9 m, given a 24,000 yr period and 40 cm/1000 yr subsidence rate (Fig. 34). Given the duration of sea-level fall, amplitudes must be greater than 7 to 9 m to get sea-level fall rates that are faster than subsidence rates. This will result in subaerial exposure of the platform and production of erosional capped cycles.

Estimating the maximum amplitude of sea-level for Rocknest cycles is more difficult, and only possible for the sequence below the lower non-cyclic interval, where the shoal-complex was permanently aggraded. Because the shoal-complex was never submerged below the upper intertidal zone during each cyclic transgression, it follows that sedimentation kept pace with sea-level rise to its maximum height during each oscillation. For the lower Rocknest, the average maximum amplitude of sea-level oscillation could not have been greater than the average thickness of shoal-complex cycles which record amplitude, minus subsidence that occurred during sea-level rise. These cycles are commonly 9 to 15 m thick (avg. 12 m), suggesting that the average maximum amplitude was approximately 10 m (12 m minus 1.9 m of subsidence during rise). This cannot be done for the upper Rocknest because the shoal-complex commonly was

Figure 34. Plot of cycle period vs. sea-level amplitude. A cycle period (24,000 yrs) is plotted along the lower horizontal axis. The percentage of time in that period (0 to 100% of 24,000 yrs) is plotted along the upper horizontal axis. Amplitude of sea-level oscillation is plotted along vertical axis. To find the minimum amplitude required for erosional caps, determine % of time involved in sea-level fall (70 to 90% of cycle period for Rocknest). Then, project down along arrows to curve (rate subs = rate sea-level fall), and then across to appropriate sea-level amplitude. This yields values where the rate of sea-level fall (determined by amplitude and duration of fall) is equal to rate of subsidence. Any amplitudes greater than this range will cause sea-level to drop faster than the subsiding platform, eventually causing subaerial exposure and erosion.

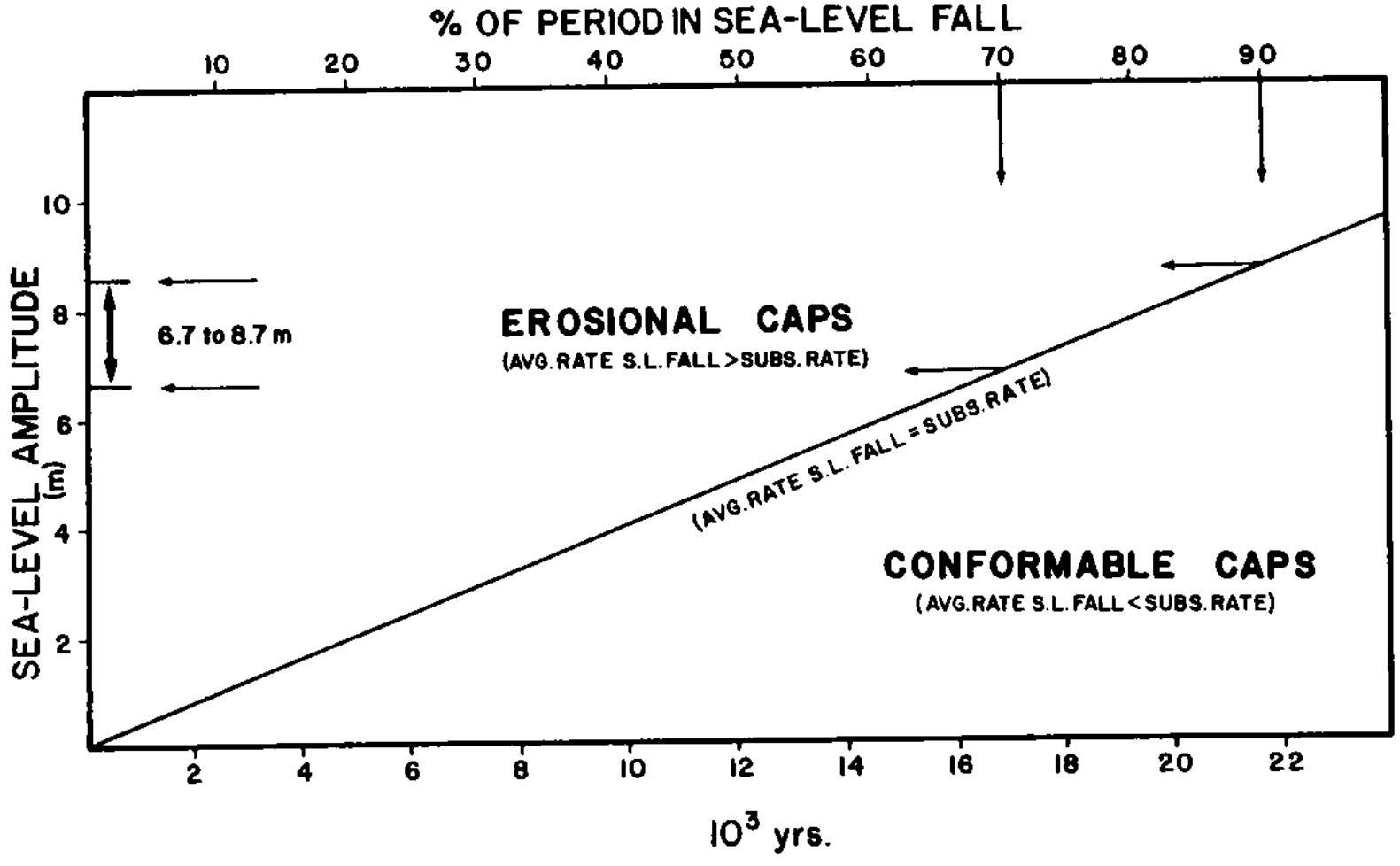
% OF PERIOD IN SEA-LEVEL FALL
10
20
30
40
50
60
70
80
90
SEA-LEVEL AMPLITUDE (m)
10
8
6
4
2
6.7 to 8.7 m
EROSIONAL CAPS
(AVG. RATE S.L. FALL > SUBS. RATE)
(AVG. RATE S.L. FALL = SUBS. RATE)
CONFORMABLE CAPS
(AVG. RATE S.L. FALL < SUBS. RATE)
2
4
6
8
10
12
14
16
18
20
22
10³ yrs.

submerged during each cyclic transgression, suggesting that amplitude may have been greater than cycle thickness, but probably not more than 15 to 20 m.

These calculations do not account for isostatic adjustment of the lithosphere due to sea-level rise. Therefore, true amplitudes probably are less than reported values. However, the calculations are still useful in that reported amplitude probably is close to the true fluctuation in water depth over the platform. This is because a water depth generated by an exaggerated amplitude without isostatic lowering of the platform, is probably similar (+ or - a few m) to a water depth resulting from a lower amplitude combined with isostatic lowering.

Inner-Shelf Slopes: Knowledge of sea-level amplitude and cycle thickness in the shoal-complex allows calculation of average inner-shelf slope and tidal flat progradation rate, given the across-strike distance over which tidal flat facies extend. Tidal flat facies (tufas and cryptalgalaminites) extend 120 to 150 km (avg. 135 km) eastward from the shoal-complex before passing into lower intertidal stromatolitic facies and subtidal thick laminites (Fig. 31). This transition marks the furthest point of tidal flat progradation and lowest sea-level stand, evidenced by lack of tidal flat facies and erosional cycle caps.

The average depositional slope at high sea-level stand during a cycle can be calculated using the height of the shoal-complex at high sea-level stand, divided by the distance over which tidal flats prograded (Fig. 35):

4) Height of shoal complex above inner shelf (135 km from shoal complex) at high sea-level stand = (thickness of shoal complex cycle - subsidence during rise) - (thickness of inner shelf layer*, 135 km from shoal complex - subsidence** during rise) = [12 m - (20% of period x 40 cm/1000 yrs)] - [0.8 m - (20% of period x 25 cm/1000 yrs)] = (12 m - 1.9 m) - (0.8 m - 1.2 m) = 10.5 m

   * layer is calculated assuming a 2,000 yr lag in sedimentation following transgression, and 30 cm/1000 yrs rate of sedimentation thereafter.

   ** subsidence on the inner-shelf, 135 km from shoal complex, was only 25 cm/1000 yrs (rather than 40).

5) Slope of inner-shelf (from shoal complex to limit of tidal flat progradation) at high sea-level stand = height of shoal-complex ÷ tidal flat progradation distance = 10.5 m ÷ 125 to 150 km (avg. 135 km) = 8 cm/km

The average depositional slope at low sea-level stand during a cycle can be calculated using the height of shoal-complex at low sea-level stand, divided by the distance over which tidal flats prograded (Fig. 35):

6) Height of shoal-complex above inner shelf (135 km from shoal complex) at low sea-level stand = (thickness of shoal complex cycle - subsidence during cycle) - (thickness of inner shelf cycle, 135 km from shoal complex - subsidence during cycle) = [12 m - (100% of period x 40 cm/1000 yrs)] - [6 m - (100% of period x 25 cm/1000 yrs)] = (12 m - 9.6 m) - (6 m - 6 m) = 2.4 m

7) Slope of inner-shelf at low sea-level stand = height

of shoal-complex ÷ tidal flat progradation distance = 2.4 m ÷ 135 km = 2 cm/km

Observed Rate Of Tidal-Flat Progradation: The observed rate of tidal-flat progradation is calculated using the distance over which tidal-flat facies extend, divided by the inferred duration of progradation (some fraction of cycle period):

8) Observed tidal flat progradation rate = distance of progradation ÷ duration of progradation = 135 km ÷ 19,200 yrs (duration of progradation = 80% of cycle period) = 7 km/1000 yrs

Expected Rate Of Tidal Flat Progradation: The expected rate of tidal flat progradation during sea-level fall may be calculated given effective rate of sea-level fall (true sea-level fall rate - subsidence rate* + sedimentation rate**), divided by observed slope (2 to 8 cm/km):

* subsidence rate is an average between shoal complex subsidence and that at 135 km to east.

** sedimentation rate at 135 km = average cycle thickness at 135 km (6 m) minus sedimentation during rise (0.8 m), divided by duration of fall.

9) Effective rate of sea level fall = true rate of sea sea level fall (amplitude ÷ duration of fall) - subsidence rate ÷ sedimentation rate = [10.1 m ÷ 80% of period] - [(40 cm/1000 yrs ÷ 25 cm/1000 yrs) ÷ 2] ÷ [5.2 m ÷ 80% of period] = 45 cm/1000 yrs

Assuming an average slope of 5 cm/km [(8 cm/km + 2 cm/km) ÷ 2], and effective sea-level fall rate of 45 cm/1000 yrs, the expected rate of tidal flat progradation can be calculated:

10) Expected rate of progradation = effective rate of sea level fall ÷ slope = (45 cm/1000 yrs) ÷ (5 cm/km) = 9 km/1000 yrs

The expected rate of tidal progradation (9 km/1000 yrs) is faster than the observed rate of progradation (7 km/1000 yrs). In part, the lack of agreement may be due to systematic errors in the calculation of subsidence, sedimentation, and true sea-level fall rates. It also may result from inability to resolve the evolving morphology of the inner-shelf during progradation, which changes shape and average slope through time (see Fig. 36a,b).

Development of Cycle Types and Profiles

Cycle types of the Rocknest Formation (Fig. 19) occur within three separate profiles which reflect different conditions of sea-level amplitude (Fig. 36a-d). During sea-level fall and development of a "complete" cycle profile (Fig. 36a-b), facies belts on the inner-shelf slope have constant water depth during migration, reflecting a balance between rate of sea-level fall, subsidence rate and sedimentation rate. The faster the rate of sea-level fall,

Figure 35. "Geohistory" diagram of Rocknest cycles. Plot is for cycles formed at shoal-complex, and cycles formed 135 km to east on the inner-shelf. Two succesive cycles (A,B) at each location are analyzed at high and low sea-level stand, calculating incremental sedimentation, incremental subsidence, and average depostional slope. 1) Initial high stand. Duration of sea-level rise was 20% of cycle period (4,800 yrs). Note greater amount of sedimentation and subsidence at shoal-complex to form cycle "A", in contrast with inner-shelf where "A" is much thinner. 2) Subsequent low stand. No further sedimentation has occurred at shoal-complex, which is now exposed in vadose zone because during sea-level fall, only 770 cm of subsidence occurred in contrast to 1000 cm of sea-level lowering. In contrast, most of cycle "A" formed during sea-level fall and the sediment surface has built up to low stand, but is not subaerially exposed. Note that the change in average depositional slope from 8 cm/km at high stand to 2 cm/km at low stand relates to sedimentation on shoal-complex ocurring primarily during sea-level rise, and sedimentation on inner-shelf occurring primarily during sea-level fall. 3,4) development of cycle "B" is identical to cycle "A" except that less sedimentation occurs at shoal-complex because of remnant topography. Thus, at the shoal-complex, cycle "B" is thinner than "A" (990 cm vs. 1190 cm) and all subsequent cycles formed after "B" will have thickness of "B". In general, for any platform, cycle thickness will almost always be somewhat less than true sea-level amplitude, unless the amplitude of sea-level oscillations is equal to or less than the amount of subsidence which can occur in one cycle period.

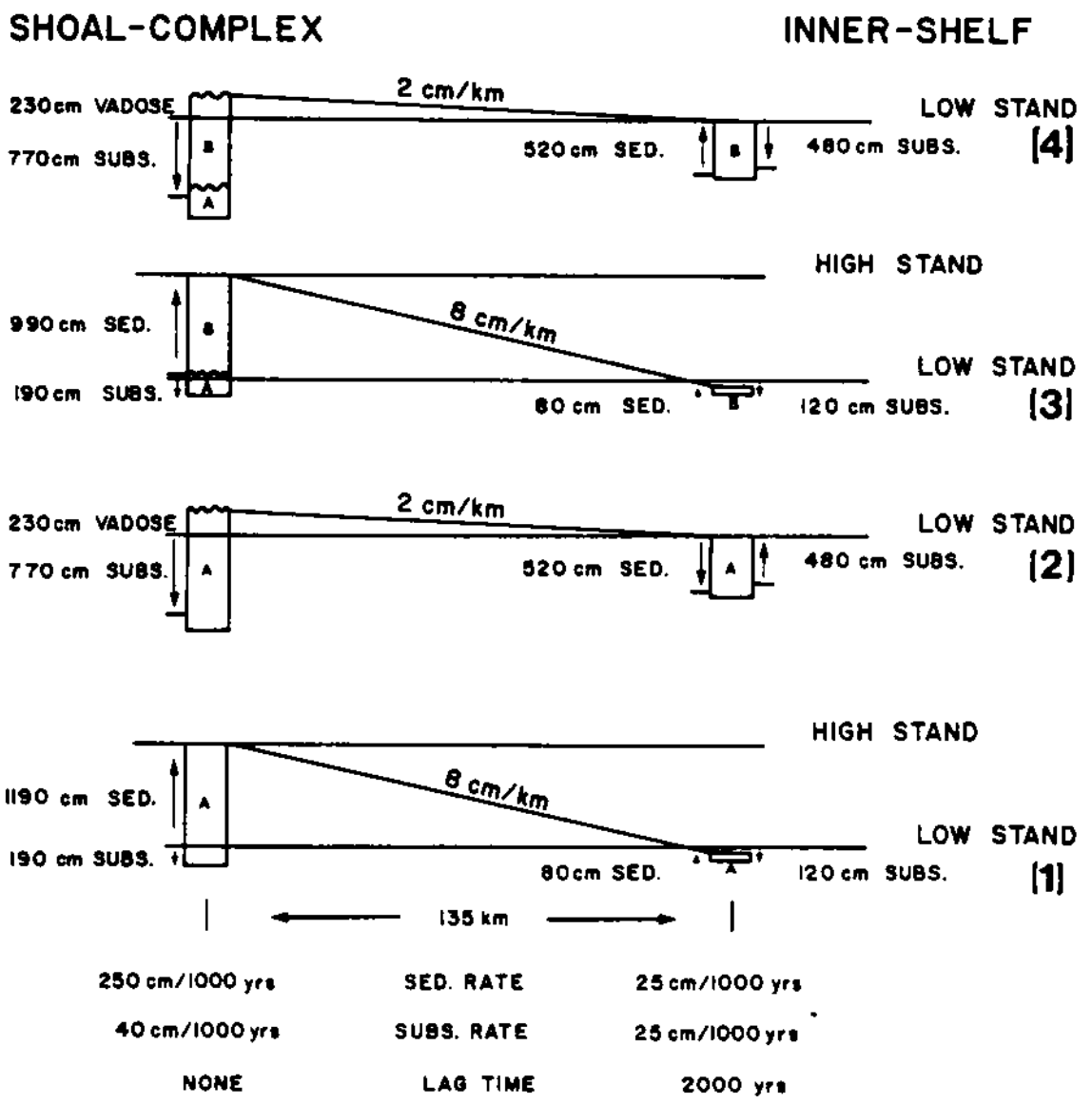
SHOAL-COMPLEX
INNER-SHELF
230cm VADOSE
770cm SUBS.
2 cm/km
520cm SED.
480cm SUBS.
LOW STAND
[4]
HIGH STAND
990cm SED.
190cm SUBS.
8 cm/km
LOW STAND
60 cm SED.
120 cm SUBS.
[3]
230cm VADOSE
770 cm SUBS.
2 cm/km
520 cm SED.
480 cm SUBS.
LOW STAND
[2]
HIGH STAND
1190 cm SED.
190 cm SUBS.
8 cm/km
LOW STAND
80cm SED.
120 cm SUBS.
[1]
135 km
250 cm/1000 yrs
SED. RATE
25 cm/1000 yrs
40 cm/1000 yrs
SUBS. RATE
25 cm/1000 yrs
NONE
LAG TIME
2000 yrs

Figure 36a,b. Rocknest cycle profiles. A) Inferred slope at high sea-level stand based on facies relations within cycles. Note that shoal-complex sedimentation occurs primarily during sea-level rise, and that only a thin veneer of sediment is deposited over most of inner-shelf. B) Facies relations and inferred slope of a "complete" cycle at low sea-level stand. Note that inner-shelf sedimentation occurs primarily during sea-level fall. This profile represents a balance between sea-level fall rate, sedimentation rate, and subsidence rate.

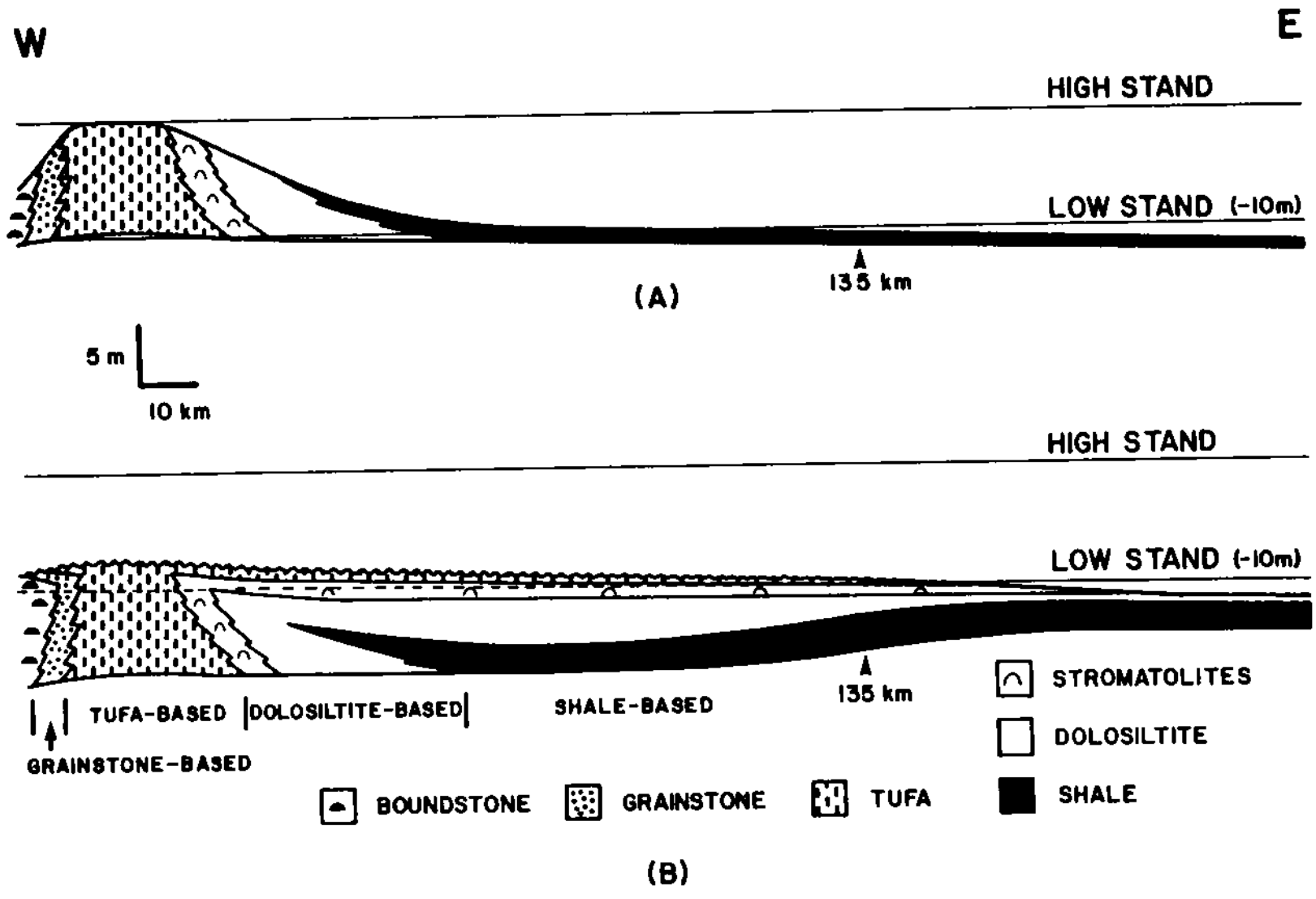
W
E
HIGH STAND
LOW STAND (-10m)
135 km
(A)
5 m
10 km
HIGH STAND
LOW STAND (-10m)
135 km
TUFA-BASED
DOLOSILTITE-BASED
SHALE-BASED
GRAINSTONE-BASED
STROMATOLITES
DOLOSILTITE
SHALE
BOUNDSTONE
GRAINSTONE
TUFA
(B)

Figure 36c,d. Rocknest cycle profiles (continued). C) Insufficient sediment supply during progradation results in facies bypassing as sea-level rapidly falls over successive lithotopes, forming "condensed" cycles over inner-shelf. Intermediate facies are omitted from inner-shelf cycles and thin tidal flat tufas are deposited directly on deepest water facies. Cycles are thinner than "complete" cycles of (B). Note greater drop in sea-level to -12 m. This makes the ratio of sea-level fall rate to sedimentation rate lower, favoring sediment starvation during progradation. D) "Expanded" cycle profile. Sediment oversupply during progradation results in faster progradation, so cycles extend farther by end of cycle. Cycles are thicker than "complete" cycles, due mostly to increase in thickness of subtidal facies. Note drop in sea-level to only -7 m. This makes the ratio of sea-level fall rate to sedimentation rate lower, favoring sediment oversupply.

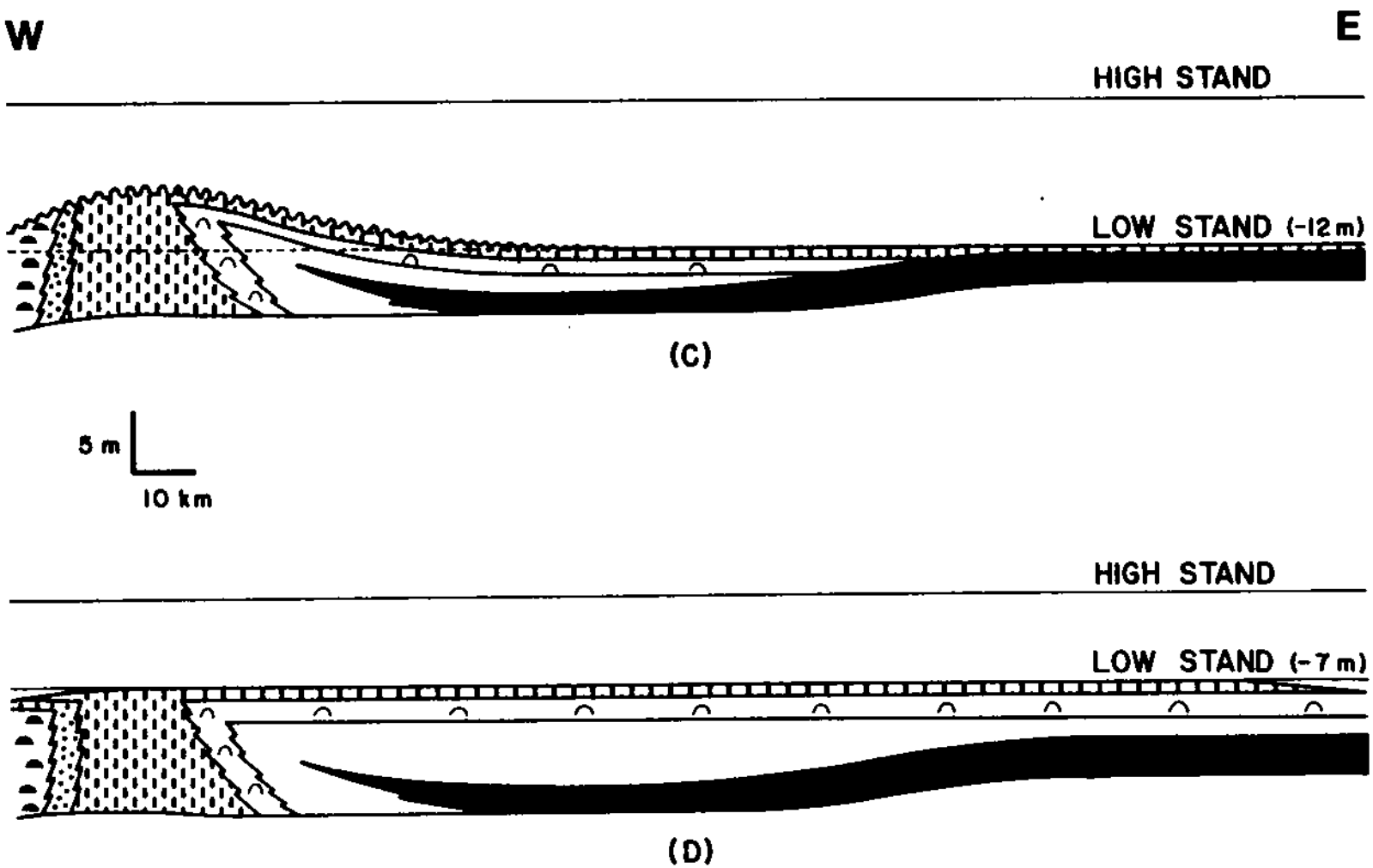
W
E
HIGH STAND
LOW STAND (-12 m)
(C)
5 m
10 km
HIGH STAND
LOW STAND (-7 m)
(D)

the faster the rate of sedimentation and progradation must be in order for a "complete" cycle profile to be formed. This process produces moderately thick, asymmetric cycles with a complete range of upward-shallowing facies. Strata deposited during progradation (this excludes deposits formed during sea-level rise) have constant thickness over the platform (Fig. 36b); any thinning (or thickening) is mostly related to differences in subsidence.

Starved progradation and development of a "condensed" cycle profile occurs when sedimentation rate is low relative to rate of sea-level fall. This results in facies being omitted from cycles because the sea recedes faster than sediment can be supplied to tidal flats. Lithotopes are progressively bypassed by the rapidly-receding shoreline, resulting in deep subtidal facies (eg. shales) being directly overlain by upper-intertidal to supratidal facies (eg. tufas), capped by well-developed erosional surfaces and breccias. Cycles thin in the direction of progradation, and where they pinch out, lack upper subtidal to lower intertidal facies, and are capped by thin beds of upper intertidal to supratidal facies with erosional tops (Fig. 36c); in the extreme case of very low sedimentation rates, "cycles" consist of subtidal facies separated only by subaerial erosional surfaces.

If sedimentation rate is high relative to rate of sea-level fall, then an "expanded" cycle profile is formed; cycles will be thicker on average (Fig. 36d), with most thickening occuring in the subtidal part of the cycle. Cycles will thicken markedly in the direction of progradation under conditions of constant or increasing differential subsidence (eg. Lohman, 1976), but may decrease in thickness under conditions of decreasing subsidence (eg. Rocknest Formation; Fig. 36d) In the extreme case, sedimentation rate is much greater than rate of sea-level fall, and progradation of flats is essentially independent of sea-level fall rate.

Additional data on these cycles can be obtained for these cycles by using a one-dimensional computer model (cf. Read et al., in prep). The model variables are: period, amplitude and symmetry of sea-level oscillation, depth-dependent sedimentation rate, lag in carbonate production following submergence, tidal range, and linear subsidence (Fig. 37a). All variables are independent of each other, but for the Rocknest Formation several variables can be fixed, permitting approximation of values for the others.

Grainstone-based cycles formed on the outer-shelf by progradation of the western margin of the shoal-complex over backreef grainstones during sea-level fall. Progradation

Figure 37. Synthetic models of Rocknest Cycles: General model and shoal-complex model. A) General Model. Period, 50,000 yrs; amplitude, 5 m; symmetrical sea-level oscillation; lag time, 5,000 yrs; subsidence, 10 cm/1000 yrs; tide range, 1 m; subtidal sedimentation rate, 100 cm/1000 yrs; intertidal sedimentation rate, 50 cm/1000 yrs. With time, sea-level rises according to sine curve, and the sediment surface subsides because of lag time. After 5,000 yrs, water depths are near the low tide zone, and sedimentation begins (fine, dotted line). Sea-level then peaks, starts to fall, but sedimentation continues to high tide (follow path of "sediment surface"). As sea-level falls, the platform is exposed because rate of sea-level fall is greater than subsidence rate; a vadose zone is formed. Subsequent cycles have well-developed subtidal bases because the subsiding platform is not submerged until about one-third of sea-level rise has been attained. B) Tufa-based cycles of Rocknest shoal-complex. Period, 24,000 yrs; amplitude, 10 m; 20% of cycle period in sea-level rise; lag time, 0 yrs; subsidence, 40 cm/1000 yrs; tide range, 1 m; sedimentation rate, 250 cm/1000 yrs. The only variables are lag time and sedimentation rate. Lag time must be zero in order not to get subtidal sedimentation, thus fixing sedimentation rate to 250 cm/1000 yrs. Tepees and breccias are formed during sea-level fall and exposure of platform.

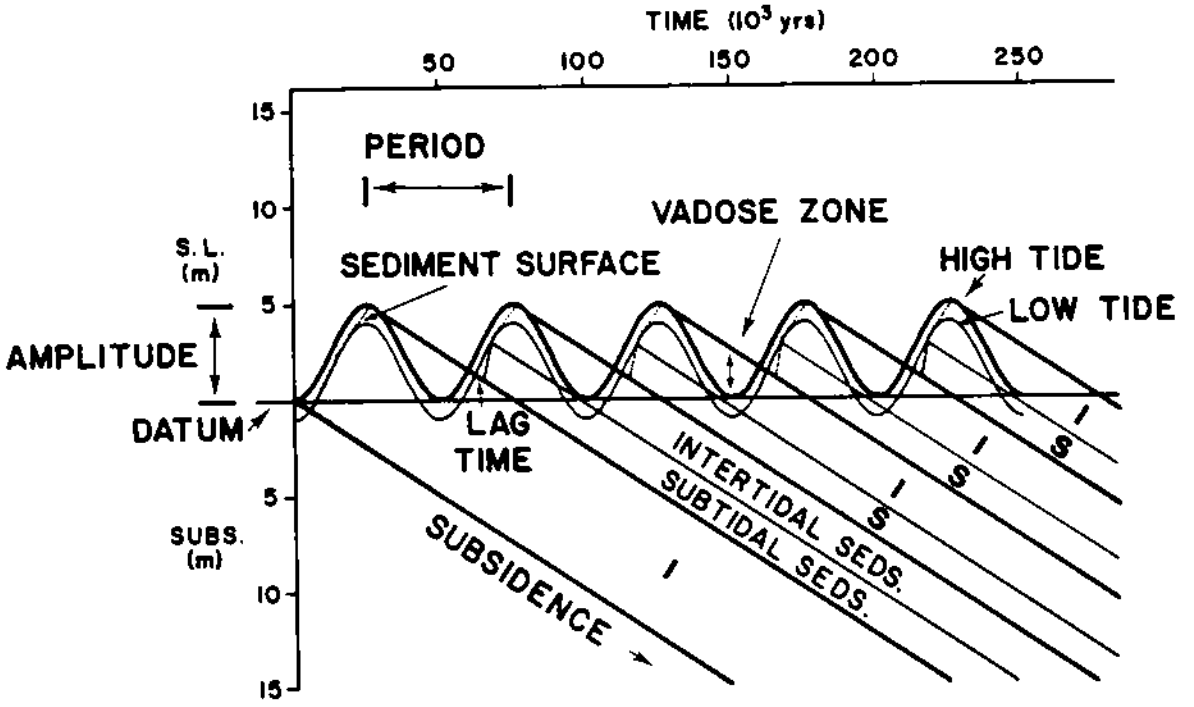
TIME (10³ yrs)
50
100
150
200
250
15
10
5
S.L. (m)
PERIOD
VADOSE ZONE
SEDIMENT SURFACE
HIGH TIDE
LOW TIDE
AMPLITUDE
DATUM
LAG TIME
INTERTIDAL SEDS.
SUBTIDAL SEDS.
SUBSIDENCE
I
S
5
10
15
SUBS. (m)

(A)

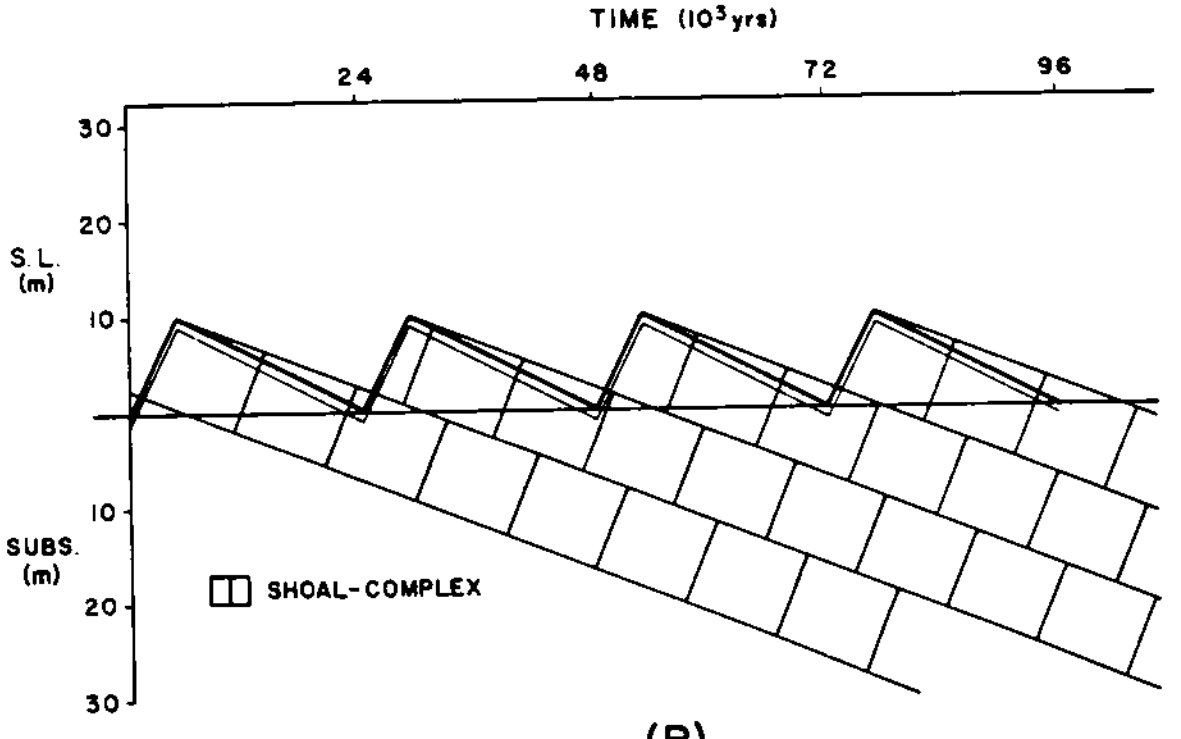
TIME (10³ yrs)
24
48
72
96
30
20
10
S.L. (m)
10
20
30
SUBS. (m)
SHOAL-COMPLEX

(B)

was very limited in extent, and consequently these cycles occupy a narrow paleogeographic tract that is rarely exposed. Therefore, they are badly constrained and cycle development is poorly understood.

Tufa-based cycles formed on the shoal-complex by vertical aggradation of upper intertidal to supratidal facies during sea-level rise (Fig. 36a). For tufa-based cycles of the shoal-complex, all variables are fixed except lag time and sedimentation rate. However, because facies indicate that significant submergence of shoal-complex did not occur, it can be assumed that lag time must be close to zero. Therefore, shoal-complex sedimentation rate is constrained by modelling to a value which matches sea-level rise rate plus subsidence rate (Fig. 37b). Sedimentation rate for the shoal-complex is approximately 250 cm/1000 yrs. This is extremely fast compared to Holocene tidal flat sedimentation rates (cf. Schlager, 1981) and probably reflects significant influx of carbonate from the rim. Note that all sedimentation on the shoal-complex occurs during sea-level rise, which generates thick tidal-flat sequences. During sea-level fall, the rate of fall is greater than platform subsidence rate, and sea-level drops below platform surface, resulting in subaerial exposure. This generates a thick vadose zone, in which tepees, breccias, and pisolite are formed.

Dolosiltite-based cycles formed on the proximal inner-shelf where subsidence rates were approximately 35 cm/1000 yrs. Cycles were initiated by shallow submergence of the platform during sea-level rise. Computer modelling constrains sedimentation rates and lag times on the proximal inner-shelf because other variables are fixed. Given these constraints, modelling shows that a lag time of 1000 yrs was long enough to allow submergence of the platform to shallow subtidal depths, but short enough to prevent further submergence to shale sedimentation depths (Fig. 38a). Following onset of sedimentation, subtidal sedimentation rate must have been greater than 80 cm/1000 yrs in order to prevent further deepening. This was followed by eastward progradation of the shoal-complex over intertidal to shallow subtidal stromatolite/thrombolite facies and thick-laminated dolosiltite facies during sea-level fall. Shallowing occurred rapidly, and a well-developed erosional cap is formed because the rate of sea-level fall is greater than subsidence rate. Note that shallowing of the platform occurred during sea-level fall; this resulted in comparatively thin tidal flat caps, which would have been thicker if shallowing had occurred during sea-level rise. Because shallowing occurred before sea-level fell to low stand, the platform had time to be exposed as sea-level fell further, producing a vadose zone and an erosional cap.

Figure 38. Synthetic models of Rocknest cycles: proximal and distal inner-shelf. A) Dolosiltite-based cycles of proximal inner-shelf. Period, 24,000 yrs; amplitude, 10 m; 20% of cycle period in sea-level rise; lag time, 1,000 yrs; subsidence rate, 35 cm/1000 yrs; shallow subtidal (dolosiltite, 5 to 3 m water depth) sedimentation rate, 80 cm/1000 yrs; stromatolite sedimentation rate (3 to 1 m water depth), 100 cm/1000 yrs; tufa sedimentation rate (1 to 0 m water depth), 50 cm/1000 yrs. All variables are fixed except lag time and sedimentation rates. The suggested values produce a model that replicates the data, although it is probably not the only solution. Lag time is long enough to allow submergence to shallow subtidal depths. Note that sediment surface rapidly builds up, intersection sea-level curve during fall. This generates relatively thin tidal flat caps, whichwould have been thicker if sediment surface had intersected sea-level curve during rise. Also, the platform is exposed during low stand, forming erosional surfaces.
B) Shale-based cycles of distal inner-shelf. Period, 24,000 yrs; amplitude, 10 m; 20% of cycle period in sea-level rise; lag time, 2,000 yrs; subsidence rate, 25 cm/1000 yrs; deep subtidal (shale, 15 to 5 m water depth) sedimentation rate, 20 cm/1000 yrs; other rates as above. All variables fixed except lag time and sedimentation rates, and suggested values produce a model that reproduces the data, although other solutions are possible. A lag time of at least 2,000 yrs is required for initial submergence to deep subtidal depths before sedimentation begins. A sedimentaton rate of 20 cm/1000 yrs for shale facies prevents rapid upbuilding of platform so that it will not be significantly exposed at low stand.

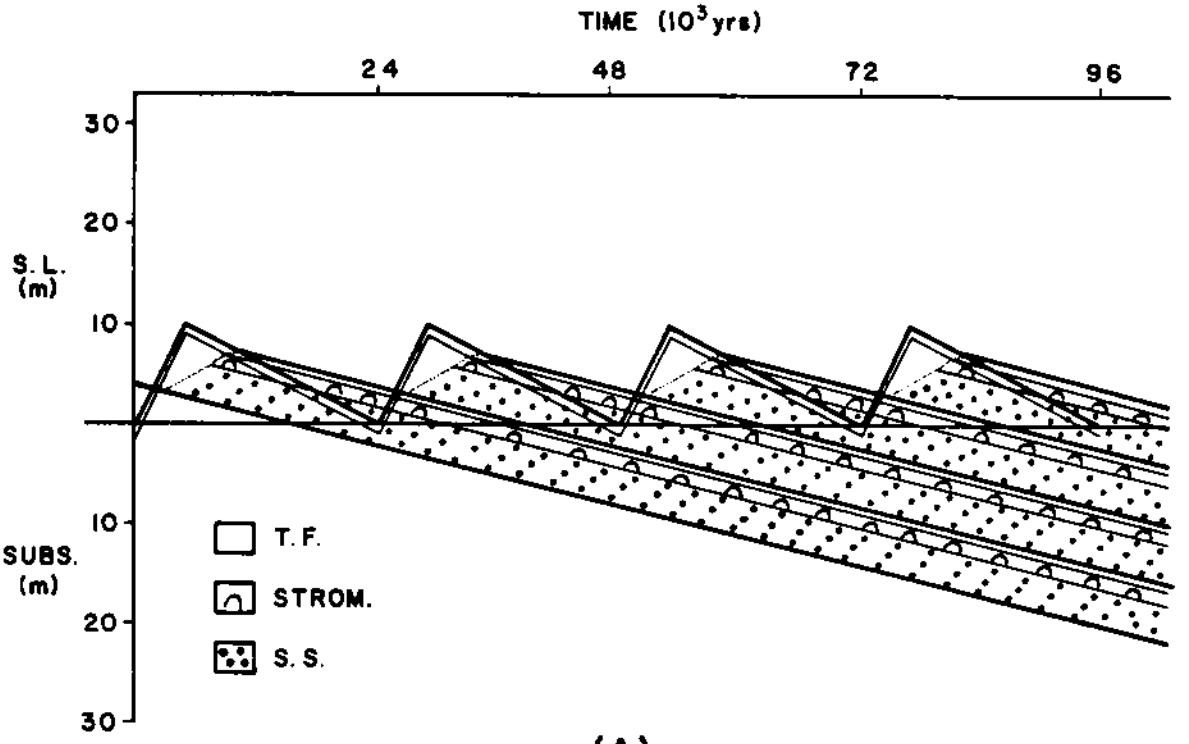
TIME (10³yrs)
24
48
72
96
30
20
S.L. (m)
10
10
SUBS. (m)
20
30
T.F.
STROM.
S.S.

(A)

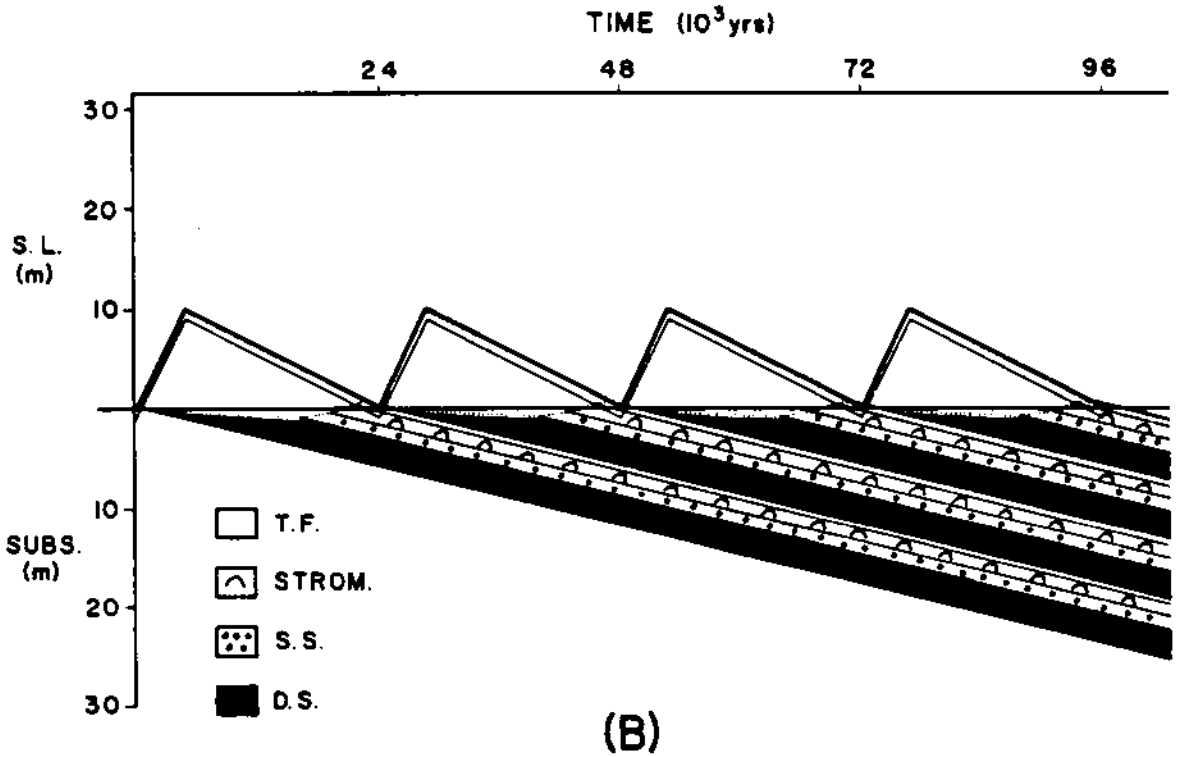
TIME (10³yrs)
24
48
72
96
30
20
S.L. (m)
10
10
SUBS. (m)
20
30
T.F.
STROM.
S.S.
D.S.

(B)

Shale-based cycles formed on the distal inner-shelf where subsidence rates were 25 cm/1000 yrs. Cycles were initiated by deeper submergence of platform during sea-level rise (as compared to the proximal inner-shelf). Modelling of a shale-based cycle at the point where tidal flat caps pinch-out (135 km from the western shoal-complex), suggests that lag time must have been at least 2000 yrs in order to get submergence to depths (> 5m) where mixed carbonate/siliciclastic (deeper subtidal) sedimentation occurred (Fig. 38b). Given a 2000 yr lag time, the rate of deeper subtidal sedimentation must have been close to 20 cm/1000 yrs. Rates faster than that would have caused shallowing to sea-level before the end of the cycle, generating thicker tidal flat caps, as opposed to thin caps that typify these cycles. Furthermore, premature shallowing would have allowed time for exposure of platform during final sea-level lowering, which is not indicated due to absence of vadose features capping these cycles. Deeper subtidal sedimentation rates significantly slower than 20 cm/1000 yrs would have incipiently drowned the platform. Note that shallowing occurred during the final stage of sea-level fall. This prevented subaerial exposure of platform. Thus, shale-based cycles that formed on the distal inner-shelf, where tidal flat caps pinch-out, have thick shale

bases, thin to absent tidal-flat units, and are separated by conformable surfaces.

"GRAND CYCLES" AND NON-CYCLIC SEDIMENTATION ON INNER-SHELF

There are 7-8 "grand cycles" (cf. Aitken, 1978) in the Rocknest Formation which range in thickness from 75 to 200 m (Figs. 3,25). Most "grand cycles" show changes in ratio of shale to dolomite within small-scale cycles such that the lower part of a "grand cycle" consists of shale-based small-scale cycles, that pass up into carbonate-based or tufa-based small-scale cycles in the upper part of a "grand cycle". However, three "grand cycles" have non-cyclic shelf intervals as their lower parts.

Lower Non-Cyclic Interval

This interval is a westward-thickening (up to 100 m) wedge of interbedded, partially-linked columnar stromatolites and intraclast/ooid grainstone (Figs. 3,23a). Generally, the abundance of grainstone/packstone increases upwards and uppermost beds may contain wavy-bedded dolosiltite, cryptalgalaminite or tufa. Intraclast grainstone/packstone is common in the western shelf, passing

laterally into rhythmite facies which mantles the lower rim. To the east, the sequence thins and intraclast grainstone/packstone passes into stromatolitic facies of the eastern shelf, and then into dolosiltite- or grainstone-based cycles.

Intraclast Grainstone/Packstone: Facies consist of massive to trough and planar cross-bedded, intraclast-ooid grainstone/packstone as thick units (up to 60 m), or laterally continuous sheets (up to 5m thick), or lenses (1 to 2 m thick, 2 to 15 m wide) within stromatolitic intervals (Fig. 39a). Paleocurrent data on cross-bed foresets indicate northeast transport (onshelf) of clastic carbonate, consistent with the inferred direction of wave propagation. Partial silicification is common throughout the sequence.

Partially-Linked Columnar Stromatolites: This facies is similar to that described from the rim sequences. Stromatolites occur as laterally continuous beds (up to 30 m thick), or as isolated buildups (1 to 4 m high, 5 to 20 m wide); individual columns are 10 to 30 cm wide, 10 to 50 cm high and have up to 20 cm synoptic relief (Fig. 39a). Columns have high inheritance of succesive laminae and are strongly elongate subnormal to regional shelf-edge trend. Narrow (3 to 10 cm wide) "gutters" between columns are filled with intraclast grainstone/packstone.

Figure 39. Non-cyclic facies. A) Partially-linked columnar stromatolites and channel grainstone, lower non-cyclic interval, eastern shelf. B) Wave-rippled cherty dolosiltite, middle non-cyclic interval, central shelf. C) Reverse-graded ooid packstone, upper non-cyclic interval, central shelf.

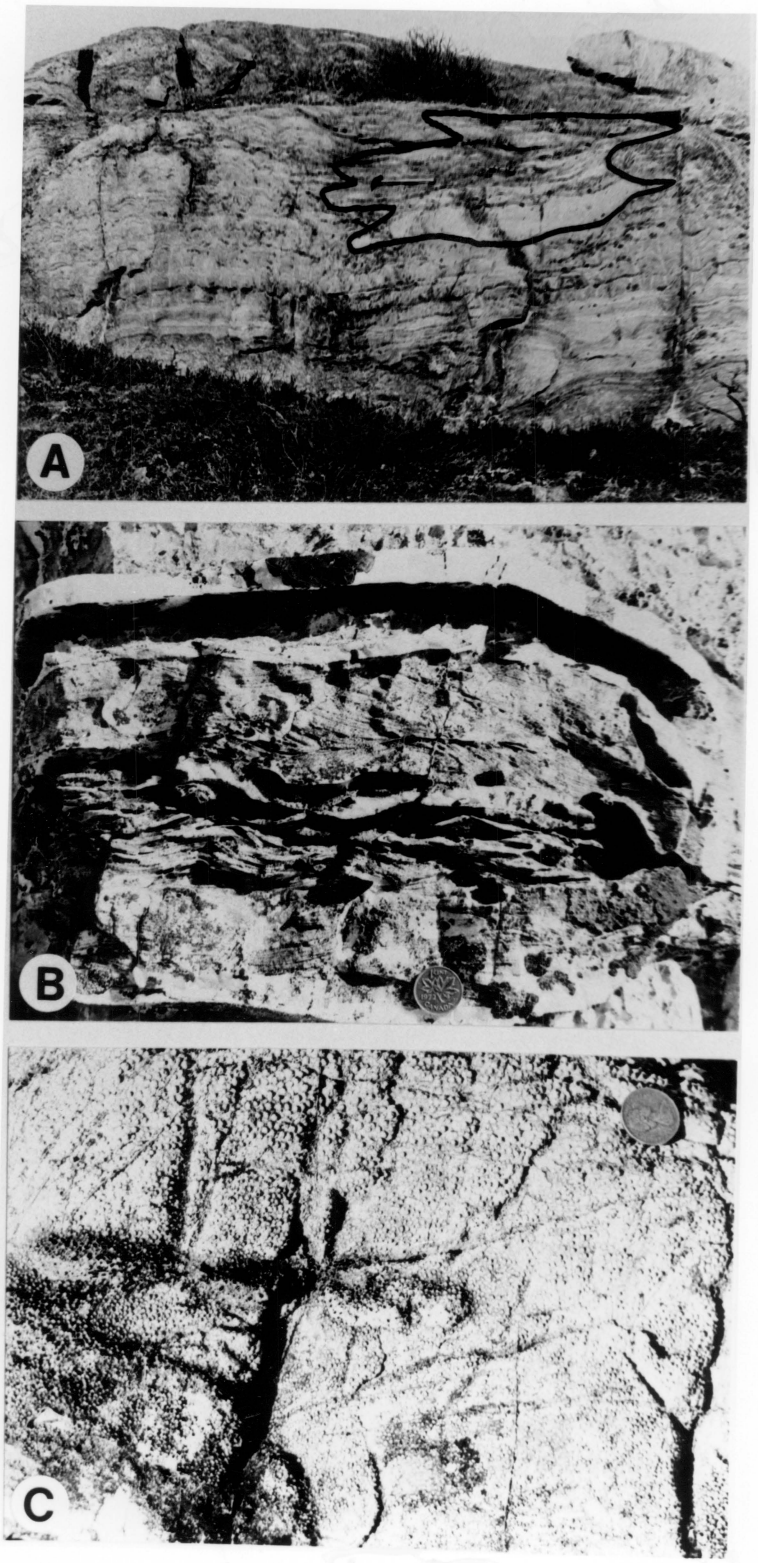
A
B
C

Development of Lower Non-Cyclic Interval: The lower non-cyclic interval formed during drowning of the lowermost rim sequence and incipient drowning of the inner-shelf. The Rocknest inner-shelf became a high-energy platform, open to the west, and lacking a reefal rim (Figs. 3,24a). This allowed coarse, intraclast grainstone to be spread over the inner-shelf. Thick beds of grainstone/packstone and strongly elongate stromatolites, similar to the reefal rim, reflect sustained high-energy conditions over the inner-shelf. High wave-energy probably was responsible for development of strongly elongate stromatolites and onshore transport (parallel to stromatolite elongation) of intraclastic material.

West-to-east transgression of the shoal-complex and incipient drowning of the inner-shelf was rapid, as indicated by the near parallelism of the base of the lower non-cyclic interval and underlying cycle boundaries (Fig. 3). Open-marine conditions prevailed over most of the shelf, except in the autochthon where it periodically shoaled to sea-level to form grainstone- or dolosiltite-based cycles. This indicates that the shoal-complex had backstepped to the easternmost part of the shelf, allowing mixed carbonate/siliciclastic "lagoonal" sedimentation to occur farther east. This suggests that the lower non-cyclic

interval may be correlative with the thin sequence of cyclic carbonates present in the Peacock Hills area of Kilohigok Basin, which thins to a feather edge 75 km further east (cf. Campbell and Cecile, 1981; Hoffman et al., 1983). By this correlation, Peacock Hills cycles would form by eastward expansion of the backstepped shoal-complex over the remaining part of the "lagoon". However, it is also possible that the Peacock Hills cycles are correlative with the upper part of the Rocknest Formation (Top member of Grotzinger and Hoffman, 1983). Reestablishment of cyclic sedimentation over the Rocknest shelf occurred when the shoal-complex prograded westward across the inner-shelf to within several kilometers east of its original location.

Middle Non-Cyclic Interval

This interval is a westward-thickening (0 to 120 m) wedge of cherty, wave-rippled dolosiltite-dolarenite grainstone/packstone, thin interbeds of partially-linked columnar stromatolites (Figs. 3,23b), and minor thin beds of ooid-intraclast packstone and argillaceous dololutite. It passes westward into rim facies consisting of stromatolitic boundstone and intraclast-ooid grainstone/packstone. Eastward, it thins and passes into shale-based cycles and minor dolosiltite-based cycles.

Cherty Dolosiltite-Dolarenite: This facies forms beds (few meters thick) of wave-rippled dolosiltite and doloarenite with abundant pink to cream colored chert nodules (Fig. 39b), with thin beds of wavy cryptalgalaminite and small, elongate, partially-linked columnar stromatolites. In the east, thin interbeds of argillaceous dololutite are present. To the west, ooid grainstone/packstone beds are up to 2 meters thick and contain herringbone cross-bedding; ooid beds of the central and eastern shelf are thinner (less than 30 cm), dominantly packstones, and commonly reverse graded with large ooids up to 2.5 mm wide.

Stromatolite Boundstone: This facies includes wavy cryptalgalaminite, small irregular-laminated domes and, near the rim, elongate partially-linked columns. Wavy cryptalgalaminite commonly is developed on beds of wave-rippled dolosiltite-dolarenite and may pass up into small domes with irregular lamination. Partially-linked columns usually form small mounds 1 to 2 m wide and up to 50 cm thick.

Development Of Middle Non-Cyclic Interval: The middle non-cyclic interval formed during a second event of incipient drowning of the inner-shelf when the rim was drowned and backstepped (Figs. 3,24b). Thick sequences of

dolosiltite and dolarenite formed during prolonged, open marine conditions. The Rocknest inner-shelf was open to the west and unrestricted by a barrier shoal-complex (Fig. 3). In contrast to the lower non-cyclic interval, the dominance of finer grained sediments in the middle non-cyclic interval, and absence of thick stromatolitic sequences in the central and eastern part of the shelf, may indicate some restriction of wave energy due to the presence of a reefal rim, but without adjacent shoal-complex.

The middle non-cyclic interval passes eastward into dolosiltite-based or shale-based cycles. However, carbonate sediments do not extend into siliciclastic shelf deposits of the central and eastern "lagoon" (Kilohigok Basin), suggesting that transgression was less extensive than during deposition of the lower non-cyclic interval. Cyclic sedimentation was reestablished over the Rocknest shelf when the shoal-complex prograded westward over the inner-shelf to within a few kilometers of its previous location.

Upper Non-Cyclic Interval

This interval is an eastward-thickening (0 to 70 m) wedge of argillaceous dololutite (Figs. 3,23c), lithologically similar to mixed carbonate/siliciclastic facies of the cyclic inner-shelf. Intercalated dolosiltites

are more common in the western part of the interval, whereas thin beds of siliciclastic siltstone/sandstone are more common in the east. The interval passes westward into shoal-complex facies and eastward into siliciclastic facies of the Goulburn Group, Kilohigok Basin. Thin beds of intraclast packstone and reverse-graded ooid packstone are common throughout the interval (Fig. 39c), and rare ooid beds are overlain by wave-rippled dolosiltite and/or wavy cryptalgalaminite.

Development Of Upper Non-Cyclic Interval: This interval formed during a third event of incipient drowning of the inner-shelf, concomitant with drowning and backstepping of the rim. However, the shoal-complex was not drowned and backstepped (Fig. 3), thus the inner-shelf was effectively shielded from high-energy, open marine conditions, allowing deposition of mixed siliciclastic-carbonate muds. Water depths were close to storm wave-base as shown by the presence of both hummocky cross-bedding and turbidites. Ooid beds formed during periodic shoaling of the "lagoon" to wave-base, related to falls in sea-level and limited, progradation of the shoal-complex. Ooids were not transported from the eastern margin of the shoal-complex because ooid shoals are absent from eastern margin of the shoal-complex and the number of ooid beds does not increase

with decreasing distance from the shoal-complex. An autochtonous origin of ooids beds is supported by common reverse grading, and association with wave-rippled dolosiltite and wavy cryptalgalaminite.

During deposition of the upper non-cyclic interval, the rim and shoal-complex were less than 30 to 40 km wide, which persisted until the shoal-complex prograded eastward, back over the inner-shelf at the end of the upper non-cyclicic deposition. Water depths during sedimentation probably were similar to those associated with submergence events which formed cyclic sequences. During the upper non-cyclic interval, the shoal-complex only prograded 10 to 20 km back over the inner-shelf after each submergence event. Consequently, much of the inner-shelf underwent a prolonged period of lagoonal sedimentation.

Origin of Non-Cyclic Intervals and "Grand Cycles"

Several alternatives may explain the origin of non-cyclic intervals. Firstly, non-cyclic intervals may have been formed during times when small-scale sea-level fluctuations did not occur. However, this is not reasonable because non-cyclic intervals are laterally equivalent to cyclic sequences, and thus sea-level must have been oscillating over parts of the platform that ultimately became non-cyclic.

Another possibility is that small-scale sea-level oscillations did occur, but the platform was too deep to experience significant changes in environment and facies. This alternative also is unlikely because most sediments were deposited in relatively shallow water. Note that even the shales of the upper non-cyclic interval are relatively shallow water facies that formed behind the shoal complex, possibly in similar water depths as grainstone-boundstone of the lower and middle non-cyclic intervals, which were not protected by the shoal-complex.

A third possibility is that the apparent "non-cyclic" interbedding of facies actually may be a response to oscillating sea-level, with incomplete shoaling during each "cycle". This final alternative is preferred in that it is possible to relate apparently random interbedding of "non-cyclic" facies to sea-level oscillations, in combination with longer-term changes in sea-level that ultimately produced "grand cycles".

Each non-cyclic interval represents incipient drowning of the inner-shelf, and inhibition of tidal flat sedimentation. In order to maintain this condition under oscillatory sea-level, without shoaling to sea-level, a long-term net increase in sea-level must be involved. Superimposition of long-term rise in sea-level on

oscillatory sea-level results in increased rates of sea-level rise and decreased rates of sea-level fall. Furthermore, succeeding sea-level high stands are greater than preceeding high stands, as are low stands, resulting in a net increase in sea-level. The rate of net increase in sea-level must initially be greater than the rate of subtidal sedimentation (to incipiently drown shelf), followed by a rate of net rise that is equal to the rate of subtidal sedimentation (to avoid complete drowning), followed by a rate of net rise to that is lower than rate of subtidal sedimentation (to end incipient drowning).

"Grand cycles" are produced by changes in the rate of long-term sea-level rise or fall, with superimposed small-scale oscillations in sea-level. Increasing the rate of longer-term sea-level rise or decreasing the rate of longer-term sea-level fall probably initiates "grand cycles" (cf. Pitman, 1978). This is followed by a decrease in rate of longer-term sea-level rise or increase in rate of longer-term sea-level fall, which results in net shoaling and the transition from lower to upper parts of "grand cycles". "Grand cycles" with non-cyclic bases reflect more extreme increases in longer-term rate of sea-level rise or decreases in longer-term rate of sea-level fall.

A "grand cycle" can be synthetically modelled to replicate the gradual transition from the upper non-cyclic interval into overlying cyclic facies (Fig. 40). Most variables are fixed as before, with subsidence rate at 25 cm/1000 yrs. Long-term sea-level rise is constant and less than subtidal sedimentation rates, allowing slow shoaling to sea-level over the course of several cycle periods. The model reveals that subtidal sedimentation rates, and rates of subsidence and long term sea-level change are important variables. It also reveals that much apparently "random" interbedding of shale and dolosiltite in "non-cyclic" facies actually may be related to cyclically oscillating sea-level. Deposition of shale occurred near the peak of sea-level rise and maximum water depths, followed by deposition of dolosiltite near the limit of sea-level fall and shallower water depths.

CONCLUSIONS

1: The restored early Proterozoic Rocknest shelf sequence contains well-developed shoal-complex and inner-shelf cyclic facies which interfinger westward with grainstone/boundstone outer-shelf facies and rhythmite/breccia slope facies, and eastward with "lagoonal"

Figure 40. Synthetic model of "grand cycle". "Grand cycle" forms as a result of small-scale sea-level oscillations superimposed on longer-term relative drop in sea-level. Small-scale cycle period, 24,000 yrs; amplitude, 10 m; 20% of cycle period in sea-level rise; lag time, 2,000 yrs (only after platform builds to sea-level); subsidence rate, 25 cm/1000 yrs; below wave-base sedimentation rate, 35 cm/1000 yrs (40 to 15 water depth); storm wave-base sedimentation rate, 50 cm/1000 yrs (15 to 10 m water depth); fairweather wave-base sedimentation rate, 70 cm/1000 yrs (10 to 5 m water depth); shallow subtidal sedimentation rate, 90 cm/1000 yrs (5 to 1 m water depth); tidal flat sedimentation rate, 50 cm/1000 yrs (1 to 0 m water depth). Initial water depth is 20 m, and platform slowly aggrades to sea-level with time. Note that much "random" interbedding of deeper water facies is related to cyclic oscillation of sea-level, which raises and lowers wave-base. This model replicates the transition from upper non-cyclic interval (Red Shale member) into overlying cyclic sequence (Thin member).

"GRAND CYCLE"

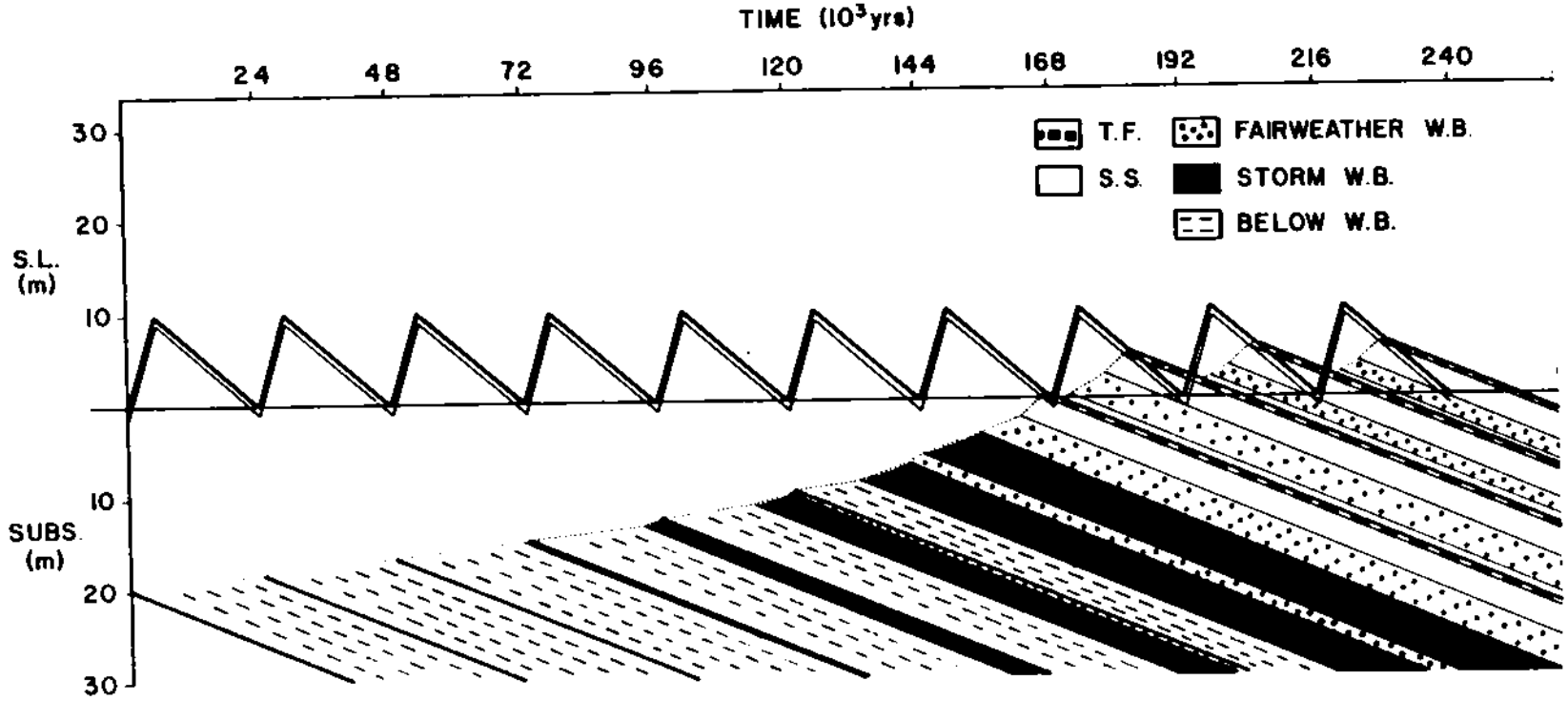
TIME (10^3yrs)
24
48
72
96
120
144
168
192
216
240
T.F.
S.S.
FAIRWEATHER W.B.
STORM W.B.
BELOW W.B.
S.L. (m)
30
20
10
SUBS. (m)
10
20
30

siliciclastics. Cyclic shoal-complex facies consist of cryptalgalaminite, tufa, and laminated dolosiltite/lutite, overlain by disrupted equivalents, developed as tepees and breccias with associated pisolite. Inner-shelf facies comprise upward-shallowing sequences of intraclastic transgressive lags, mixed carbonate/siliciclastic lagoonal sediments, shallow subtidal thick-laminated dolosiltite, shallow subtidal to intertidal stromatolitic/thrombolitic dolomite, and upper intertidal to supratidal tufa. Cycles are bounded by erosional surfaces that become less pronounced away from the shoal-complex.

2: Cycles formed during periodic sea-level rise when rapid transgression and flooding of carbonate tidal flats along the eastern margin of the shoal-complex occurred, followed by eastward expansion of the shoal-complex and slow progradation of tidal flat facies over lagoonal facies during sea-level fall. Grainstone-based cycles formed along the western margin of shoal-complex, tufa-based cycles formed within the shoal-complex, and dolosiltite-based/shale-based cycles formed along the eastern margin of the shoal-complex.

3: Detailed stratigraphy and field mapping demonstrates that individual cycles at several different levels in the Rocknest Formation can be correlated for over

200 km parallel to depositional strike and over 120 km perpendicular to strike. Generally, shale-based inner-shelf cycles pass westward (toward shoal-complex) into dolosiltite-based cycles and then into tufa-based cycles of the shoal-complex. These in turn pass westward (toward the rim) into grainstone-based cycles of the outer-shelf. Cycle types are a product of variable paleogeography/topography during sedimentation and progradation. Because the shoal-complex was seldom submerged during sea-level rise it became a paleotopographic high, restricting an eastern "lagoon" from the western ocean. Consequently, it exerted a strong control over cyclic facies patterns.

4: Given radiometric constraints on the duration of the passive-margin sequence, average cycle period is bracketed between 18,000 to 30,000 yrs and is similar to the range of values reported for perturbations of Earth's orbital parameters. These are believed to have generated Pleistocene glacio-eustatic sea-level oscillations, suggesting that Rocknest cyclcity may relate to early Proterozoic glacio-eustacy. Relative sea-level oscillation was approximately 10 m for lower Rocknest cycles, and thus alpine glaciation is favored over continental glaciation.

5: From estimates of the amplitude and period of sea-level oscillation and distance over which tidal flat facies

extend from shoal-complex (approx. 135 km for lower Rocknest), average inner-shelf slopes were calculated to range from 8 cm/km at high sea-level stand to 2 cm/km at low sea-level stand. The accuracy of these estimates is supported by the close agreement between observed progradation rate of tidal flats (7 km/1000 yrs) and expected progradation rate of tidal flats (9 km/1000 yrs), calculated from platform slopes, distance over which tidal flat facies extend, and amplitude and period of sea-level oscillation.

6: Examination of cycle types reveals that progradation is controlled by sedimentation rate, sea-level fall rate, and inclination of inner-shelf slope from western shoal-complex into "lagoon". "Complete" cycle profiles of moderate thickness are formed when there is a balance between sedimentation and sea-level fall such that water depths over each facies tract remain constant during progradation. Decreased sediment supply relative to rate sea-level fall produces thinner, "condensed" cycle profiles by ommision of facies during progradation. Conversely, sediment oversupply during sea-level fall produces thicker, "expanded" cycle profiles because tidal flats recieve more sediment than that required for complete progradation under the given rate of sea-level fall and slope inclination.

7: Non-cyclic intervals formed during incipient drowning of the inner-shelf, associated with drowning and backstepping of the rim, in response to longer-term relative sea-level rise. During the lower non-cyclic interval, the shelf was a ramp, open to the west, allowing high-energy grainstone/boundstone to form over most of the shelf; cyclic tidal flat sedimentation occurred over the easternmost part of the shelf. During sedimentation of the middle non-cyclic interval, the inner-shelf was partially restricted by growth of a rim. The upper non-cyclic interval formed during a prolonged period of "lagoonal" sedimentation, due to the presence of a rim and shoal-complex near the shelf margin. Non-cyclic intervals or bundles of shale-based cycles grade up into bundles of dolosiltite-based or tufa-based cycles to form "grand cycles", 75 to 100 m thick. "Grand cycles" are produced by changes in rates of sea-level rise and fall related to longer-term, higher amplitude oscillations.

8: Data derived from study of Rocknest cycles should be useful in the interpretation of other Proterozoic and even Phanerozoic cyclic sequences. Although the values of parameters responsible for cyclic sedimentation will change for different platforms, the general relationships controlling those parameters should be similar, leading to a restricted number of cycle types and profiles in the record.

Consequently, in cyclic sequences that are not as tightly constrained as the Rocknest Formation, reasonable assumptions with testable predictions can be made concerning the origin of cycles, using the principles outlined here.

REFERENCES

Aigner, T., 1984. Dynamic stratigraphy of epicontinental carbonates, Upper Muschelkalk (M. Triassic), South-German Basin. N. Jb. Geol. Palaont. Abh. v. 169, no. 2, p. 127-159.

Aitken, J. D., 1967. Classification and environmental significance of cryptalgal limestones and and dolomites, with illustrations from the Cambrian and Ordovician of southwestern Alberta. Journal Sedimentary Petrology, v. 37, p. 1163-1178.

Aitken, J. D., 1978. Revised models for depositional grand cycles, Cambrian of the southern Rocky Mountains, Canada. Bulletin of Canadian Petroleum Geology, v. 26, p. 515-542.

Allen, P. A., 1981. Wave-generated structures in the Devonian lacustrine sediments of south-east Shetland and ancient wave conditions. Sedimentology, v. 28, p. 369-379.

Anderson, E. K., Goodwin, P., and Sobieski, T., 1974. Episodic accumulation and the origin of formation boundaries in the Helderberg Group of New York State. Geology, v. 12, p. 120-123.

Assereto, R.L.A.M., and Kendall, C.G.St.C., 1977. Nature, origin and classification of peritidal tepee structures and related breccias. Sedimentology, v. 24, p. 153-210.

Bally, A. W., 1983. Seismic expression of structural styles. American Association of Petroleum Geologists Studies in Geology Series 15, v.2, sec. 2.2.3.

Berger, A., 1980. The Milankovitch astronomical theory of paleoclimates: a modern review. Vistas in Astronomy, v. 24, p. 103-122.

Bond, G. C. and Kominz, M. A., 1984. Construction of tectonic subsidence curves for the early Paleozoic miogeocline, southern Canadian Rocky Mountains: implications for subsidence mechanisms, age of breakup, and crustal thinning. Geol. Soc. America Bull., v. 95, p. 155-173.

Bova, J. A., 1982. Peritidal cyclic and incipiently drowned platform sequences: Lower Ordovician Chepultepec Formation, Virginia. unpubl. Master's Thesis, Virgina Tech, Blacksburg, p. 184.

Brown, M. B., 1983. Two-way and multiway frequency tables - measures of association and the log-linear model (complete and incomplete tables). Dixon, W. J., et al., eds., BMDP Statistical Software, 1983 revised edition, Los Angeles, Univ. California Press, p. 143-206.

Caldwell, J. G., and Turcotte, D. L., 1979. Dependence of the thickness of the elastic oceanic lithosphere on age. Journal of Geophysical Research, v. 84, p. 7572-7576.

Campbell, F. H. A., and Cecile, M. P., 1976. Geology of the Kilohigok Basin, Goulburn Group, Bathurst Inlet, N. W. Territories. in Report of Activities, Part A, Geological Survey of Canada, Paper 76-1A, p. 369-377.

_____, 1981. Evolution of the Early Proterozoic Kilohigok Basin, Bathurst Inlet - Victoria Island, N. W. Territories. in Proterozoic Basins of Canada. F. H. A. Campbell, ed., Geological Survey of Canada, Paper 81-10, p. 103-131.

_____, 1978. Regressive stromatolite reefs and associated facies, Middle Goulburn Group (lower Proterozoic), in Kilohigok Basin, N.W. Territories: An example of environmental control of stromatolite form. Bulletin of Canadian Petroleum Geology, v. 26, p. 237-267.

Carr, T. R., 1982. Log-linear models, markov chains and cyclic sedimentation. Jour. Sed. Pet., v. 52, no. 3, p. 905-912.

Chappell, J., 1974. Geology of coral terraces, Huon Peninsula, New Guinea: a study of Quaternary tectonic movements and sea level changes. Geologic Society America Bulletin, v. 85, p. 553-570.

Cook, H. E. 1979. Ancient continental slope sequences and their value in understanding modern slope development. in Geology of Continental Slopes. L. J. Doyle and O. H. Pilkey, eds., Soc. Econ. Paleont. Mineral., Special Publication, v. 27, 287-305.

Cook, H. E., and Mullins, H. T., 1983. Basin margin environment. in Carbonate Depositional Environments. P. A. Scholle and D. G. Bebout, eds., American Association of Petroleum Geologists, Memoir 33, p. 540-617.

Davies, G. R., 1970. Algal-laminated sediments, western Australia. in Carbonate Sediments and Environments, Shark Bay, Western Australia. B. W. Logan et al., eds., American Association Petroleum Geologists, Memoir 13, p. 169-205.

Donaldson, J. A., 1976. Aphebian stromatolites in Canada: implications for stromatolite zonation. in Stromatolites. M. R. Walter, ed., Developments in Sedimentology, v. 20, p. 371-380.

Dunham, R. J., 1970. Stratigraphic reefs versus ecologic reefs. American Association of Petroleum Geologists Bulletin, v. 54, 1931-1932.

_____, 1972. Capitan reef, New Mexico and Texas: facts and questions to aid interpretation and group discussion. Permian Basin Section, Soc. Econ. Paleont. Mineral., Publication 72-14.

Easton, R. M., 1981. Stratigraphy of the Akaitcho Group and the development of an early Proterozoic continental margin, Wopmay Orogen, N. W. Territories. in Proterozic Basins of Canada. F. H. A. Campbell, ed., Geological Survey of Canada Paper 81-10, p. 79-96.

Esteban, M., and Klappa, C. F., 1983. Subaerial exposure environment. in Carbonate Depositional Environments. P. A. Scholle, et al., eds., American Association Petroleum Geologist, Memoir 33, p. 1-95.

Fairbridge, R. W., 1976. Convergence of evidence on climatic change and ice ages. Annals of the New York Acad. Sci., v. 91, no. 1, p. 542-579.

Fischer, A. G., 1964. The Lofer cyclothems of the Alpine Triassic. in Symposium on Cyclic Sedimentation. D. F. Merriam, ed., State Geological Survey of Kansas, Bulletin 169, v. 1, p. 107-149.

Ginsburg, R. N., 1971. Landward movement of carbonate mud: new model for regressive cycles in carbonates (Abstract). American Association of Petroleum Geologists Bulletin, v. 55, p. 340.

Ginsburg, R. N., and James, N. P., 1974. Holocene carbonate sediments of continental shelves. in The Geology of Continental Margins. C. A. Burke and C. L. Drake, eds., Springer-Verlag, New York, p. 137-157.

Grotzinger, J. P., 1981. The stratigraphy and sedimentation of the Wallace Formation, northwest Montana and Idaho. unpubl. Master's Thesis, Univ. Montana, Missoula, p. 153.

Grotzinger, J. P., and Hoffman, P. F., 1983. Quantitative paleobathymetry of Early Proterozic (1.9 b.y.) continental slope, Rocknest Formation, Wopmay Orogen, N. W. Territories, Canada. American Assiciation of Petroleum Gelolgists Bulletin, v. 67, p. 475.

Hamblin, A. P., and Walker, R. G., 1979. Storm-dominated shallow marine deposits: The Fernie-Kootenay (Jurrassic) transition, southern Rocky Mountains. Canadian Journal Earth Science, v. 16, p. 1673-1690.

Hays, J. D., Imbrie, J., and Shackleton, J. J., 1976. Variations in the Earth's orbit: Pacemaker of the Ice Ages. Science, v. 194, p. 1121-1132.

Hays, J. D., and Pitman, W. C., III, 1973. Lithospheric plate motion, sea-level changes and climatic and ecological consequences. Nature, v. 246, p. 18-22.

Heckel, P. H., 1974. Carbonate buildups in the geologic record: a review. in Reefs in Time and Space. L. F. Laporte, ed., Soc. of Econ. Paleont., and Mineral., Special Publication 18, p. 90-155.

Hileman, M. E., and Mazzullo, S. J., eds., 1977. Upper Guadalupian facies, Permian reef complex, Guadalupe Mountains, New Mexico and West Texas. in 1977 Field Conference Guidebook, Pub 77-16, p. 508.

Hine, A. C., and Neumann, A. C., 1977. Shallow carbonate-bank-margin growth and structure, Little Bahama Bank, Bahamas. American Association of Petroleum Geologists, Bulletin, v. 61, p. 376-406.

Hoffman, P. F., 1969. Proterozoic paleocurrents and depositional history of the East Arm Fold Belt, Great Slave Lake, Northwest Territories. Canadian Journal of Earth Sciences, V. 6, no. 3, p. 441-462.

_____, 1973. Evolution of an early Proterozoic continental margin: The Coronation geosyncline and associated aulacogens of the northwestern Canadian shield. Royal Society of London Philosophical Transactions, ser. A, v. 273, p. 547-581.

_____, 1974. Shallow and deepwater stromatolites in Lower Proterozoic platform-to-basin facies change, Great Slave Lake, Canada. American Association of Petroleum Geologists Bulletin, v. 58, no. 5, p. 856-867.

_____, 1975. Shoaling-upward shale-to-dolomite cycles in the Rocknest Formation (Lower Proterozoic), N.W. Territories, Canada. in Tidal Deposits. R. N. Ginsburg, ed., Springer-Verlag, New York, p. 257-265.

_____, 1976. Environmental diversity of Middle Precambrian stromatolites. in Stromatolites. M. R. Walter, ed., Developments in Sedimentology, v. 20, p. 599-611.

_____, 1980. Wopmay Orogen: A Wilson cycle of early Proterozoic age in the northwest of the Canadian Shield. in The continental crust and its mineral deposits. D. W. Strangway, ed., Geological Association of Canada Special Paper 20, p. 523-549.

_____, Supercontinents, "world-wide" orogenies, anorogenic magmatism and the North American Precambrian; submitted to Geology.

Hoffman, P. F., and Bowring, S. A., 1984. Short-lived 1.9 Ga continental margin and its destruction, Wopmay Orogen, northwest Canada. Geology, v. 12, p. 68-72.

Hoffman, P. F., Tirrul, R., and Grotzinger, J. P., 1983. The externides of Wopmay Orogen, Point Lake and Kikerk Lake map areas, District of Mackenzie. in Current Research, Part A, Geological Survey of Canada, Paper 83-1A, p. 429-435.

Hoffman. P. F., Tirrul, R., Grotzinger, J. P., Lucas, S. B., and Eriksson, K. A., 1984. The externides of Wopmay Orogen, Takijuq Lake and Kikerk Lake map areas, District of Mackenzie. in Current Research, Part A, Geological Survey of Canada, Paper 84-1A, p. 383-395.

Jackson, G. D., and Iannelli, T. R., 1981. Rift-related cyclic sedimentation in the Neohelikian Borden Basin, northern Baffin Island. in Proterozoic Basins of Canada. F.H.A. Campbell, ed., Geological Survey of Canada, Paper 81-10, p. 269-302.

Imbrie, J., and Imbrie, J. Z., 1980. Modeling the climatic response to orbital variations. Science, v. 207, no. 4434, p. 943-952.

Jackson, M. J., 1982. Correlations of stromatolites between northern Australia and U.S.S.R. in Abstracts of Papers, International Association of Sedimentologists, Hamilton, p. 161.

_____, 1984. Sedimentology of an early Proterozoic calc-flysch to molasse transition in northwestern Canada; rhythmite to reef to river. in Abstracts, Geological Association of Canada, v. 9.

James, N. P., 1983. Reef Environment. in Carbonate Depositional Environments. P. A. Scholle, D. G. Bebout, C. H. Moore, eds., American Association of Petroleum Geologists, Memoir 33, p. 345-462.

_____, 1984a. Shallowing-upward sequences in carbonates. in Facies Models, second edition. R. G. Walker, ed., Geoscience Canada, Reprint Series 1, p. 213-228.

_____, 1984b. Reefs. in Facies Models, second edition. R. G. Walker, ed., Geoscience Canada, Reprint Series 1, p. 229-244.

James, N. P., Ginsburg, R. N., Marszalek, D., and Choquette, P. W., 1976. Facies and fabric specificity of early subsea cementation in shallow Belize (British Honduras) reefs. Journal of Sedimentary Petrology, v. 46, p. 523-544.

James, N. P., and Mountjoy, E. W., 1983. Shelf-slope break in fossil carbonate platforms: an overview. in The shelfbreak: critical interface on continental margins. D. J. Stanley and G. T. Moore, eds., Soc. Econ. Paleont. Mineral., Special Publication 33, p. 189-206.

Kendall, C.St.G.C., and Skipwith, P.A.d'E., 1969. Holocene shallow-water carbonate and evaporite sediments of Khor al Bazam, Abu Dhabi, Southwest Persian Gulf. Journal of Sedimentary Petrology, v. 38, p. 1040-1058.

Kerans, C., 1982. Sedimentology and stratigraphy of the Dismal Lakes Group. Ph.D thesis, unpublished; Carleton University, Ottawa, Ontario.

Koerschner, W. F., III, 1983. Cyclic peritidal facies of a Cambrian aggraded shelf: Elbrook and Conococheague Formations, Virginia Appalachians. unpubl. Master's Thesis, Virginia Tech, Blacksburg, p. 184.

Kominz, M. A., and Bond, G. C., 1984. Thermal modeling of foreland basins: effects on flexure and uplift. in Abstracts with Programs, Geological Society of America, v. 16, no. 6, p. 564.

Krause, F. F., and Oldershaw, A. E., 1979. Submarine carbonate breccia beds - a depositional model for two-layer, sediment gravity flows from the Sekwi Formation (Lower Cambrian), Mackenzie Mountains, N.W. Territories. Canadian Journal of Earth Sciences, v. 16, p. 189-199.

Logan, B. W., Harding, J. L., Ahr, W. M., Williams, J. D., and Snead, R. G., 1969. Carbonate sediments and reefs, Yucatan shelf, Mexico. American Association of Petroleum Geologists, Memoir 11, p. 1-198.

Logan, B. W., Hoffman, P. F., and Gebelein, C., 1974. Evolution and diagenesis of Quaternary carbonate sequences, Shark Bay, Western Australia. American Association of Petroleum Geologists, Memoir 22, p. 358.

Lohmann, K. C., 1976. Lower Dresbachian (Upper Cambrian) platform to deep-shelf transition in Eastern Nevada and Western Utah: an evaluation through lithologic cycle correlation. in Paleontology and Depositional Environments: Cambrian of Western North America. R. A. Robison and A. J. Rowell, eds., Geological Studies, Brigham Young University, v. 23, p. 111-122.

Lucas, S. B., 1984. Low-grade metamorphism in the externides of Wopmay Orogen, N. W. Territories. in Program with Abstracts, Geological Association of Canada, v. 9, p. 85.

Major, R. P., and Matthews, R. K., 1983. Isotopic composition of bank margin carbonates on Midway Atoll: Amplitude constraint on post-early Miocene eustasy. Geology, v. 11, p. 335-338.

Malek-Aslani, M., 1970. Lower Wolfcampian reef in Kemnitz Field, Lea County, New Mexico. Ammerican Association Petroleum Geologists Bulletin, v. 54, p. 2317-2335.

Margara, K., 1973. Compaction and fluid migration in Cretaceous shales of Western Canada. Canada Geological Survey Paper 72-18,

Mathews, R. K., 1984. Dynamic Stratigraphy: An Introduction to Sedimentation and Stratigraphy, second edition. Prentice-Hall, Inc., Englewood Cliffs, N.J.

McGlynn, J. C. and Ross, J. V., 1963. Arseno Lake map-area, District of Mackenzie (86 b/12). Geological Survey of Canada Paper 63-26, p. 7.

McKenzie, D., 1978. Some remarks on the development of sedimentary basins. Earth and Planet. Science Lett. (Neth.), v. 40, p. 25-32.

Mesolella, K. J., Matthews, R. K., Broecker, W. S., and Thurber, D. L., 1969. The astronomical theory of climatic changes: Barbados data. Journal Geology, v. 77, p. 250-274.

Mial, A. D., 1983. Glaciomarine sedimentation in the Gowganda Formation (Huronian), northern Ontario. Journal of Sedimentary Petrology, v. 53, no. 2, p. 477-491.

Moore, C. H., and Druckman, Y., 1981. Burial diagenesis and porosity evolution, Upper Jurassic Smackover, Arkansas and Louisiana. American Association of Petroleum Geologists Bulletin, v. 65, p. 597-628.

Moore, R. C., 1964. Paleoecological aspects of Kansas Pennsylvanian and Permian cyclothems. in Symposium on Cyclic Sedimentation. Daniel F. Merriam, ed., Kansas Geological Survey Bulletin 169, v. 1, p. 287-380.

Morner, N., 1976. Eustasy and geoid changes. The Journal of Geology, v. 84, no. 2, p. 123-151.

_____, 1981. Eustasy, paleoglaciation and paleoclimatology. Geologische Rundschau, v. 70, p. 691-702.

_____, 1983. Sea levels. in Mega-Geomorphology. R. Gardner and H. Scoging, eds., Oxford University Press, p. 74-91.

Mullins, H. T., and Neumann, A. C., 1979. Carbonate slopes along open seas and seaways in the northern Bahamas. in Geology of continental slopes. L. A. Doyle and O. H. Pilkey, eds., Soc. Econ. Paleont. Mineral., Special Publication 27, p. 165-192.

Peltier, W. R., 1984. A model of the ice age cycle. Terra Cognita, v. 4, no. 2, p. 261-262.

Peltier, W. R., and Hyde, W., 1984. A model of the ice age cycle. in Milankovitch and Climate; Part 2. A. L. Berger et al., eds., D. Reidel Publishing Co., p. 565-580.

Pitman, W. C., III, 1978. Relationship between eustacy and stratigraphic sequences of passive margins. Geological Society of America Bulletin, v. 89, p. 1389-1403.

Playford, P. E., 1980. Devonian "Great Barrier Reef" of the Canning Basin, Western Australia. American Association of Petroleum Geologists Bulletin, v. 64, p. 814-840.

Pratt, Brian R., and James, Noel P., 1982. Cryptalgal-metazoan bioherms of early Ordovician age in the St. George Group, western Newfoundland. Sedimentology, v. 29, p. 543-569.

Read, J. F., 1973. Carbonate cycles, Pillara Formation (Devonian), Canning Basin, Western Australia. Bulletin of Canadian Petroleum Geology, v. 21, p. 38-51.

____, 1980. Carbonate ramp-to-basin transitions and foreland basin evolution, Middle Ordovician, Virgina Appalachians. American Association of Petroleum Geologists Bulletin, v. 64, p. 1575-1612.

____, 1982. Carbonate platforms of passive (extensional) continental margins: Types, characteristics, and evolution. Tectonophysics, v. 81, p. 195-212.

Read, J. F., and Grotzinger, J. P., in prep. Models for shallowing-upward cycles in carbonates.

Royden, L., and Keen, C. E., 1980. Rifting process and thermal evolution of the continental margin of eastern Canada determined from subsidence curves. Earth and Planetary Science Letters, v. 51, p. 343-361.

Ruppel, S. C., and Walker, K. R., 1984. Petrology and depositional history of a Middle Ordovician carbonate platform: Chickamauga Group, northeastern Tennessee. Geological Society of America Bulletin, v. 95, p. 568-583.

Schlager, W., 1981. The paradox of drowned reefs and carbonate platforms. Geological Society of America Bulletin, Part I, v. 92, p. 197-211.

Shinn, E. A., 1969. Submarine lithification of Holocene carbonate sediments in the Persian Gulf. Sedimentology, v. 12, p. 109-144.

Sleep, N. H., 1971. Thermal effects of the formation of Atlantic continental margins: evidence from older margins by continental breakup. Geophys. J.R. Astr. Soc., v. 24, p. 325-350.

Sneh, A., and Friedman G. M., 1980. Spur and groove patterns on the reefs of the northern gulfs of the Red Sea. Journal of Sedimentary Petrology, v. 50, no. 3, p. 981-986.

Soegaard, K., 1984. Sedimentological constraints on Precambian crustal evolution in northern New Mexico. unpubl. Ph.D Dissertation, Virginia Tech, Blacksburg.

Steinen, R. P., Harrison, R. S., and Mathews, R. K., 1973. Eustatic low stand of sea level between 125,000 and 105,000 B.P.: Evidence from the subsurface of Barbados, West Indies. Geological Society of America Bulletin, v. 84, p. 63-70.

Thompson, P. H., and Ashton, K., 1984. Preliminary report on the geology of the Tinney Hills-Overby Lake (W 1/2) map area - a look at the Thelon Tectonic Zone northeast of the Bathurst Fault. in Current Research, Part A, Geological Survey of Canada, Paper 84-1A, p. 415-423.

Tirrul, R., 1982. Frontal thrust zone of Wopmay Orogen, Takijuq Lake map area, District of Mackenzie. in Current Research, Part A, Geological Survey of Canada, Paper 82-1A, p. 119-122.

_____, 1983. Structure cross-sections across Asiak Foreland Thrust and Fold Belt, Wopmay Orogen, District of Mackenzie. in Current Research, Part B, Geological Survey of Canada Paper 83-1B, p. 253-260.

_____, 1985. Nappes in the Kilohigok Basin, N. W. Territories and their relation to the Thelon Tectonic Zone. in Current research, Part A, Geological Survey of Canada Paper 85-1A.

Vail, P. R., Mitchum, R. M., and Thompson, S., III, 1977. Seismic stratigraphy and golobal changes of sea level, Part 3: Relative changes of sea level from coastal onlap. in Seismic stratigraphy - Applications to hydrocarbon exploration. C. Payton, ed., American Association of Petroleum Geologists Memoir 26, p. 63-81.

Walker, R. G., 1984. Shelf and shallow marine sands. in Facies Models, second edition. R. G. Walker, ed., Geoscience Canada, Reprint Series 1, p. 141-170.

Wilkinson, B. R., 1982. Cyclic cratonic carbonates and Phanerozoic calcite seas. Journal of Geological Education, v. 30, p. 180-203.

Wilson, J. L., 1975. Carbonate Facies in Geologic History. Springer-Verlag, New York.

Appendix A

MEASURED SECTIONS

This appendix contains 22 measured sections of the Rocknest Formation. The location of sections is shown in Figure 41. Note that section 12 is located in the Peacock Hills area of Kilohigote Basin.

Because of the scale of the sections, beds thinner than 1 m plot poorly. Consequently, the thickness of intraclast packstone beds at cycle bases is exaggerated. These beds are actually 10 to 30 cm thick, but the sections are shown to be up to 1 m thick. Also, there commonly is a transitional interval, 30 to 50 cm thick, of thick-laminated dolosilitite, between argillaceous dololutites and overlying stromatolites/thrombolites or crytalgalamite. In the measured sections, this facies is often incorporated as part of the underlying argillaceous dololutite. Finally, the argillaceous dololutite facies contains locally abundant cross-bedded and hummocky, cross-stratified sands (carbonate and silliclastic) that are 10 to 30 cm thick, and therefore cannot be plotted.

Sections 11, 20, 21, and 22 contain slope rhythmites which consist of thin to thick laminated dololutite and dolosiltite. However, in the measured sections, they are

represented by using the symbols for "cryptalgalamite" or "thick-laminated dolosiltite" (see key). These rhythmites should not be confused with true cryptalgalaminites and thick laminated dolosiltites of the shelf.

Boundaries between the Rocknest Formation (R. FM.), and Odjick Formation (O. FM.) and Recluse Group (R. GRP.) are plotted on the measured sections where they occur. Note that in section 12, the Burnside River Formation encloses the Rocknest Formation. With regard to all sections, many stratigraphic contacts with the Odjick Formation or Recluse Group are either covered or structurally displaced.

Figure 41. Location of measured sections for Appendix A. See text and figure 1 for discussion of geology and regional setting of map units. Note that section 12 is located at the Peacock Hills area of Kilohigok Basin. All sections are approximately located; exact coordinates will be provided upon request.

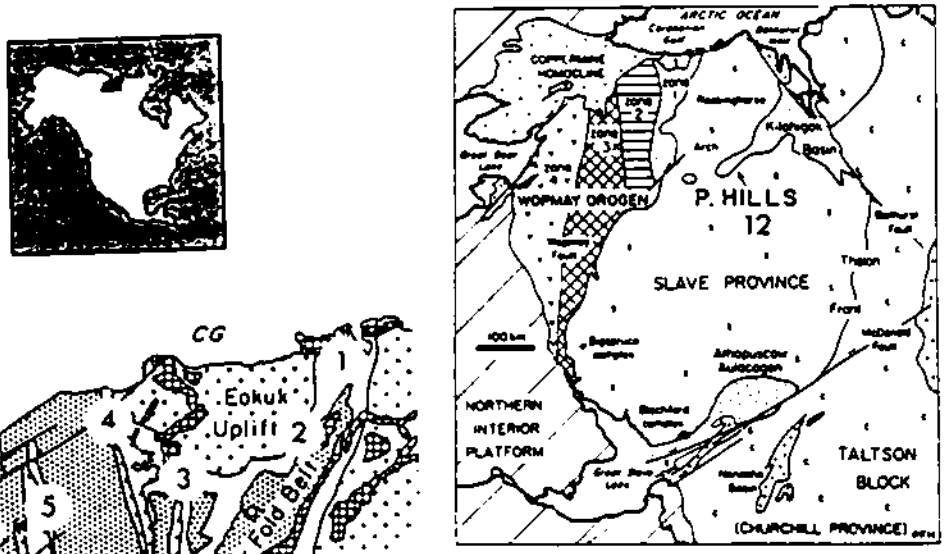

(A)

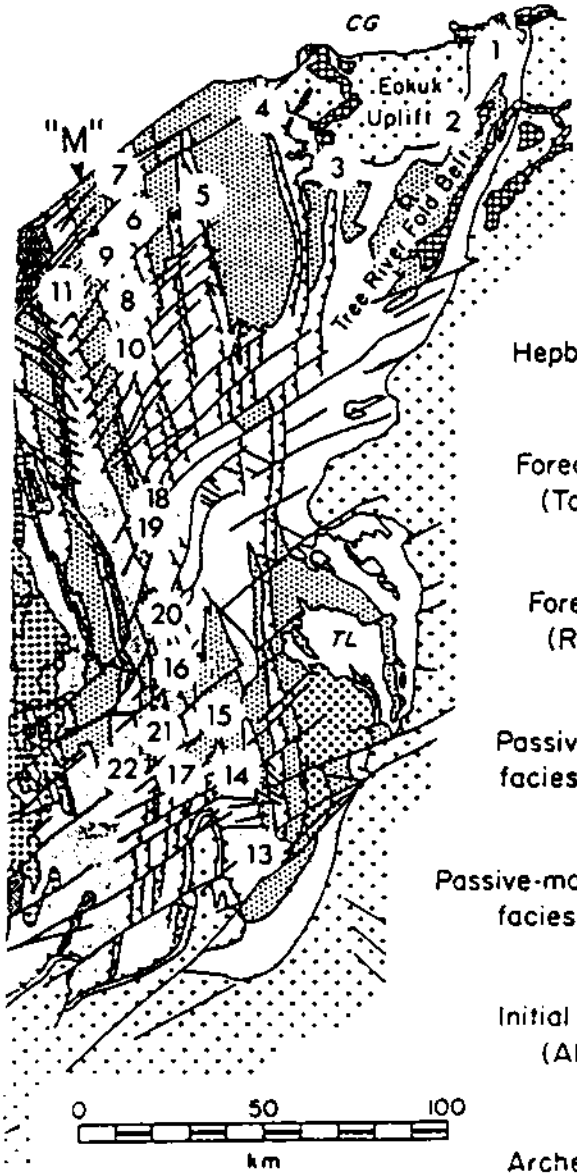

Hepburn Intrusives

Foredeep molasse (Takiyuak Fm)

Foredeep flysch (Recluse Gp)

Passive-margin shelf facies (Epworth Gp)

Passive-margin slope-rise facies (Epworth Gp)

Initial rift sequences (Akaitcho Gp)

CORONATION SUPERGROUP

Archean basement

(B)

The vita has been removed from the scanned document

KEY

LITHOFACIES

- SILICICLASTIC SANDSTONE
- " SILTSTONE
- S " DETRITUS ABUNDANT
- ARGILLACEOUS DOLOLUTITE/SILTITE
- THICK LAMINATED DOLOSILTITE
- CRYPTALGALAMINITE
- LAMINAR TO INCIPIENTLY MICRODIGITATE TUFA
- MICRODIGITATE TUFA
- INTRACLAST GRAINSTONE
- " PACKSTONE
- OOID/INTRACLAST GRAINSTONE/PACKSTONE
- DOLARENITE

STROMATOLITES

- DOMES; SMOOTH, FENESTRAL, THROMBOLITIC
- PEAKED DOMES
- WAVY-LAMINATED DOMES
- MOUNDS, TANGENTIAL-LAMINATED
- MOUNDS, LAMINATED W/ DIGITATE FINGERS
- COLUMNS; SMOOTH, FENESTRAL, THROMBOLITIC
- COLUMNS, CONICAL
- BRANCHING COLUMNS
- " "
- " "

SEDIMENTARY STRUCTURES

- CROSS-BEDDING; PLANAR, HERRINGBONE, FESTOON
- CROSS-LAMINATION; UNIDIRECTIONAL, WAVE
- PLANAR LAMINATION
- ELONGATE STROMATOLITES
- RIP-UP INTRACLASTS, EDGEWISE CONGLOMERATE
- OOIDS, PISOLITHS, ENCRUSTED BLOCKS
- DESICCATION CRACKS, SYNAERESIS CRACKS
- TEPEES, FIBROUS CEMENT-FILLED FISSURES
- HALITE CASTS
- CHERT; LIGHT, BLACK, NODULAR, "SPLOTCHY"

SECTION 1

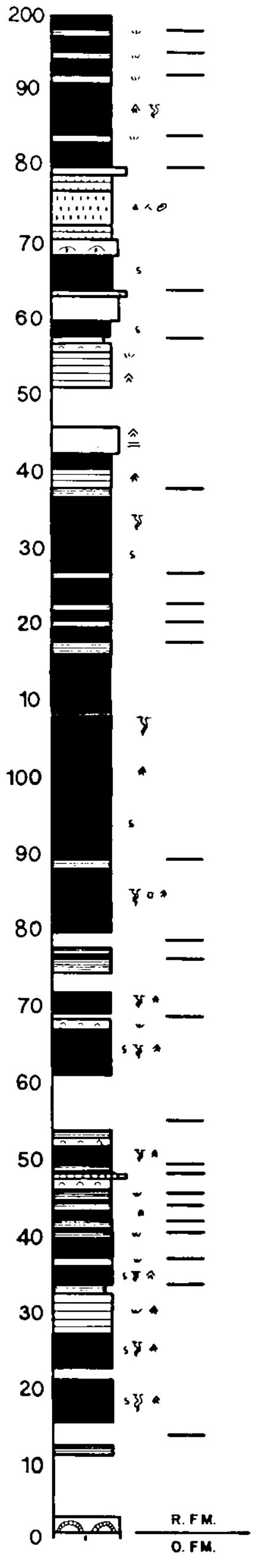
200
90
80
70
60
50
40
30
20
10
100
90
80
70
60
50
40
30
20
10
0
R. FM.
O. FM.

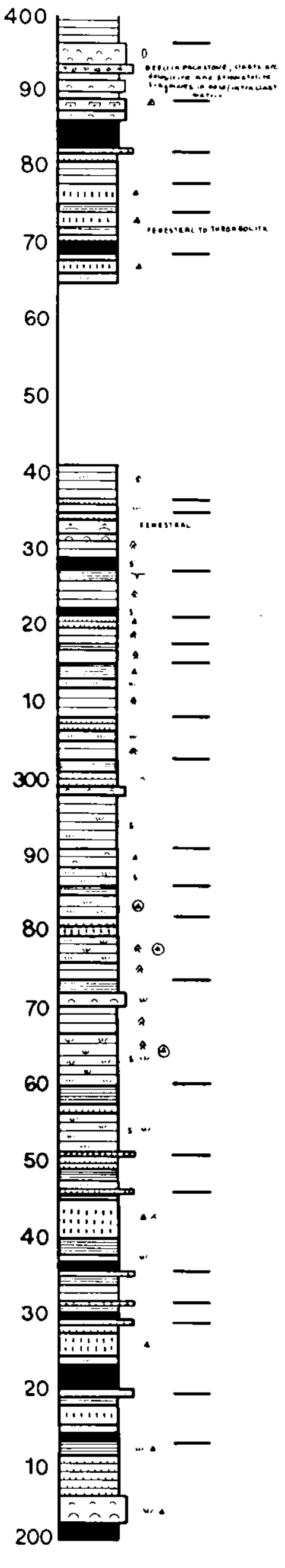
400
90
80
70
60
50
40
30
20
10
300
90
80
70
60
50
40
30
20
10
200
D
FENESTRAL TO THROMBOLITIC
FENESTRAL

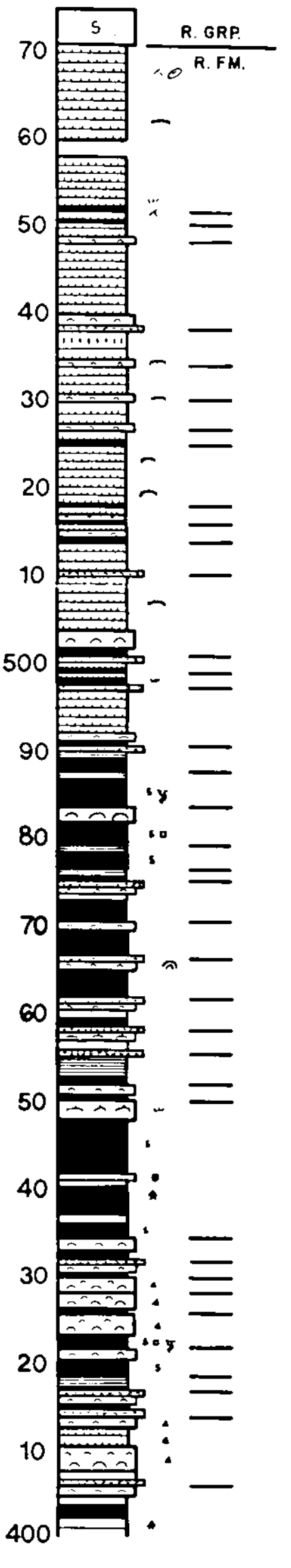
S
R. GRP.
R. FM.
70
60
50
40
30
20
10
500
90
80
70
60
50
40
30
20
10
400

SECTION 2

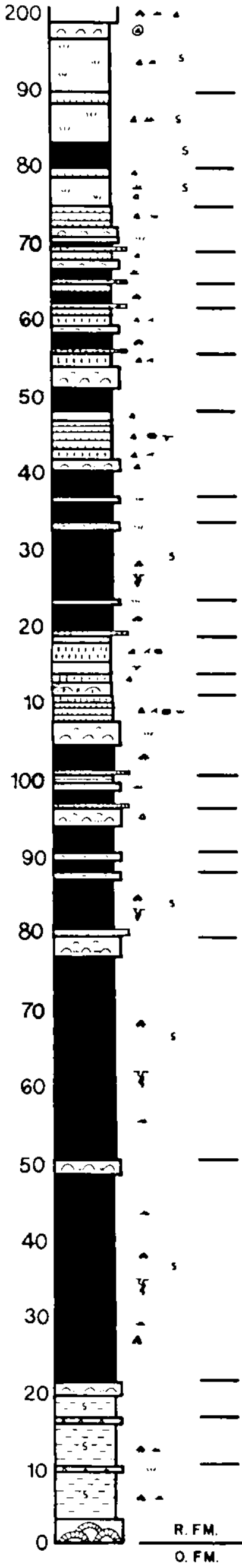
200
90
80
70
60
50
40
30
20
10
100
90
80
70
60
50
40
30
20
10
0
R. FM.
O. FM.

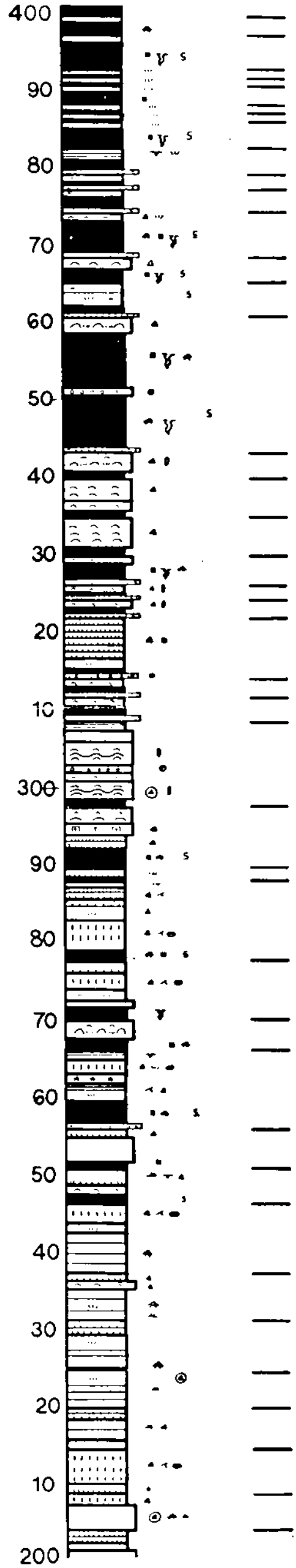
400
90
80
70
60
50
40
30
20
10
300
90
80
70
60
50
40
30
20
10
200

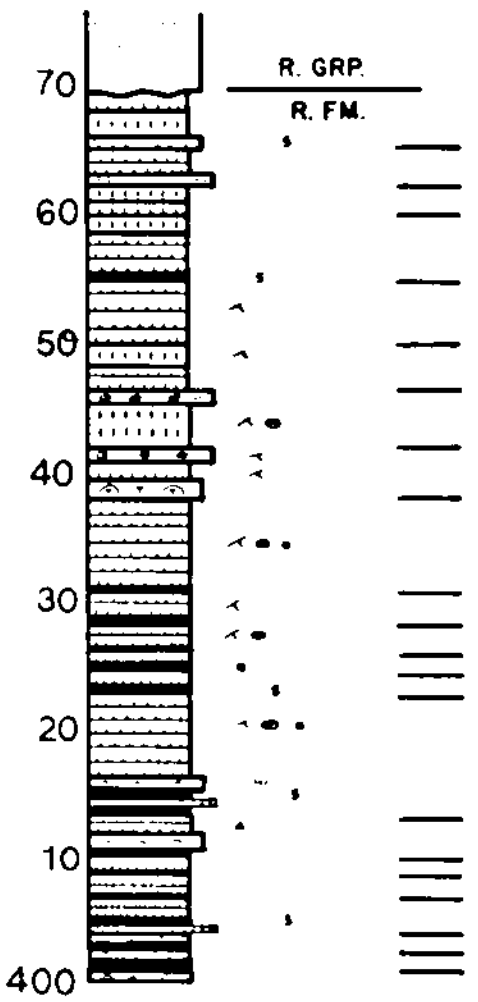
70
60
50
40
30
20
10
400
R. GRP.
R. FM.

SECTION 3

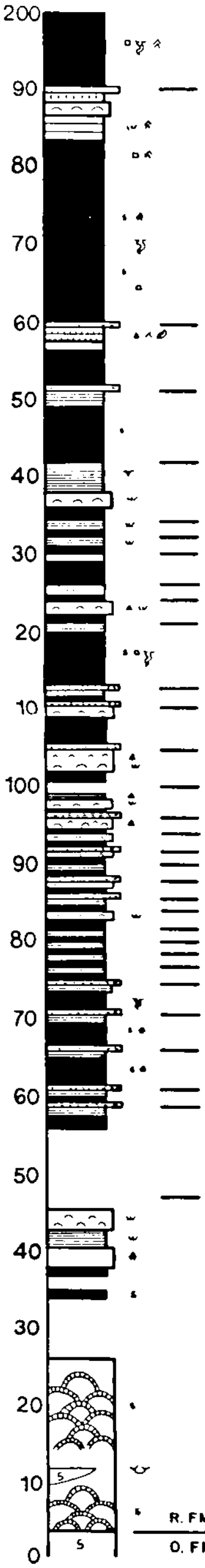
200
90
80
70
60
50
40
30
20
10
100
90
80
70
60
50
40
30
20
10
0
5
5
R. FM.
O. FM.

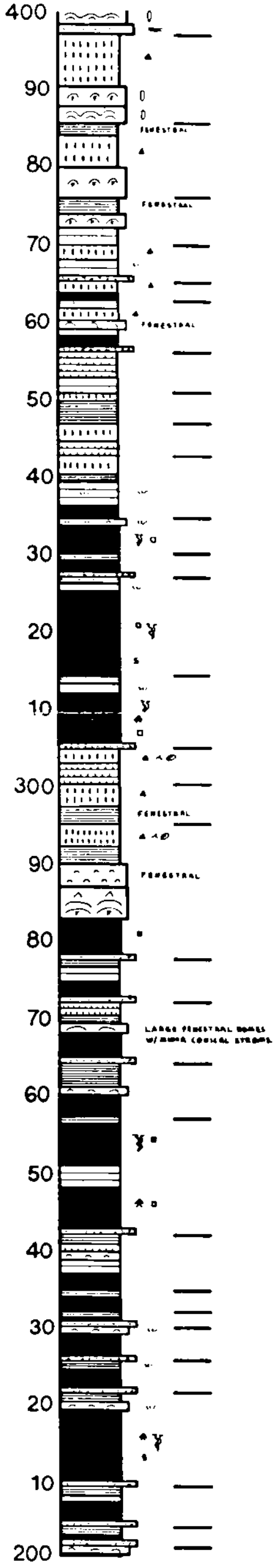
400
90
80
70
60
50
40
30
20
10
300
90
80
70
60
50
40
30
20
10
200
FENESTRAL
FENESTRAL
FENESTRAL
FENESTRAL
FENESTRAL
LARGE FENESTRAL DOMES

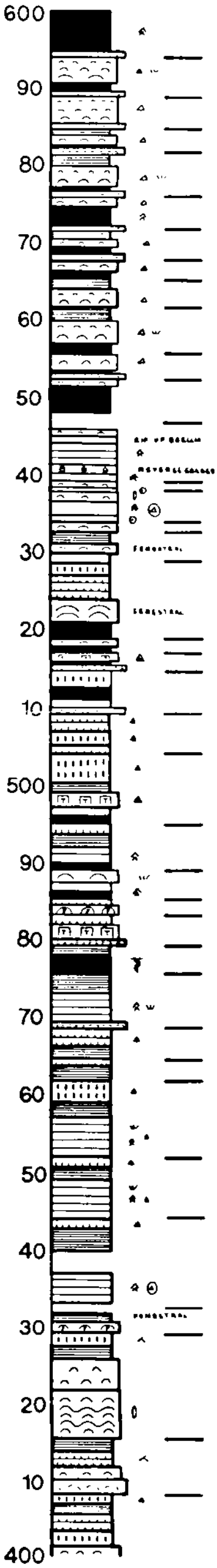
600
90
80
70
60
50
40
30
20
10
500
90
80
70
60
50
40
30
20
10
400
FENESTRAL
FENESTRAL
FENESTRAL

SEC. 3 CONT.

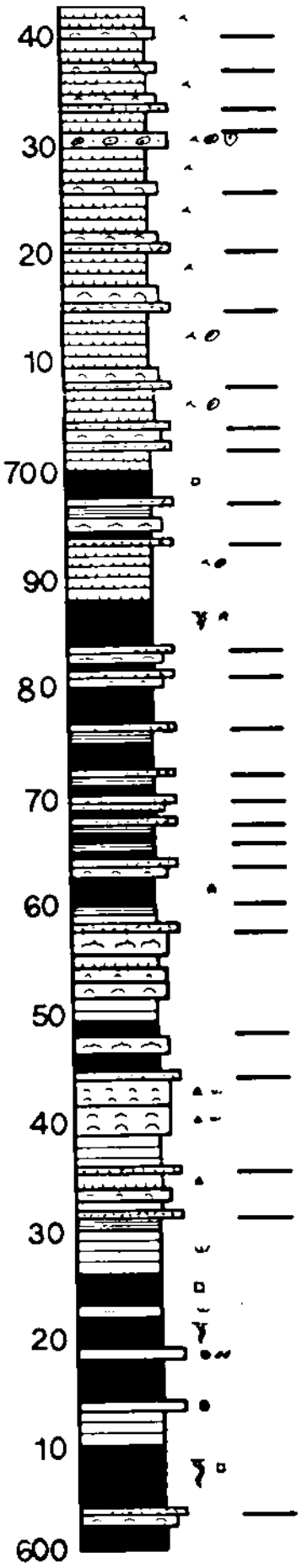

SECTION 4

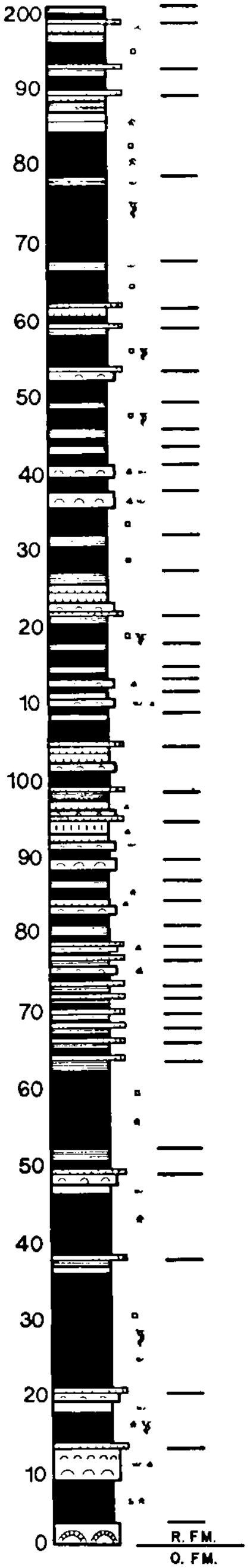
200
90
80
70
60
50
40
30
20
10
100
90
80
70
60
50
40
30
20
10
0
R. FM.
O. FM.

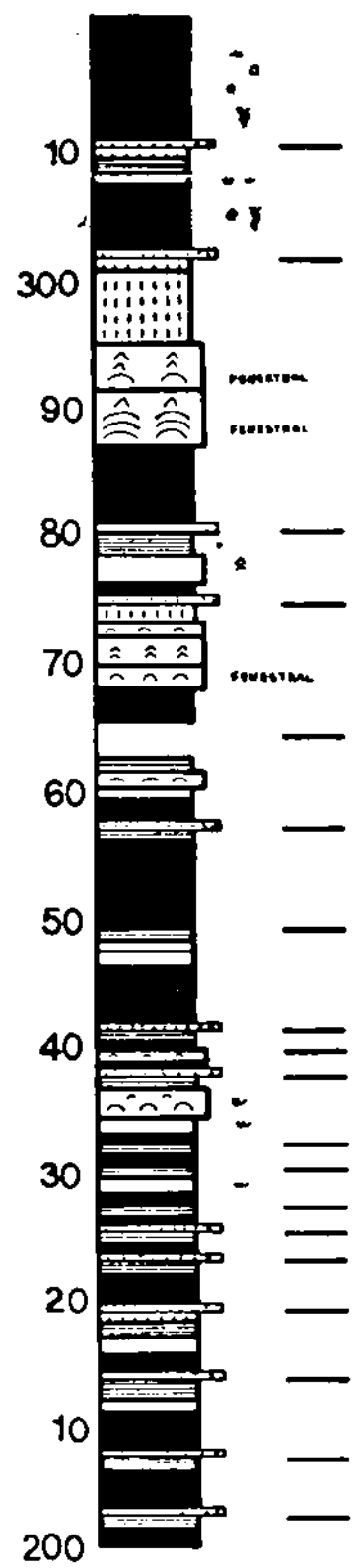
10
300
90
80
70
60
50
40
30
20
10
200

SEC. 4 CONT.

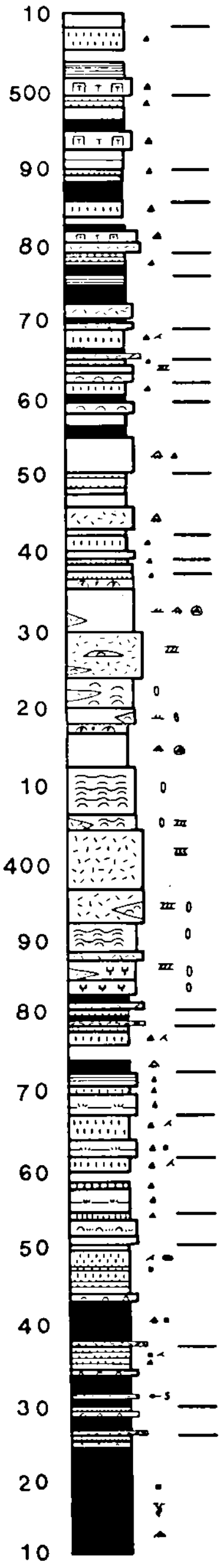
10
500
90
80
70
60
50
40
30
20
10
400
90
80
70
60
50
40
30
20
10

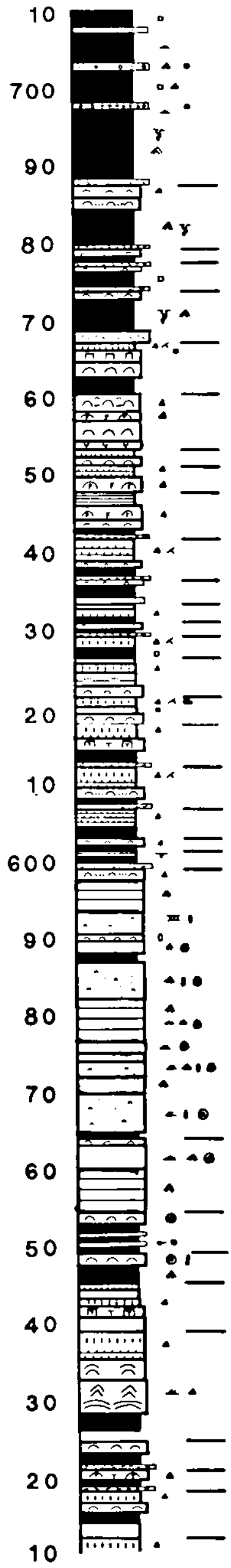
10
700
90
80
70
60
50
40
30
20
10
600
90
80
70
60
50
40
30
20
10

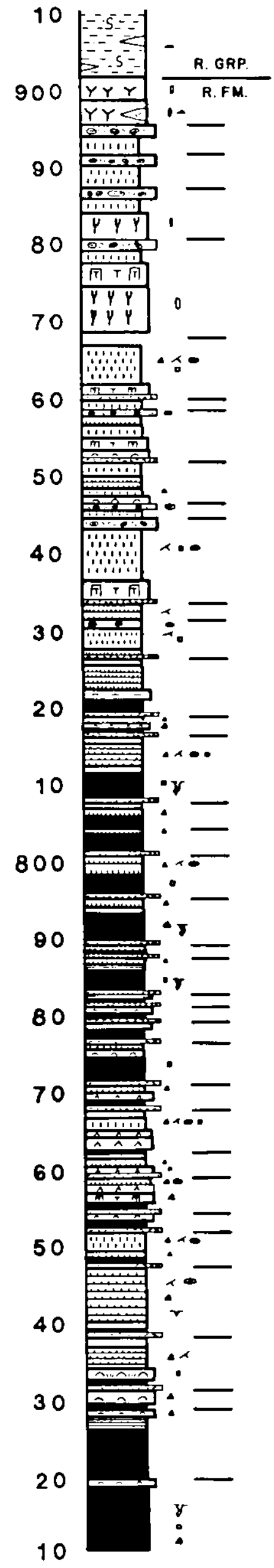
R. GRP.
R. FM.
10
900
90
80
70
60
50
40
30
20
10
800
90
80
70
60
50
40
30
20
10

SEC. 5 CONT.

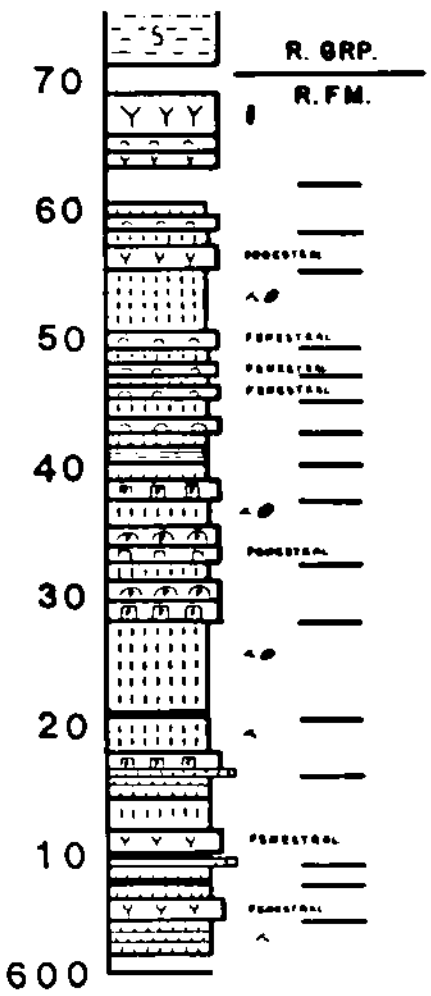

SECTION 6

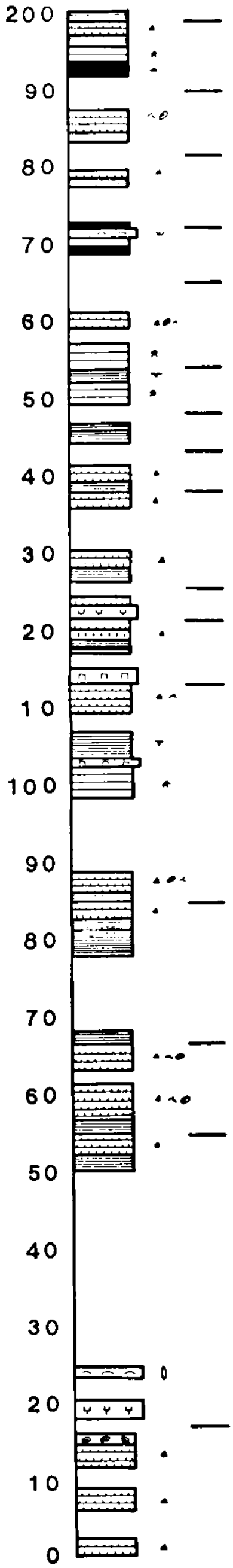
200
90
80
70
60
50
40
30
20
10
100
90
80
70
60
50
40
30
20
10
0

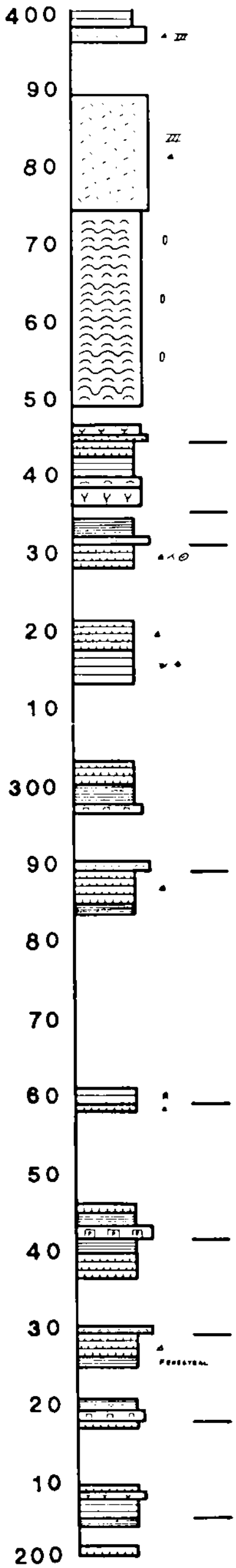
400
90
80
70
60
50
40
30
20
10
300
90
80
70
60
50
40
30
20
10
200

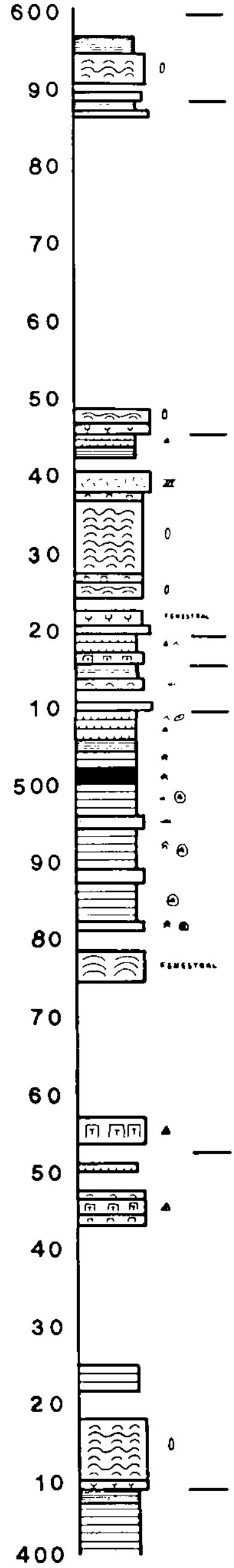
600
90
80
70
60
50
40
30
20
10
500
90
80
60
50
40
30
20
10
400

SEC. 6 CONT.

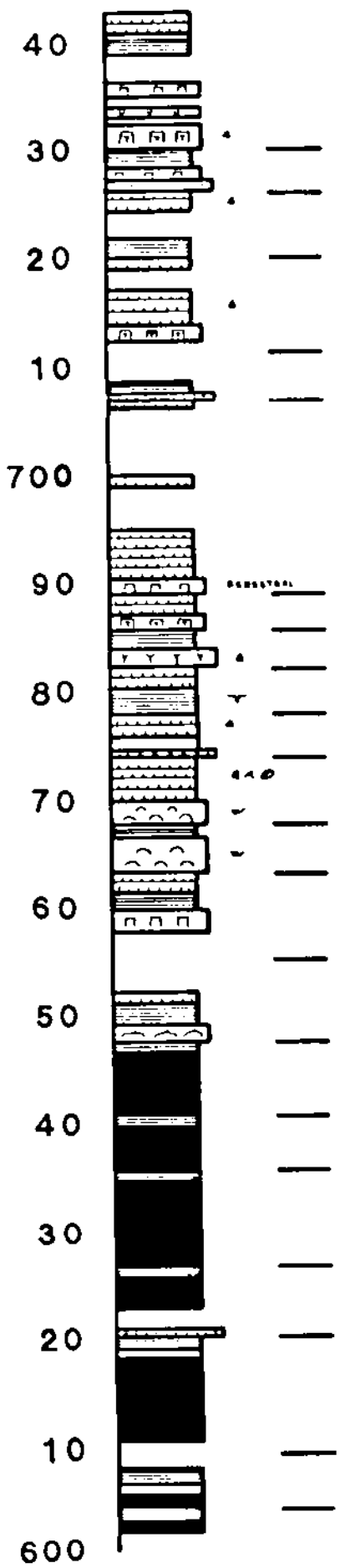

SECTION 7

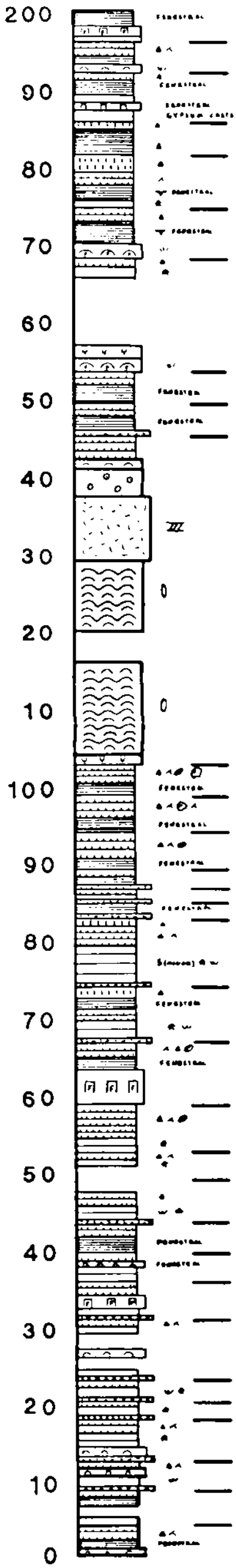
200
90
80
70
60
50
40
30
20
10
100
90
80
70
60
50
40
30
20
10
0

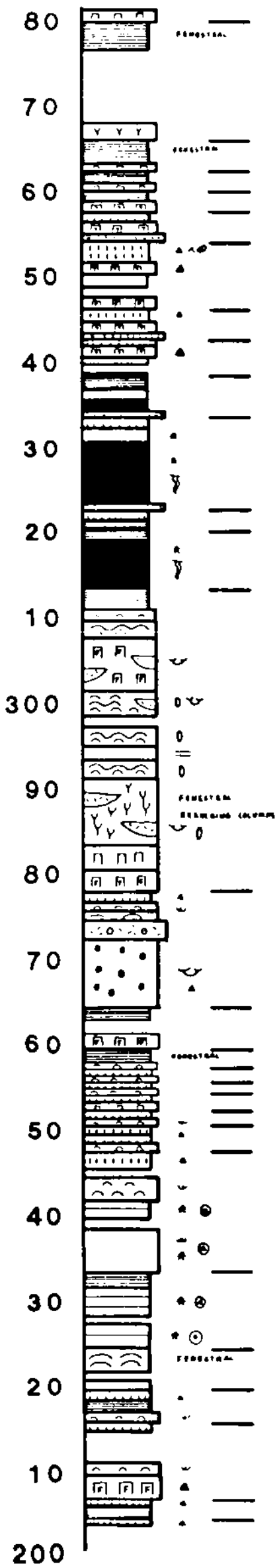
80
70
60
50
40
30
20
10
300
90
80
70
60
50
40
30
20
10
200

SECTION 8

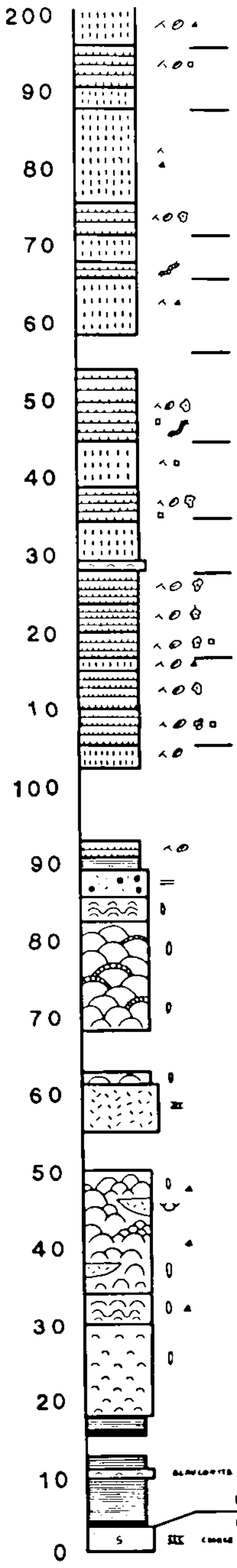
200
90
80
70
60
50
40
30
20
10
100
90
80
70
60
50
40
30
20
10
0
R. FM.
O. FM.
S

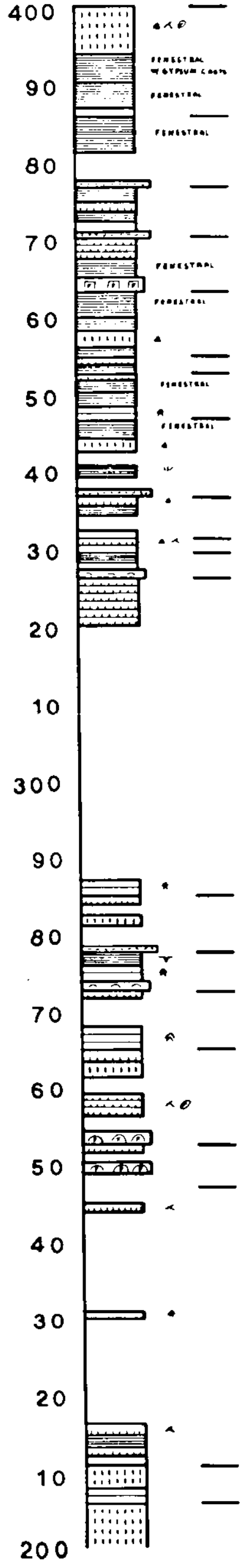
400
90
80
70
60
50
40
30
20
10
300
90
80
70
60
50
40
30
20
10
200

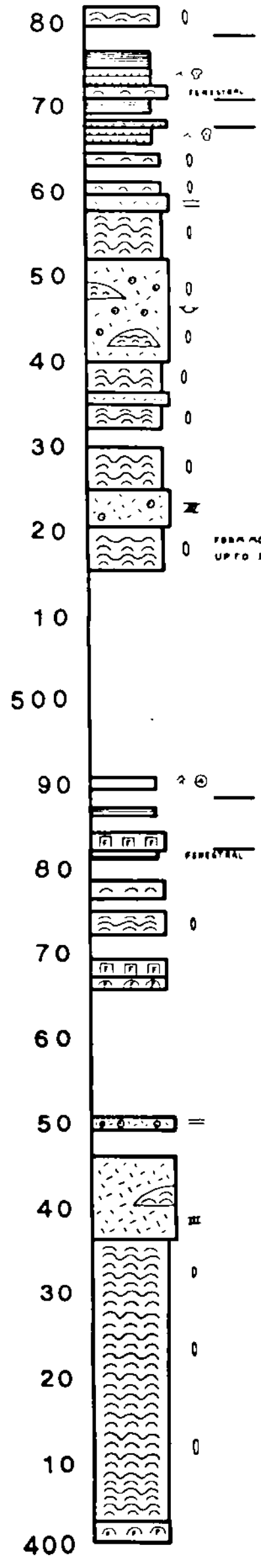
80
70
60
50
40
30
20
10
500
90
80
70
60
50
40
30
20
10
400

SECTION 9

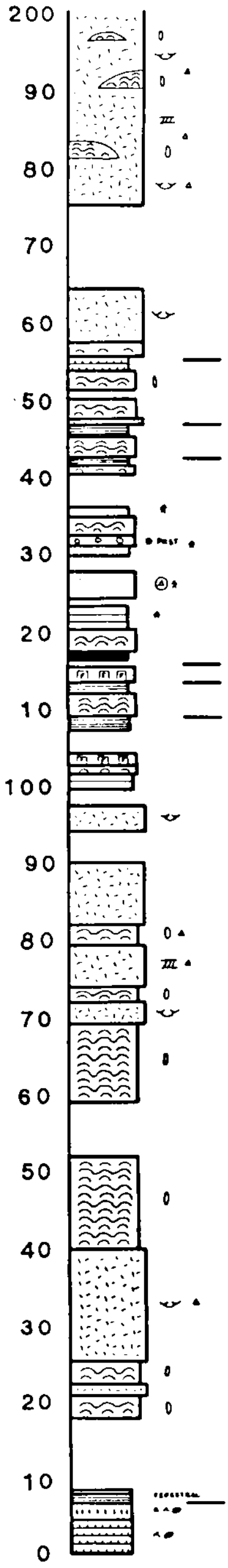
200
90
80
70
60
50
40
30
20
10
100
90
80
70
60
50
40
30
20
10
0

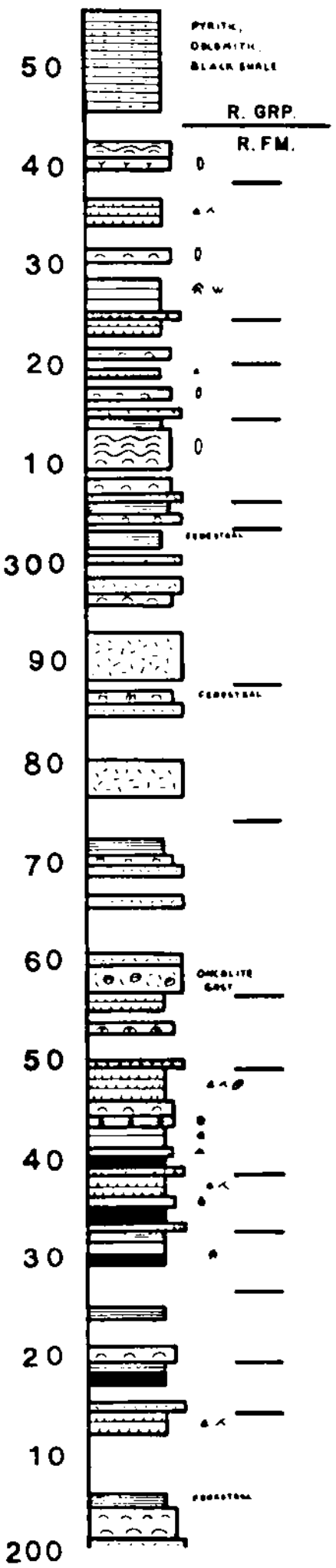
50
40
30
20
10
300
90
80
70
60
50
40
30
20
10
200
R. GRP.
R. FM.

SECTION 10

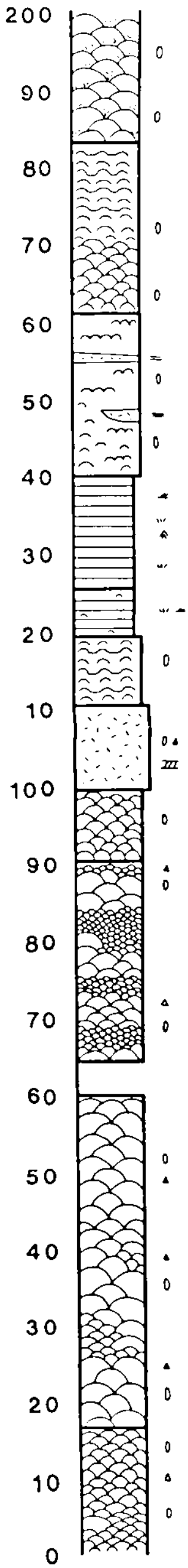
200
90
80
70
60
50
40
30
20
10
100
90
80
70
60
50
40
30
20
10
0

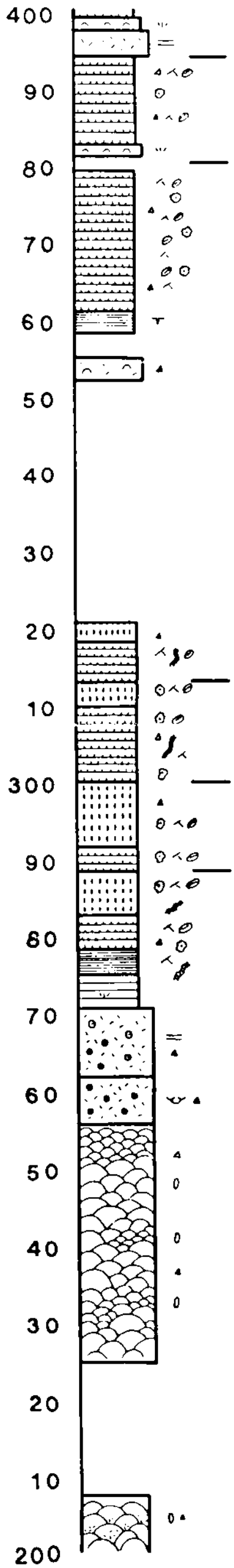
400
90
80
70
60
50
40
30
20
10
300
90
80
70
60
50
40
30
20
10
200

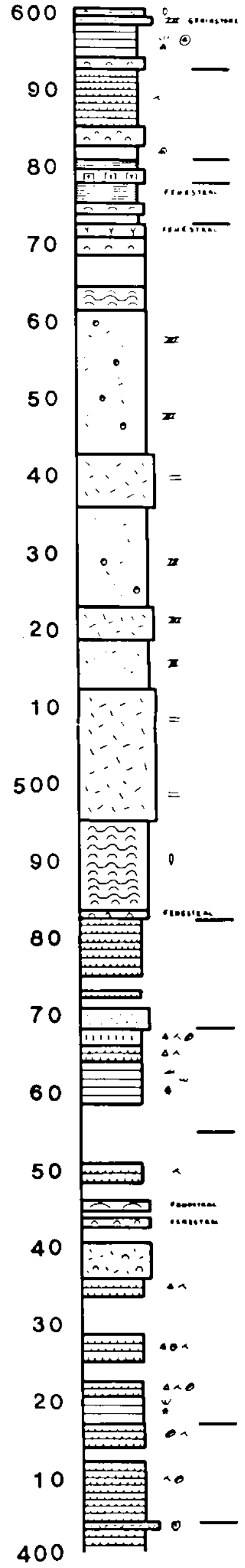
600
90
80
70
60
50
40
30
20
10
500
90
80
70
60
50
40
30
20
10
400

SEC. 10 CONT.

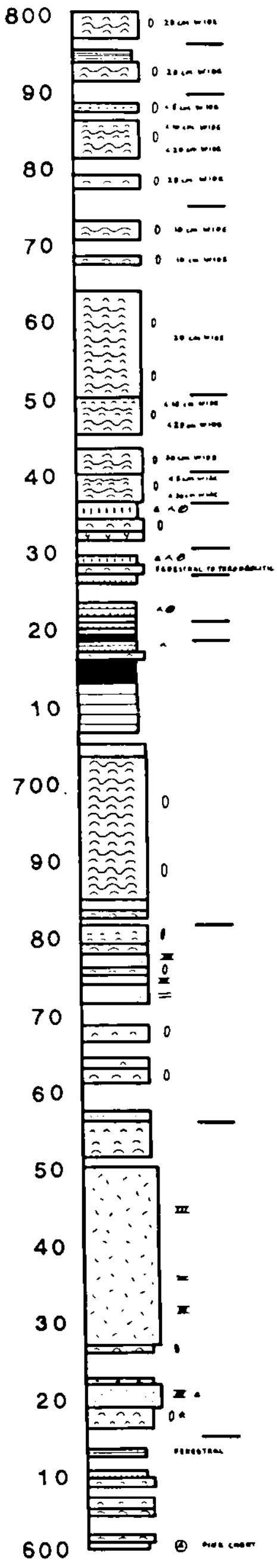

SECTION 11

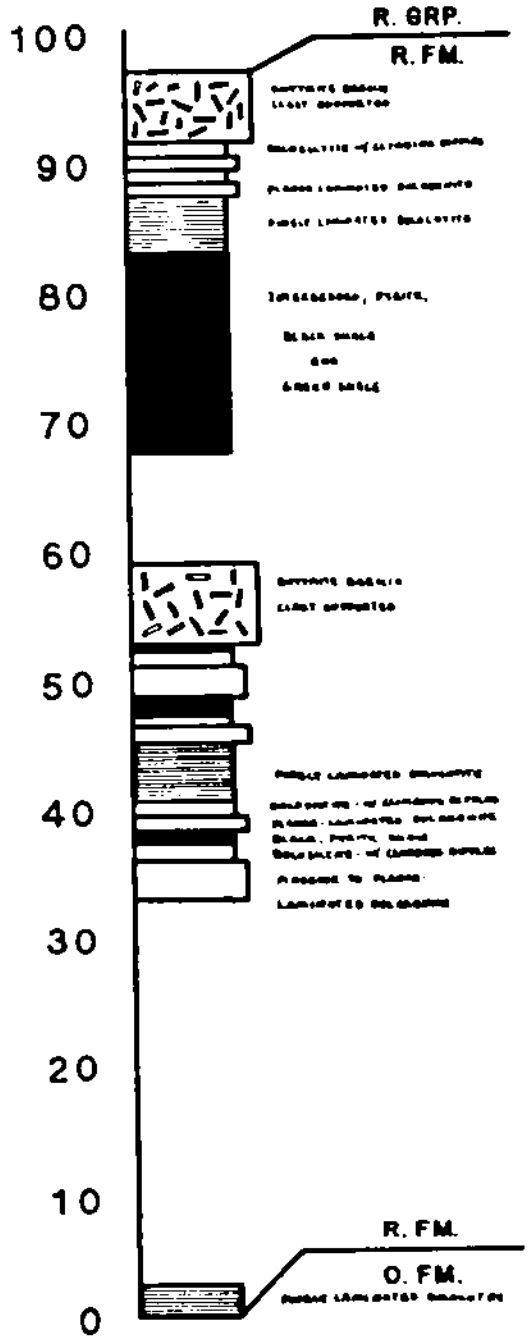

SECTION 12

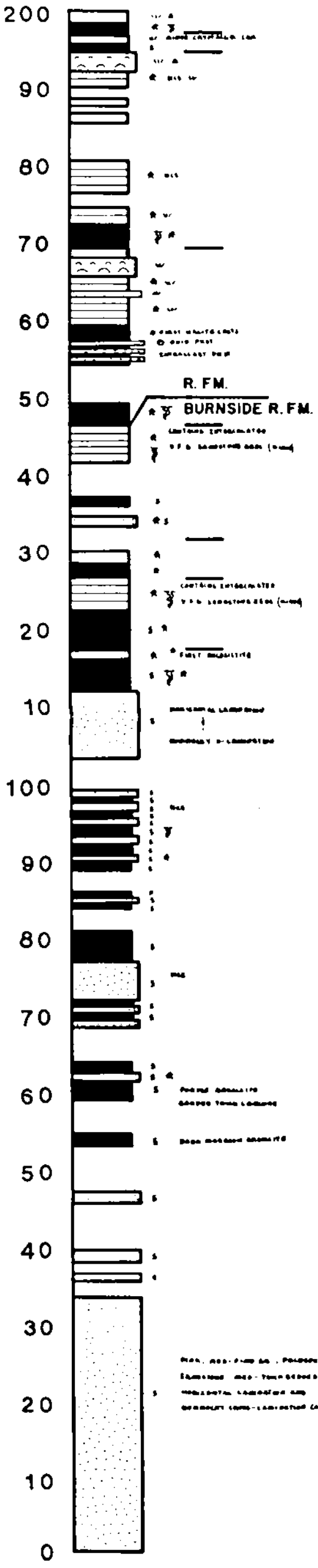
200
90
80
70
60
50
40
30
20
10
100
90
80
70
60
50
40
30
20
10
0
R. FM.
BURNSIDE R. FM.


10
200
BURNSIDE R. FM.
R. FM.

SECTION 13

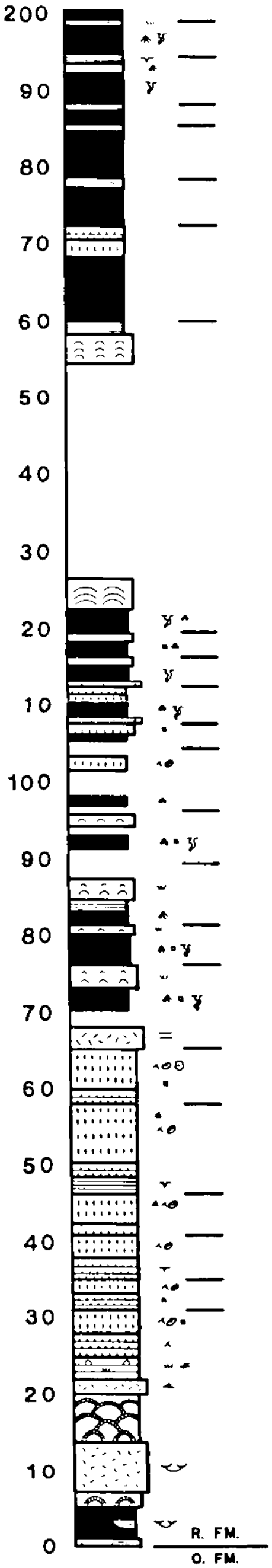
200
90
80
70
60
50
40
30
20
10
100
90
80
70
60
50
40
30
20
10
0
R. FM.
O. FM.

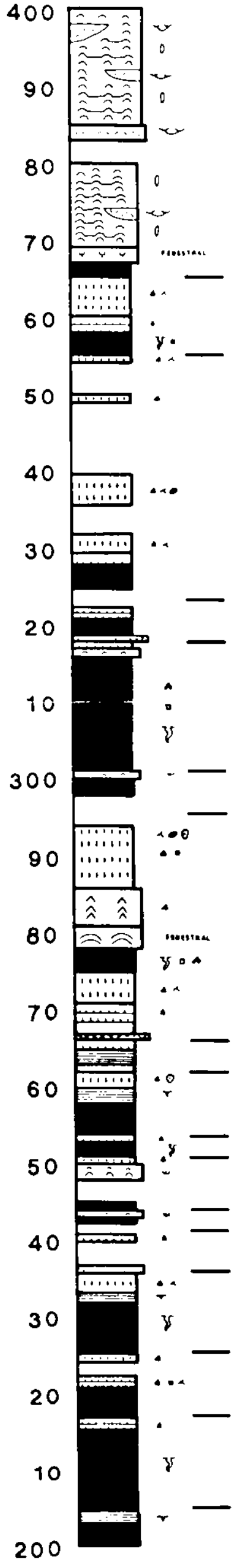
400
90
80
70
60
50
40
30
20
10
300
90
80
70
60
50
40
30
20
10
200

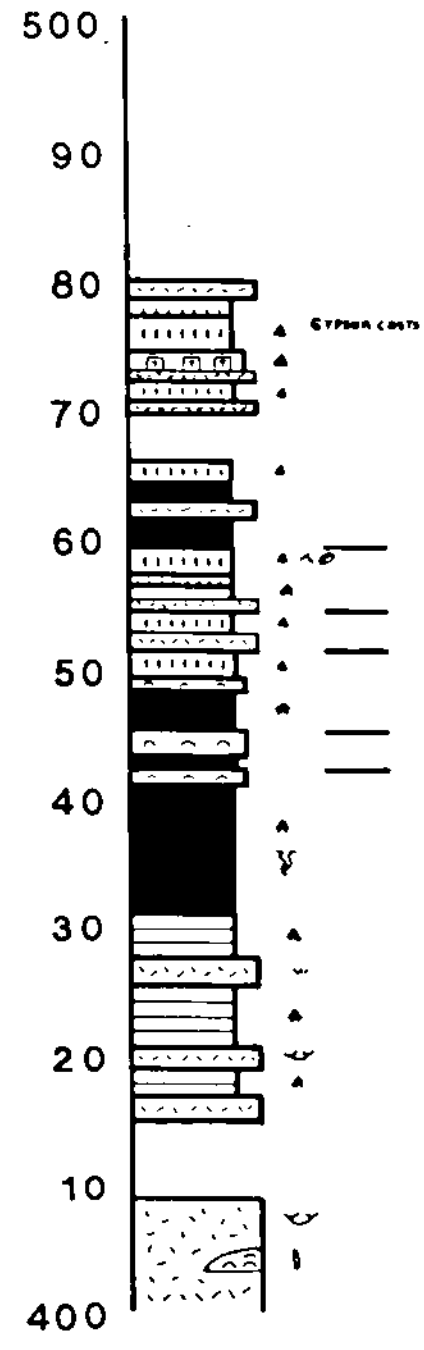
500
90
80
70
60
50
40
30
20
10
400

SECTION 14

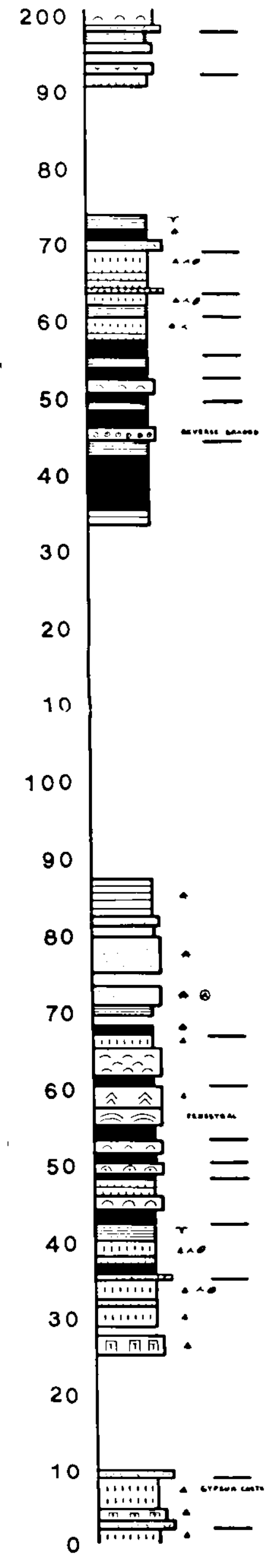
200
90
80
70
60
50
40
30
20
10
100
90
80
70
60
50
40
30
20
10
0

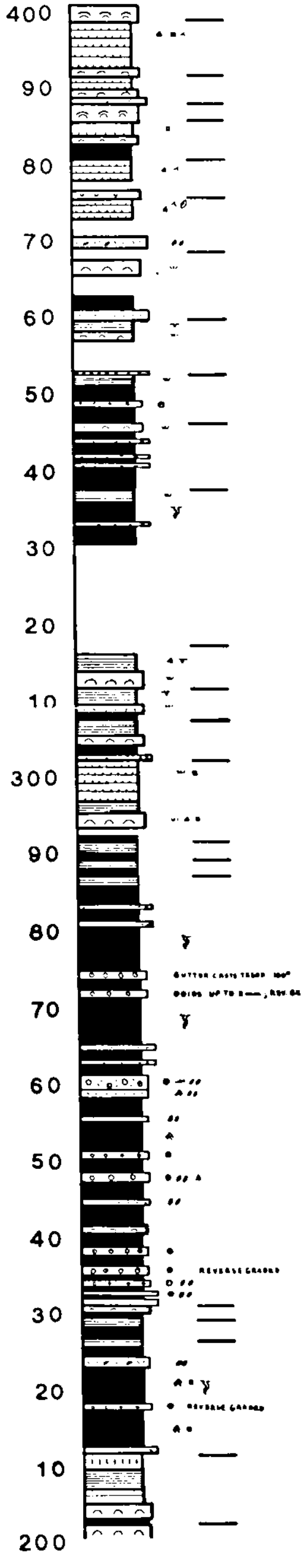
400
90
80
70
60
50
40
30
20
10
300
90
80
70
60
50
40
30
20
10
200

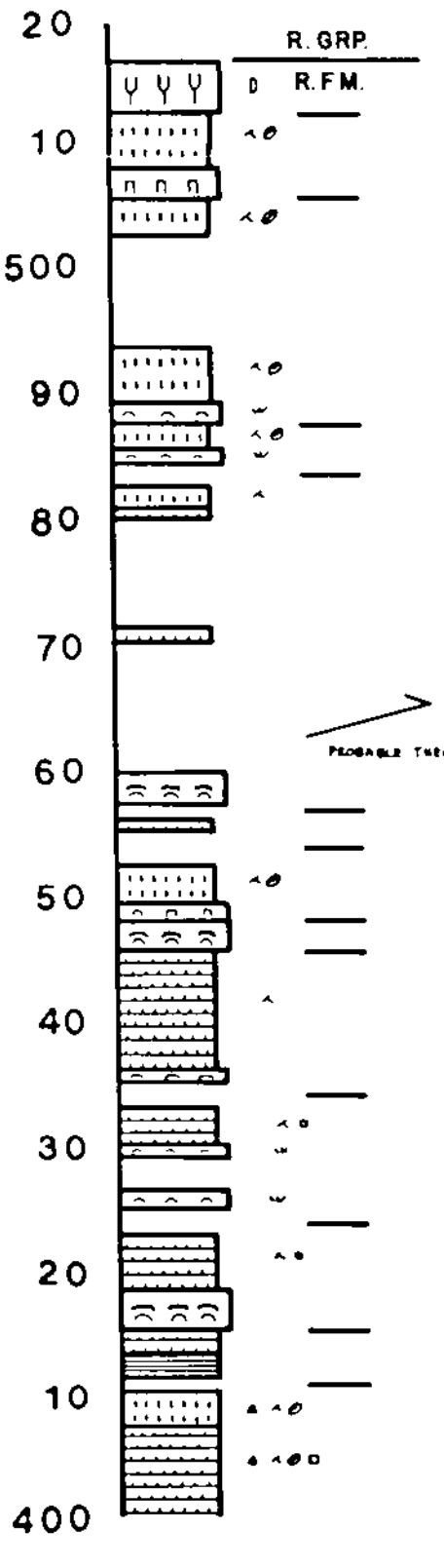
20
R. GRP.
R.F.M.
10
500
90
80
70
60
50
40
30
20
10
400

SECTION 15

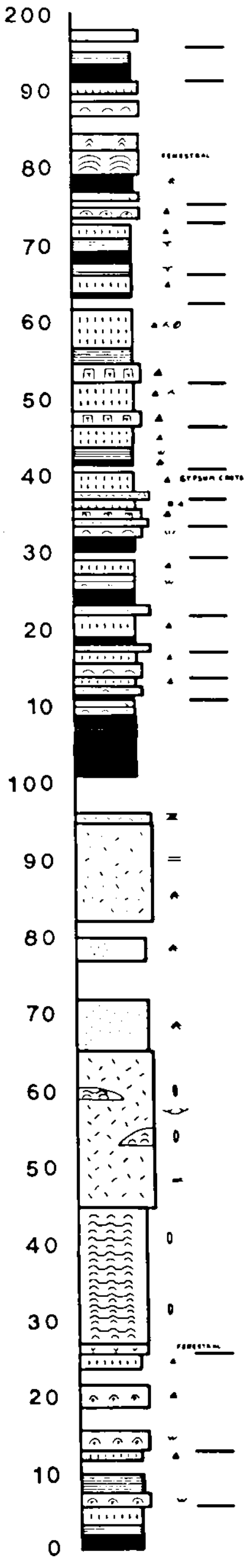
200
90
80
70
60
50
40
30
20
10
100
90
80
70
60
50
40
30
20
10
0

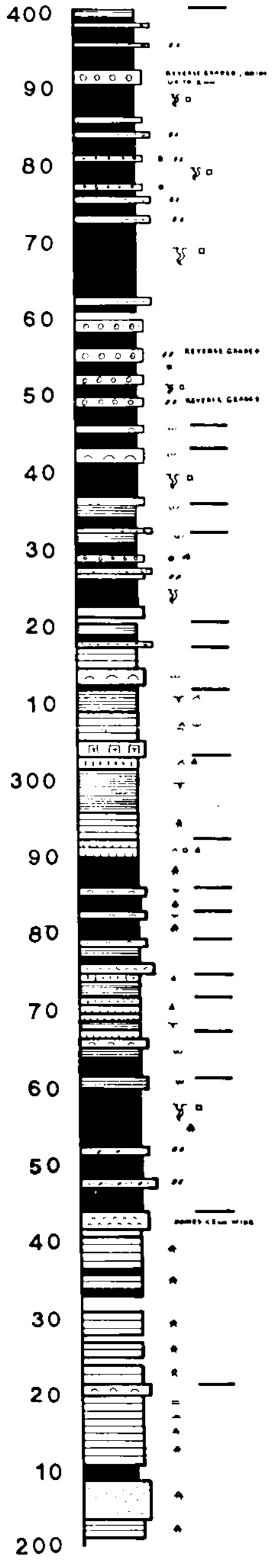
400
90
80
70
60
50
40
30
20
10
300
90
80
70
60
50
40
30
20
10
200

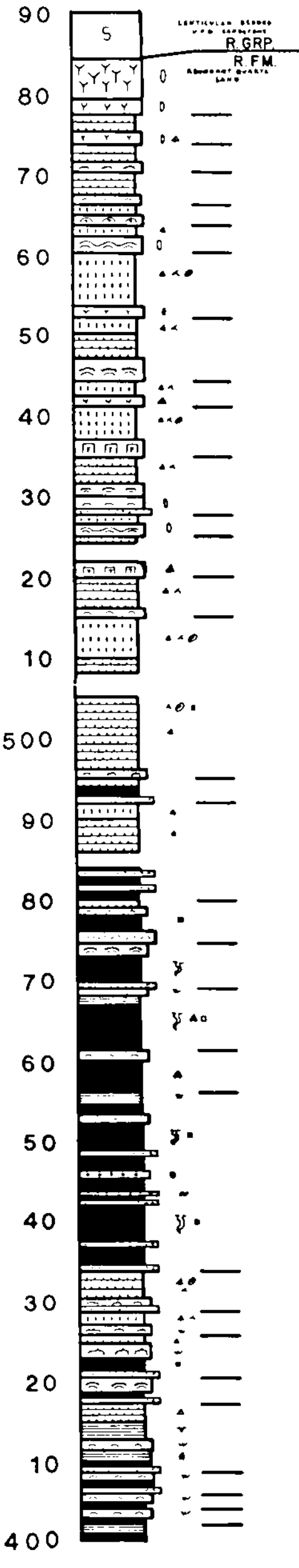
90
S
R.GRP.
R.FM.
80
70
60
50
40
30
20
10
500
90
80
70
60
50
40
30
20
10
400

SECTION 16

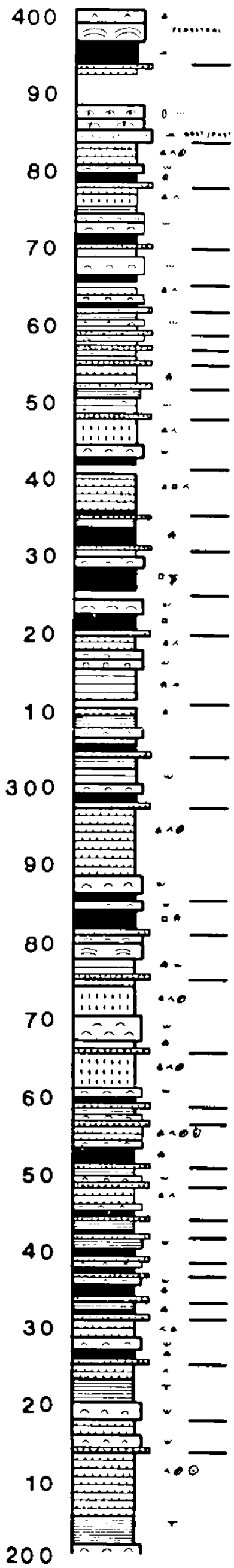

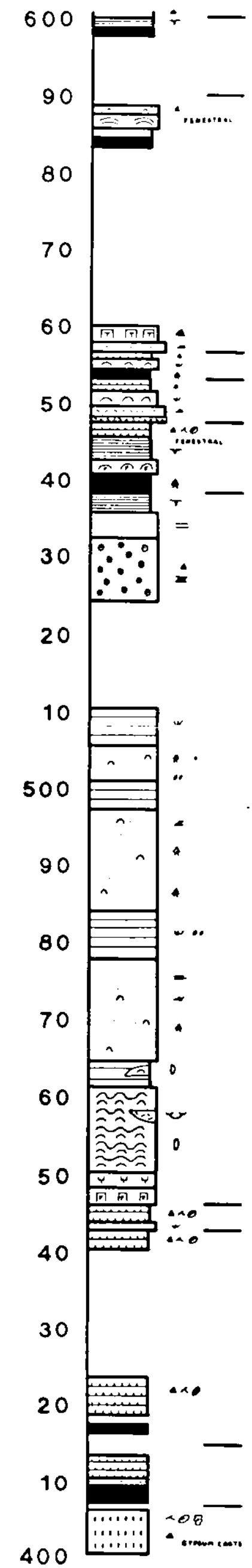

SEC. 16 CONT.

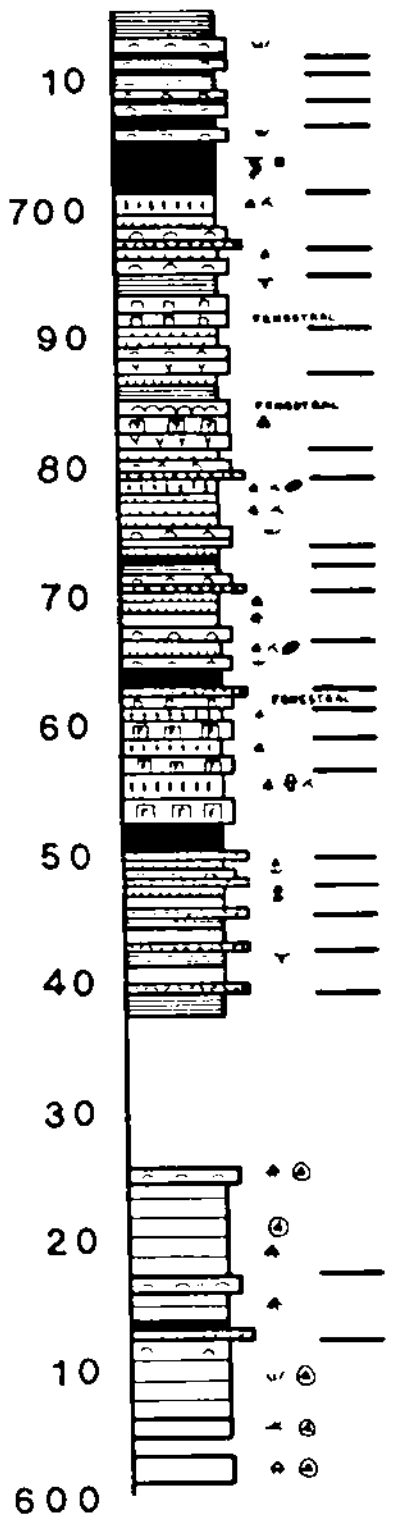

SECTION 17

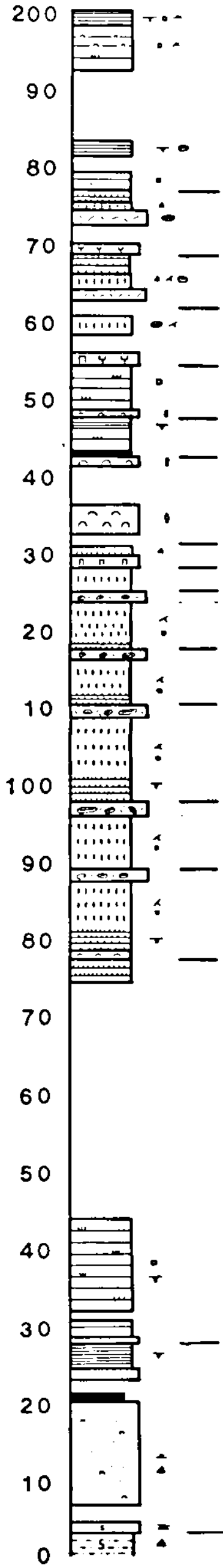
200
90
80
70
60
50
40
30
20
10
100
90
80
70
60
50
40
30
20
10
0
R. FM.
O. FM.

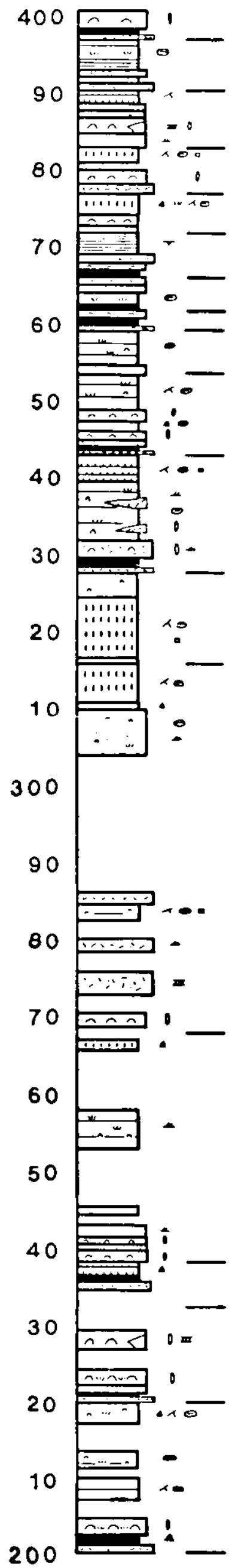
400
90
80
70
60
50
40
30
20
10
300
90
80
70
60
50
40
30
20
10
200

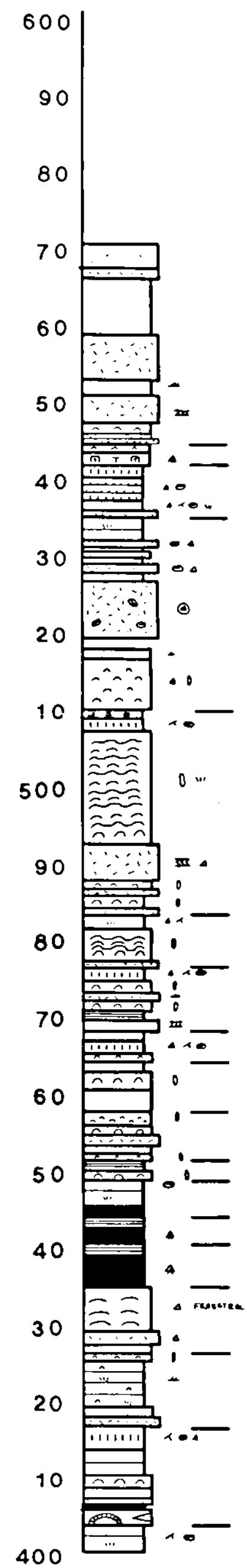
600
90
80
70
60
50
40
30
20
10
500
90
80
70
60
50
40
30
20
10
400

SEC. 17 CONT.

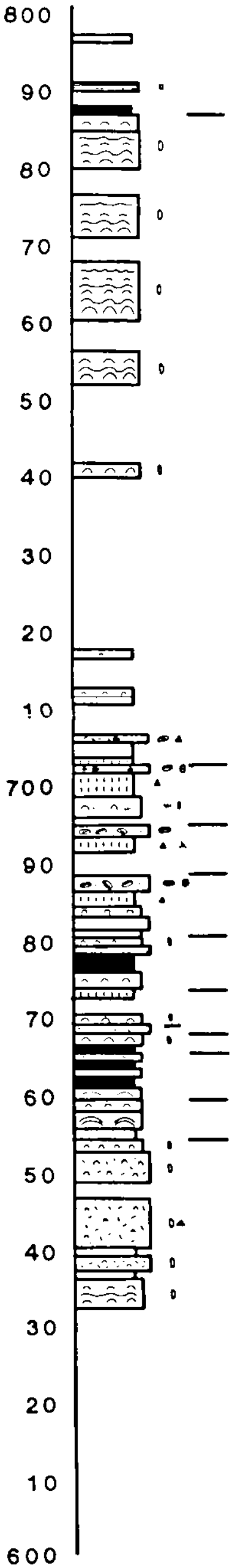
800
90
80
70
60
50
40
30
20
10
700
90
80
70
60
50
40
30
20
10
600

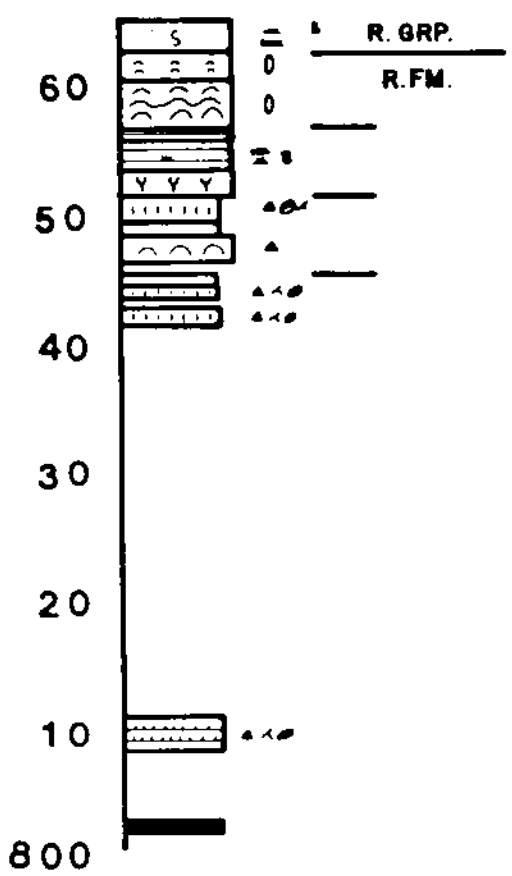
R. GRP.
R.FM.
60
50
40
30
20
10
800

SECTION 18

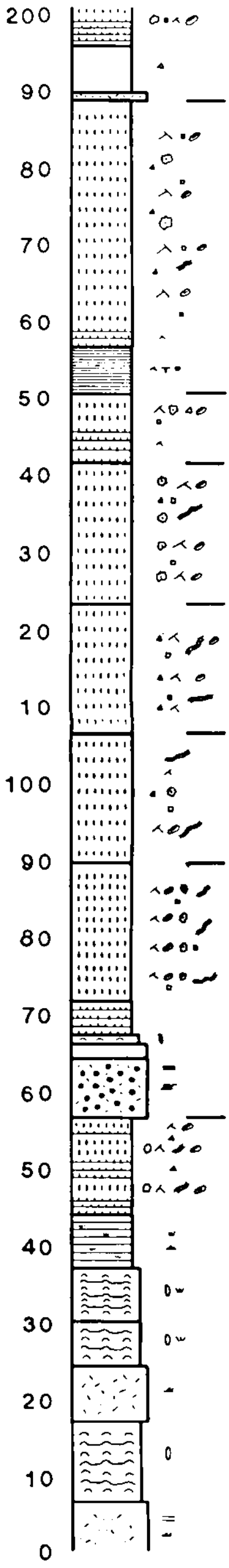
200
90
80
70
60
50
40
30
20
10
100
90
80
70
60
50
40
30
20
10
0

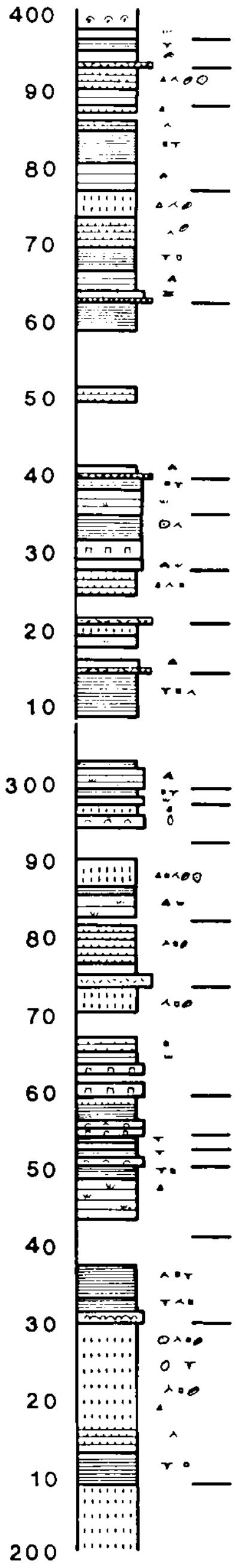
400
90
80
70
60
50
40
30
20
10
300
90
80
70
60
50
40
30
20
10
200

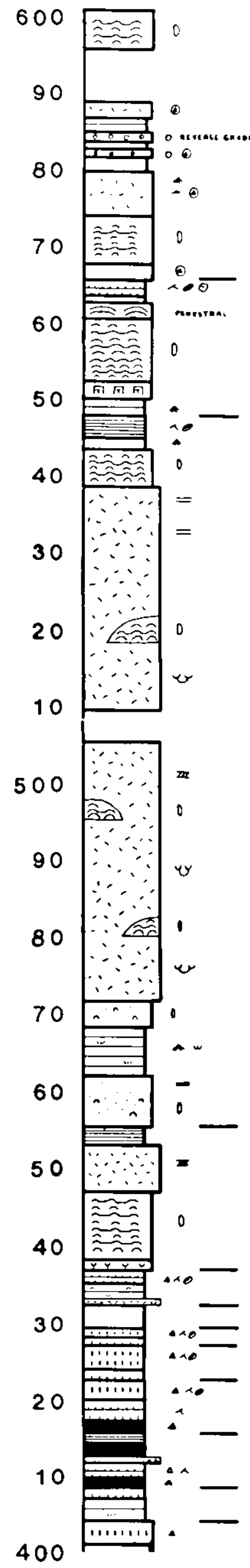
600
90
80
70
60
50
40
30
20
10
500
90
80
70
60
50
40
30
20
10
400

SEC. 18 CONT.

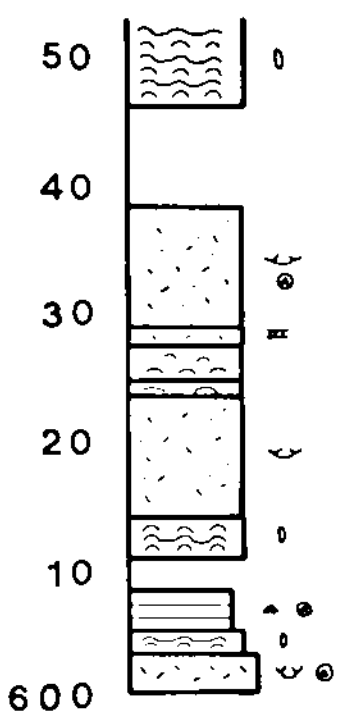

SECTION 19

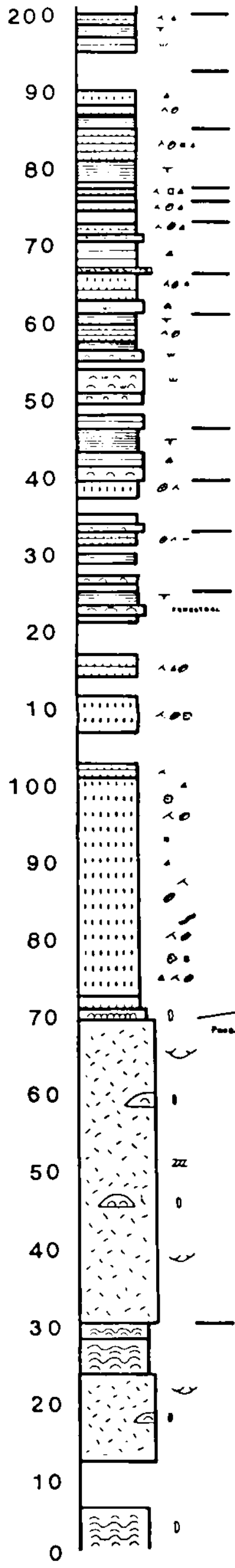
200
90
80
70
60
50
40
30
20
10
100
90
80
70
60
50
40
30
20
10
0

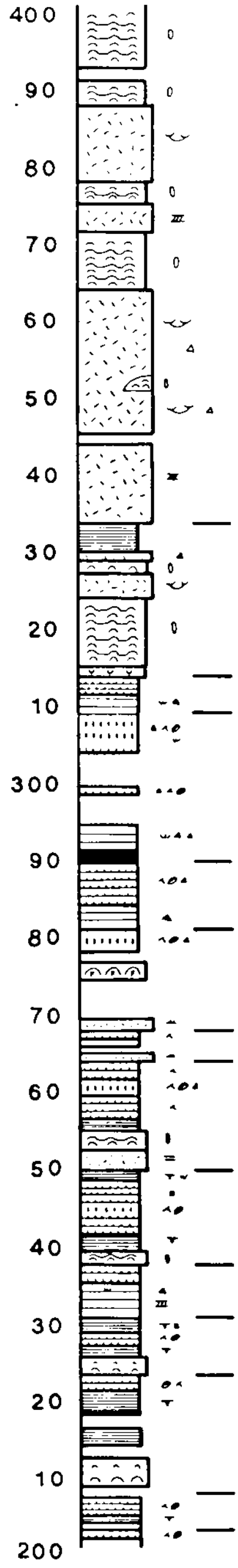
400
90
80
70
60
50
40
30
20
10
300
90
80
70
60
50
40
30
20
10
200

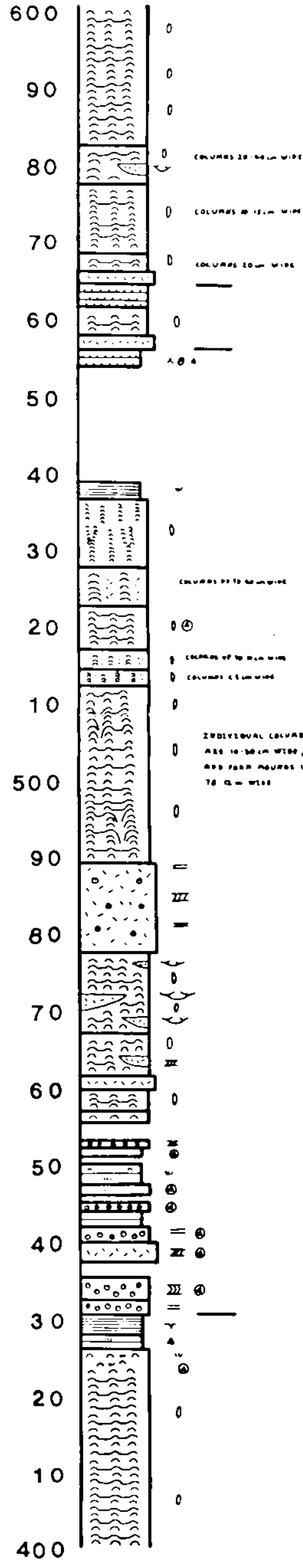
600
90
80
70
60
50
40
30
20
10
500
90
80
70
60
50
40
30
20
10
400

SEC. 19 CONT.

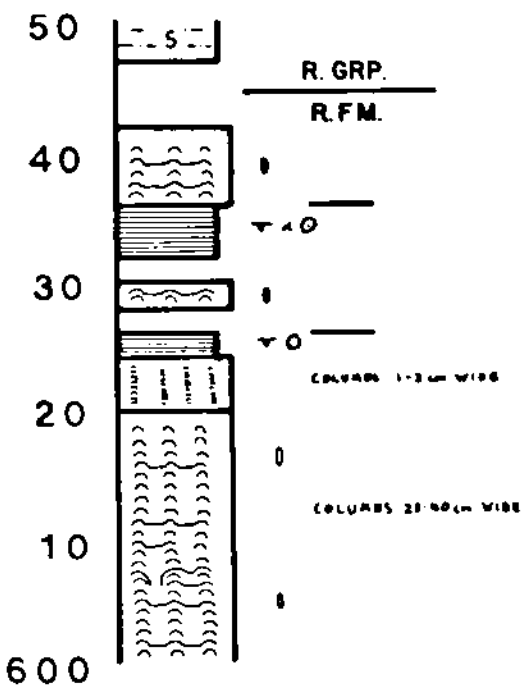

SECTION 20

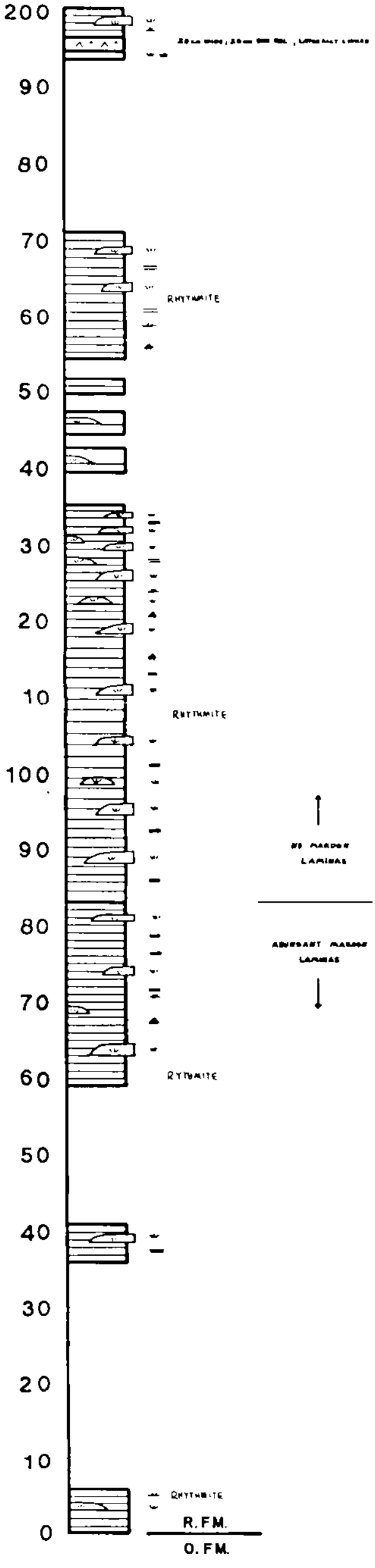
200
90
80
70
60
50
40
30
20
10
100
90
80
70
60
50
40
30
20
10
0
RHYTHMITE
RHYTHMITE
RYTHMITE
RHYTHMITE
R.FM.
O.FM.

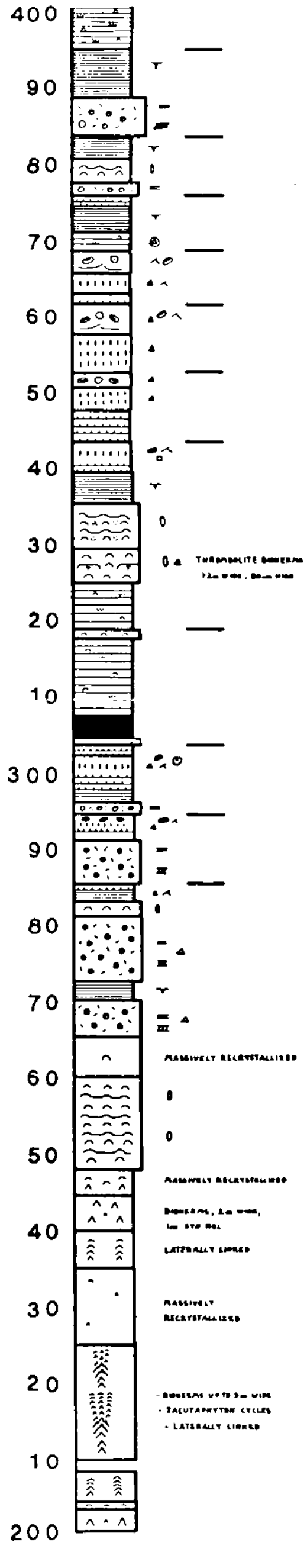
400
90
80
70
60
50
40
30
20
10
300
90
80
70
60
50
40
30
20
10
200
MASSIVELY RECRYSTALLISED
MASSIVELY RECRYSTALLISED
LATERALLY LINKED
MASSIVELY
RECRYSTALLISED
- LATERALLY LINKED

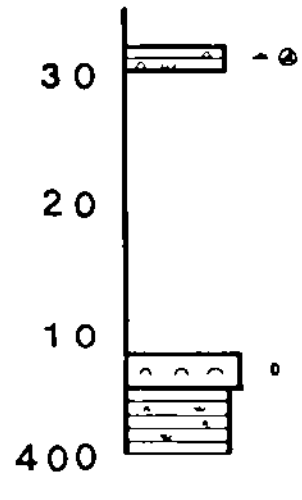
30
20
10
400

SECTION 21

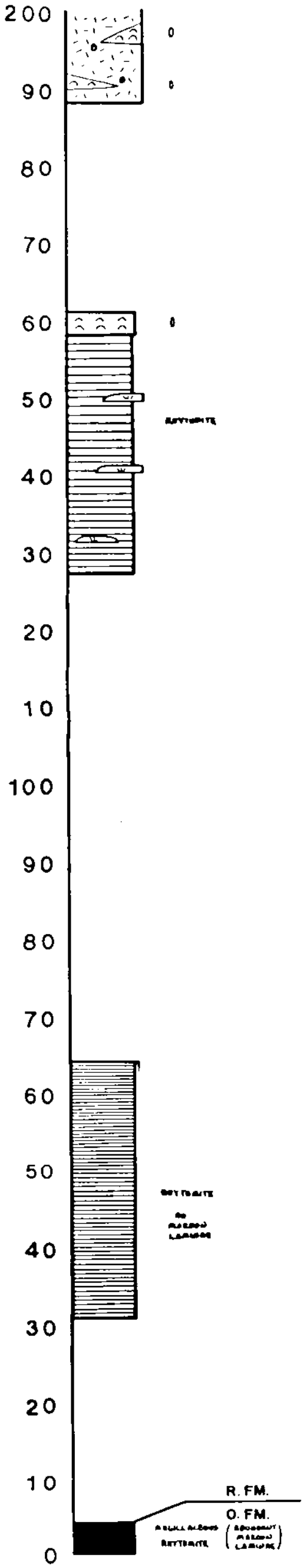
200
90
80
70
60
50
40
30
20
10
100
90
80
70
60
50
40
30
20
10
0
R. FM.
O. FM.

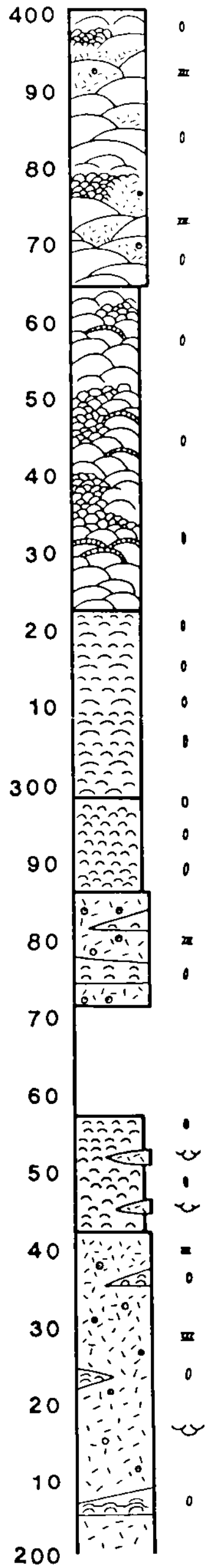
400
90
80
70
60
50
40
30
20
10
300
90
80
70
60
50
40
30
20
10
200

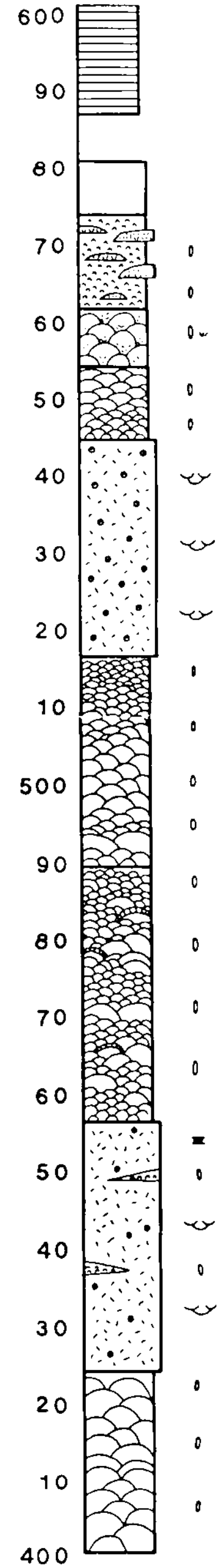
600
90
80
70
60
50
40
30
20
10
500
90
80
70
60
50
40
30
20
10
400

SEC. 21 CONT.

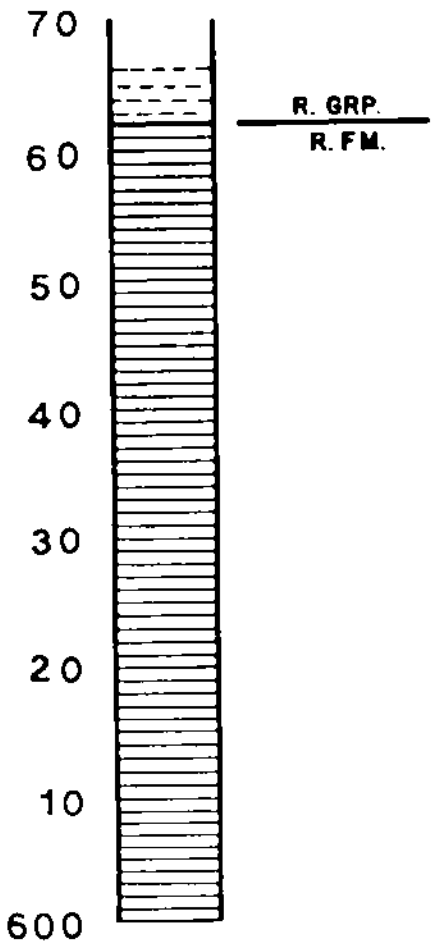

SECTION 22

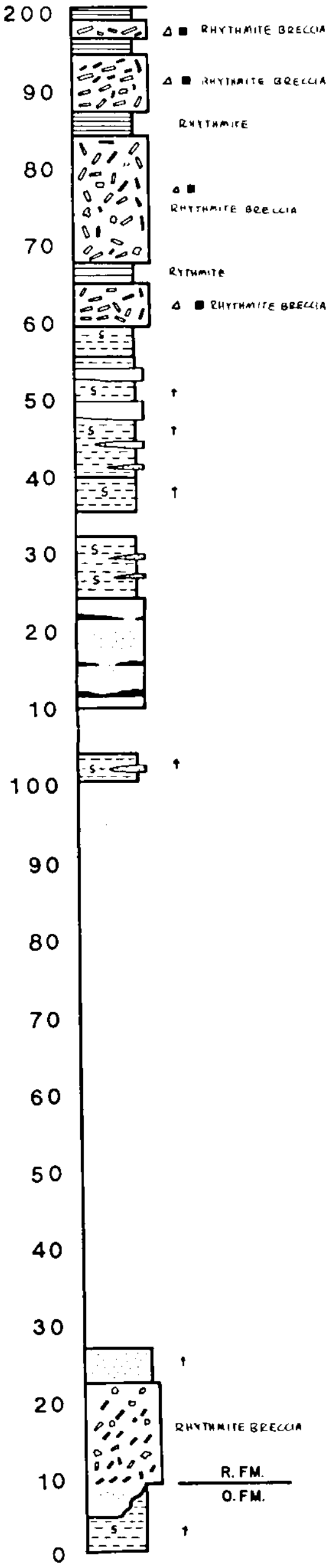
200
90
80
70
60
50
40
30
20
10
100
90
80
70
60
50
40
30
20
10
0
RHYTHMITE BRECCIA
RHYTHMITE BRECCIA
RHYTHMITE
RHYTHMITE BRECCIA
RYTHMITE
RHYTHMITE BRECCIA
RHYTHMITE BRECCIA
R. FM.
O. FM.

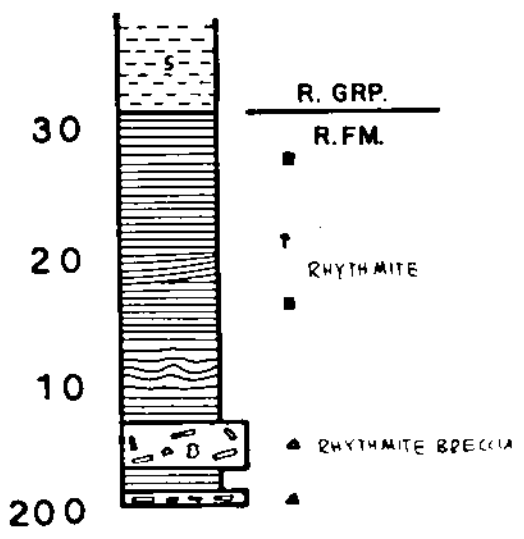
30
20
10
200
R. GRP.
R. FM.
RHYTHMITE
RHYTHMITE BRECCIA